



University of Sussex

A University of Sussex DPhil thesis

Available online via Sussex Research Online:

<http://sro.sussex.ac.uk/>

This thesis is protected by copyright which belongs to the author.

This thesis cannot be reproduced or quoted extensively from without first obtaining permission in writing from the Author

The content must not be changed in any way or sold commercially in any format or medium without the formal permission of the Author

When referring to this work, full bibliographic details including the author, title, awarding institution and date of the thesis must be given

Please visit Sussex Research Online for more information and further details

Developmental failure in cochlear hair
cells from mouse models of Usher
syndrome and the identification of an
acid sensitive ionic current in Inner
and Outer hair cells

Submitted for the degree of D. Phil.

December 2012

Terri Patricia Roberts

DECLARATION

I hereby declare that this thesis has not been submitted, either in the same or different form, to this or any other University for a degree.

Terri Patricia Roberts

ACKNOWLEDGEMENTS

I would like to say a massive thank you to my supervisors Corne Kros and Guy Richardson for their un-wavering support throughout the course of my DPhil. This extends no end to Corne who has become a friend throughout the last 4 years, being both a shoulder to cry on and an open ear when the course of PhD life has become tough.

I would also like to say thank you to Kishani Ranatunga for all of the time and dedication that was spent teaching me the intricacies of patch clamping, along with days of solution making and hours of pulling electrodes together. Without you by my side during the early years of my PhD I would never have become the scientist I am today. I must also thank you for the contribution of data towards my thesis, providing data on the development of the Myo7a^{+/sh6j} and Myo7a^{sh6j/sh6j} IHCs.

A big thank you to Shinya Ugawa all the way in Japan, for providing the mouse models for my work on identifying the acid sensitive ion current.

To Sonia, Jasmine and Guleid, I cannot begin to express how much I appreciate your hours of hard work proof reading my work I can only imagine just how difficult I made this for you, we all know how poor my typing skills are! I will never forget this along with the numerous panic stricken phone calls you have all received and your abilities to calm me down and make me see sense once more.

Many of my friends and family including Mum, Gemma, Ruth, Gareth, Taz, Kim, Nicola, Mikey, Freya and too many more to name deserve a special thank you for listening to hours of my ranting and moaning about the goings on in the lab. You guys really made it what it was I couldn't have got through it without the laughs! A special shout out to Gemma for giving me her laptop in my hour of need, I could never have finished without your generosity, Gareth for hours of constructing scaffold supports, lending of equipment for recording videos and answering the hundreds of questions I had about PhD life in general, and finally Nicola for helping me master photoshop at the final hurdle, proof reading the final version and keeping me sane in the lead up to my viva.

All of you guys mentioned here have made the last 4 years bearable and without that who knows what state this would be in so I truly thank you all from the bottom of my heart!

ABSTRACT

Inner hair cells (IHCs) are the primary sensory receptors of the mammalian cochlea. I employed the whole-cell patch-clamp technique to study voltage responses and ionic currents of IHCs in mice bearing mutations in hair bundle proteins. These mutations, all associated with Usher syndrome, lead to structural and functional defects of the mechanosensory hair bundle. I observed developmental failure in the electrical properties of IHCs from these mutants: a continuation of neonatal spiking instead of the graded receptor potentials seen in control adult IHCs. Voltage-clamp recordings revealed the main cause as the absence of the adult fast potassium ($I_{K,f}$) current.

Outer hair cells (OHCs) are required to amplify the travelling wave to be detected by the IHCs. Optical and whole-cell patch clamp techniques in these same mutants were employed to investigate the development of adult OHCs. I observed a developmental failure in the electrical properties of these OHCs, seen by an absence of the potassium current $I_{K,n}$. Electromotility and the associated non-linear capacitance were however observed, indicating that prestin is expressed in the mutants.

Acid sensitive ion channels (ASICs) have recently been found to be present within the organ of Corti. Here I present data showing the presence of an acid sensitive ion current in both IHCs and OHCs. ASIC1b knockout mice show a response to changes in the extracellular pH suggesting that the current may be carried through a different channel subtype or that compensatory changes occur. The electrical properties of the IHCs develop to maturity in these mice, however the OHCs appear to remain functionally immature displaying a lack of expression of the $I_{K,n}$ current and electromotility. This lack of electromotile function suggests that ASIC1b may be required either for the function of prestins electromotility or for the targeting of prestin to the cell membrane.

TABLE OF CONTENTS

Declaration	2
Acknowledgements.....	3
Abstract.....	4
Table of Contents.....	5
1 Introduction	8
1.1 The structure and function of the mammalian ear	9
1.1.1 Anatomy of the outer and middle ear	9
1.1.2 Anatomy of the inner ear.....	11
1.2 Development of the inner hair cells	13
1.3 Development of the outer hair cells	21
1.4 The hair bundle	27
1.5 Acid sensitive currents and ASIC channels	32
1.6 Thesis aims.....	36
2 Methods.....	37
2.1 Tissue Preparation.....	38
2.1.1 Mouse models.....	38
2.1.2 Immature preparation	39
2.1.3 Mature preparation	40
2.2 Experimental equipment	40
2.3 Experimental solutions	43
2.4 Whole cell recording.....	44
2.5 Mechanoelectrical transduction.....	45
2.6 DIC imaging	45
2.7 Data acquisition and analysis.....	45
2.7.1 Current measurement.....	45
3 Development of the inner hair cells in mouse models of Usher syndrome	48

3.1	Introduction	49
3.2	Results	49
3.2.1	Neonatal Myo7a ^{+/sh6j} and Myo7a ^{sh6j/sh6j} IHCs	49
3.2.2	Steady state currents in mature IHCs	51
3.2.3	Presence of I _{K,f} in mature IHCs	52
3.2.4	Presence of I _{K,n} in mature IHCs	52
3.2.5	Voltage responses in mature IHCs	53
3.2.6	Cellular properties of mature IHCs	54
3.2.7	Adult Pcdh ^{+/AV6j} and Pcdh ^{AV6j/AV6j} IHCs	55
3.3	Discussion	57
3.4	Conclusions	60
3.5	Future experiments	60
4	Development of outer hair cells in myo7a^{+/sh6j} and myo7a^{sh6j/sh6j} mouse models	83
4.1	Introduction	84
4.2	Results	84
4.2.1	Steady state currents in neonatal and mature OHCs	84
4.2.2	The I _{K,n} current in the neonatal and mature OHCs	85
4.2.3	Cellular properties of the OHCs	86
4.2.4	Presence of prestin in the mature OHCs	87
4.2.5	Effect of linopirdine on the basolateral currents	88
4.3	Discussion	89
4.4	Conclusions	90
4.5	Future experiments	90
5	Presence of an acid sensitive current in the hair cells	103
5.1	Introduction	104
5.2	Results	104
5.2.1	Acid sensitive currents in the inner and outer hair cells	104
5.2.2	Effect of nafamostat on the pH sensitive current in the hair cells.	108

5.2.3	Effect of amiloride on the pH sensitive current in the hair cells.	109
5.2.4	Effect of nafamostat on the resting current in the hair cells.....	111
5.2.5	Effect of amiloride on the baseline currents in the hair cells.	112
5.3	Discussion	113
5.4	Conclusions	117
5.5	Future experiments	117
6	Basolateral currents in the hair cells of ASIC1b mouse models	134
6.1	Introduction	135
6.2	Results	135
6.2.1	Steady state currents in the hair cells.....	135
6.2.2	Presence of adult current $I_{K,f}$	137
6.2.3	Presence of $I_{K,s}$	138
6.2.4	Presence of adult current $I_{K,n}$	138
6.2.5	Presence of prestin	139
6.2.6	Cellular properties.....	140
6.2.7	Mechanoelectrical transduction current	142
6.3	Discussion	143
6.4	Conclusions	144
6.5	Future experiments	145
6.6	Amendment	169
7	Final conclusions.....	170
8	Supplementary information	173
9	References.....	175

1 INTRODUCTION

Language and music are an integral part of life and social interactions; without the ability to hear, those who suffer from hearing impairments may feel isolated. Understanding the ear and the causes underlying impediments to hearing will in time improve the quality of life of those with auditory impairment. The auditory system is beautifully engineered to transfer sound vibrations from the environment into electrical signals for perception by the brain. The early parts of this chapter are centred around the physiology of the auditory system, with later parts providing a more specific background and introduction to the research reported in this thesis.

1.1 The structure and function of the mammalian ear

Noise or sound is carried by a travelling pressure wave caused by vibrating air molecules (Geisler, 1998; Purves et al., 2007). Humans can detect sounds between 20 Hz and 20 kHz, with this higher end gradually decreasing with age (Purves et al., 2007). Sound intensity levels are measured in decibels sound pressure level (dB SPL), humans can detect sounds as quiet as 0 dB SPL with loud sounds becoming painful at around 130 dB SPL. The organ responsible for sound detection is the ear; this can be divided into three main parts: the outer ear, the middle ear and the inner ear. The anatomy of the ear is shown in Figure 1-1. The structure and function of each part will now be described.

1.1.1 Anatomy of the outer and middle ear

The mammalian outer ear consists of the pinna, concha and the auditory meatus (ear canal). The pinna is the cartilaginous flange that sits on the external surface of the head. The concha is the resonance cavity within the pinna. The auditory meatus is the canal connecting the pinna to the tympanic membrane (ear drum) (Figure 1-1). The role of the pinna and the concha is to collect and amplify incoming sound waves and channel them down the auditory meatus (Geisler, 1998; Pickles, 2008; Purves et al., 2007). The pinna and concha are also able to selectively filter incoming sound waves depending on their direction to give cues about the location of the source of the sound (Pickles, 2008; Purves et al., 2007). Due to passive resonance effects the auditory meatus is able to amplify sounds with frequencies in the range of 2 – 5 kHz (Purves et al., 2007). Once directed down the ear canal the sound wave causes the tympanic membrane to vibrate.

The tympanic membrane is the division between the outer and middle ears and vibration of this structure causes the movement of the three middle ear bones; the ossicles (Geisler, 1998; Pickles, 2008; Purves et al., 2007). The malleus, which contacts the tympanic membrane, is joined rigidly to the incus meaning that the two bones rotate together upon vibration of the ear drum and the force is transferred to the stapes (Figure 1-1). The stapes is attached to the flexible oval window of the cochlea and causes this to vibrate. The oval window is the division between the middle and inner ear and the consequences of movement of this structure will be discussed in the next section.

The majority of sound waves travelling through air are reflected when they come into contact with fluid. The role of the middle ear is to reduce this reflection by matching the low impedance of the air filled external ear with the high impedance of the fluid filled inner ear. This occurs through two mechanisms, the first due to the tympanic membrane being roughly 20 times larger than the oval window. This would result in the pressure at the oval window being 20 times larger than that at the tympanic membrane. The second mechanism is through the lever action of the ossicles increasing the force on the oval window by a factor of 2. Together these amplify the pressure sound wave about 40 fold, so that even with reflection of the incoming signal it is still large enough to be detected in the cochlea (Geisler, 1998; Pickles, 2008; Purves et al., 2007).

There are two muscles within the middle ear which allow for modification of the incoming sound wave. The stapedius muscle is connected to the stapes and contraction of the muscle causes a sideways movement of the stapes. The footplate of the stapes is kept in place in the opening of the oval window, and so the bone tilts and stretches the annular ligament. This increase in stiffness thus increases the reflection of the incoming sound wave (Geisler, 1998). The tensor tympani is connected to the malleus. Contraction of the muscle results in an inward movement of the tympanic membrane causing a reduction in the size of the sound wave that is transmitted (Geisler, 1998). Contraction of these muscles is initiated through a reflex in response to loud noises and also during periods of self vocalization (Geisler, 1998; Pickles, 2008).

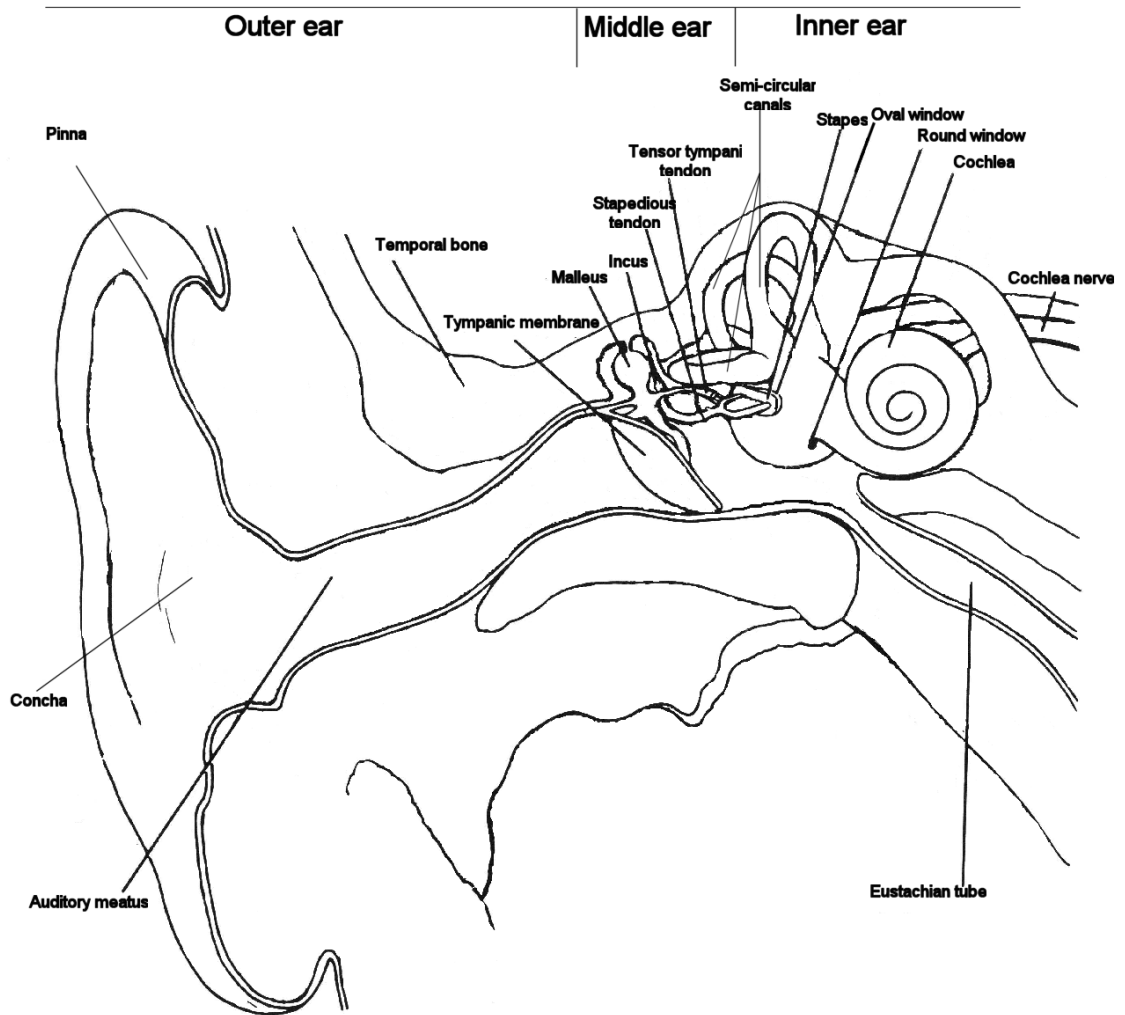


Figure 1-1 Structure of the mammalian ear. Modified from Pickles, 2008.

1.1.2 Anatomy of the inner ear

The inner ear consists of the cochlea (the organ of hearing) and the vestibular system (the organ of balance) (Figure 1-1). The vestibular system will not be discussed any further in this work as it is beyond the scope of this research.

The cochlea is the spiral shaped organ within the inner ear that contains the sensory cells for sound detection. The cochlea can be divided into three fluid filled chambers, the scala vestibuli (SV), the scala media (SM) and the scala tympani (ST). These three chambers run the length of the cochlea and are spiralled around a central bone which is called the central modiolus (Geisler, 1998; Pickles, 2008; Purves et al., 2007). The oval window is connected to the SV and

movement of the oval window causes displacement of the fluid within this chamber. The SV is connected to the ST through the helicotrema at the apex of the cochlea. The ST is connected to the middle ear through the round window, and so displacement of the fluid in the SV is transferred to the ST and then emitted back into the air of the middle ear (Geisler, 1998; Pickles, 2008). Although this seems wasteful it is important because the movement of the oval window would not be able to displace the fluid within these two chambers (the SV and ST) as fluid is incompressible and there would be nowhere for it to travel if the cochlea was a closed system (Geisler, 1998). Between the SV and the ST sits the SM. The SV is separated from the SM by Reissner's membrane, whilst the basilar membrane (BM) separates the ST from the SM. The fluid within the SV and the ST is called perilymph and is similar in composition to typical extracellular solution in that it has a high Na^+ concentration and a low K^+ concentration. The fluid within the SM known as endolymph, is however an atypical extracellular fluid in that it contains a high concentration of K^+ ions and low Na^+ ions (Geisler, 1998; Pickles, 2008; Purves et al., 2007). The purpose of this fluid in the auditory system will become evident when discussing activation of the sensory cells.

The sensory tissue of the cochlea called the organ of Corti sits upon the BM (Geisler, 1998; Pickles, 2008; Purves et al., 2007). The organ of Corti contains a single row of inner hair cells (IHCs) and 3 rows of outer hair cells (OHCs). These cells have bundles protruding from the apical surface. These bundles are V shaped in the OHCs and are slightly straighter in the IHCs. These hair cells are surrounded by a host of supporting cells and sit under the tectorial membrane (TM) (Figure 1-2). The TM is a gelatinous structure which is attached to the supporting cells at the modiolar side of the organ of Corti where it then protrudes over the top of the hair cells where it is again held by the stereocilia of the OHCs. The stereocilia of the IHCs do not contact the TM but sit in a groove called Hensen's stripe (Geisler, 1998; Pickles, 2008).

The displacement of the fluid in the ST moves the BM, which in turn causes the movement of the organ of Corti. The TM does not move and so movement of the sensory tissue causes a relative movement of the stereocilia of the hair cells which are deflected (Pickles, 2008; Purves et al., 2007). Deflection of the stereocilia causes the opening and closing of mechanotransducer channels dependent on the movement of the bundle. These will be discussed in more detail later in this chapter. Opening of mechanotransducer channels in the stereocilia cause a depolarisation of the hair cells, whereas closing of the channels causes a hyperpolarisation of the hair cells. The IHCs are able to convert the sound signal into an electrical signal which is transferred to the auditory region of the central nervous system as distinct patterns of neural activity in the afferents of the auditory nerve. OHCs only have a

sparse afferent innervation but are important in the amplification of the incoming signal (Pickles, 2008), as discussed later in this chapter.

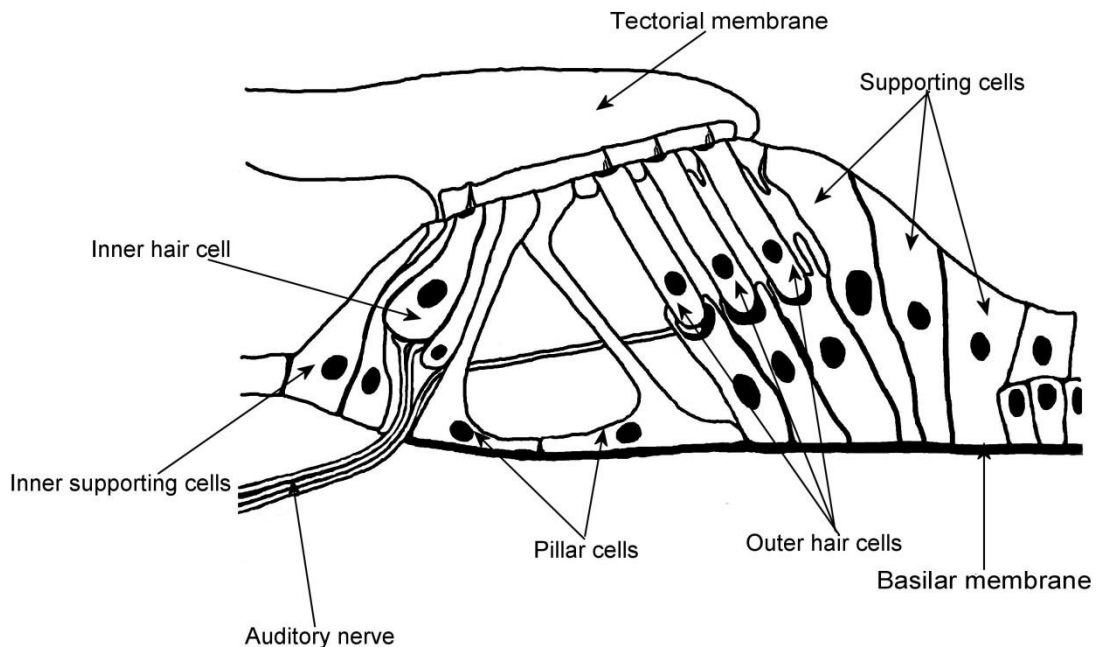


Figure 1-2 Structure of the organ of Corti modified from (Pickles, 2008)

1.2 Development of the inner hair cells

Inner hair cells (IHCs) are the primary sensory receptors that are able to detect sound and convert this signal into an electrical form that is processable by the brain. IHCs can be first identified just after terminal differentiation at E14.5 in the basal coil of the organ of Corti and E15.5 in the apical coil (where E19.5 is equal to P0 and P0 is the day of birth) (Ruben, 1967). At this stage of development the IHCs express only a small delayed rectifier K^+ current called $I_{K,emb}$, which shows slow activation kinetics that are voltage dependant and at -4 mV reach a size of around 200 pA. At this age the IHCs have a resting membrane potential of around -50 mV (Kros, 2007; Marcotti et al., 2003a). IHCs at this time are quiescent and unable to fire action potentials which are seen in the more developed cells.

Over the next two days the IHCs develop the inward rectifier current $I_{K,1}$, this current is important hyperpolarising the resting membrane potential to around -67 mV. At this age the IHCs also acquire small Na^+ and Ca^{2+} currents, all three of which increase in size until E18.5 (Marcotti et al., 2003a, 2003b). At this stage of development the IHCs are then able to produce slow spontaneous action potentials.

Unusually action potentials in the IHCs are Ca^{2+} dependant and upon removal of extracellular Ca^{2+} both spontaneous and evoked spiking activity can be abolished (Marcotti et al., 2003b). The calcium current in the IHCs is carried by the voltage dependant $\text{Ca}_v1.3$ channels (Marcotti et al., 2003b; Platzner et al., 2000). Small depolarisations of the resting membrane potential activate these channels causing an inward Ca^{2+} current and further depolarisation of the membrane opening more Ca^{2+} channels and so on. Increasing the extracellular Ca^{2+} concentration increased the rate of the upstroke of the action potentials that were generated as well as the maximum potential that was reached at the peak of the spike (Marcotti et al., 2003b). Increased extracellular Ca^{2+} had no effect on the frequency of the action potentials that were generated, whilst modulation of the Na^+ current altered the firing frequency (Marcotti et al., 2003b). An increase in the I_{Na} caused an increase in the action potential frequency, reducing the time required for the membrane potential to reach threshold for triggering this regenerative activity.

Action potentials recorded from embryonic IHCs have a slow time course compared to those seen neonatally. This is likely to be due to the smaller I_{Ca} and I_{Na} in the former, which will slow the upstroke of the action potential and cause a slower depolarisation of the membrane potential (Marcotti et al., 2003b). This will in turn result in a slower recruitment of the $I_{K,\text{emb}}$ current, slowing the repolarisation of the membrane. The $I_{K,\text{emb}}$ current is also smaller meaning that it will take longer for the repolarisation to occur.

In neonatal IHCs the downward stroke of the action potential is also regulated by the SK current. This current is not intrinsically voltage dependant and is activated by increases in the intracellular calcium concentration, which binds the calcium binding protein calmodulin and activates the SK channel (Marcotti et al., 2004a; Xia et al., 1998). The increase in intracellular Ca^{2+} occurring during the depolarisation phase of an action potential results in the activation of the SK2 channel and contributes to the repolarisation of the membrane potential. Block of the SK2 channel by apamin results in a progressively reduced repolarization phase causing a steady depolarisation of the membrane potential. Eventually the membrane potential is too depolarised to sustain action potential generation (Marcotti et al., 2004a). Before the resting

membrane potential becomes too depolarised to sustain action potential generation there is often an increase in the firing frequency, likely to be linked to the more depolarised resting membrane potential (Marcotti et al., 2004a). Genetic deletion of the SK2 channels does not result in IHCs being unable to produce action potentials, but as with the apamin block, the action potentials produced have a progressively smaller repolarisation phase until the cell is too depolarised for action potential generation. The cell then slowly returns to its resting membrane potential when it is again able to produce action potentials (Johnson et al., 2007). In neonatal IHCs the $I_{k,emb}$ current develops into $I_{k,neo}$ and although this current is required for the repolarisation phase of the action potentials in these cells it alone is not sufficient, probably due to its steady state inactivation (Marcotti et al., 2003a).

The intracellular Ca^{2+} required to activate the SK2 channel does not arise from the L-type voltage gated Ca^{2+} channels alone but also through Acetylcholine (ACh) receptors (AChRs). Neonatal IHCs are known to receive a transient efferent innervation, which is no longer present when the cells are fully mature (Pujol et al., 1998). These efferent terminals release the neurotransmitter ACh onto the IHCs activating AChRs. These non-selective cation channels act, just like the Ca^{2+} channels, by increasing intracellular Ca^{2+} levels. This activates the SK2 channel resulting in an outward K^+ current and hyperpolarisation of the IHC resulting in a reduction in the spiking of the cell (Marcotti et al., 2004a). Conversely application of strychnine, a blocker of the $\alpha 9\alpha 10$ AChR subunits caused an increase in the frequency of action potentials in IHCs and turned the bursting activity seen in apical IHCs into activity similar to that seen in basal cells, with a more sustained firing rate (Johnson et al., 2011).

Action potential frequency in IHCs changes along the apical to basal gradient of the organ of Corti. Apical IHCs tend to fire in a burst like manner, showing a period of activity followed by a quiescent phase. Basal IHCs tend to fire in a much more sustained manner with a similar frequency of activity to apical IHCs but without the longer quiescent phases (Johnson et al., 2011).

Experimentation with BAPTA, a fast calcium chelating agent, and EGTA, a slow calcium chelating agent, has shown that AChR are co-localized with the SK2 channels whereas the L-type Ca^{2+} channels are located further away. This means the activation of the SK2 channel through depolarisation of the membrane potential and the voltage gated Ca^{2+} channel will require more time, allowing the membrane to depolarise fully and the upward stroke of action potential generation to occur before the membrane is repolarised (Marcotti et al., 2004a).

At the end of the second postnatal week there is a reduction in the expression of the SK2 channels and the AChRs, which coincides with the down-regulation of the efferent innervation of the IHCs. Mature IHCs do not respond to ACh and show no SK2 current (Glowatzki and Fuchs, 2000; Marcotti et al., 2004a).

Although neonatal mice are deaf due to the blockage of the ear canal preventing sound signals entering the ear, the IHCs do possess the hair bundle structure and transduction current required to encode sound detection. The transduction current (I_T) is a non-specific cation current carried through the as of yet unidentified mechanoelectrical transducer (MET) channel. It is thought that the finite open probability of the MET channel may cause small depolarisations, which can trigger action potential generation in the IHCs (Johnson et al., 2012).

Neonatal IHCs also express P2X and P2Y receptors, which carry a non-specific cationic current activated by the presence of extracellular ATP. Activation of these channels causes an inward current consisting of mainly Na^+ and Ca^{2+} , which lead to depolarisation of the IHCs membrane potential and can trigger action potential generation (Tritsch et al., 2007). Extracellular ATP is thought to be released by the inner supporting cells of Köllikers organ (KO) through unconnected connexons. The supporting cells of the cochlea are known to be connected to one another via gap junctions formed of connexin 26 (6 connexin subunits form a connexon, 2 connexons form a gap junction) and so the putative presence of unpaired connexons in the inner supporting cells is not impossible (Tritsch et al., 2007). Application of ATP increased the frequency of the spontaneous inward currents recorded in the IHCs and the non-specific purinergic receptor blockers pyridoxalphosphate-6-azophenyl-2',4'-disulfonic acid (PPADS) and suramin, reduced the likelihood of these events occurring. These results suggest that release of ATP from the inner supporting cells of the KO is an important activator of the spontaneous electrical activity recorded in the IHCs. However, more recent work has found that the story is likely to be more complex with low concentrations of extracellular ATP inhibiting the generation of action potentials (Johnson et al., 2011). This is thought to be due to an interaction with the SK2 channels, nanomolar extracellular ATP concentrations are thought to cause a small sustained influx of Ca^{2+} into the IHC activating the SK2 channels hyperpolarizing the cell and reducing the frequency of spontaneous action potentials. Block of the purinergic receptors through either application of PPADS or 2',3'-O-(2,4,6-trinitrophenyl)adenosine-5'-triphosphate (TNP-ATP), a P2X receptor blocker resulted in depolarisation of the membrane potential and an increase in the frequency of action potential generation. This is likely to be due to removal of the hyperpolarisation by activation of the SK2 channels. When this has been

replicated with mouse models lacking the SK2 channel the blocking of the purinergic receptors has no effect on the membrane potential again suggesting that this hyperpolarisation is being carried through activation of the SK2 channels. In vivo it is probable that these low ATP concentrations are found around the IHCs. Due to the low nanomolar sensitivity of the purinergic receptors it is likely that this hyperpolarising effect is being mediated by the P2X₃ receptor. It is interesting to note that there is an apical to basal gradient in the expression of the P2X₃ receptor with it being higher in the apical regions than in the basal. This may account in part for the bursting activity seen in the apical IHCs, with a more hyperpolarised resting membrane potential (-58 mV in apical IHCs compared to -55 mV in basal) the IHCs are much less likely to randomly fire action potentials and so would require a trigger to depolarise the membrane to fire a train of spikes, although this idea is still being debated. Small current injections causing a small depolarisation in the apical IHCs causes the cells to fire in a manner similar to that seen in the basal IHCs, suggesting that it is this small difference in resting membrane potential that causes the difference in spiking activity. Larger ATP concentrations cause a larger inward current depolarizing the cell triggering action potential formation (Johnson et al., 2011).

The production of these action potentials persists until the end of the first postnatal week, when the cells become quiescent. Interestingly though the IHCs can be triggered to produce action potentials in the second postnatal week, suggesting that the cells are able to produce action potentials but their resting membrane potentials sit too negative and so the threshold for action potential generation is not reached. It has recently been suggested that *in vivo* IHCs are able to produce spontaneous action potentials at this time (Johnson et al., 2012). From the second postnatal week the apical surface of the hair cells is surrounded by an endolymph extracellular solution with a reduced calcium concentration compared to the typical perilymph extracellular solution. Calcium is a known permeant blocker of the MET channel and so reducing the calcium concentration from 3 mM to 0.3 mM closer to that found in endolymph removed this block and caused the resting membrane potential to be more depolarised. This was sufficient to allow the IHCs to generate action potentials spontaneously (Johnson et al., 2012). A summary of the currents expressed in neonatal IHCs is shown in (

Figure 1-3).

This electrical activity is thought to be important for the modelling of synaptic connections between the IHCs and the spiral ganglion neurons (SGNs), and further downstream in the auditory nerve and within the brain. It has been shown in neonatal IHCs that one action

potential is sufficient to drive exocytosis and release of the neurotransmitter glutamate onto its post-synaptic targets on the SGNs (Johnson et al., 2005). The inward calcium current required for the upstroke of the action potential is also required to drive the fusion of vesicles with the pre-synaptic membrane. Neonatal IHCs show spherical bodies in the pre-synaptic structure. At P6 it is estimated that 1 action potential causes the fusion of around 310 vesicles (Johnson et al., 2005). Each fusion event requires 4 calcium binding events to occur; this is probably mediated by synaptotagmin. The large I_{Ca} and comparatively low calcium efficiency seen in the neonatal IHCs is likely to be important for refinement of the downstream synaptic connections ensuring that vesicle fusion and glutamate release only occurs during periods of IHC activity. After the onset of hearing I_{Ca} is reduced to 30% of its maximal size in the mature IHCs, but the rate of exocytosis measured as an increase in membrane capacitance remains the same for the same level of depolarisation (Johnson et al., 2005). This suggests that the calcium efficiency is increased throughout development and fewer calcium binding events are required for the fusion of vesicles with the pre-synaptic membrane. In fact the relationship between calcium binding and vesicle fusion is almost linear with only 1 calcium ion required for the fusion of 1 vesicle (Johnson et al., 2005). This low calcium dependence in the mature IHCs promotes spontaneous fusion events, but the near-linear calcium requirements allow broadening of the dynamic range of the cell so that the cell can respond as efficiently to small and large stimuli (Johnson et al., 2005). The reduction in I_{Ca} is probably due to a reduction in the $Ca_v1.3$ channels rather than a change in expression of channel subtypes as there is no difference in the kinetics of the current just a reduction in the size (Johnson et al., 2005). There is also a structural difference in the pre-synaptic machinery in the mature IHCs with flat plate-like ribbon structures, a multi-protein structure that tethers vesicles at the pre-synaptic membrane developing after the onset of hearing. This structure ensures there is a large readily releasable pool of vesicles for fusion events to occur (Meyer et al., 2009). This structure holds more vesicles close to the pre-synaptic membrane allowing for more efficient transmitter release via the vesicle fusion events. Each IHC is synaptically connected to several SGNs whilst each SGN is only coupled to one IHC. Although the size of each synaptic ribbon does not vary the density of afferent innervation of the IHCs varies along the length of the cochlea with the most sensitive region having the highest number of synapses (around 17 synapses per IHC at the 20 kHz region). This density declines laterally towards the basal and apical extremes (Meyer et al., 2009).

Besides the reduction in I_{Ca} , mature IHCs (after the onset of hearing - P14 and above) have a very different expression in their currents compared to the neonatal IHCs. Both I_{Na} and the

potassium currents, I_{K1} and I_{SK} , are completely down regulated and not expressed at all (Marcotti and Kros, 1999; Marcotti et al., 2003a, 2003b, 2004a). The delayed rectifier potassium current $I_{K,neo}$ develops into the $I_{K,s}$ current and although there is no clear point of change between the two. The mature $I_{K,s}$ current is much more sensitive to block by 4-aminopyridine (4-AP) than the current seen in the neonatal IHCs. The $I_{K,s}$ and $I_{K,neo}$ currents are thought to be carried by two different currents: one sensitive to 4-AP and one that is insensitive to 4-AP. The neonatal current is carried mostly by the 4-AP insensitive current (Marcotti et al., 2003a). $I_{K,s}$ also differs from $I_{K,neo}$ in that it is activated at more hyperpolarised potentials and shows less inactivation to depolarisation of the membrane potential (Kros and Crawford, 1990; Kros et al., 1998). The $I_{K,s}$ current is activated at potentials positive to -65 mV and fully activates within 10 ms of depolarisation (Kros and Crawford, 1990). Mature IHCs see a 2 fold increase in the cell size measured through the whole cell capacitance (Kros et al., 1998). Mature IHCs also have a more hyperpolarised resting membrane potential (Marcotti et al., 2003a) due to the presence of the $I_{K,n}$ current.

The inward rectifier current $I_{K,1}$ rapidly declines in size after the onset of hearing and is replaced with the $I_{K,n}$ current (Marcotti et al., 2003a). The $I_{K,n}$ current is carried by the KCNQ4 channel and is activated at extremely hyperpolarised potentials meaning that at rest it is around 65% activated and plays a disproportionately large contribution to the resting membrane potential compared to the other currents that are present. The $I_{K,n}$ current is linopirdine sensitive and appears to be similar to the main current expressed in the mature OHCs (Kros, 2007; Marcotti et al., 2003a).

Mature IHCs also express the fast activating K^+ current $I_{K,f}$ carried through the BK channel (Kros et al., 1998; Marcotti et al., 2003a). The $I_{K,f}$ current is fully activated within 0.35 ms (Kros and Crawford, 1990) and does not inactivate upon depolarisation. The $I_{K,f}$ current is activated at potentials depolarised to -65 mV and does not saturate at membrane potentials of +25 mV, and continues to increase in size at potentials more positive to this. This current is much larger than those seen in neonatal IHCs reaching a size up to 16 nA at a membrane potential of 0 mV (Kros and Crawford, 1990). This fast activating current inhibits the production of action potentials in the mature IHCs, acting to repolarise the membrane potential much before the calcium current would be large enough to depolarise the membrane for action potential generation, this current allows the IHCs to respond to depolarisation with graded receptor potentials (Kros et al., 1998). This $I_{K,f}$ current is sensitive to block by iberiotoxin (IbTx) and TEA and insensitive to block by 4-AP. The current is also independent of extracellular calcium concentrations but does appear to be dependent on the voltage sensitive calcium stores in

addition to its intrinsic voltage dependant properties (Kros and Crawford, 1990; Marcotti et al., 2004b). The effects of intracellular calcium concentrations on $I_{K,f}$ have been investigated by the addition of BAPTA or caffeine and thapsigargin. BAPTA is a fast calcium buffer and in conjunction with each other, caffeine and thapsigargin work to empty intracellular Ca^{2+} stores. Application of these drugs results in a reduction in the size of the initial and steady state currents (Marcotti et al., 2004b). The channels carrying this current are likely to be localised with the L-type calcium channels, $Ca_v1.3$, as block of these channels by nifedipine reduced the total size of the $I_{K,f}$ current (Marcotti et al., 2004b). The features of this current are unusual for a potassium current carried through the BK channel, however a small typical BK current is also expressed in the mature IHCs and is called $I_{K(Ca)}$ this current is much smaller in size than the $I_{K,f}$ current, is less sensitive to IbTx block and is sensitive to changes in extracellular Ca^{2+} concentration (Marcotti et al., 2004b). The function of this current is as of yet unknown. Figure 1-4 shows a summary of the ionic currents in the mature IHC.

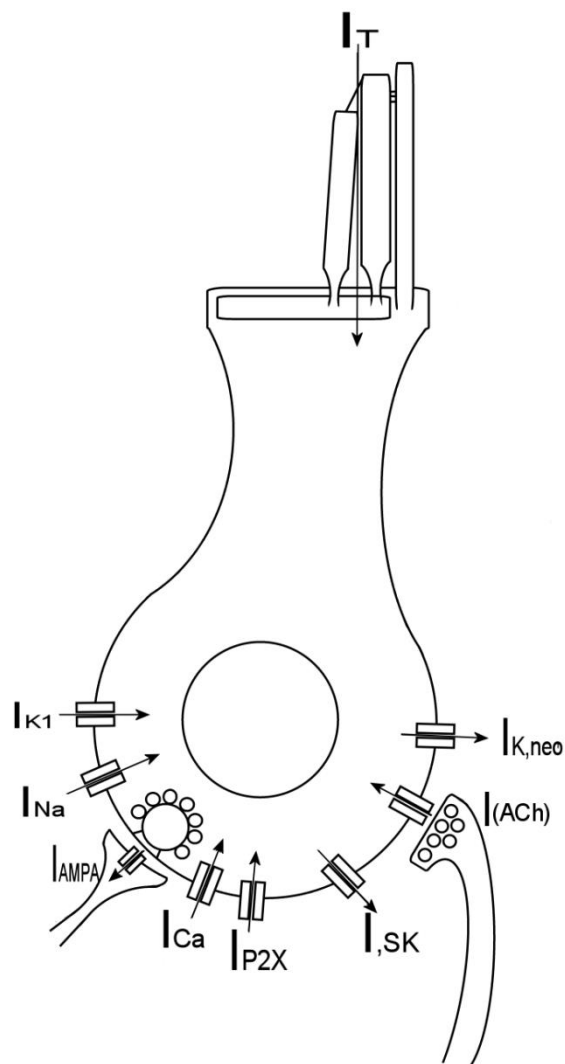


Figure 1-3 Ionic currents in the neonatal IHC

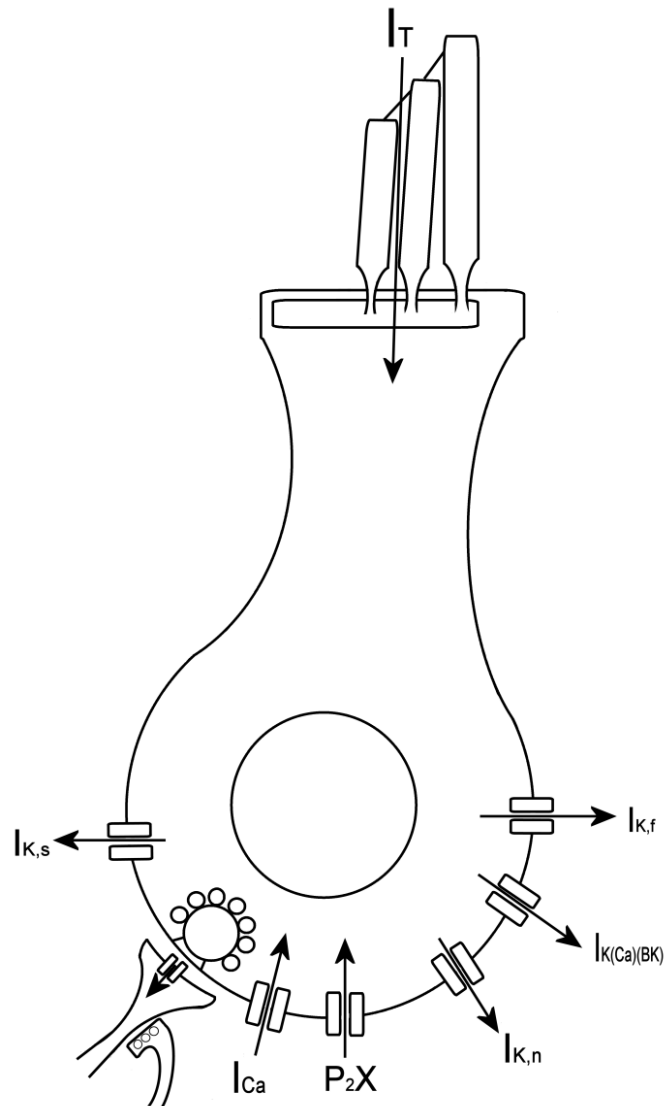


Figure 1-4 Ionic currents in the mature IHC

1.3 Development of the outer hair cells

Outer hair cells (OHCs) are found in three rows sitting parallel to the singular row of IHCs and function to amplify the incoming sound signal for detection by the IHCs (Dallos and Harris, 1978; Müller and Gillespie, 2008; Ryan and Dallos, 1975). OHCs can first be identified at E15 by the presence of the hair bundle (Anniko, 1983).

Neonatal OHCs express a similar complex of currents to those seen in the neonatal IHCs but overall the individual current sizes are all much smaller. In response to depolarising steps in the membrane potential a slowly activating outward current can be seen, the delayed rectifier

current $I_{K,neo}$ (Helyer et al., 2005; Marcotti and Kros, 1999). There is also a voltage gated calcium current, again like the IHCs this current is carried through L-type Ca^{2+} channels (Michna et al., 2003), and a sodium current (Oliver et al., 1997). Although expressing a similar complement of currents to IHCs, OHCs are unable to fire spontaneous action potentials, likely to be due to the smaller I_{Ca} and I_{Na} . In response to current injections OHCs show a single spike followed by oscillations in the membrane potential (Marcotti and Kros, 1999). In rat OHCs held at a resting potential of -100 mV action potentials could also be evoked (Oliver et al., 1997), thought to be due to relief of the inhibition on the sodium channels, which are thought to be almost completely inhibited at a holding potential close to -70 mV. It may be the case that *in vitro* conditions are unfavourable for the generation of this activity in neonatal OHCs in much the same way as second postnatal week IHCs (Johnson et al., 2012) and that *in vivo* the OHCs are electrically active during this time.

The $I_{K,neo}$ current in the neonatal OHCs develops into the I_K current in the mature cells. This current is a delayed rectifier current and in response to depolarising steps in the membrane potential reached a steady state current within 20 ms of step onset and did not decay (Mammano and Ashmore, 1996). The I_K current is sensitive to block by 4-AP.

At around P6 in the rat OHCs begin to respond to application of ACh, this is at the same time that efferent innervation is first established with these cells (Dulon and Lenoir, 1996; Lenoir et al., 1980). It is believed that the current activated by application of ACh is carried through $\alpha 9\alpha 10$ subunits similar to that seen in neonatal IHCs (Elgoyhen et al., 2001; Lustig et al., 2001; Sgard et al., 2002). The inward calcium current carried by the $\alpha 9\alpha 10$ channel is difficult to see as it is dwarfed by a much larger outward K^+ current carried through the SK channels which is activated by the inward flux of Ca^{2+} ions (Blanchet et al., 1996; Dulon et al., 1998; Evans, 1996; Nenov et al., 1997). A summary of the ionic currents expressed in neonatal OHCs can be seen in Figure 1-5.

At P8 the current complex in the OHCs becomes dominated by the appearance of the $I_{K,n}$ current (Housley and Ashmore, 1992; Mammano and Ashmore, 1996; Marcotti and Kros, 1999). The channel carrying $I_{K,n}$ has been identified as the KCNQ4 subtype of the m current family (Brown and Adams, 1980; Kubisch et al., 1999; Selyanko et al., 2000) and is known to be sensitive to block by linopirdine. At the resting membrane potential of the OHCs this current is 50% active. Its hyperpolarized activation range brings the resting membrane potential close to the K^+ equilibrium potential, at least *in vitro* to around -75 mV (Marcotti and Kros, 1999). Block of the channel by application of linopirdine results in a 20 mV depolarizing shift in the resting

membrane potential of the OHCs (Marcotti and Kros, 1999). In response to hyperpolarizing voltage steps the current shows an instantaneous inward peak current followed by a decay with a time constant between 10-30 ms known to be caused by deactivation rather than inactivation (Housley and Ashmore, 1992; Mammano and Ashmore, 1996; Nenov et al., 1997). $I_{K,n}$ current is necessary for OHC survival as it provides an efficient route for K^+ exit after entry through the MET channel (Oliver et al., 2003). Mutations in KCNQ4 result in a depolarisation of the resting membrane potential and leads to progressive hearing loss through degeneration of the OHCs (Kharkovets et al., 2006; Kubisch et al., 1999).

Temporary tinnitus and hearing threshold elevation of between 20 and 40 dB is seen with patients who are prescribed the anti-inflammatory drug salicylate. Although previous work has shown that salicylate concentrations up to 10 mM can block the electromotile activity in mature OHCs (Kakehata and Santos-Sacchi, 1996) more recent work has also suggested that lower more clinically relevant concentrations of between 0.1 and 1 mM salicylate also block the $I_{K,n}$ current (Wu et al., 2010). It is believed that salicylate blocks $I_{K,n}$ by two methods: the first is a direct blockage of the channel pore, the second is due to the acidification of the OHC cytoplasm causing an increase in the intracellular calcium concentration. The increased calcium is known to decrease the $I_{K,n}$ current through the activity of calmodulin or an as of yet unidentified pathway (Chambard and Ashmore, 2005; Gamper and Shapiro, 2003; Xu et al., 2007). The KCNQ4 channel is also known to be regulated by the activity of the cAMP/protein kinase A (PKA) pathway. Phosphorylation of the channel causes an increase in channel activity whilst dephosphorylation by protein phosphatases down regulates the channels activity resulting in a shift in the V_{half} (Chambard and Ashmore, 2005; Jagger and Ashmore, 1999).

Mature OHCs show faster and smaller voltage responses than immature OHCs, with large inward current injections causing a large transient peak followed by a steady state level of depolarization. The mature voltage response can be returned to a neonatal like response by the application of linopirdine, with a single spike followed by membrane potential oscillations being observed, suggesting that it is activity of the $I_{K,n}$ current that is dampening the electrical activity of the mature OHCs. The membrane potential oscillations observed under these conditions in mature OHCs are reduced in size compared to the neonatal OHCs, likely due to the down regulation of the calcium current (Marcotti and Kros, 1999; Michna et al., 2003). Mature OHCs also lack I_{Na} , which declines rapidly after the onset of hearing (Oliver et al., 1997). Figure 1-6 shows a summary of the compliment of ionic currents expressed in mature OHCs.

The most distinguishing feature of a mature OHC is its electromotility, first identified in 1985 (Brownell et al., 1985). It can be described as a change in the length of the cell body of the OHC: In response to depolarising membrane potentials the cell body shortens, and hyperpolarising membrane potentials result in an elongation of the cell body (Frank et al., 1999). The molecular basis underlying this activity has been identified as prestin (Zheng et al., 2000). Prestin is a member of the SLC26A family of membrane antiporters that transport anions across the plasma membrane (Muallem and Ashmore, 2006), although prestin itself appears to be a modified antiporter and seems unable to undergo a full transport cycle failing to unload the anion at the extracellular face of the protein (Schaechinger and Oliver, 2007). It has been shown that the electromotility of the mature OHC is able to follow changes in the membrane potential with contractions and elongations in the cell length up to a frequency of 100 kHz, with this value currently being limited by experimental conditions rather than by the OHC itself (Frank et al., 1999). The function of this electromotile behaviour is believed to be amplification of the incoming mechanical stimulus so that it can be detected by the IHCs. This amplification is thought to arise by enhancing the vibration of the basilar membrane (Müller and Gillespie, 2008). Ablation of the OHCs through chemical disruption has shown an increase in the hearing threshold of up to 50 dB (Ryan and Dallos, 1975), agreeing with more recent work on prestin knockout mouse models showing an increase of between 40 and 60 dB in the hearing threshold compared to wild type mice (Liberman et al., 2002). OHCs from prestin^{-/-} OHCs do not show electromotility, and this activity is reduced by half in prestin^{+/-} OHCs. Although this model suggests that prestin is responsible for amplification in the mammalian organ of Corti, shortening of the overall OHC cell body length, due to prestin being reduced or absent, may alter some of the cochlear mechanics and so a mouse knock-in model was developed in which prestin was still expressed in the cell membrane but was rendered non-functional. Investigation with these mice matched findings with prestin knock-out mouse models with an increase in the hearing thresholds (Dallos, 2008). Interestingly immunolabelling of prestin in neonatal OHCs shows that the protein is present in the cell membrane from as early as P0 despite electromotility not being recorded until P8 (Belyantseva et al., 2000; Marcotti and Kros, 1999). Electromotile behaviour is likely to not be functional in the first postnatal week due to low levels of the protein in the plasma membrane. In order to coordinate contraction of the entire cell body high levels of prestin expression would be required so that the activity of individual prestin molecules could be coupled together and have an effect (Goodyear et al., 2006). As well as observing the electromotile behaviour, its presence can be detected by the presence of a fast transient current upon voltage steps that cannot be compensated consistently for steps of different size and polarity (Mammano and

Ashmore, 1996). This transient is identified as the voltage sensitive component of the cell capacitance termed the non-linear capacitance and is associated with changes in the OHC length (Mammano et al., 1995; Santos-Sacchi, 1991).

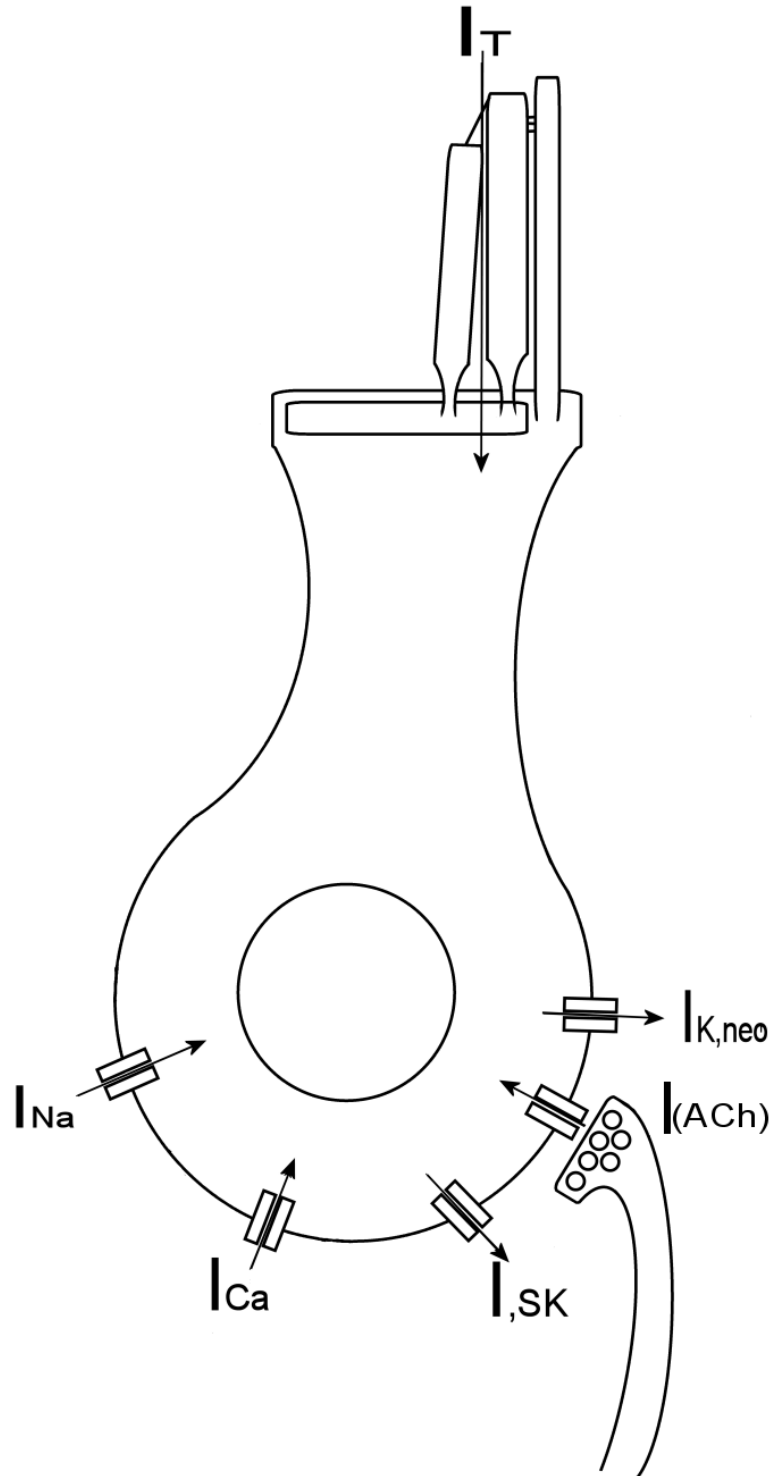


Figure 1-5 Ionic currents in the neonatal OHC

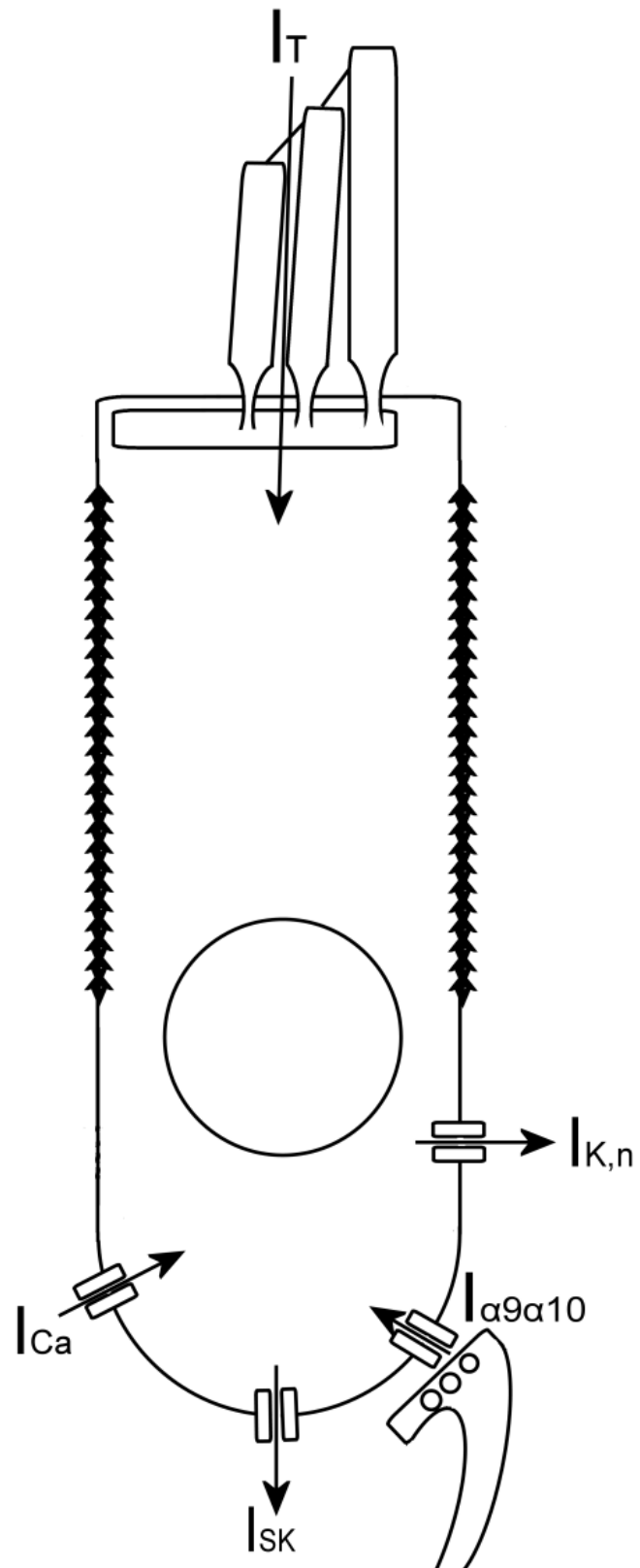


Figure 1-6 Ionic currents in the mature OHC. The jagged line in the apical pole of the mature OHC represents the presence of prestin in the cellular membrane.

1.4 The hair bundle

The transduction current (I_T) is a non-specific cation current carried through the as of yet unidentified mechano-electrical transducer (MET) channel. Although it is thought that TMC1 and TMC2 channels are strong candidates (Kawashima et al., 2011). The MET channel is mechanically gated with movements of the hair bundle directly opening and closing the channel. The location and function of the MET channel is discussed later.

The hair bundle is composed of finger-like stereocilia, projections that protrude from the apical surface of the hair cell. These stereocilia are arranged in a V shape and when deflected modulate the probability of the mechano-electrical transducer (MET) channels being open. The stereocilia contain an actin-based cytoskeleton, in which the actin filaments are uniformly polarised with the fast growing ends being at the tip of the stereocilia. A mature stereocilium contains around 2000 actin filaments (Revenu et al., 2004; Schneider et al., 2002). The hair bundle can first be detected at E15 in the basal regions of the cochlea and are composed of 30-300 stereocilia (Anniko, 1983; El-Amraoui and Petit, 2005). The stereocilia emerge from the apical membrane as a homogenous group of equally sized microvilli clustered around a single kinocillium. The kinocillium then migrates to the peripheral edge of the apical surface of the hair cell and this dictates the polarity of the hair bundle. The stereocilia closest to the kinocillium then begin to elongate and widen, with this process then continuing in the next row to form a staircase pattern within the rows of stereocilia. Each hair bundle consists of 3-5 rows of stereocilia. Some actin filaments then extend down into the apical region of the hair cell into an actin based horizontal network called the cuticular plate, where the stereocilia are stabilised. The region of the stereocilia that connects to the cuticular plate is called the rootlet and is thinner than the rest of the stereocilia. This tapering is important for the pivoting of the hair bundle. After the formation of the rootlets the stereocilia then continue to elongate to reach mature levels. At this stage any stereocilia that are not fully incorporated in to the hair bundle regress. The kinocillium also disappears in the mature hairs cells of the mammalian auditory system (El-Amraoui and Petit, 2005; Tilney et al., 1992).

The structure of the hair bundle is stabilised through several different connections between individual stereocilia. At the earliest stages of development the stereocilia are connected by transient lateral links that diminish during the early postnatal period, coincidental with the appearance of ankle links at the base of the stereocilia. Mature stereocilia lose the ankle links and gain horizontal top connectors (Kremer et al., 2006). These links connect the stereocilia

perpendicular to the direction of activation (towards the tallest stereocilia). The tip links however run parallel to this direction and connect the tip of one stereocilium to the shaft of the neighbouring taller stereocilium (Pickles et al., 1984). The kinocillium of immature hair bundles is connected to the tallest stereocilia through the kinocillial link (Michel et al., 2005).

The MET channel is thought to be mechanosensitive, meaning that it is directly gated by a mechanical energy rather than, for example, a second messenger system. This is because the opening of the channel occurs very quickly, within microseconds of stimulation (Corey and Hudspeth, 1979). The MET channel is now known to be located at the top of the shorter stereocilia at the base of the tip link (Beurg et al., 2009). It is believed there is a gating spring present between adjacent stereocilia that becomes stretched upon deflection of the hair bundle and that this pulls the MET channel open. The tip link is believed to be the gating spring of the MET channel, it is now known that the tip link is composed of two homodimers, one formed of protocadherin 15 (Pcdh) connecting to the top of the lower stereocilium, forming the bottom of the tip link and the other formed of cadherin 23 (Cdh) connecting to the shaft of the taller stereocilium, forming the top of the tip link (Ahmed et al., 2006; Kazmierczak et al., 2007; Siemens et al., 2004). The stability of the tip link appears to be highly calcium dependent, with application of zero calcium solution or the fast calcium buffer BAPTA breaking these links (Assad et al., 1991; Goodyear and Richardson, 1999, 2003; Kachar et al., 2000; Kazmierczak et al., 2007; Rzadzinska et al., 2004; Sellick et al., 2007). It was originally thought that it was the stretching of the tip link that directly gated the MET channel, however understanding the molecular basis has changed this idea as the elasticity of CDH23 is very limited and the tip links themselves are now known to be stiff filaments that buckle under strain (Kachar et al., 2000; Sotomayor and Schulten, 2008).

Due to this discrepancy there are now two models to explain the gating of the MET channel (Gillespie and Müller, 2009), the first is called the tethered channel model and states that the MET channel is attached both to the tip link and the cytoskeleton either directly or through a tethering protein. The channel is tightly tethered to Pcdh and deflection of the bundle pulls the tip link and so the MET channel, which would pull the tether that opens the MET channel. In this model it is the tether to the cytoskeleton that is the gating spring. The second model is called the lateral tension model and says that upon deflection of the hair bundle Pcdh pulls on the stereociliary membrane increasing the tension and it is this which directly opens the MET channel (Gillespie and Müller, 2009). The tension of the tip link is very important in maintaining the open probability of the MET channel at rest; Cdh inserts into the membrane of the shaft of the taller stereocilium and is able to form a ternary complex with the scaffold

protein harmonin b (Hrm) and myosin VIIa (Myo7a). Both Hrm and Myo7a are also able to directly bind to the actin cytoskeleton (Bahloul et al., 2010; Berg et al., 2001; Boëda et al., 2002; Hasson et al., 1997; Küssel-Andermann et al., 2000; Müller, 2008; Senften et al., 2006). When in the complex Myo7a is able to climb up the actin filaments to create the desired tension in the tip link and when in the correct position this is thought to be stabilised by Hrm shown by Myo7a not concentrating at the stereocilia tips in mice lacking Hrm (Boëda et al., 2002; Lefèvre et al., 2008).

This complex is also important in the slow adaptation of the MET current. Adaptation is a reduction in the size of the MET current in response to sustained deflection of the hair bundle. Fast adaptation occurs through the binding of calcium ions (entering the stereocilia via activation of the MET channel) to the MET channel itself or binding to a calcium release element altering the relationship between the MET channel and the gating spring, thus reducing its open probability (Stepanyan and Frolenkov, 2009). Slow adaptation is also thought to be calcium dependent but happens through a variety of proteins. Calcium entering the stereocilia diffuses across the tip of the stereocilium to the top of the tip link connected to the next shorter stereocilium (Ricci and Fettiplace, 1998; Wu et al., 1999). This then affects the interaction between myosin 1c (myo1c) and CDH23, which is important in maintaining tip link tension (Siemens et al., 2004). The interaction between myo1c and Cdh is dependent on calmodulin so that upon binding calcium the interaction between the two is disrupted and the complex at the top of the tip link is able to slip, thereby decreasing the tension in the tip link (Kros et al., 2001; Michalski et al., 2009; Phillips et al., 2006; Siemens et al., 2004). Adaptation is associated with bundle movement in the direction of stimulation, this is believed to be due to relaxation of the gating spring allowing for continued movement of the stereocilia (Kennedy et al., 2003).

Mutations in Myo7a show that despite the hair bundle being unable to transduce with physiological stimulation, deflections of the bundle large enough (e.g. 150 nm) to open the MET channel have an increased rate of adaption, this is likely to be due to increased slipping of the complex at the tip of the tip link (Kros et al., 2001). Mutations in Hrm also show altered rates of adaptation, likely to be due to reduced stability of the ternary complex at the top of the tip link (Michalski et al., 2009). The developmental appearance of Hrm at the upper end of the tip link is correlated with increased rate of adaptation, increased open probability of the MET channel at rest and increased sensitivity of transduction, implying that Hrm is important in the function of the tip link and gating of the MET channel (Lefèvre et al., 2008; Lelli et al., 2009; Waguespack et al., 2007). The open probability of the MET channel at rest is also

decreased in mouse models lacking the function of either Myo7a, Hrm or Pcdh (Kros et al., 2001; Michalski et al., 2009; Senften et al., 2006), this is likely to be due to these proteins being needed to maintain the required tension in the tip link and so the tip link is slacker than usual thus decreasing the chances of the MET channel being open (Grillet et al., 2009; Kros et al., 2001; Michalski et al., 2009). The importance of the MET channel having an open probability of ~5% at rest becomes apparent when considering negative deflections of the hair bundle, i.e. away from the tallest stereocilia. This decreases the tension of the tip link and results in a decrease in the open probability of the MET channel, this reduces the current flowing through the channel and as such causes a hyperpolarisation of the hair cell (Gillespie and Cyr, 2004; Howard and Hudspeth, 1987).

Along with maintaining tip link tension and being important in tip link function and gating of the MET channel, many of the proteins that have been described here are also important in the development of the stereocilia and hair bundle. Myo7a is an unconventional myosin motor that moves towards the plus end of actin filaments, up the stereocilia, using energy from ATP hydrolysis. It has functions in carrying cargo and as such the relocation of proteins within the hair cell and bundle (Inoue and Ikebe, 2003; Müller, 2008). Myo7a shows localization across the entire hair cell, with labelling showing its presence in the cell body, along with the stereocilia and kinocilium and particularly high expression in the cuticular plate and the pericuticular necklace – a vesicle dense region surrounding the cuticular plate (el-Amraoui et al., 1996; Grati and Kachar, 2011; Hasson et al., 1995; Howard and Hudspeth, 1987; Weil et al., 1996). Mutations in Myo7a result in improper Hrm localization with the latter remaining at the base of the stereocilia (Boëda et al., 2002). The hair bundles of the immature hair cells in homozygous myosin7a mutant mice have a misplaced kinocilium, and the bundles themselves have an irregular shape with the disorganization increasing after birth (Self et al., 1998). Myo7a is thought to be involved in stabilising the stability of the stereociliary rootlet – cuticular plate connection. Myo7a is known to interact with vezatin, a component of the ankle links and is thought to stabilise this link. This motor protein is also thought to be important in stabilizing the cuticular plate and so strengthening the stereocilia (Küssel-Andermann et al., 2000; Tilney et al., 1992). Hrm, a scaffold protein, is thought to be important in stabilising the actin filament structure of the stereocilia, with increased expression leading to abnormally enlarged F-actin bundles being formed (Boëda et al., 2002). Again Hrm is found throughout the cell body and stereocilia (Verpy et al., 2000) Hrm is found to be co-localized with Myo7a in the cuticular plate and may be involved in its stabilization through its actin cross-linking behaviour (Boëda et al., 2002; Hasson et al., 1995). The localization of Myo7a has been shown to be

dependent on Hrm with mutations in Hrm resulting in the lack of myo7a expression at the tips of the stereocilia. Hrm malfunction causes disorganized hair bundles that become progressively worse throughout development.

Cdh is a cell to cell adhesion molecule (Bolz et al., 2001) and although forming part of the tip link it is also known to be present in the transient lateral links and the kinocilial link (Michel et al., 2005). In the stereocilia expression is found along the entire length during the early postnatal period with the localization progressively becoming more and more restricted to the tips of the stereocilia when fully mature (Lagziel et al., 2005; Michel et al., 2005; Di Palma et al., 2001). Cdh expression is also found within the cell body of the hair cell (Garner et al., 2000). Pcdh, like Cdh, is a cell to cell adhesion molecule that is also found in the transient lateral links and kinocilial links (Lelli et al., 2010). Pcdh is also known to be present within the cuticular plate and through its interactions with Myo7a and Hrm it may be important for the stabilization of the cuticular plate (Kikkawa et al., 2008; Reiners et al., 2005; Senften et al., 2006). Mutations in Pcdh result in disrupted hair bundle morphology with the polarity often being misdirected (Kikkawa et al., 2008).

Myosin 6 (Myo6) is an actin based transporter and an anchoring protein that moves towards the minus end of an actin filament, down the stereocilia (Wells et al., 1999). It is localized to the cuticular plate and pericuticular necklace (Hasson et al., 1997). Mutations in Myo6 cause disordered hair bundles, which in humans cause both recessive and dominant forms of hearing impairment. It has also been shown that defects in Myo6 expression can result in a lack of development of the IHCs, with mature IHCs displaying an immature compliment of K^+ currents with no $I_{K,f}$ and $I_{K,n}$ expression (Roux et al., 2009). These mature IHCs also show the generation of action potentials which suggests the presence of other immature currents such as I_{Na} and a larger I_{Ca} . The exocytotic activity of mature IHCs with lack of Myo6 function also appears to remain functionally immature with reduced ribbon synapses and those that are present remaining immature (Roux et al., 2009).

Mutations in the proteins described above have also been described in humans resulting in the deaf – blindness disease Usher syndrome. Usher syndrome is the most common cause of deaf – blindness in the human population accounting for more than 50% of cases. There are three forms of Usher syndrome, types I, II and III. Usher syndrome type I (USH1) is the most severe form with patients presenting with profound deafness, vestibular defects and pre-pubertal onset of retinitis pigmentosa (RP). RP is a form of blindness which first shows as night blindness, loss of peripheral vision and the accumulation of intra – retinal pigment deposits (EL-

Amraoui and Petit, 2005; Petit, 2001). USH1 has been linked to 7 genes, 5 of which have been identified: USH1b is linked to Myo7a, USH1c to Hrm, USH1d to Cdh, USH1f to Pcdh and USH1g to sans (Ahmed et al., 2001; Alagramam et al., 2001; Bolz et al., 2001; Bork et al., 2001; Verpy et al., 2000; Weil et al., 1995, 2003). Sans is a scaffold protein located in the kinocilium and cuticular plate of the hair bundle. It is known to interact with both Hrm and Myo7a and is thought to be important in the localization of the Usher proteins by regulating the trafficking of these proteins to the stereocilia. Mutations in sans results in mis-localization of Hrm similar to that seen with Myo7a mutations, with Hrm being found at the base of the stereocilia (Adato et al., 2005; Boëda et al., 2002). Mutations in any of these 5 proteins results in a condition that is clinically indistinguishable. As all of these proteins are known to interact with each other and all result in hair bundle deformities this suggests that the activity of this complex of proteins is required for the correct development of the hair bundle in auditory hair cells. Interestingly all of the Usher proteins described here also appear in the ribbon synapses of retinal cells (Reiners et al., 2005). All of the Usher proteins described here are known to have cellular expression at the ribbon synapse of the hair cells (Adato et al., 2005; Boëda et al., 2002; Gregory et al., 2011; Reiners et al., 2005; Senften et al., 2006; Siemens et al., 2002). Mouse models with mutations in any of the USH1 proteins exhibit deafness and vestibular defects shown as head tossing and circling behaviour, but interestingly no blindness. In this body of work I will be examining the effect of mutations in Myo7a, PCDH15 and Hrm on the development of the basolateral currents of the IHCs and OHCs.

1.5 Acid sensitive currents and ASIC channels

Proton sensitive currents were first discovered in 1981 in rat trigeminal ganglia cells, and were described as an inward Na^+ current (Krishtal and Pidoplichko, 1981). It wasn't until 1992 that an acid sensitive ion channel (ASIC) was cloned from the rat brain and it was shown that the channel was directly gated by H^+ (Waldmann et al., 1997). To date seven different ASIC subtypes have been identified, being encoded by four different ASIC genes: 1a, 1b1, 1b2, 2a, 2b, 3 and 4 (Krishtal, 2003; Waldmann and Lazdunski, 1998). ASICs are distributed around the body with high expression found within the nervous system, subtypes 1a, 2a, 2b and 4 are found in the central nervous system (CNS) and are likely to be involved in sensing ischemia during times of damage such as epilepsy (Baron et al., 2002). Loss of ASIC function has been shown to increase the length of seizures, indicating that the change of pH within the brain

from 7.3-6.8 is an important communication signal in ceasing seizures (Ziemann et al., 2008). All subtypes with the exception of 4 are found in the peripheral nervous system (PNS) (Chu et al., 2011). Subtypes 2b and 4 do not appear to show any sensitivity to H^+ , but as all ASICs are defined by their sequence homology, they are members of this family of proteins, which themselves belong to the ENaC/DEG superfamily of proteins (Akopian et al., 2000; Gründer et al., 2000; Lingueglia et al., 1997). The function of these subtypes remains unclear but it is thought they may offer some modulation of activity and are involved in the formation of heteromeric channels (Lingueglia et al., 1997). ASICs are formed of several subunits, prior to 2007, it was believed that they were formed of tetramers similar to that seen with ENaC channels (Firsov et al., 1998), however when the crystal structure of chick ASIC1a was published this data suggested that ASICs are formed of trimers (Jasti et al., 2007). Multimeric ASICs are commonly found with ASIC1a/ASIC2a being the most common heteromeric channels found within the CNS (Askwith et al., 2004).

ASICs open in response to a rapid drop in the extracellular pH and are voltage independent. ASICs are highly sensitive to an increase in the extracellular H^+ concentration with ASIC1a channels beginning to open when the pH reduces to 6.9 from 7.5 (Babini et al., 2002; Waldmann et al., 1997). The inward peak current increases in size until pH 6 upon which the currents begin to saturate. ASIC currents also show strong desensitization in response to activation by H^+ , with ASIC1a desensitizing within 1-2 seconds of an H^+ application. This desensitization recovers quickly within a further few seconds (Babini et al., 2002; Bässler et al., 2001; Waldmann et al., 1997). ASIC1a and ASIC1b are known to have similar activation and desensitization kinetics (Bässler et al., 2001). ASIC3 is the most sensitive subtype opening with a drop in pH from 7.4 to 7 (Sutherland et al., 2001), this channel also desensitizes much faster than ASIC1a and ASIC1b likely because of the increased sensitivity of the ASIC3 subtype (Bässler et al., 2001). Previous work has shown that ASICs are 50% open at pH 7.5 (Immke and McCleskey, 2003). Given this high sensitivity shown by ASICs it is also conceivable that a population of ASICs could go undetected as they sit in a desensitized state with resting extracellular pH levels.

The ASIC is cation selective, but the current carried is predominantly sodium. The channel has a moderate selectivity for Na^+ over K^+ ions with $P_{Na}/P_K = 10$, meaning that at the cells' resting potential the current carried would be predominantly Na^+ (Bässler et al., 2001; Waldmann et al., 1997). The ASIC are also permeable to H^+ ions with $P_{Na}/P_H < 0.3$, but as the H^+ concentration is very low in the extracellular environment these ions make up only a small part of the ASIC current (Chen and Gründer, 2007; Chu et al., 2011). Homomeric ASIC1a is the only ASIC known

to have some permeability to Ca^{2+} ions with $P_{\text{Na}}/P_{\text{Ca}} = 15$ (Bässler et al., 2001; Sutherland et al., 2001; Yermolaieva et al., 2004), although due to low extracellular calcium concentrations this again contributes to the current minimally. Calcium also acts as a permeant blocker of the ASICs. It is thought that both Ca^{2+} and H^+ compete for the same binding site within the ASIC protein, with Ca^{2+} stabilizing the closed state of the ion channel. H^+ displaces Ca^{2+} from its binding site increasing the open probability of the channel (Gründer and Chen, 2010; Paukert et al., 2004; Waldmann et al., 1997).

Amiloride is a classic ASIC blocker and is known to inhibit all ASICs (Waldmann et al., 1997; Xiong et al., 2008). This drug is known to plug the ion channel pore inhibiting the flow of ions (Paukert et al., 2004), this drug however is not specific to ASIC channels and is able to block the activity of other members of the ENaC superfamily along with T-type calcium channels, the Na^+/H^+ exchanger (Xiong et al., 2008) and the MET channel (Jørgensen and Ohmori, 1988; Rüscher et al., 1994). Amiloride blocks ASIC subtypes 1a, 1b, and 2a with an $\text{IC}_{50} \sim 20 \mu\text{M}$ and for ASIC3 this value is slightly higher $\sim 60 \mu\text{M}$ (Basilana et al., 1997; Champigny et al., 1998; Chen et al., 1998; Lingueglia et al., 1997). Nafamostat is a serine protease which has recently been identified as a blocker of the ASIC channels. Nafamostat blocks ASIC 1a, 2a and 3 with IC_{50} values of 13.5 μM , 70.6 μM and 2.5 μM respectively (Ugawa et al., 2007).

Other modulators of ASICs are heavy metals including Zn^{2+} , Cu^+ , Pb^+ , Ni^+ , Cd^+ and Gd^+ which decrease the acid sensitive current (Babinski et al., 2000; Chu et al., 2004; Staruschenko et al., 2007; Wang et al., 2006, 2007). Aminoglycosides such as neomycin and gentamicin have also been shown to have modulatory effects on ASICs decreasing the inward peak current and slowing the rate of desensitization (Garza et al., 2010). Aminoglycosides are well known for their ability to block the MET channel (Kroese et al., 1989; Marcotti et al., 2005). It has also been shown that temperature has an effect on the current flowing through ASICs with cold temperatures (7°C) potentiating the ASIC current by slowing the rate of desensitization (Askwith et al., 2001). Although this function may seem redundant ASIC channels are highly involved in the perception of taste and so temperature regulation maybe important in the detection of chemical stimuli in the mouth. ASIC1a is specifically blocked by Psalmotoxin1 (PcTx1), this drug ($\text{IC}_{50} = 0.9 \text{ nM}$) acts as a gating modifier increasing the channels affinity for H^+ which then forces the channel into its desensitized state leaving it unable to respond to changes in the extracellular pH (Chen et al., 2005). Interestingly PcTx1 is also able to modulate the activity of ASIC1b, this time however the drug stabilizes the open state of the channel increasing the channels activity however a much higher concentration is required to see this

effect with more than 10 nM needed (Chen et al., 2006). As previously mentioned Ca^{2+} can modulate ASIC function, co-application of Ca^{2+} and H^+ results in a reduction in the ASIC current, pre-treatment of Ca^{2+} before Ca^{2+} and H^+ treatment results in a complete block of the ASIC current, whilst pre-treatment of Ca^{2+} and then H^+ alone results in an enhancement of the ASIC current (Immke and McCleskey, 2003; Paukert et al., 2004; Wang et al., 2006; de Weille and Bassilana, 2001). The enhancement described in the last experimental condition is likely to arise from the Ca^{2+} increasing the likelihood of the ASICs being in the closed state rather than the desensitized state at rest and so upon application of H^+ more ion channels are available to respond.

Recent work has identified ASIC channels within the hearing organ (Ugawa et al., 2006). ASIC1a has been shown to be present within the organ of Corti, but is found only within the supporting cells of the tissue (Ugawa et al., 2006). ASIC1b has been shown to be present in both the IHCs and OHCs and is located at the base of the hair bundles in these cells (Ugawa et al., 2006). Loss of function of ASIC1b results in an increase in the hearing threshold by around 20 dB compared to wild-type (Ugawa, personal communication). ASIC2 and 3 are also found within the hearing organ and are particularly expressed in the spiral ganglion neurons (Hildebrand et al., 2004; Peng et al., 2004). ASIC2 null mouse models are resistant to noise induced hearing threshold shifts important in protecting against damage caused by loud sounds; whilst ASIC3 null mouse models develop hearing loss during early development. The function of ASIC channels within the organ of Corti is unknown but it is known that cochlea hypoxia and ischemia are accompanied by tissue acidosis so they may be important in signalling tissue damage in times of stress (Mazurek et al., 2003).

Recent work (Petroff et al., 2008) has shown a physical interaction between the ASIC1a channel and the BK channel. The interaction between the ASIC1a channel and the BK channel inhibits the $I_{K,f}$ current and this inhibition is removed when the pH of the extracellular solution is dropped to pH 6 (Petroff et al., 2008). ASIC2a and 2b are also able to interact with BK channel and cause an inhibition of the $I_{K,f}$ (Petroff et al., 2008). ASIC1a and ASIC1b are splice variants and as such have a very similar structure and pattern of behaviour (Waldmann et al., 1997). Given that ASICs have a very similar structure it is conceivable that ASIC1b present within the hair cells is able to interact with BK channels and modulate the $I_{K,f}$ current. The interaction between the BK channel and ASIC1a channel also affects the proton activated current that is seen in response to H^+ (Petroff et al., 2008). When the BK channel is present the desensitization of the ASIC current is slower this would suggest that the mature IHCs are likely to respond with a larger ASIC current compared to mature OHCs.

In the hair cells there are other channels that also show some pH sensitivity. The first being the TRPV4 channel (Suzuki et al., 2003). These channels carry a mixed cation current and so at a resting membrane potential the current is likely to be inward. The current carried by these channels does however not desensitise or decrease in size with prolonged H^+ application (Suzuki et al., 2003). P2X receptors have also shown that they can be modulated by H^+ , with H^+ potentiating the current elicited when applied with ATP compared to ATP alone (Burgard et al., 1999). Acidic conditions alone were able to produce currents through the P2X receptors but these were small suggesting that the presence of ATP is necessary for full P2X receptor activation (Burgard et al., 1999).

1.6 Thesis aims

The aims of this thesis can be broadly divided into two main areas of research: The effect of Usher protein mutations on the development of the electrical properties of the hair cells and identifying the presence of an acid sensitive ion current in the hair cells, including the effects of lack of ASIC1b function on the electrical development of the hair cells. More specifically the aims of each chapter are:

Chapter 3: Investigate the effects of mutations in $Myo7a^{+/sh6j}$, $Myo7a^{sh6j/sh6j}$, $Ush1c^{+/-}$, $Ush1c^{-/-}$, $Pcdh^{+/AV3J}$, $Pcdh^{AV3J/AV3J}$ and $Pcdh^{+/AV6J}$, $Pcdh^{A63J/AV6J}$ mouse models on the electrical properties of neonatal, mature and adult IHCs, looking at the presence of the $I_{K,f}$, $I_{K,n}$ and $I_{K,s}$ currents along with the ability of these cells to produce action potentials.

Chapter 4: Investigate the effect of loss of myo7a function on the electrical development of OHCs, looking at the presence of $I_{K,n}$ and the ability of the mature OHC to be electromotile.

Chapter 5: Identify the presence of an acid sensitive ion current in neonatal and mature IHCs and OHCs and attempt to identify the ASIC subtype carrying this current using mouse models with loss of ASIC1b function.

Chapter 6: Investigate the effect of loss of ASIC1b function on the transduction currents in neonatal OHCs, basolateral currents in neonatal and mature IHCs and OHCs and on the electromotile activity in mature OHCs.

2 METHODS

2.1 Tissue Preparation.

IHCs and OHCs were studied in acutely dissected organ of Corti from both immature and mature preparations of Myo7a^{+/sh6j}, Myo7a^{sh6j/sh6j}, Ush1c^{+/-}, Ush1c^{-/-}, Pcdh^{+/AV3J}, Pcdh^{AV3J/AV3J}, Pcdh^{+/AV6J}, Pcdh^{A63J/AV6J}, ASIC1b^{+/+} and ASIC1b^{-/-} mouse models.

2.1.1 Mouse models

Myo7a^{sh6j/sh6j} mice carry a non-conservative missense, R241P mutation (Gibson et al., 1995) in a highly conserved region, close to the ATP-binding site in the N-terminal myosin motor domain. This leads to an 80% reduction in Myo7a expression as well as presumed dysfunction in the expressed protein (Hasson et al., 1997). The mutation is on a mixed 25% BALBc, 75% C57BL/6J background (Self et al., 1998).

Ush1c^{-/-} mice carry a 1 base pair deletion which results in a transcriptional frame shift, changing 38 amino acids before introducing a premature stop codon. The mutation is on a C57BL/6J background (Johnson et al., 2003).

The Pcdh^{AV3J/AV3J} mice are on a C57BL/6J background and carry a mutation rendering a presumed null allele of protocadherin 15 (Alagramam et al., 2001). The mutation carried by Pcdh^{AV6J/AV6J} mice, also on the C57BL/6J background causes a 47 amino acid deletion in the 9th extracellular cadherin domain, the result of which is less severe on protocadherin 15 function (Zheng et al., 2006).

All four of the above mouse models were maintained in closed colonies. Mice used for experimenting were taken from litters of heterozygous and homozygous mutant matings. The genotype of the offspring (either heterozygous or homozygous) was identified from the phenotype of the mouse which was visible from P2 onwards. Homozygous mutants displayed behavioural defects associated with vestibular malfunction such as circling and head tossing (Johnson et al., 2003, Gibson et al., 1995). At the cellular level, the hair bundle stereocilia of both inner and outer hair cells were highly disorganised (Johnson et al., 2003; Self et al., 1998). Heterozygotes had normal phenotypes at the behavioural and cellular level.

Limited availability of mice due to low reproduction rates of the more elderly mating pairs results for the low n numbers in the Ush1c^{-/-} data sets. Whilst recording from technically

difficult preparations of the adult $Pcdh^{+/AV6J}$ and $Pcdh^{AV6J/AV6J}$ and having limited numbers of mice caused the low n numbers for this set of experiments.

The $ASIC1b^{-/-}$ mice are on a C57BL/6 background and carry a partial knock out deletion of the $ASIC1b$ specific N-terminal region (Ugawa, personal communication). These mice were maintained in closed colonies. Mice used for experimenting came from litters of either $ASIC1b^{+/+}$ or $ASIC1b^{-/-}$ mutant matings. The genotype of the mouse has been assumed from the mating pairs of the parent mice, tail clippings, obtained post mortem from animals have been kept and genotyping although not completed can be investigated in the future if there are any queries. These homozygous mutants do not display any phenotypic defects, but are likely to have abnormalities in their pain perception (Ugawa, personal communication). At the cellular level, the hair bundle stereocilia of both inner and outer hair cells were normal.

Immature IHCs and OHCs were studied from mice aged between P1 and P6 (where P0 is the day of birth). Mature OHCs were studied from mice between P12 and P16, and mature IHCs were recorded from mice between P20 and P30. For some recordings IHCs have been recorded from adult mice between P254-549 (Average P377, n = 7 mice). All mice were killed by rapid cervical dislocation followed by decapitation. The cochlea were then removed and placed in a dissection chamber with standard extracellular solution (ECS), the constituents of which are described in Table 2-1.

The dissection method differs between neonatal and mature mice. Dissections were performed under a light microscope (Leica) using two pairs of grade 5 watchmaker's forceps.

2.1.2 Immature preparation

The cartilaginous casing of the cochlea was removed and the tissue unwound from the central modiolus bone. The tissue was then gently split in two by pulling on the stria vascularis to isolate the organ of Corti. The entire organ of Corti was cut in half to separate into basal and apical sections. The apical section was then transferred into a recording chamber and held under a nylon grid attached to a stainless steel ring, (**Figure 2-1**). This process can be seen in Figure 8-1.

2.1.3 Mature preparation

The bone casing of the apex of the cochlea is gently chipped away and then removed to reveal the organ of Corti. The edge casing is then removed, which also detaches the stria vascularis from the tissue. The apical region of the organ of Corti was then released by gently pushing the osseous spiral lamina down and lifting the tissue up. One full turn of the apical organ of Corti was then cut from the remaining tissue and transferred to a recording chamber and held under a nylon grid attached to a stainless steel ring (**Figure 2-1**). The process can be seen in Figure 8-2.

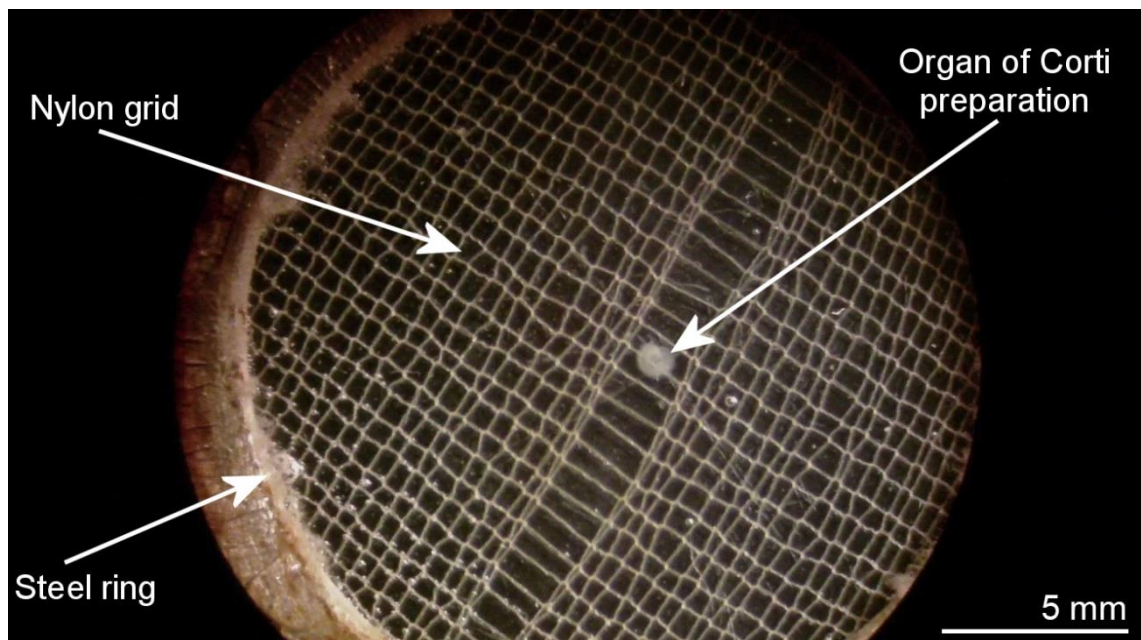


Figure 2-1 Neonatal (P4) Organ of Corti preparation held under a nylon grid

2.2 Experimental equipment

The equipment used to perform electrophysiology experiments is shown in Figure 2-2.

The cells on the acute preparation were viewed using an upright microscope (Olympus BX50, Tokyo, Japan) using Nomarski Differential Interference Contrast (DIC) optics (40 X water immersion objective plus 15 X eyepiece). The microscope was positioned inside a Faraday cage to reduce electrical noise and on an anti-vibration table (TMC) to avoid movements and

slipping of microelectrodes. The recording chamber was positioned on a rotating stage (Olympus, Tokyo, Japan) to allow access to all hair cells along the preparation. The chamber was continuously perfused with standard ECS using a peristaltic pump (Cole-Palmer, IL, USA) at a rate of 16 ml h^{-1} . To ensure complete isolation from the pump the stainless steel inlet of the recording chamber was connected in series to a $63 \mu\text{F}$ capacitor and the earth electrode.

In order to locally modulate the external conditions e.g. pH changes or application of drugs (linopirdine, nafamostat and amiloride) a large-tipped ($\sim 200 \mu\text{M}$) applicator was placed close to and above the preparation. This applicator was gravity driven and was connected to four 10 ml syringes which were controlled manually using tap-switches. This allowed rapid changes of up to 4 different solutions in the local environment of the cell recorded from.

Some experiments were performed around body temperature (37°C), this was maintained manually. A silicon coated probe was placed in the recording chamber close to the preparation to monitor the temperature. The rotating stage acts as the heating plate. The temperature was set to a couple of degrees below the desired temperature (35°C) to prevent overheating as the base of the recording chamber is warmer than the recorded temperature.

Patch electrodes were pulled from soda glass capillaries using an upright puller (Narishige, Tokyo, Japan) and had resistances between 1.8 and $3.3 \text{ M}\Omega$ when in standard ECS and filled with KCl intracellular solution. To reduce the fast electrode capacitive transients the shank of the electrode was coated in wax (coconut flavour, Mr. Zoggs SexWax, CA, USA). The patch electrode is held in place using an electrode holder which is connected to a Cairn Optopatch head-stage and optopatch. To prevent aliasing artefacts all signals were filtered through an 8-pole Bessel filter before data acquisition.

Cleaning pipettes were pulled from borosilicate glass capillaries using an upright puller and had an internal diameter $\sim 5 \mu\text{m}$. These were held by a pipette holder (Harvard Apparatus, Edenbridge, UK) and connected via thin plastic tubing to a 10 ml syringe. This was completely filled with standard ECS.

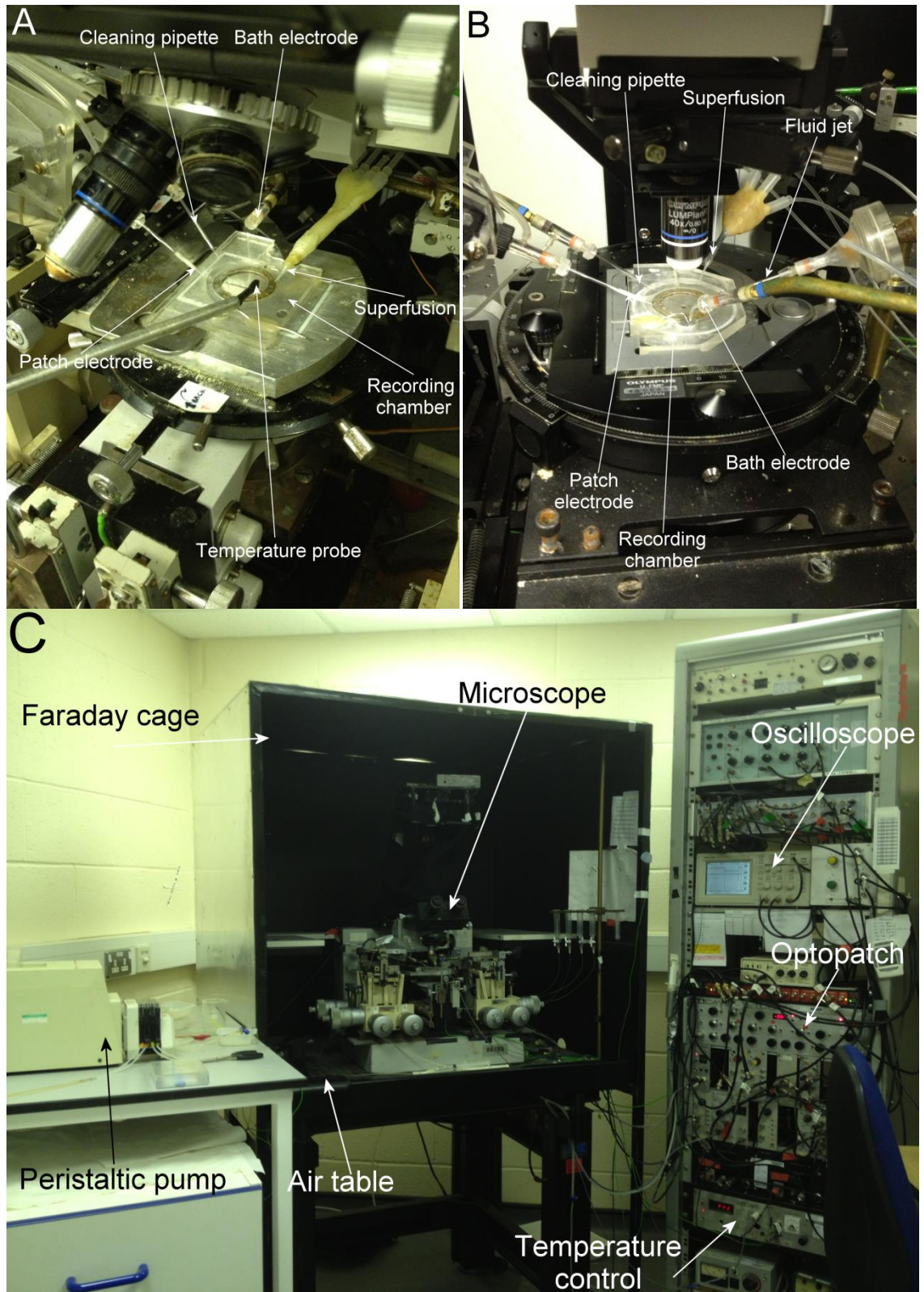


Figure 2-2 Equipment used to perform electrophysiological experiments. A. Close up of equipment used for most electrophysiology experiments. B. Close up of equipment used for mechano-electrical transduction experiments. C. All equipment used for most transduction experiments.

2.3 Experimental solutions

The extracellular solutions used to perform electrophysiology experiments are described in Table 2-1. The standard ECS also contained vitamins and amino acids for Eagle's Minimum Essential Medium, which were added from concentrates. The pH of the standard ECS, control ECS and control ECS pH 7.5 was adjusted to pH 7.48 using 1 M NaOH. The pH of control ECS pH 5.0 was adjusted to pH 5 using 1 M NaOH. The osmolarity was around 308 mOsm and measured using an osmometer (Advanced Instruments, MA, USA).

The intracellular solutions used are described in Table 2-2. The pH of K⁺ICS and CsCl ICS solutions was adjusted to pH 7.28 using 1 M KOH and 1 M CsOH respectively. The osmolarity was around 295 mOsm, measured using an osmometer.

Various drugs were used to modulate the electrical behaviour of the hair cells: nafamostat (100 μ M) (Tocris), amiloride (100 μ M) (RBI) and linopirdine (10 μ M) (sigma-Aldrich).

The sources of all chemicals and modulators are listed in the representative Table 2-1 for extracellular solutions and Table 2-2 for intracellular solutions.

Chemical	Conc. (mM)				Supplier
	Standard ECS	Control ECS	Control ECS pH7.5	Control ECS pH5	
NaCl	135	145	148	153	VWR
CaCl ₂	1.3	1.3	1.3	1.3	VWR
KCl	5.8	5.8	5.8	5.8	VWR
MgCl ₂	0.9	0.9	0.9	0.9	VWR
HEPES	10	10	10		Calbiochem
MES				10	Calbiochem
Glucose	5.6	5.6	5.6	5.6	VWR
NaH ₂ PO ₄	0.7	0.7			VWR
Napyruvate	2	2			Fisher

Table 2-1: Description of the components of extracellular solutions used in electrophysiology experiments.

Chemical	Conc. (mM)		Supplier
	K ⁺ ICS	CsCl ICS	
K ⁺ Cl	135		VWR
MgCl ₂	2.5	2.5	VWR
Na ₂ ATP	2.5	2.5	Roche
EGTA-KOH	1		VWR
HEPES	5	5	Calbiochem
Na ₂ phosphocreatine	10	10	Fluka
CsCl		137	Sigma-Aldrich
EGTA-CsOH		1	VWR, Sigma-Aldrich

Table 2-2: Description of the components of intracellular solutions used in electrophysiology experiments.

2.4 Whole cell recording

The recording of whole-cell current and voltage responses from inner and outer hair cells was achieved using the patch clamp technique (Hamill et al., 1981). Cells were chosen by their healthy appearance shown by a well formed bundle, smooth membrane, the absence of vacuoles and a clear nucleus. Supporting cells around the basal area of the hair cell were removed using the cleaning pipette. This exposed the membrane of the cell of interest and allowed a tight Gigaohm seal to be formed with the patch electrode. Once the seal had been formed the fast capacitive transients formed between the patch electrode and the bath were compensated for. Gentle suction was applied causing the patch of membrane within the electrode to rupture reaching the whole-cell configuration.

The cell membrane capacitance (C_m) and series resistance (R_s) were compensated for so that the capacitive transient was no longer visible and these values were documented for later reference about the cell size and quality of the seal. The zero current potential was also documented for further off-line analysis. Due to R_s there is an error between the clamped potential of the pipette and the membrane potential of the cell. R_s compensation was applied (between 50-80%) to reduce this error voltage in voltage clamp recordings (Ogden, 1994).

Voltage clamp recordings were performed at either room temperature (20-25°C) or closer to body temperature (33-35°C). All current clamp recordings were performed between 33-35°C.

2.5 Mechanoelectrical transduction

Hair bundles of OHCs were stimulated using a fluid jet. Figure 2-2B shows the equipment used to perform these experiments. The pipettes were pulled from borosilicate glass and their tips had an internal diameter of $\sim 10 \mu\text{m}$. The pipette was positioned close to the hair bundle. The sine wave stimulus was created using a single channel function generator (Tektronix, USA) with an output of 1.6 Vpp amplitude and 22 ms period. This signal was then amplified through a pre filter of 1 kHz (5 times) and the piezo driver (10 times) for a final amplitude of 80 Vpp.

2.6 DIC imaging

DIC images and movies were captured using Hamamatsu EM-CCD digital camera. The software used to acquire all images was Voxcell Scan version 4 (VisiTech, Sunderland). Camera settings were: 99 ms exposure, 200 direct EM gain and 1x1 binning. Movies to capture electromotility in mature OHCs had a sampling rate of 4 Hz. All images were captured at room temperature (18-21°C). Image acquisition was monitored by PClamp so that all frames of movies could be time stamped in reference to the voltage clamp protocol. For the electromotility movies the sampling frequency was 25 kHz and the step duration was 500 ms.

2.7 Data acquisition and analysis

Data acquisition and application of current and voltage commands were carried out using Signal version 4 (Cambridge Electronic Design) and PClamp version 10 (Axon Instruments). The sampling rates and filtering rates for the different protocols are shown in Table 2-3.

2.7.1 Current measurement

Steady state currents were measured as an average of the current magnitude between time 40 and 50 ms from the beginning of the command voltage step onset. Early or $I_{K,f}$ currents were measured as an average of the current magnitude between time 6 and 8 (average 7) ms after

the step onset of the command voltage. $I_{K,s}$ is measured as the difference between the steady state and $I_{K,f}$ currents. Peak currents are measured as the largest current elicited during the 50 ms command voltage step. For inward currents personal judgement was used to discard data if capacitive transients were larger than currents and peak current sizes were measured by hand in this instance (Figure 2-3). $I_{K,n}$ is measured as the difference between the steady state and peak currents.

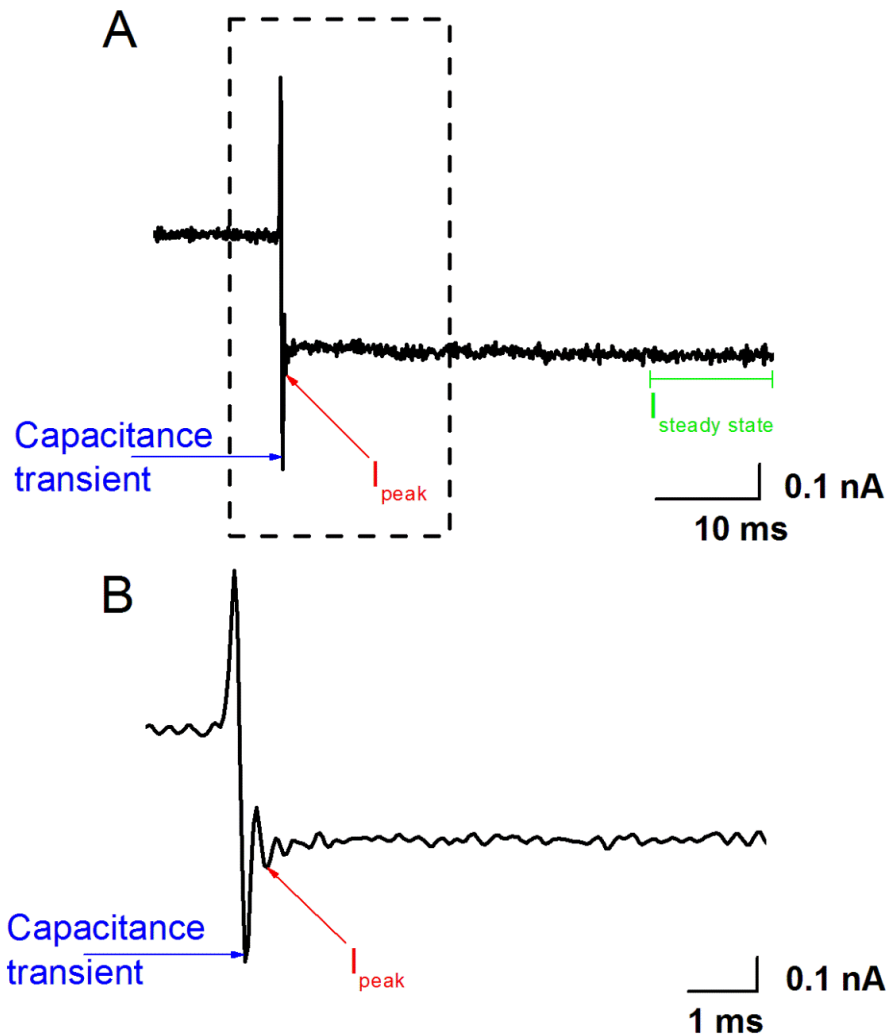


Figure 2-3 Example trace where the capacitance transient is larger than the peak current.

In this example trace the holding potential is -84 mV and the voltage command is stepped to -164 mV to investigate the inward potassium current $I_{K,n}$.

The capacitance transient highlighted by the blue arrow is larger than the peak current, highlighted by the red arrow. In this example I would manually measure the size of the peak current so that the value is not obscured by the capacitance transient. The steady state current highlighted in green is measured as an average over a 10 ms duration at the end of the voltage command step. $I_{K,n}$ is measured as the difference between the peak and steady state currents.

- A. Shows the capacitance transient, the peak current and the steady state current
- B. Shows an enlarged image of the box in A, with only the capacitance transient and the peak current to highlight the difference between the two.

Peak Δ pH responses were measured as the most negative (largest Inward) current during the 10 second period of extracellular solution at pH 5 minus the steady state current before change of extracellular solution. The steady state Δ pH response was measured as the average current magnitude between 8 and 9 seconds after the change in extracellular solution minus the steady state current before exchanging the extracellular solution.

Data analysis was performed offline using Clampfit version 10 (Axon Instruments, CA USA), Signal and Origin software version 7.0 (OriginLab, MA, USA). Where stated current traces from voltage clamp recordings have been corrected offline for leak conductance (g_{leak}). Leak conductance was measured between -84 mV and -94 mV for $I_{K,f}$, $I_{K,s}$ and some $I_{K,n}$ recordings. For $I_{K,n}$ traces from mature OHCs measuring leak conductance was measured between -164 mV and -154 mV to exclude the presence of the $I_{K,n}$ current itself. Membrane potentials for all currents were corrected for any residual R_s after compensation. Membrane potentials were also corrected for the liquid junction potential, which arises from a difference in the mobility of ions at the interface between the bath and pipette solution (Neher, 1992). With KCl intracellular solution the liquid junction potential is -4 mV and with CsCl intracellular solution it is -4 mV. Voltage responses were recorded using the current clamp configuration of the Optopatch, which automatically applies the R_s compensation. The zero-current potential was measured using an external calibrator, this was subtracted along with the -4 mV error from the liquid junction potential from all voltage traces.

Statistical comparison of means was carried out using a two-tailed *t*-test for the direct comparisons in chapters 3 and 4. Two way ANOVAs were used for the statistical comparisons of multiple groups of data in chapters 5 and 6. Statistical significance was determined with $P < 0.05$.

Protocol	Use	Sampling rate	Filtering rate
VCIKOUT	50 ms steps from -104 mV to +46 mV to measure steady state currents	25 kHz	2.5 kHz
VCIKf	5 ms steps from -104 mV to +46 mV to measure instantaneous currents	25 kHz	2.5 kHz
VCIKn	50 ms steps from -164 mV to +46 mV to measure steady state currents	25 kHz	2.5 kHz
CC10pA	100 ms steps from -20 pA to +50 pA to measure voltage responses	25 kHz	5 kHz
CC100pA	100 ms steps from -200 pA to +1000 pA to measure voltage responses	25 kHz	5 kHz
VC2min	2 minutes at -84 mV for determining ASIC responses	1 kHz	200 Hz

Table 2-3 Sampling rates and filtering rates for all protocols used.

3 DEVELOPMENT OF THE INNER HAIR CELLS IN MOUSE MODELS OF USHER SYNDROME

3.1 Introduction

Previous work investigating the development of the basolateral currents in IHCs without functional Myo6 showed that the IHCs didn't reach maturity and remained functionally immature (Roux et al., 2009). Mature IHCs with dysfunctional Myo6 fail to display the mature $I_{K,f}$ current and are still able to produce action potentials, indicative of the expression of a neonatal complement of currents. Mutations in myo6 much like mutations in Usher proteins result in a disorganised hair bundle which, is the primary cause of deafness in these mice. In this chapter I investigate the effects of several mutations (Myo7a, Hrm and Pcdh) on the electrical development of the IHCs, allowing us to see whether the lack of development previously reported is directly related to Myo6 function or due to loss of the MET current and hair bundle function. I have investigated the development of $I_{K,s}$, $I_{K,f}$ and $I_{K,n}$ currents along with the voltage responses in IHCs of neonatal (P2-4), mature (P20-30) and adult (~1 year) mice.

3.2 Results

All electrophysiological recordings were performed using standard ECS and K^+ ICS (see Table 2-1 and Table 2-2 for composition), and cells were held at 35°C. All statistical comparisons were carried out using a two-tailed *t*-test, significant differences were achieved with a *p* value of <0.05 (NS for non-significant differences *p* = >0.05).

3.2.1 Neonatal Myo7a^{+/sh6j} and Myo7a^{sh6j/sh6j} IHCs

At BT (35°C) neonatal Myo7a^{+/sh6j} and Myo7a^{sh6j/sh6j} IHCs both display typical K^+ currents for this age (P2 - 4) with slow activation reaching a steady state level within 25 ms in response to a depolarising membrane potential of -4 mV (Figure 3-1A and B). At -24 mV neonatal Myo7a^{+/sh6j} and Myo7a^{sh6j/sh6j} IHCs have a steady state current of 2470 ± 290 pA (mean \pm SEM) (*n* = 9) and 2470 ± 330 pA (*n* = 8) (NS) respectively. The IV plot in Figure 3-1C shows that there is no difference between the currents seen in response to changes in the membrane potential in Myo7a^{+/sh6j} and Myo7a^{sh6j/sh6j} neonatal IHCs. The basolateral currents seen in both IHC

genotypes are comparable to those previously recorded (Kros et al., 1998), this suggests that Myo7a is not required for the IHCs to develop a neonatal complement of currents.

Neonatal IHCs are known to produce both spontaneous and evoked calcium based action potentials in response to small depolarisations in the cells resting membrane potential (Marcotti et al., 2003b). Figure 3-2 shows the voltage responses of the neonatal Myo7a^{+/sh6j} and Myo7a^{sh6j/sh6j} IHCs. Both IHC types show production of action potentials in response to positive injections of current (Figure 3-2). In response to negative current injections there is a large deviation from the resting membrane potential.

Figure 3-1D shows a VI plot for the variation in the resting membrane potential in response to sustained current injections, this variation is similar between the neonatal Myo7a^{+/sh6j} and Myo7a^{sh6j/sh6j} IHCs. The membrane potentials were measured as the average potential over 50 ms during the current injection. It is interesting to note that the Myo7a^{sh6j/sh6j} IHCs sit more hyperpolarised than the Myo7a^{+/sh6j} IHCs.

The resting membrane potential for the neonatal Myo7a^{+/sh6j} and Myo7a^{sh6j/sh6j} IHCs is -55.8 ± 4.1 mV (n = 8) and -69.6 ± 3.2 mV (n = 10) (p = 0.0166) respectively. This difference is likely to be due to a lack of the mechano-electrical transducer (MET) current, and has been previously reported (Kros et al., 2001). The MET current has a finite open probability at rest of ~5% and lack of Myo7a function reduces this probability to close to zero, this would cause decrease in the inward flow of a cationic current causing the cell to be more hyperpolarised. This difference in the resting membrane potential may cause a difference in the firing of spontaneous action potentials which are produced in the neonatal IHCs (Johnson et al., 2012). Myo7a^{+/sh6j} IHCs fired spontaneous action potentials in 60% (3 out of 5 cells) of cells recorded from compared to 29% (2 out of 7 cells) in Myo7a^{sh6j/sh6j} IHCs. The difference in action potential generation does not extend to triggered events as these could be elicited in 63% (5 out of 8 cells) and 70% (7 out of 10 cells) of Myo7a^{+/sh6j} and Myo7a^{sh6j/sh6j} IHCs respectively, showing that lack of Myo7a function does not alter the ability of the IHCs to produce action potentials just reduces the probability of these happening spontaneously.

The whole cell capacitance for the neonatal Myo7a^{+/sh6j} and Myo7a^{sh6j/sh6j} IHCs is 6.3 ± 0.4 pF (n = 9) and 6.6 ± 0.5 pF (n = 8) (NS) respectively (Figure 3-13A). Neonatal Myo7a^{+/sh6j} IHCs have a linear leak measured during a -10 mV step of 3.3 ± 0.6 nS (n = 9) compared to 3.6 ± 0.7 nS (n = 8) (NS) in the neonatal Myo7a^{sh6j/sh6j} IHCs. The whole cell capacitance recorded here is similar to that previously shown (Kros et al., 1998). This suggests that the function of Myo7a is not required for the development of the neonatal IHC when investigating both the cellular

properties and the basolateral currents. As the neonatal Myo7a^{+/sh6j} IHCs are comparable to those previously reported the investigation of the Myo7a^{+/+} IHCs is not required as Myo7a^{+/sh6j} can be thought of as wild-type-like.

3.2.2 Steady state currents in mature IHCs

Mature (P20-P30) Myo7a^{+/sh6j}, Hrm^{+/-} and Pcdh^{+/AV3J} IHCs display K⁺ currents with fast activation kinetics in response to a depolarising membrane potential around -4 mV, that reach a steady state level within 0.5 ms. Myo7a^{sh6j/sh6j}, Hrm^{-/-} and Pcdh^{AV3J/AV3J} mature IHCs show K⁺ currents which are much smaller in size and have slower activation kinetics than those seen with the mature wild-type-like IHCs at a comparable membrane potential, similar to those seen with the neonatal IHCs (Figure 3-3). At -24mV the mature IHC steady state currents measures: Myo7a^{+/sh6j} and Myo7a^{sh6j/sh6j} 5050 ± 280 pA (n = 6) and 2410 ± 240 pA (n = 9) (p<0.0001), Hrm^{+/-} and Hrm^{-/-} 3380 ± 14 pA (n = 14) and 874 ± 338 pA (n = 3) (p=0.0032) and Pcdh^{+/AV3J} and Pcdh^{AV3J/AV3J} 6133 ± 867 (n = 10) and 1321 ± 254 pA (n = 12) (p<0.0001). A summary of these data can be seen in Figure 3-12A and Table 3-1.

Error! Reference source not found. A, B and C show the IV plots for the steady state currents in the IHCs described above. What can be noted is that in the heterozygous wild-type-like (+/x) IHCs the steady state current is much larger than in the homozygous mutant (x/x) IHCs. The currents recorded here in the heterozygous wild-type-like IHCs (+/x) are comparable to those previously recorded in mature IHCs (Kros et al., 1998), suggesting that these cells have developed to maturity normally and can be used as wild-type-like recordings (**Error! Reference source not found.**). Comparison between mature Myo7a^{sh6j/sh6j} IHCs and neonatal Myo7a^{+/sh6j} and Myo7a^{sh6j/sh6j} IHCs show that there is no difference in the steady state currents. These currents are also comparable to steady state currents previously recorded in neonatal IHCs (Kros et al., 1998), suggesting that the currents do not develop to maturity. As there is no difference in the steady state currents recorded in the homozygous mutant (x/x) IHCs this suggests that the steady state currents remain immature in these IHCs and that loss of function of the Usher complex is responsible for this.

3.2.3 Presence of $I_{K,f}$ in mature IHCs

Mature $Myo7a^{+/sh6j}$, $Hrm^{+/-}$ and $Pcdh^{+/AV3J}$ IHCs show currents that are fully activated within 0.5 ms whereas mature $Myo7a^{sh6j/sh6j}$, $Hrm^{-/-}$ and $Pcdh^{AV3J/AV3J}$ IHCs activate much slower and are not fully activated within the first 5 ms after the membrane potential has depolarised to -4 mV (Figure 3-4). At -24mV the mature IHC early currents measures: $Myo7a^{+/sh6j}$ and $Myo7a^{sh6j/sh6j}$ 1850 ± 280 pA ($n = 6$) and -250 ± 30 pA ($n = 9$) ($p < 0.0001$), $Hrm^{+/-}$ and $Hrm^{-/-}$ 2232 ± 183 pA ($n = 14$) and -394 ± 100 pA ($n = 3$) ($p = 0.0259$) and $Pcdh^{+/AV3J}$ and $Pcdh^{AV3J/AV3J}$ 3766 ± 490 pA ($n = 10$) and -252 ± 23 pA ($n = 12$) ($p < 0.0001$). The IV plots shown in in **Error! Reference source not found.**E, F and G show the size of the early current measured in the mature IHCs as a function of voltage. It can be seen that in the wild-type-like IHCs the $I_{K,f}$ current (measured as the early current) is much larger than the early current measured in the mutant homozygous IHCs. The small but negative early currents recorded in the $Myo7a^{sh6j/sh6j}$, $Hrm^{-/-}$ and $Pcdh^{AV3J/AV3J}$ IHCs are likely to be dominated by the Ca^{2+} currents present in these cells rather than the large outward K^+ currents recorded in the wild-type-like mature IHCs. The size of the $I_{K,f}$ currents recorded here in the heterozygous mature IHCs are comparable to those previously recorded (Kros et al., 1998) in mature IHCs. The early currents seen in homozygous mature IHCs are comparable to those measured previously in the neonatal IHCs (Kros et al., 1998), suggesting that the $I_{K,f}$ current does not appear in these IHCs and that the Usher protein complex is required for the development of this current. These data are summarised in **Error! Reference source not found.**B and **Error! Reference source not found.**.

The size of the $I_{K,s}$ current can be determined by subtracting the early current from the steady state current measured from the same voltage clamp recording. At -24 mV the mature $I_{K,s}$ current measures: $Myo7a^{+/sh6j}$ and $Myo7a^{sh6j/sh6j}$ 3206 ± 261 pA ($n = 6$) and 2658 ± 231 pA ($n = 9$) (NS), $Hrm^{+/-}$ and $Hrm^{-/-}$ 1148 ± 192 pA ($n = 14$) and 1267 ± 275 pA ($n = 3$) (NS) and $Pcdh^{+/AV3J}$ and $Pcdh^{AV3J/AV3J}$ 2367 ± 509 pA ($n = 10$) and 1573 ± 248 pA ($n = 12$) (NS). The size of the $I_{K,s}$ current recorded here is comparable to that previously recorded (Kros et al., 1998). These data are summarized in **Error! Reference source not found.**C and **Error! Reference source not found.**.

3.2.4 Presence of $I_{K,n}$ in mature IHCs

Mature $Myo7a^{+/sh6j}$, $Hrm^{+/-}$ and $Pcdh^{+/AV3J}$ IHCs have inward K^+ currents at hyperpolarizing potentials that are instantly activate reaching a maximal size that then slowly deactivate to a steady state level. Mature $Myo7a^{sh6j/sh6j}$, $Hrm^{-/-}$ and $Pcdh^{AV3J/AV3J}$ IHCs display inward currents at hyperpolarizing potentials which activate quickly but do not inactivate (Figure 3-5).

The $I_{K,n}$ current is defined at the peak current minus the steady state current (Marcotti and Kros, 1999) as described in chapter 2 and Figure 2-3, a full description of the peak and steady state currents can be seen in Figure 3-511 and Table 3-1. At -124 mV in mature IHCs measures: $Myo7a^{+/sh6j}$ and $Myo7a^{sh6j/sh6j}$ -288 ± 87 pA (n = 5) and -89 ± 48 pA (n = 4) (NS), $Hrm^{+/-}$ and $Hrm^{-/-}$ -235 ± 25 pA (n = 12) and -43.7 pA (n = 1) (NS) and $Pcdh^{+/AV3J}$ and $Pcdh^{AV3J/AV3J}$ -216 ± 17 pA (n = 8) and -68 ± 11 pA (n = 8) ($p < 0.0001$). The size of the peak currents recorded here in the heterozygous wild-type-like IHCs are comparable to those previously recorded for mature IHCs, with those recorded for the homozygous mutant IHCs are similar to those seen before for neonatal IHCS (Marcotti et al., 2003a). **Error! Reference source not found.** A, B and C show the IV plots for the peak currents described above. It can be seen that with the exception of the $Hrm^{-/-}$ IHCs the peak current is larger in the wild-type-like IHCs than in the mutant IHCs.

The larger peak current seen with the $Hrm^{-/-}$ mature IHCs is likely to be due to a large leak and n of only one. The $I_{K,n}$ current recorded in the heterozygous wild-type-like mature IHCs is much larger than that seen in the homozygous mutant mature IHCs despite this difference only reaching a statistical difference with $Pcdh^{+/AV3J}$ and $Pcdh^{AV3J/AV3J}$ IHCs. The $I_{K,n}$ currents recorded here in the heterozygous wild-type-like IHCs are similar to those previously recorded for mature IHCs showing that this current develops normally in these IHCs (Marcotti et al., 2003a). This current in the homozygous mutant mature IHCs is comparable to that seen in the neonatal IHCs from work that has been previously published (Marcotti et al., 2003a). The small $I_{K,n}$ current measured in the homozygous mature IHCs is likely to be due to leak currents and would be insensitive to the application of the KCNQ4 channel blocker linopirdine.

This work suggests that the $I_{K,n}$ current does not develop in the mature homozygous IHCs and that function of the Usher protein complex is required for this to happen.

3.2.5 Voltage responses in mature IHCs

Immature IHCs fire spontaneous calcium based action potentials (Kros et al., 1998). After the onset of the $I_{K,f}$ current mature IHCs can no longer produce these action potentials, the voltage

response seen during a current injection is instead like a graded receptor potential, even with current injections up to 1000 pA action potentials cannot be triggered and the resting membrane potential is quickly clamped by the presence of the $I_{K,f}$ current inhibiting oscillations of the membrane potential and large deviations from the resting membrane potential of the cell.

Mature $Myo7a^{+/sh6j}$, $Hrm^{+/-}$ and $Pcdh^{+/AV3J}$ IHCs show a mature response to current injections, with fast clamping of the membrane potential and the lack of action potential generation. Current injections between -20 and +30 pA cause very little deviation from the resting membrane potential (Figure 3-7). In response to larger current injections a graded receptor potential is recorded (Figure 3-6). Mature $Myo7a^{sh6j/sh6j}$ and $Pcdh^{AV3J/AV3J}$ IHCs show the production of action potentials in response to positive current injections, and although not seen in $Hrm^{-/-}$ IHCs there is a larger deviation from the resting potential in response to the same current injections when compared to mature $Hrm^{+/-}$ IHCs (Figure 3-6). Negative current injections cause a much larger hyperpolarization in the membrane potential in all homozygous mature mutant IHCs than seen in the heterozygous wild-type-like IHCs (Figure 3-7).

The VI plots shown in **Error! Reference source not found.** E, F and G allow us to see the difference between the wild-type-like and mutant IHCs much clearer. The heterozygous wild-type-like IHCs have a much smaller variation in the membrane potentials than is seen in the homozygous mutant IHCs in response to the same current injections.

3.2.6 Cellular properties of mature IHCs

IHCs are known to increase in size throughout their maturation (Marcotti et al., 2003a). The whole cell capacitance in mature IHCs measures: $Myo7a^{+/sh6j}$ and $Myo7a^{sh6j/sh6j}$ IHCs is 11 ± 1.6 pF ($n = 6$) and 8.3 ± 0.5 pF (NS), $Hrm^{+/-}$ and $Hrm^{-/-}$ 9.8 ± 0.2 pF ($n = 29$) and 6.4 ± 0.4 pF ($n = 6$) ($p = <0.0001$) and $Pcdh^{+/AV3J}$ and $Pcdh^{AV3J/AV3J}$ 10.0 ± 0.4 pF ($n = 13$) and 7.1 ± 0.4 pF ($n = 15$) ($p = <0.0001$) (**Error! Reference source not found.**A). It is interesting to note that the cell size measured by the whole cell capacitance does differ between the mature heterozygous wild-type-like IHCs and the homozygous mutant IHCs. Mature $Myo7a^{+/sh6j}$ IHCs have a larger whole cell capacitance than the mature $Myo7a^{sh6j/sh6j}$ IHCs and although not significantly different it does agree with the other data here to suggest that the homozygous mutant IHCs do not increase in size. The whole cell capacitance of the heterozygous wild-type-like mature

IHCs is similar to that previously seen for mature IHCs, whereas the cell size for the homozygous mutant mature IHCs is much closer to previously recorded values for the neonatal IHC (Marcotti et al., 2003a). This suggests that loss of the Usher complex also stunts the development of the IHC size.

The resting membrane potential in mature IHCs measures: $Myo7a^{+/sh6j}$ and $Myo7a^{sh6j/sh6j}$ IHCs is -68.1 ± 1.5 mV ($n = 4$) and -75.8 ± 4.6 mV ($n = 8$) (NS), $Hrm^{+/-}$ and $Hrm^{-/-}$ -70.3 ± 1.3 mV ($n = 24$) and -71 ± 0.4 mV ($n = 6$) (NS) and $Pcdh^{+/AV3J}$ and $Pcdh^{AV3J/AV3J}$ -76.1 ± 2.1 mV ($n = 13$) and -81.8 ± 2.9 mV ($n = 13$) (NS). Although the difference between the two does not reach significance it is interesting to note that the heterozygous wild-type-like IHCs have a more depolarised resting membrane potential than that seen in the homozygous mutant IHCs. Loss of the MET current is likely to contribute towards this, in much the same way as seen in the neonatal IHCs. The transducer channel has a finite open probability at rest and this is reduced to close to zero in the homozygous mutant IHCs, the decrease in the inward cationic current causes a negative shift in the resting membrane potential of the cells.

Under our recording conditions the cell membranes of the mature IHCs become more fragile when compared to neonatal IHCs, this often presents itself with an increase in the linear leak measurements. The linear leak in mature IHCs measures: $Myo7a^{+/sh6j}$ and $Myo7a^{sh6j/sh6j}$ IHCs 8.4 ± 1.4 nS ($n = 6$) and 3.1 ± 0.7 nS ($n = 9$) (0.0002), $Hrm^{+/-}$ and $Hrm^{-/-}$ 6.8 ± 0.3 nS ($n = 33$) and 6.4 ± 0.7 nS ($n = 7$) (NS) and $Pcdh^{+/AV3J}$ and $Pcdh^{AV3J/AV3J}$ 7.1 ± 0.8 nS ($n = 10$) and 3.0 ± 0.4 nS ($n = 12$) ($p = 0.0002$) (**Error! Reference source not found.C**). In the mature heterozygous wild-type-like IHCs the leak measurements are increased when compared to their homozygous mutant equivalents. The leak values seen here for the homozygous mutant IHCs are comparable to those recorded in the neonatal $Myo7a$ IHCs, again suggesting that the homozygous mutant IHCs have remained neonatal-like. There does not however appear to be a difference in the leak measurements between mature $Hrm^{+/-}/Hrm^{-/-}$ IHCs, this may be because the data collected for the $Hrm^{-/-}$ was not as good as seen with the other IHC types, but could not be improved upon because $Hrm^{-/-}$ mice were no longer forthcoming.

3.2.7 Adult $Pcdh^{+/AV6J}$ and $Pcdh^{AV6J/AV6J}$ IHCs

Recordings from adults IHCs (~1 year) were attempted to be made from $Pcdh^{AV3J/AV3J}$ however there were no IHCs remaining on the organ of Corti preparation, this was not a consequence of

the dissection technique as data could be recorded from adult $Pcdh^{+/AV3J}$ IHCs (data not shown). In order to investigate the electrical properties of IHCs at this age a less severe $Pcdh15$ mutation was investigated in the $Pcdh^{AV6J/AV6J}$ mouse model. IHCs were present on these preparations at ~1 year and they showed the following activity.

Adult (~1 year) $Pcdh^{+/AV6J}$ IHCs display fast outward K^+ currents that reach a steady state level within 0.5 ms, whereas adult $Pcdh^{AV6J/AV6J}$ IHCs display slower activating K^+ currents which reach a steady state level within 25 ms (**Error! Reference source not found.A,B,C and D**). At -24 mV adult $Pcdh^{+/AV6J}$ and $Pcdh^{AV6J/AV6J}$ IHCs have a steady state current of 2351 ± 571 pA ($n = 7$) and 1536 ± 571 pA ($n = 4$) (NS) respectively. At -24 mV adult $Pcdh^{+/AV6J}$ and $Pcdh^{AV6J/AV6J}$ IHCs have an early current of 1092 ± 295 pA ($n = 7$) and 24 ± 54 pA ($n = 4$) ($p = 0.0259$). At -24 mV adult $Pcdh^{+/AV6J}$ and $Pcdh^{AV6J/AV6J}$ IHCs have an $I_{K,s}$ current of 1339 ± 295 pA ($n = 7$) and 1512 ± 439 pA ($n = 4$) (NS) respectively. The IV plot in **Error! Reference source not found.D** shows that the steady state currents are larger in the $Pcdh^{+/AV6J}$ adult IHCs than those seen in the $Pcdh^{AV6J/AV6J}$ IHCs. It can also be seen in **Error! Reference source not found.H** that the early current $I_{K,f}$ is much larger in the $Pcdh^{+/AV6J}$ IHCs than what is recorded in the $Pcdh^{AV6J/AV6J}$ IHCs. There is no difference in the $I_{K,s}$ current between the adult $Pcdh^{+/AV6J}$ and $Pcdh^{AV6J/AV6J}$ IHCs, agreeing with the findings in the mature IHCs. A summary of these data can be seen in **Error! Reference source not found.A, B and C and Error! Reference source not found..**

In response to hyperpolarizing membrane potentials adult $Pcdh^{+/AV6J}$ IHCs display an inward current which activates instantly and then deactivates to a steady state level. A full description of the peak and steady state currents can be seen in Figure 3-511 and Table 3-1. Adult $Pcdh^{AV6J/AV6J}$ IHCs show inward currents which activate quickly but do not inactivate in response to hyperpolarizing membrane potentials (**Error! Reference source not found.A**). At -124 mV adult $Pcdh^{+/AV6J}$ IHCs and $Pcdh^{AV6J/AV6J}$ have an $I_{K,n}$ current that measures -213 ± 64 pA ($n = 6$) and -53 pA (NS) respectively. The IV plot in **Error! Reference source not found.D** shows that the peak and $I_{K,n}$ currents are larger in the $Pcdh^{+/AV6J}$ adult IHCs than those seen in the $Pcdh^{AV6J/AV6J}$ adult IHCs (**Error! Reference source not found.F**). This again agrees with the data in the mature IHCs suggesting that the $I_{K,n}$ current has not developed in the adult $Pcdh^{AV6J/AV6J}$ IHCs. A summary of this data can be seen in **Error! Reference source not found.D, E and F and Error! Reference source not found..**

Adult $Pcdh^{+/AV6J}$ IHCs show a mature response to current injections between -20 pA and +30 pA with small deviations from the resting membrane potential (**Error! Reference source not found.** with a graded receptor potential seen with current injections up to 1000 pA.

Although spiking was not recorded in the adult $Pcdh^{AV6J/AV6J}$ IHCs, there are large deviations in the membrane potential in response to small injections of current. The VI plot in **Error! Reference source not found.H** highlights this showing that the membrane potential varies less in the $Pcdh^{+/AV6J}$ adult IHCs than in the adult $Pcdh^{AV6J/AV6J}$ IHCs.

Adult $Pcdh^{+/AV6J}$ and $Pcdh^{AV6J/AV6J}$ IHCs have a whole cell capacitance of 8.0 ± 0.5 pF ($n = 7$) and 7.0 ± 1.8 pF ($n = 5$) (NS) (**Error! Reference source not found.A**). The resting potential measured -58.2 ± 3.3 mV ($n = 6$) and -68.5 ± 1.5 mV ($n = 2$) (NS) in the adult $Pcdh^{+/AV6J}$ and $Pcdh^{AV6J/AV6J}$ IHCs respectively (**Error! Reference source not found.B**). Adult $Pcdh^{+/AV6J}$ IHCs have a linear leak of 4.1 ± 0.9 nS ($n = 19$) compared to 22.7 ± 9.8 nS ($n = 9$) ($p = 0.0103$) in adult $Pcdh^{AV6J/AV6J}$ IHCs (**Error! Reference source not found.C**).

3.3 Discussion

The differences seen between the heterozygous and homozygous IHCs can be explained by lack of development of the $I_{K,f}$ current. The production of action potentials in the IHCs through to maturity is likely to be a consequence of lacking this current, as a fast activating current small depolarisations in the membrane potential will be sufficient to activate this current and bring the membrane potential back to more hyperpolarising potentials inhibiting the generation of action potentials (Kros et al., 1998).

The resting membrane potentials of the mature homozygous mutant IHCs are more hyperpolarized than seen in the heterozygous wild-type-like IHCs. Loss of the MET current is likely to contribute towards this, in much the same way as seen in the neonatal IHCs the transducer channel has a finite open probability and this is reduced to close to zero in the homozygous mutant IHCs, the decrease in the inward cationic current causes a negative shift in the resting membrane potential of the cells.

The production of action potentials in the mature $Myo7a^{sh6j/sh6j}$ and $Pcdh^{AV3J/AV3J}$ IHCs shows that the voltage responses of these cells have remained immature. The continuation of this immature response is likely to be due to the lack of development of the $I_{K,f}$ current. It has previously been shown that activation of this current quickly clamps the membrane of the cell in response to depolarizations of the resting membrane potential (Kros et al., 1998). This means that the membrane will never depolarise enough to trigger an action potential.

After the first postnatal week the calcium currents in the IHCs begin to progressively decline in size until around P12 when they reach their steady state mature level (Beutner and Moser, 2001a; Marcotti et al., 2003b). The reduced calcium currents in the mature IHCs are unlikely to be large enough to sustain spontaneous action potential generation although this has not been investigated. Mature $Myo7a^{sh6j/sh6j}$ IHCs are able to produce spontaneous action potentials without any current injection in 29% of the IHCs investigated. This suggests that the calcium currents have remained large enough to sustain action potential generation, however further investigation would be required to confirm this.

Although action potential generation was not seen in mature $Hrm^{-/-}$ (0 out of 6 cells) IHCs, this does not rule out the possibility that these cells are able to produce them. The voltage responses seen are still large in response to small current injections and the membrane does become depolarised enough to trigger action potentials. Production of action potentials is not seen in every cell recorded from even with neonatal IHCs and so it may be that if more cells had been investigated spiking would have been seen. This does not however detract from the voltage responses remaining immature in the mature $Hrm^{-/-}$ IHCs. All together this data shows that the Usher protein complex is required for the development of the voltage responses in the IHCs towards the generation of graded receptor potentials.

Investigation of the steady state currents in the mature IHCs show that loss of function of the Usher complex proteins causes a reduction in the size of the current recorded. The currents recorded here in the heterozygous wild-type-like IHCs are comparable to those previously recorded in mature IHCs (Kros et al., 1998), suggesting that these cells have developed to maturity normally and can be used as wild-type-like recordings. Comparison between mature $Myo7a^{sh6j/sh6j}$ IHCs and neonatal $Myo7a^{+/sh6j}$ and $Myo7a^{sh6j/sh6j}$ IHCs show that there is no difference in the steady state currents. These currents are also comparable to steady state currents previously recorded in neonatal IHCs (Kros et al., 1998), suggesting that the currents do not develop to maturity. As there is no difference in the steady state currents recorded in the homozygous mutant IHCs this suggests that the steady state currents remain immature in these IHCs and that loss of function of the Usher complex is responsible for this.

The $I_{K,s}$ current as previously described is thought to be a mixed current formed by a mixture of two potassium currents. Measured by the subtraction of the $I_{K,f}$ current from the steady state current (Kros and Crawford, 1990). In neonatal IHCs this current is termed $I_{K,neo}$ and is carried by a mixture of a 4-AP insensitive I_K current mostly and a smaller 4-AP sensitive I_K current, this current then develops to the $I_{K,s}$ current where it is carried more dominantly by the 4-AP

sensitive I_k current and has a smaller contribution from the 4-AP insensitive I_k current. In mature $Myo7a^{+/sh6j}/Myo7a^{sh6j/sh6j}$, $Pcdh^{+/AV3J}/Pcdh^{AV3J/AV3J}$ and $Hrm^{+/-}/Hrm^{-/-}$ IHCs there is no difference in the size of the $I_{k,s}$ current suggesting that the difference seen in the steady state currents is due to lack of development of the $I_{k,f}$ and $I_{k,n}$ current.

The steady state currents in the adult $Pcdh^{+/AV6J}$ IHCs are much larger than those seen in the adult $Pcdh^{AV6J/AV6J}$ IHCs however this difference is not significant, this is likely to be because of few recordings and increased leak in the $Pcdh^{AV6J/AV6J}$ IHCs. The early current recorded in the adult $Pcdh^{+/AV6J}$ IHCs is larger than that in the $Pcdh^{AV6J/AV6J}$ IHCs and this difference is significant. There is no difference in the $I_{k,s}$ current between the adult $Pcdh^{+/AV6J}$ and $Pcdh^{AV6J/AV6J}$ IHCs, agreeing with the findings in the mature IHCs. Although there is only 1 recording for the $I_{k,n}$ current in the adult $Pcdh^{AV6J/AV6J}$ IHCs, it can be seen that this current is reduced when compared to the current seen in the adult $Pcdh^{+/AV6J}$ IHCs. This again agrees with the data in the mature IHCs suggesting that the $I_{k,n}$ current has not developed in the adult $Pcdh^{AV6J/AV6J}$ IHCs. Although the production of action potentials has not been recorded in the adult $Pcdh^{AV6J/AV6J}$ IHCs, the voltage responses that have been recorded are immature like showing larger deviations from the resting potential in response to small current injections. Taken together this suggests that there is a stunting rather than delay of the development in the mutant IHCs.

Although it is easy to forget, the stunting of development seen in the IHCs here is not the cause for the deafness in these mice, which is due to lack of hair bundle function and reduced MET currents meaning that incoming sounds cannot be detected and converted to electrical signals to be passed to the brain.

This work along with previous work using $Myo6$ mouse models (Roux et al., 2009) suggests that loss of function of the hair bundle causes a lack of development of the IHCs from neonatal to mature. It might be that the spontaneous action potential activity in the neonatal IHCs is important for the development of the mature basolateral currents. As this is reduced in the homozygous mutant (x/x) IHCs it may be enough to cause the stunting of maturation. This has also been seen with $Ca_v1.3^{-/-}$ IHCs, which are not able to elicit action potentials at any point and do not develop the $I_{k,f}$ current (Brandt et al., 2003a), although interestingly the $I_{k,n}$ current develops normally. This suggests that action potential activity may not be important for the development of the $I_{k,n}$ current. It may also be important that the resting potential is more negative in the $Myo7a^{sh6j/sh6j}$ IHCs and that a slightly more depolarised potential may be required for the development of the mature basolateral currents.

All of the Usher proteins investigated here also have structural functions within the synaptic region of the IHCs (Adato et al., 2005; Boëda et al., 2002; Gregory et al., 2011; Reiners et al., 2005; Senften et al., 2006; Siemens et al., 2002). It has also been shown that loss of function in Myo6 results in dysfunctional exocytosis in the mature IHCs but this activity is normal in the neonatal IHCs, this suggests that exocytotic activity would also be normal in the neonatal Myo7a^{sh6j/sh6j}, Hrm^{-/-} and Pcdh^{AV3J/AV3J} IHCs and would not affect the development of the IHCs. The exocytotic activity in these cells at both neonatal and mature has not however been investigated and so this cannot be stated for certain. The stunting of development seen in mature Myo7a^{sh6j/sh6j}, Hrm^{-/-} and Pcdh^{AV3J/AV3J} IHCs and adult Pcdh^{AV6J/AV6J} IHCs are likely to be caused by loss of function of the hair bundle and MET channel rather than secondary actions of the proteins in the synaptic machinery.

3.4 Conclusions

Voltage responses remain immature in the mutant mature IHCs, with production of action potentials seen in Myo7a^{sh6j/sh6j} and Pcdh^{AV3J/AV3J} IHCs, and large deviations from the membrane potential seen in Hrm^{-/-} IHCs in response to small positive current injections. Adult marker currents $I_{K,f}$ and $I_{K,n}$ do not appear upon maturation of the mutant IHCs, suggesting that Usher complex proteins are required for the development of the IHCs. This is supported by the smaller whole cell capacitance seen in the mutant mature IHCs. It is also important to note that this is a stunting of the development rather than a delay as IHCs at one year in Pcdh^{AV6J/AV6J} mouse models still do not show the adult marker currents, still have an immature response to current injections and the whole cell capacitance is reduced similar to that seen in neonatal IHCs.

3.5 Future experiments

As there is a reduction in the size of the calcium currents in the IHCs upon maturation (Marcotti et al., 2003b), it would be interesting to investigate whether these changes occur in the Myo7a^{sh6j/sh6j} mature IHCs. The ability of these mature IHCs to produce action potentials suggests that the calcium currents do not decline in size as they would in wild-type-like mature

IHCs. The IHCs become much more efficient in releasing neurotransmitters via exocytosis throughout development (Beutner and Moser, 2001b; Johnson et al., 2005). Less intracellular calcium is required for vesicle fusion with the pre-synaptic membrane of the mature IHC. It would be interesting to investigate this process in the mature $Myo7a^{+/sh6j}$ and $Myo7a^{sh6j/sh6j}$ IHCs to see if the developmental stunting that has been recorded here extends to the exocytosis in these IHCs.

It would also be interesting to try and investigate the basolateral currents in the adult $Myo7a^{sh6j/sh6j}$ IHCs to see if they confirm the results found in the adult $Pcdh^{AV6J/AV6J}$ IHCs relating to the stunting of development. However I expect that at 1 year of age there will be no IHCs to record from left in the organ of Corti, it may however be possible to look at the currents at a more intermediate age (~6 months) rather than at 1 year, where the IHCs will be fully adult but may be still present in the tissue.

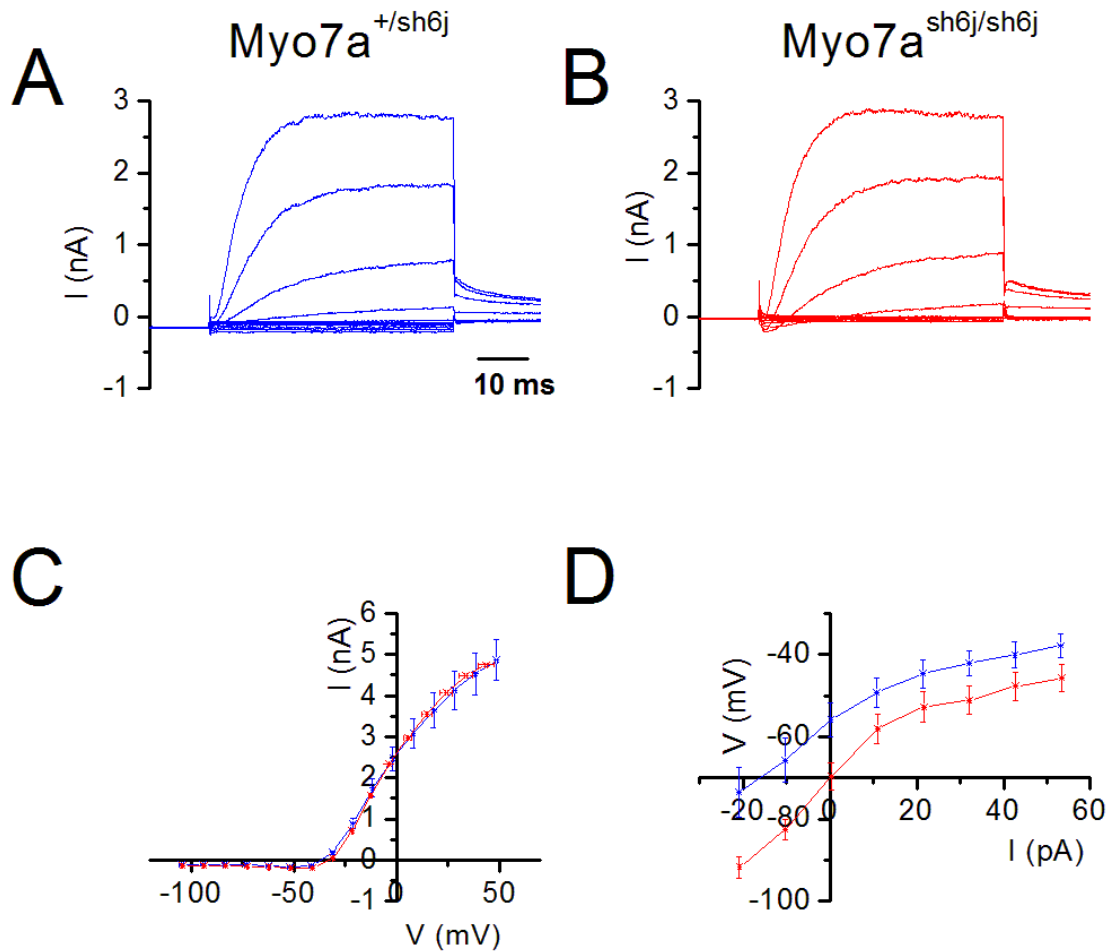


Figure 3-1 Basolateral currents in neonatal $Myo7a^{+/sh6j}$ and $Myo7a^{sh6j/sh6j}$ IHCs

Typical whole cell current recordings seen in response to voltage steps in:

- $Myo7a^{+/sh6j}$ neonatal IHCs (C_m 6.8 pF, R_s 1.0 M Ω , Leak 2.9 nS, P4)
- $Myo7a^{sh6j/sh6j}$ neonatal IHC (C_m 6.8 pF, R_s 0.8 M Ω , Leak 2.6 nS, P3)
- IV plot for the steady state currents in neonatal IHCs $Myo7a^{+/sh6j}$ (blue) (n = 9) and $Myo7a^{sh6j/sh6j}$ (red) (n = 8)
- Plot of the mean membrane voltage versus current injection measured between 100 and 250 ms after step onset. $Myo7a^{+/sh6j}$ (blue) (n = 9) and $Myo7a^{sh6j/sh6j}$ (red) (n = 8).

Traces have been corrected for linear leak conductance assuming Ohms law, baselines haven't been adjusted to 0 pA.

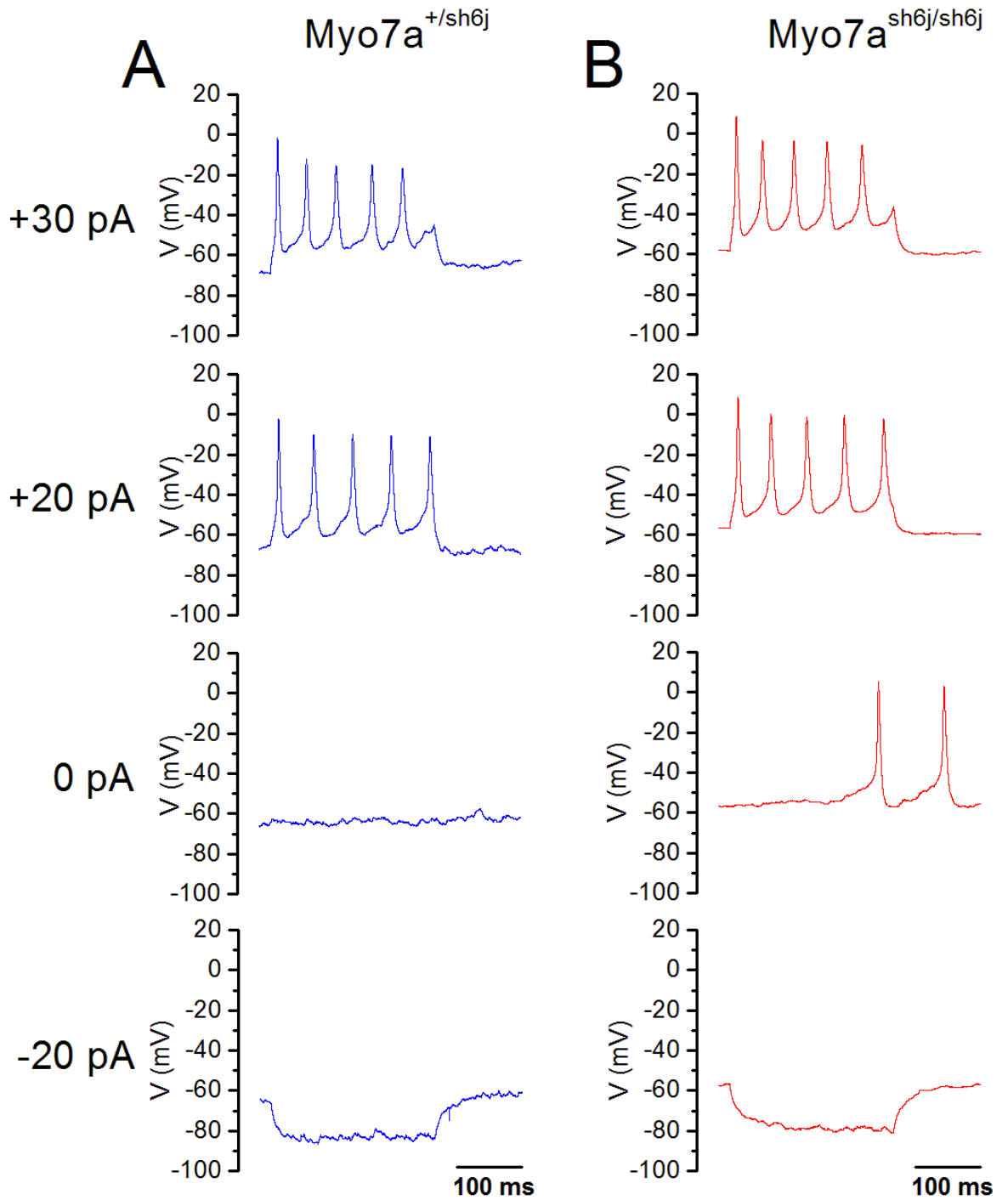


Figure 3-2 Voltage responses in neonatal *Myo7a*^{+/sh6j} and *Myo7a*^{sh6j/sh6j} IHCs

Typical voltage responses seen in:

- A. *Myo7a*^{+/sh6j} neonatal IHCs at 30, 20 and -20 pA current injection (C_m 6.9 pF, R_s 3.8 M Ω , P3)
- B. *Myo7a*^{+/sh6j} neonatal IHCs at 30, 20 and -20 pA current injection (C_m 6.1 pF, R_s 4.0 M Ω , P3)

Series resistance compensation was employed in current clamp.

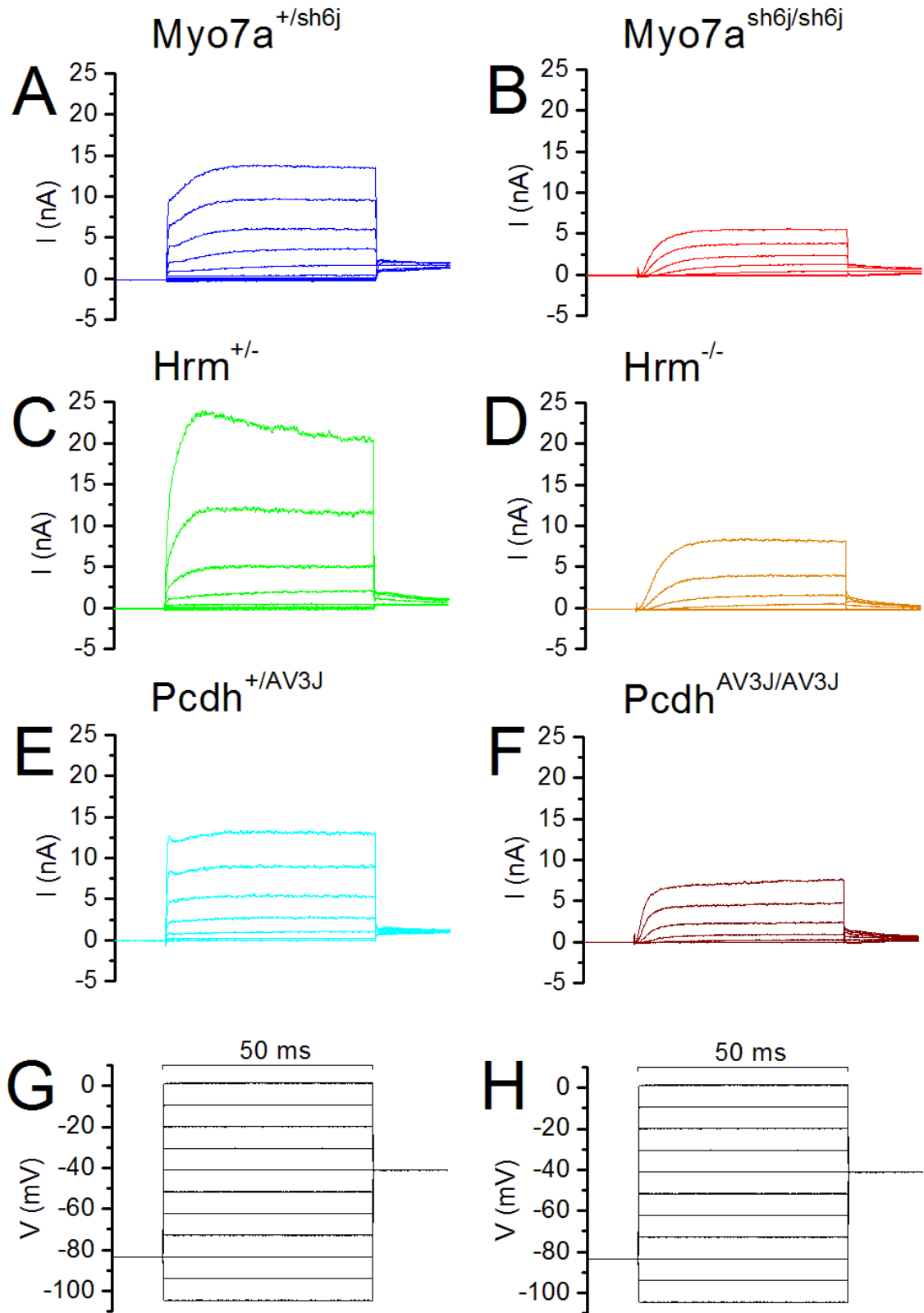


Figure 3-3 Steady state currents in mature IHCs from mouse models of Usher syndrome.

Figure 3-3 Steady state currents in mature IHCs from mouse models of Usher syndrome.

Typical whole cell current recordings seen in response to voltage steps in:

- A. $Myo7a^{+/sh6J}$ mature IHC (C_m 7.4 pF, R_s 1.4 M Ω , Leak 7.6 nS, P22)
- B. $Myo7a^{sh6J/sh6J}$ mature IHC (C_m 7.4 pF, R_s 1.1 M Ω , Leak 5.0 nS, P25)
- C. $Hrm^{+/-}$ mature IHC (C_m 9.9 pF, R_s 0.7 M Ω , Leak 6.5 nS, P22)
- D. $Hrm^{-/-}$ mature IHC (C_m 7.0 pF, R_s 0.6 M Ω , Leak 6.6 nS, P25)
- E. $Pcdh^{+/AV3J}$ mature IHC (C_m 10.6 pF, R_s 0.6 M Ω , Leak 4.9 nS, P23)
- F. $Pcdh^{AV3J/AV3J}$ mature IHC (C_m 6.7 pF, R_s 1.5 M Ω , Leak (11.9 nS, P21)
- G. Voltage command
- H. Voltage command

Traces have been corrected for linear leak conductance assuming Ohms law, baselines haven't been adjusted to 0 pA.

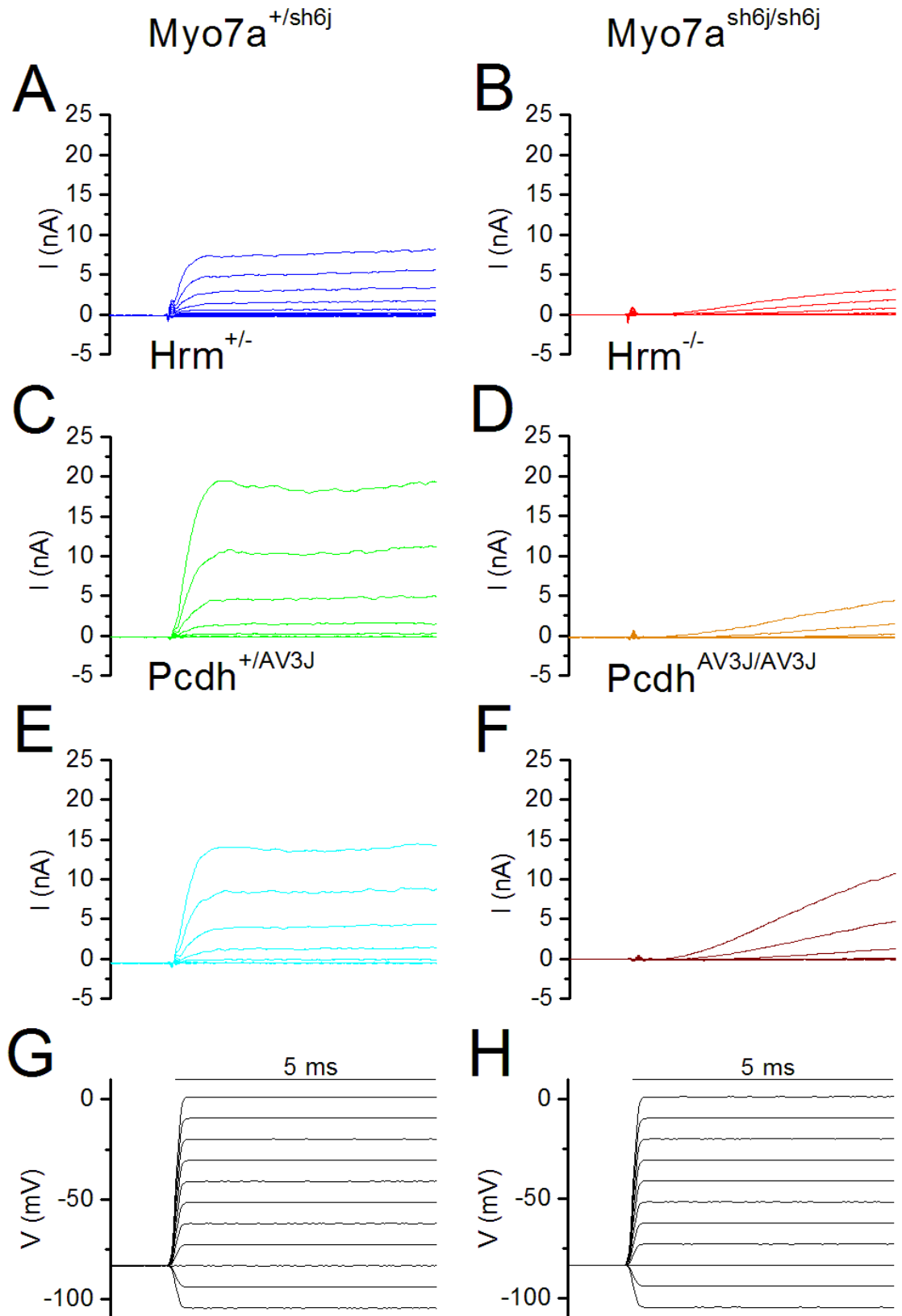


Figure 3-4 $I_{K,f}$ currents in mature IHCs from mouse models of Usher syndrome.

Figure 3-4 I_{K_f} currents in mature IHCs from mouse models of Usher syndrome.

Typical whole cell current recordings seen in response to voltage steps in:

- A. $Myo7a^{+/sh6J}$ mature IHC (C_m 7.4 pF, R_s 1.4 M Ω , Leak 7.6 nS, P22)
- B. $Myo7a^{sh6J/sh6J}$ mature IHC (C_m 7.4 pF, R_s 1.9 M Ω , Leak 2.2 nS, P21)
- C. $Hrm^{+/-}$ mature IHC (C_m 10.0 pF, R_s 0.8 M Ω , Leak 6.9 nS, P21)
- D. $Hrm^{-/-}$ mature IHC (C_m 7.2 pF, R_s 0.7 M Ω , Leak 7.2 nS, P25)
- E. $Pcdh^{+/AV3J}$ mature IHC (C_m 10.1 pF, R_s 0.8 M Ω , Leak 13.6 nS, P22)
- F. $Pcdh^{AV3J/AV3J}$ mature IHC (C_m 4.0 pF, R_s 1.3 M Ω , Leak 3.7 nS, P21)
- G. Voltage command
- H. Voltage command

Traces have been corrected for linear leak conductance assuming Ohms law, baselines haven't been adjusted to 0 pA.

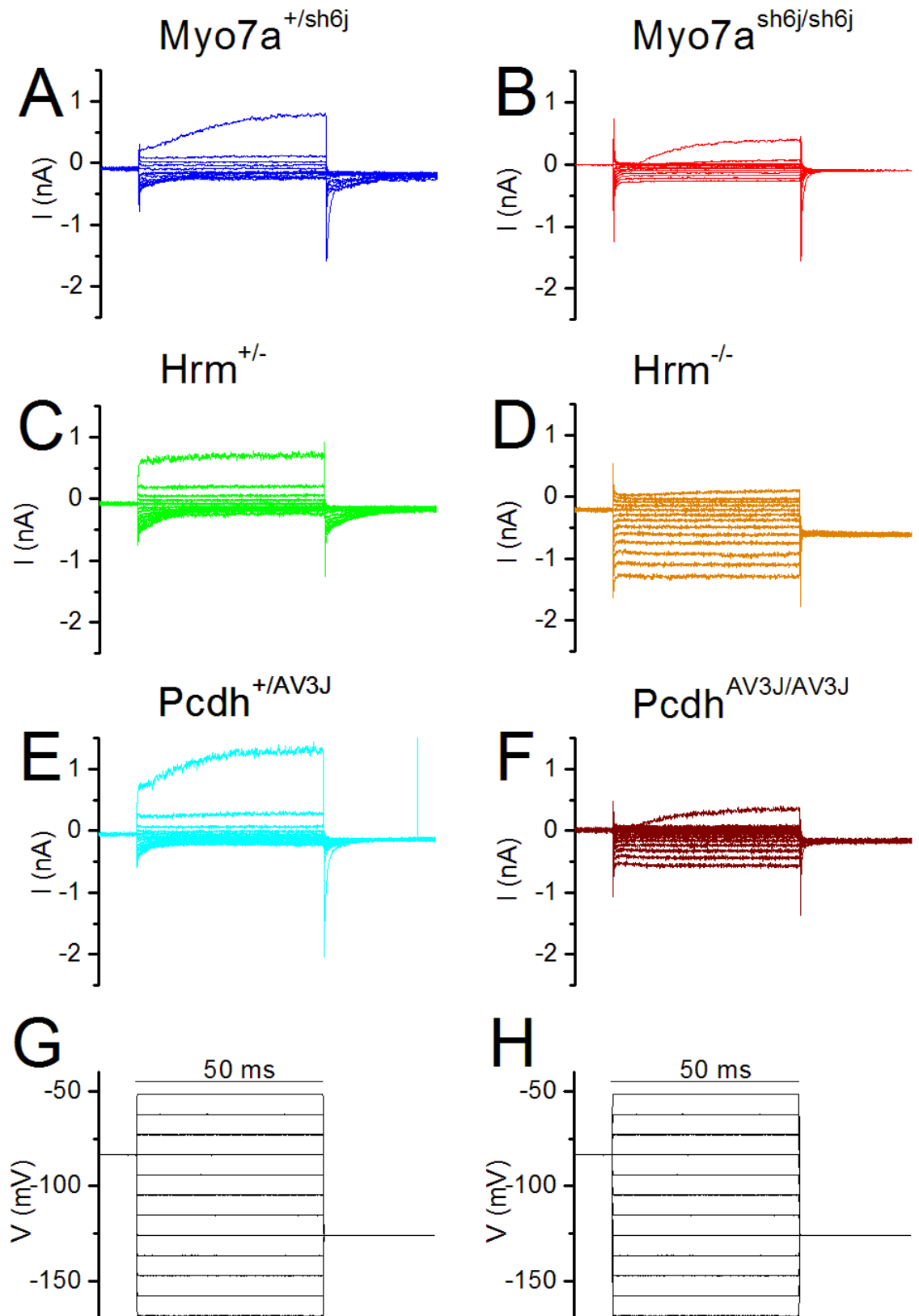


Figure 3-5 $I_{K,n}$ currents in mature IHCs from mouse models of Usher syndrome

Figure 3-5 $I_{K,n}$ currents in mature IHCs from mouse models of Usher syndrome.

Typical whole cell current recordings seen in response to voltage steps in:

- A. $Myo7a^{+/sh6J}$ mature IHC (C_m 8.0 pF, R_s 1.1 M Ω , Leak 5.0 nS, P25)
- B. $Myo7a^{sh6J/sh6J}$ mature IHC (C_m 8.1 pF, R_s 0.7 M Ω , Leak 2.0 nS, P21)
- C. $Hrm^{+/-}$ mature IHC (C_m 10.0 pF, R_s 0.5 M Ω , Leak 5.2 nS, P21)
- D. $Hrm^{-/-}$ mature IHC (C_m 7.2 pF, R_s 0.9 M Ω , Leak 7.4 nS, P25)
- E. $Pcdh^{+/AV3J}$ mature IHC (C_m 10.1 pF, R_s 0.8 M Ω , Leak 13.6 nS, P22)
- F. $Pcdh^{AV3J/AV3J}$ mature IHC (C_m 4.0 pF, R_s 1.3 M Ω , Leak 3.7 nS, P21)
- G. Voltage command
- H. Voltage command

Traces have not been corrected for linear leak conductance, baselines have not been adjusted to 0 pA.

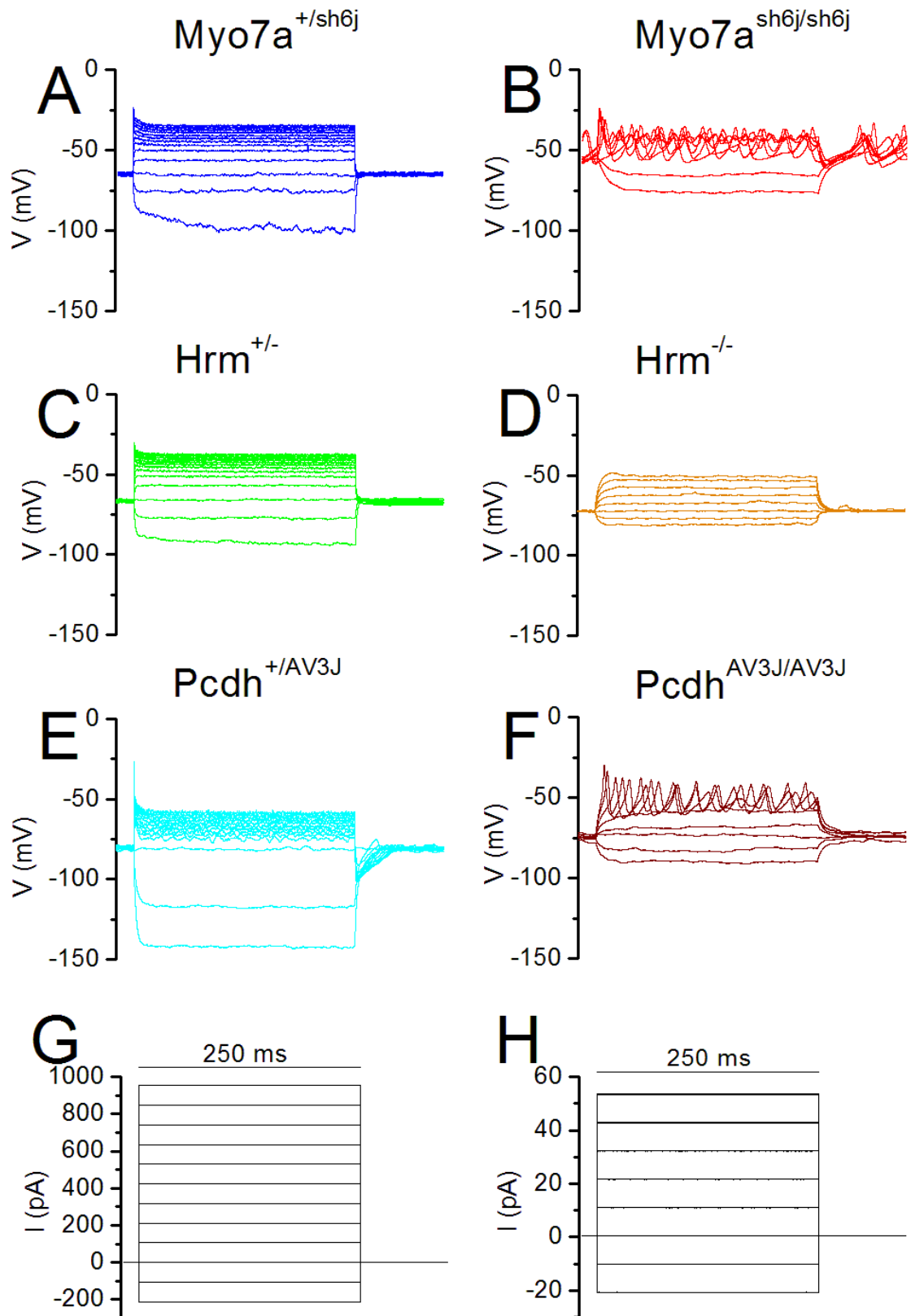


Figure 3-6 Voltage responses in mature IHCs from Usher syndrome mouse models.

Figure 3-6 Voltage responses in mature IHCs from Usher syndrome mouse models.

Typical voltage responses seen in response to current injections in:

- A. $Myo7a^{+/sh6J}$ mature IHC (C_m 9.0 pF, R_s 4.4 M Ω , P22)
- B. $Myo7a^{sh6J/sh6J}$ mature IHC (C_m 6.0 pF, R_s 6.0 M Ω , P21)
- C. $Hrm^{+/-}$ mature IHC (C_m 8.6 pF, R_s 2.9 M Ω , P24)
- D. $Hrm^{-/-}$ mature IHC (C_m 6.4 pF, R_s 3.7 M Ω , P25)
- E. $Pcdh^{+/AV3J}$ mature IHC (C_m 10.6 pF, R_s 3.4 M Ω , P23)
- F. $Pcdh^{AV3J/AV3J}$ mature IHC (C_m 2.9 pF, R_s 6.7 M Ω , P24)
- G. Current injections for A,C and E
- H. Current injections for B,D and F

Series resistance compensation was employed in current clamp.

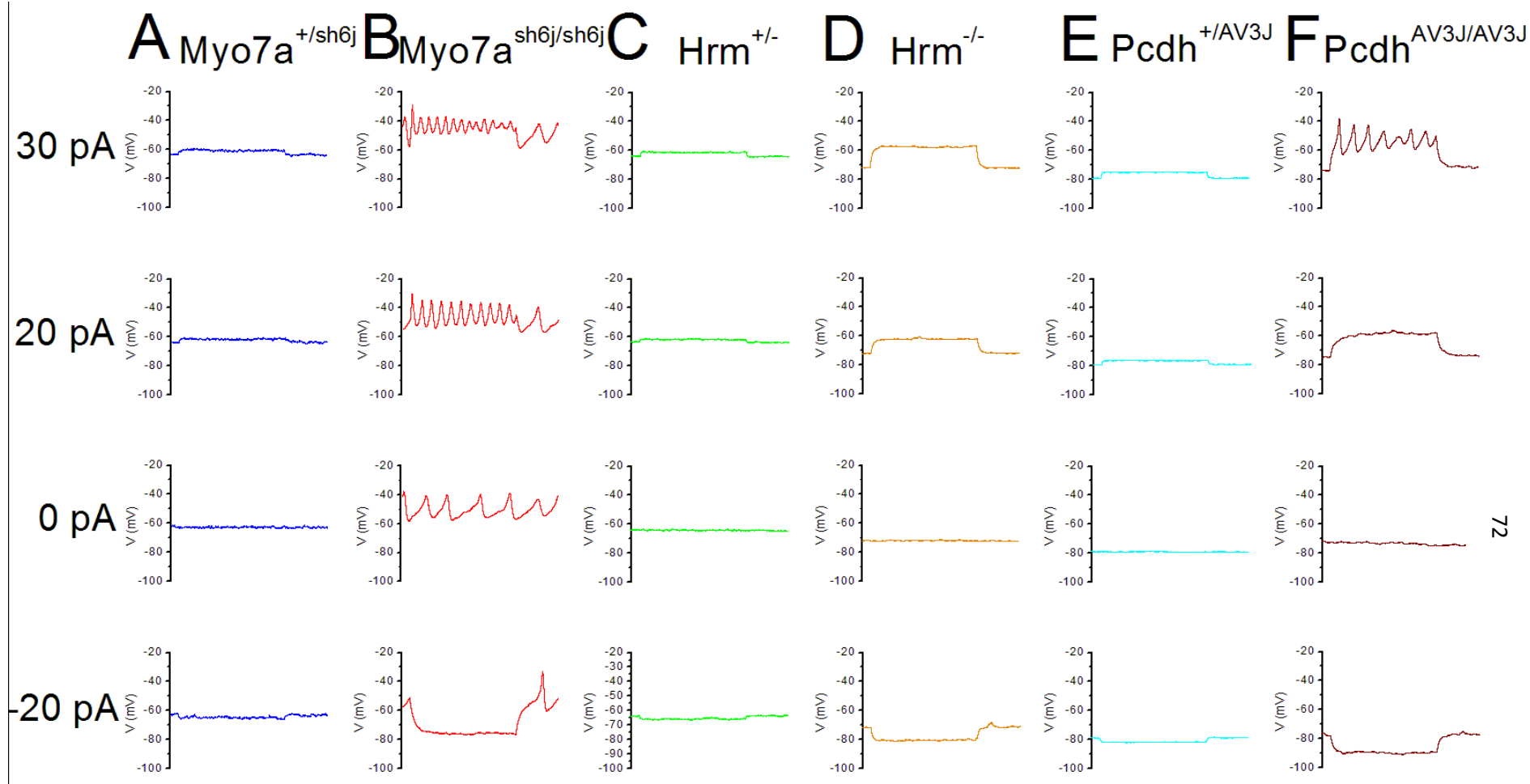


Figure 3-7 Expansion of the voltage response in mature IHCs

Figure 3-7 Expansion of the voltage response in mature IHCs

Typical voltage responses seen in response to current injections in:

- A. $Myo7a^{+/sh6J}$ mature IHC (C_m 9.0 pF, R_s 4.4 M Ω , P22)
- B. $Myo7a^{sh6J/sh6J}$ mature IHC (C_m 6.0 pF, R_s 6.0 M Ω , P21)
- C. $Hrm^{+/-}$ mature IHC (C_m 8.6 pF, R_s 2.9 M Ω , P24)
- D. $Hrm^{-/-}$ mature IHC (C_m 6.4 pF, R_s 3.7 M Ω , P25)
- E. $Pcdh^{+/AV3J}$ mature IHC (C_m 10.6 pF, R_s 3.4 M Ω , P23)
- F. $Pcdh^{AV3J/AV3J}$ mature IHC (C_m 2.9 pF, R_s 6.7 M Ω , P24)

Series resistance compensation was employed in current clamp.

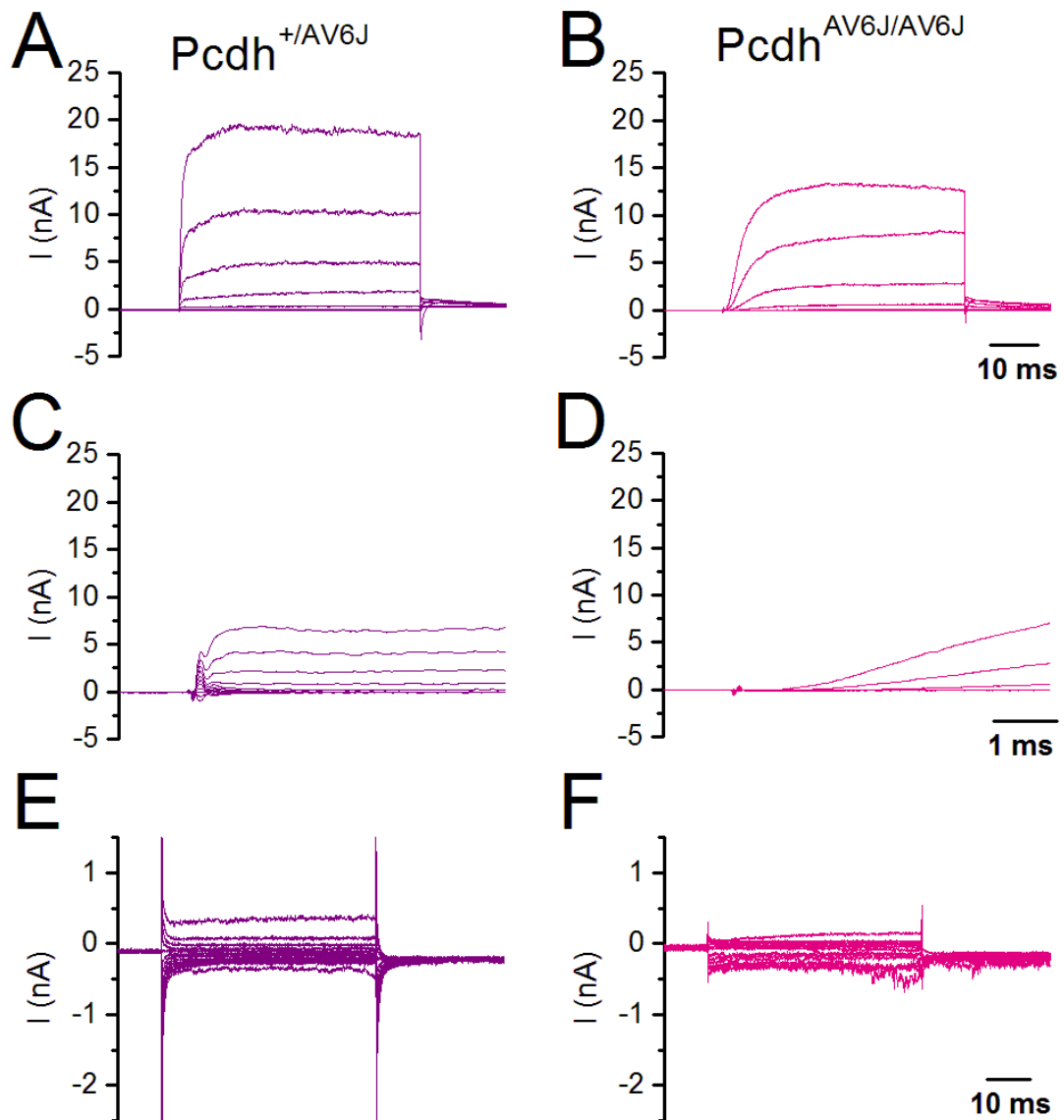


Figure 3-8 Basolateral currents in adult Pcdh^{+/AV6J} and Pcdh^{AV6J/AV6J} IHCs.

Typical whole cell current recordings seen in response to voltage steps in:

- A. Pcdh^{+/AV6J} adult IHCs (C_m 9.3 pF, R_s 0.6 M Ω , Leak 95.2 nS, P255)
- B. Pcdh^{AV6J/AV6J} adult IHCs (C_m 5.8 pF, R_s 1.2 M Ω , Leak 2.4 nS, P549)
- C. Pcdh^{+/AV6J} adult IHCs (C_m 9.3 pF, R_s 1.3 M Ω , Leak 5.2 nS, P255)
- D. Pcdh^{AV6J/AV6J} adult IHCs (C_m 5.8 pF, R_s 1.2 M Ω , Leak 2.4 nS, P549)
- E. Pcdh^{+/AV6J} adult IHCs (C_m 8.6 pF, R_s 2.0 M Ω , Leak 3.6 nS, P255)
- F. Pcdh^{AV6J/AV6J} adult IHCs (C_m 6.2 pF, R_s 1.4 M Ω , Leak 2.6 nS, P549)

Traces (A-D) have been corrected for linear leak conductance assuming Ohms law E and F have not been corrected for linear leak conductances. Baselines haven't been adjusted to 0 pA

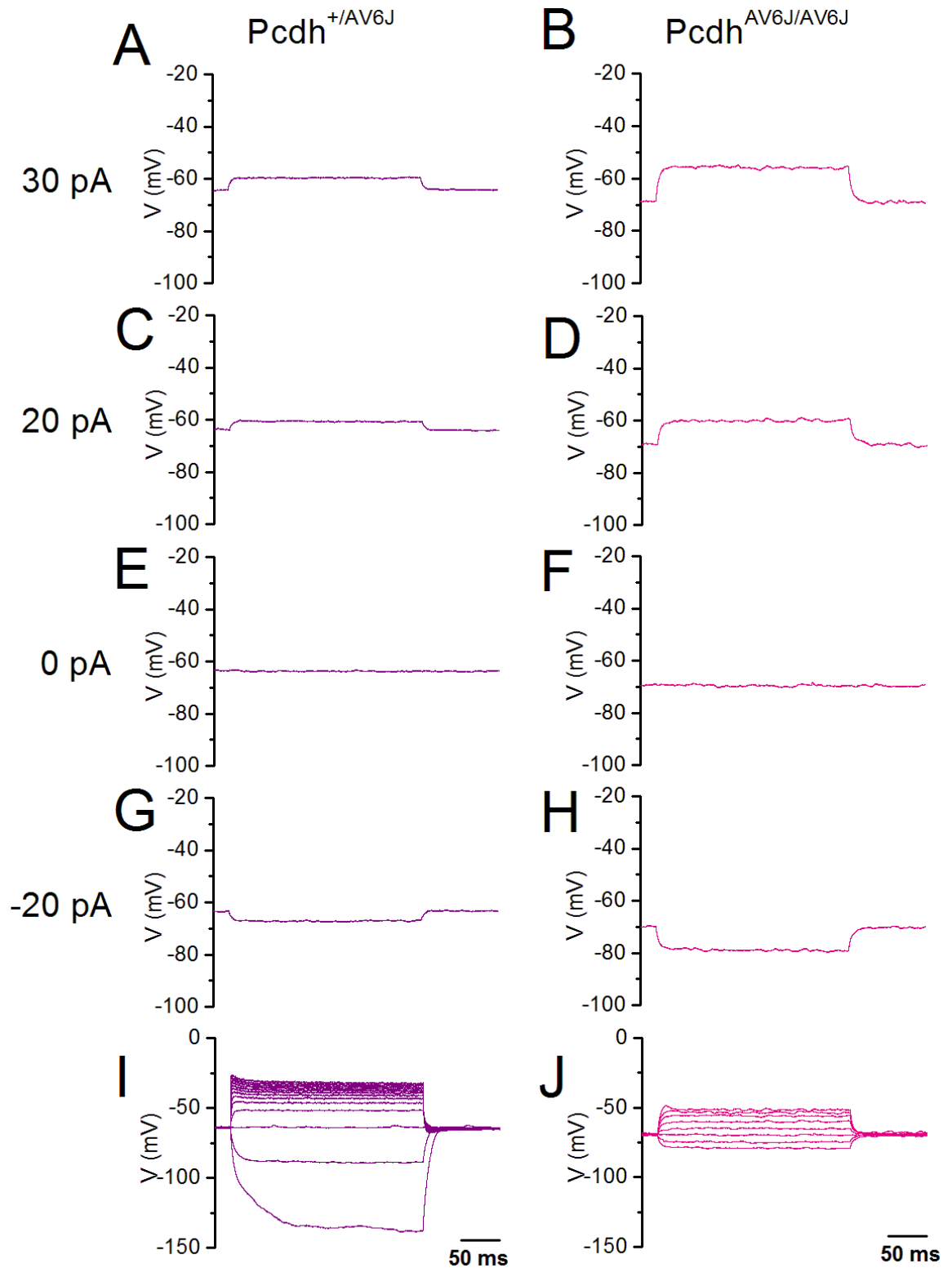


Figure 3-9 Voltage responses in adult $Pcdh^{+/AV6J}$ and $Pcdh^{AV6J/AV6J}$ IHCs.

Typical voltage responses seen in response to current injections in:

A,C,E,G,I $Pcdh^{+/AV6J}$ adult IHCs (C_m 8.0 pF, R_s 11.1 M Ω , P255)

B,D,F,H,J $Pcdh^{AV6J/AV6J}$ adult IHCs (C_m 6.0 pF, R_s 6.3 M Ω , P549)

Series resistance compensation was employed in current clamp.

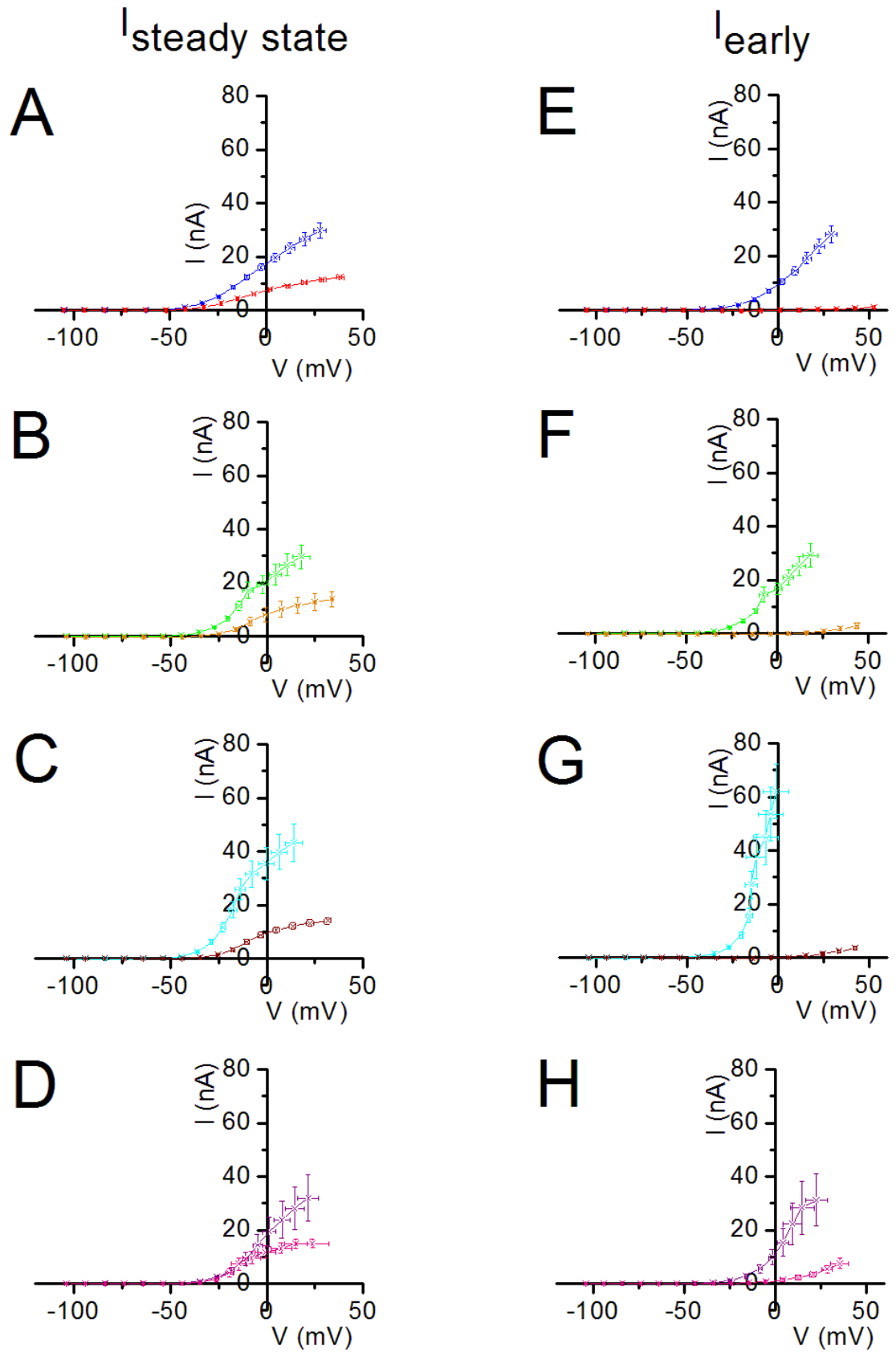


Figure 3-10 IV plots of the steady state and $I_{K,f}$ currents in the mature and adult IHCs

Figure 3-10 IV plots of the steady state and $I_{K,f}$ currents in the mature and adult IHCs.

IV plots of the leak subtracted steady state and $I_{K,f}$ currents measured during the voltage step in:

- A. Steady state currents in mature $Myo7a^{+/sh6j}$ (blue) (n = 7) and $Myo7a^{sh6j/sh6j}$ (red) (n = 8) IHCS
- B. Steady state currents in mature $Hrm^{+/-}$ (green) (n = 14) and $Hrm^{-/-}$ (orange) (n = 3) IHCs
- C. Steady state currents in mature $Pcdh^{+/AV3J}$ (blue) (n = 10) and $Pcdh^{AV3J/AV3J}$ (wine) (n = 12) IHCs
- D. Steady state currents in adult $Pcdh^{+/AV6J}$ (purple) (n = 7) and $Pcdh^{AV6J/AV6J}$ (pink) (n = 2-4) IHCs
- E. Early currents in mature $Myo7a^{+/sh6j}$ (blue) (n = 5) and $Myo7a^{sh6j/sh6j}$ (red) (n = 6) IHCS
- F. Early currents in mature $Hrm^{+/-}$ (green) (n = 14) and $Hrm^{-/-}$ (orange) (n = 3) IHCs
- G. Early currents in mature $Pcdh^{+/AV3J}$ (blue) (n = 9) and $Pcdh^{AV3J/AV3J}$ (wine) (n = 11) IHCs
- H. Early currents in adult $Pcdh^{+/AV6J}$ (purple) (n = 7) and $Pcdh^{AV6J/AV6J}$ (pink) (n = 2-4) IHCs

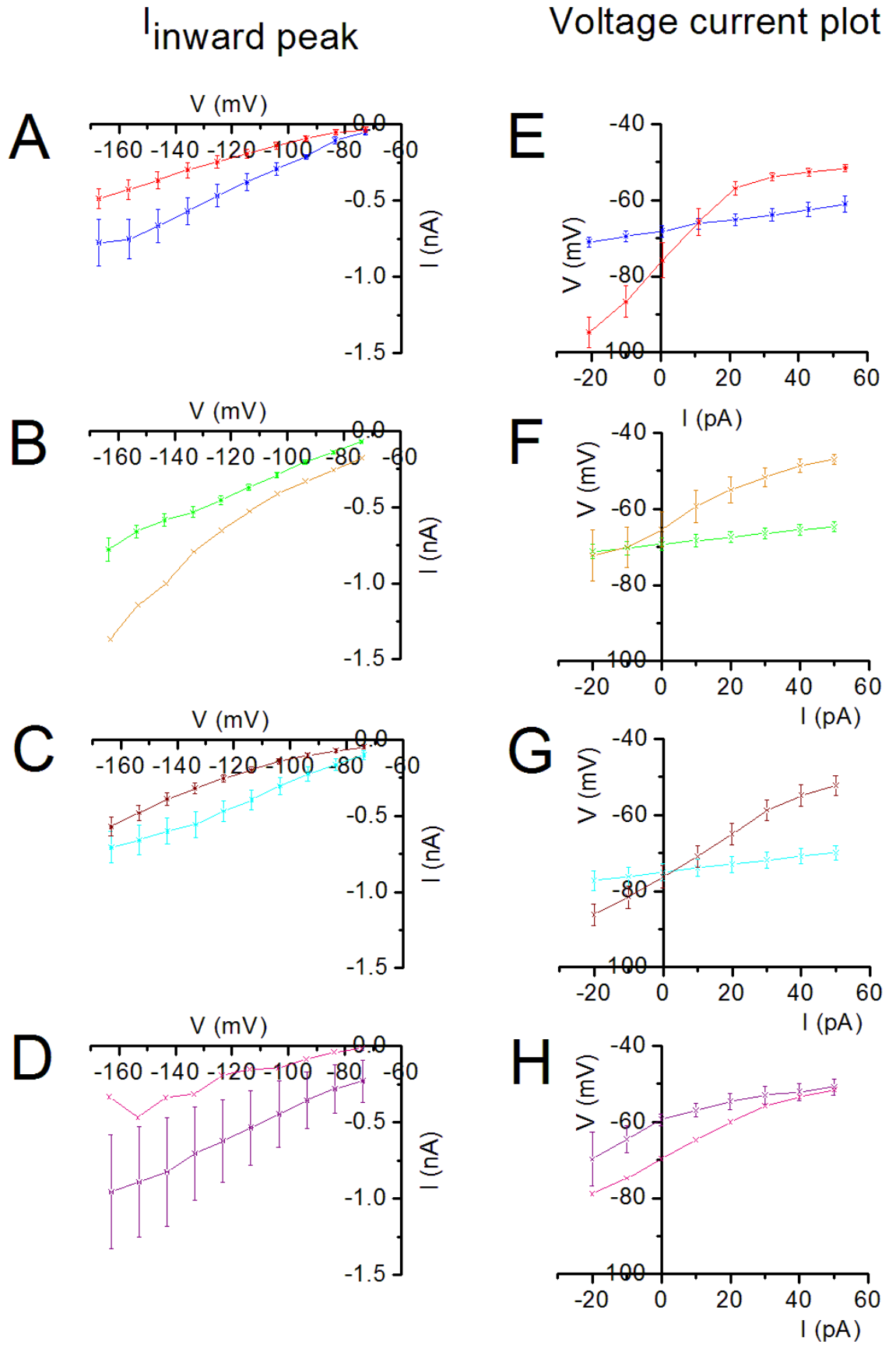


Figure 3-11 IV plots of the $I_{K,n}$ and voltage responses in the mature and adult IHCs

Figure 3-11 IV plots of the $I_{K,n}$ and voltage responses in the mature and adult IHCs.

IV plots of the $I_{K,n}$ currents measured during the voltage step and the voltage responses in:

- A. Peak currents in mature $Myo7a^{+/sh6j}$ (blue) (n = 5) and $Myo7a^{sh6j/sh6j}$ (red) (n = 4) IHCS
- B. Peak currents in mature $Hrm^{+/-}$ (green) (n = 12) and $Hrm^{-/-}$ (orange) (n = 1) IHCs
- C. Peak currents in mature $Pcdh^{+/AV3J}$ (blue) (n = 8) and $Pcdh^{AV3J/AV3J}$ (wine) (n = 8) IHCs
- D. Peak currents in adult $Pcdh^{+/AV6J}$ (purple) (n = 6) and $Pcdh^{AV6J/AV6J}$ (pink) (n = 1) IHCs
- E. Voltage responses in mature $Myo7a^{+/sh6j}$ (blue) (n = 7) and $Myo7a^{sh6j/sh6j}$ (red) (n = 8) IHCS
- F. Voltage responses in mature $Hrm^{+/-}$ (green) (n = 10) and $Hrm^{-/-}$ (orange) (n = 6) IHCs
- G. Voltage responses in mature $Pcdh^{+/AV3J}$ (blue) (n = 8) and $Pcdh^{AV3J/AV3J}$ (wine) (n = 15) IHCs
- H. Voltage responses in adult $Pcdh^{+/AV6J}$ (purple) (n = 4) and $Pcdh^{AV6J/AV6J}$ (pink) (n = 1) IHCs

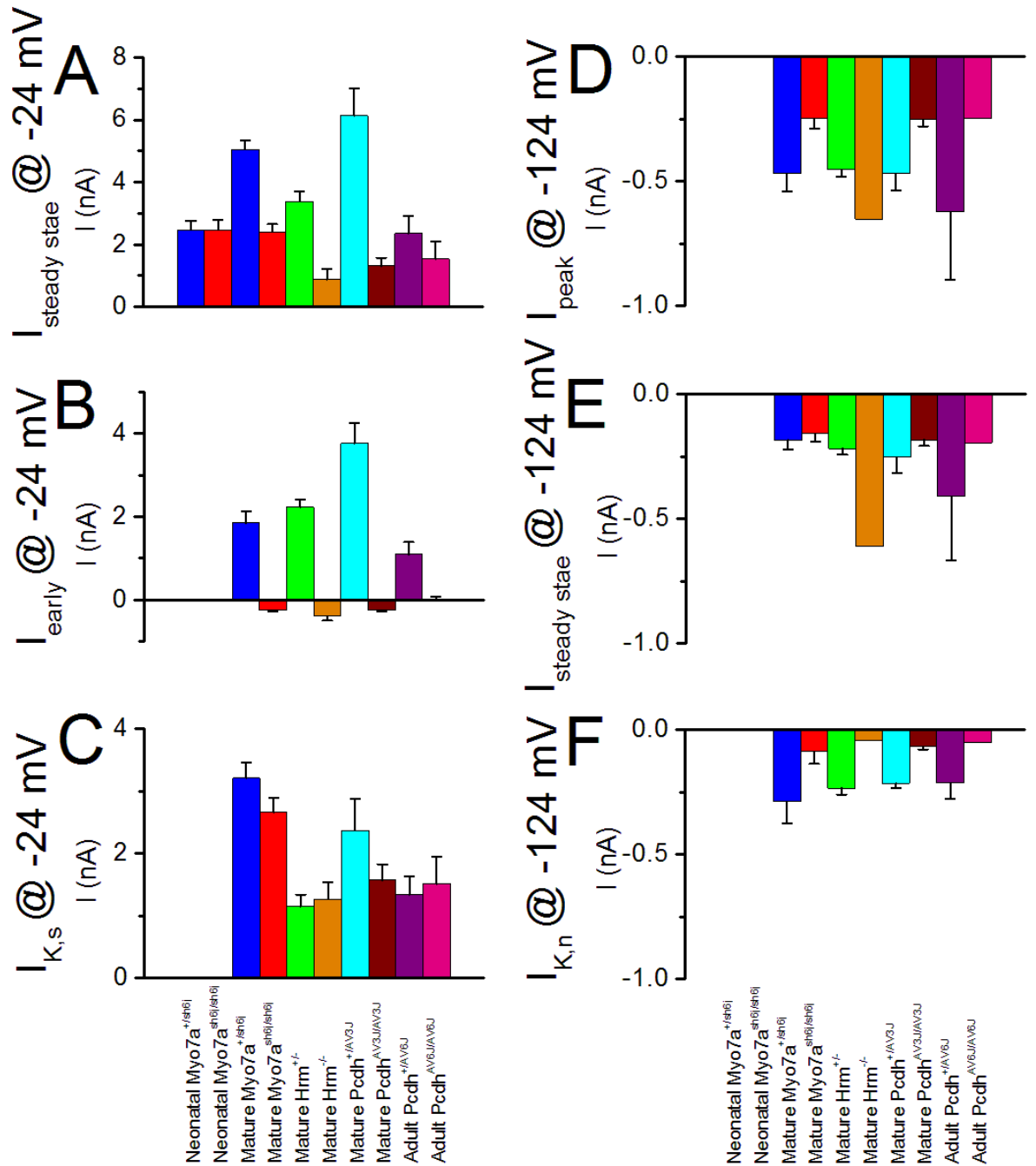


Figure 3-12 Bar graphs of the basolateral currents in the neonatal, mature and adult IHCs

Leak subtracted current measurements for:

- Steady state currents at -24 mV (n = 9,8,6,9,14,3,10,12,7,4)
- Early currents at -24 mV (n = 6,9, 14,3,10,12,7,4)
- The $I_{K,s}$ current at -24 mV (n = 6,9,14,3,10,12,7,4)

Current measurements for:

- Peak currents at -124 mV (n = 5,4,12,1,18,8,6,1)
- Steady state currents at -124 mV (n = 5,4,12,1,18,8,6,1)
- The $I_{K,n}$ current at -124 mV (n = 12,1,18,8,6,1)

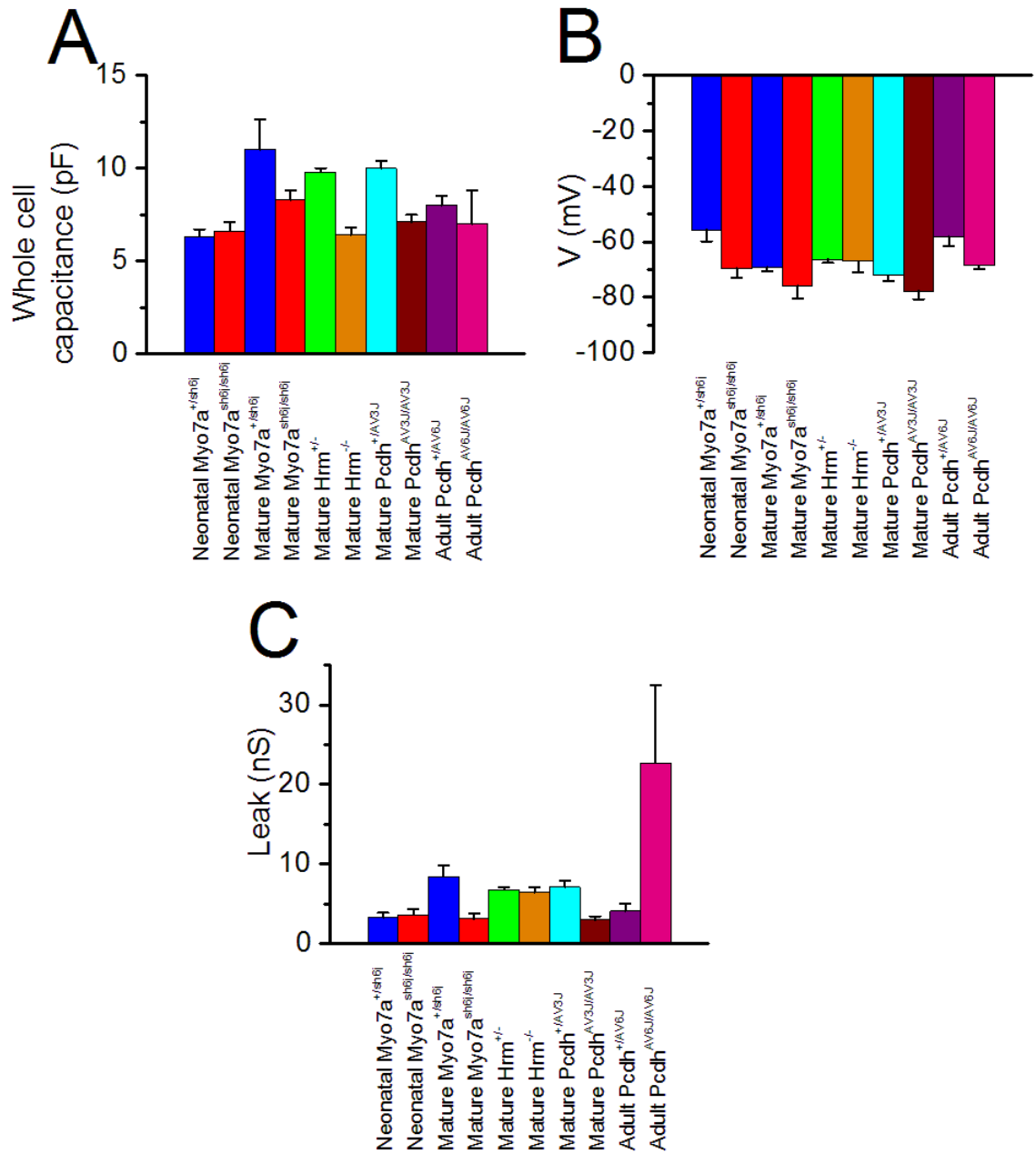


Figure 3-13 Bargraphs of the cellular properties of the IHCs

- Whole cell capacitance measurements (n = 9,8,6,9,29,33,7,10,12,19,9)
- Resting membrane potentials (n = 8,10,4,8,24,6,13,13,6,2)
- Leak measurements (n = 9,8,6,9,33,7,10,12,19,9)

	Neonatal				Mature				Mature				Mature				Adult			
	Myo7a ^{+/sh6j}		Myo7a ^{sh6j/sh6j}		Myo7a ^{+/sh6j}		Myo7a ^{sh6j/sh6j}		Hrm ^{+/-}		Hrm ^{-/-}		Pcdh ^{+/AV3J}		Pcdh ^{AV3J/AV3J}		Pcdh ^{+/AV6J}		Pcdh ^{AV66J/AV6J}	
	mean ± SEM	n	mean ± SEM	n	mean ± SEM	n	mean ± SEM	n	mean ± SEM	n	mean ± SEM	n	mean ± SEM	n	mean ± SEM	n	mean ± SEM	n	mean ± SEM	n
g_{leak} (nS)	3.3 ±0.6	9	3.6 ±0.7	8	8.4 ±1.4	6	3.1 ±0.7	9	6.8 ±0.3	33	6.4 ±0.7	7	7.1 ±0.8	10	3 ±0.4	12	4.1 ±0.9	19	22.7 ±9.8	9
$C_{whole\ cell}$ (pF)	6.3 ±0.4	9	6.6 ±0.5	8	11 ±1.6	6	8.3 ±0.5	9	9.8 ±0.2	29	6.4 ±0.4	6	10 ±0.4	13	7.1 ±0.4	15	8 ±0.5	7	7 ±1.8	5
V_m (mV)	-55.8 ±4.1	8	-69.6 ±3.2	10	-69.1 ±1.5	4	-75.8 ±4.6	8	-66.3 ±1.3	24	-67 ±4	6	-72.1 ±2.1	13	-77.8 ±2.9	13	-58.2 ±3.3	6	-68.5 ±1.5	2
$I_{steady\ state@-24mV}$ (pA)	2470 ±290	9	2470 ±330	8	5050 ±280	6	2410 ±240	9	3380 ±317	14	874 ±338	3	6133 ±867	10	1321 ±254	12	2351 ±571	7	1536 ±571	4
$I_{early@-24mV}$ (pA)					1850 ±280	6	-250 ±30	9	2232 ±183	14	-394 ±99.9	3	3766 ±490	10	-252 ±23	12	1092 ±295	7	24 ±54.4	4
I_{K_s} I @-24mV (pA)					3206 ±255	6	2659 ±230	9	1148 ±192	14	1267 ±275	3	2367 ±509	10	1573 ±248	12	1339 ±295	7	1512 ±439	4
$I_{steady\ state@-124mV}$ (pA)					-185 ±36	5	-159 ±32	4	-219 ±24	12	-609	1	-253 ±65	8	-185 ±23	8	-410 ±258	6	-195	1
$I_{inward\ peak@-124mV}$ (pA)					-468 ±73	5	-248 ±41	4	-454 ±28	12	-652	1	-469 ±68	8	-254 ±26	8	-622 ±273	6	-248	1
$I_{K,n@-124mV}$ (pA)					-289 ±87	5	-88.7 ±48.2	4	-235 ±25	12	-43	1	-216 ±17	8	-68 ±11	8	-213 ±64	6	-52	1

Table 3-1 Summary of the basolateral currents and cellular properties in the neonatal, mature and adult IHCs

Steady state, Inward peak, $I_{K,f}$ and $I_{K,n}$ current measurements. All current measurements are mean ± SEM. All recordings were measured from a holding potential of -84 mV. Steady state currents were measured over 10 ms towards the end of the 50 ms voltage step. Peak currents were measured as the largest current seen during the 50 ms step. $I_{K,n}$ is the subtraction between the two, $I_{K,f}$ currents are averaged over 0.2 ms 0.7 ms after the step onset, $I_{K,s}$ is the subtraction between the steady state and $I_{K,f}$ current measurements.

4 DEVELOPMENT OF OUTER HAIR CELLS IN MYO7A^{+/SH6J} AND MYO7A^{SH6J/SH6J} MOUSE MODELS

4.1 Introduction

The previous chapter has shown that loss of function of the Usher complex stunts the development of the IHCs. The purpose of this chapter is to investigate whether the development of the OHCs is affected in a similar fashion. The development of the OHCs has only been investigated in Myo7a^{+/sh6j} and Myo7a^{sh6j/sh6j} OHCs, as other mouse models were no longer available for experimentation.

4.2 Results

All electrophysiology recordings were performed using standard ECS and K⁺ ICS (see Table 2-1 and Table 2-2 for composition), and cells were held at room temperature (RT) (21°C). All statistical comparisons were carried out using a two-tailed *t*-test, significant differences were achieved with a *p* value of <0.05 (NS for non-significant differences *p* >0.05).

4.2.1 Steady state currents in neonatal and mature OHCs

Myo7a^{+/sh6j} and Myo7a^{sh6j/sh6j} neonatal (P2-P4) OHCs display outward K⁺ currents with slow activation reaching a steady state within 25 ms (Figure 4-1A and B). At -24 mV the steady state current in the neonatal Myo7a^{+/sh6j} and Myo7a^{sh6j/sh6j} OHCs measure 144 ± 26 pA (*n* = 17) and 266 ± 39 pA (*n* = 16) (*p* = 0.0124) respectively, this same difference is not seen at -4 mV with the steady state current measuring 1144 ± 102 pA (*n* = 17) and 1068 ± 66 pA (*n* = 16) (NS). The difference seen here at -24 mV may be due to differences in the calcium currents in the neonatal OHCs, but further experiments would need to be completed to determine this. The IV plot in Figure 4-2B shows the steady state currents for the neonatal OHCs, it can be seen that there is no difference between the neonatal Myo7a^{+/sh6j} and Myo7a^{sh6j/sh6j} OHCs.

Mature (P12-16) Myo7a^{+/sh6j} display inward K⁺ currents that instantly reach a peak that then deactivates to a steady state level, the outward currents are slowly activating reaching a steady state level within 25 ms. Mature Myo7a^{sh6j/sh6j} OHCs display K⁺ currents similar to neonatal OHCs with very small inward currents and slowly activating outward K⁺ currents reaching a steady state within 25 ms (Figure 4-1C and D). At -24 mV the steady state current in

the mature Myo7a^{+/sh6j} and Myo7a^{sh6j/sh6j} OHCs measure 866 ± 109 pA ($n = 23$) and 86 ± 55 pA ($n = 13$) ($p = <00001$) the significantly larger currents seen in the Myo7a^{+/sh6j} mature OHCs also extends to the steady state currents measured at -4 mV which in Myo7a^{+/sh6j} and Myo7a^{sh6j/sh6j} OHCs measure 1512 ± 188 pA ($n = 23$) and 326 ± 91 pA ($n = 13$) ($p = <00001$). A summary of this data can be seen in Figure 4-3A and B and **Error! Reference source not found.** The IV plot in Figure 4-2D shows that the steady state currents in the Myo7a^{+/sh6j} OHCs are much larger than those seen in the Myo7a^{sh6j/sh6j} OHCs. The differences show that the steady state currents are larger in the mature Myo7a^{+/sh6j} OHCs than in the Myo7a^{sh6j/sh6j} OHCs. The steady state currents seen in the mature Myo7a^{+/sh6j} OHCs are comparable with those previously recorded for mature OHCs (Marcotti and Kros, 1999), whereas those seen for the mature Myo7a^{sh6j/sh6j} OHCs are similar to those recorded for neonatal OHCs.

4.2.2 The $I_{K,n}$ current in the neonatal and mature OHCs

The $I_{K,n}$ current is defined at the peak current minus the steady state current (Marcotti and Kros, 1999) as described in chapter 2 and Figure 2-3, a full description of the peak and steady state currents can be seen in Figure 4-2, 4 and Table 4-1. The decaying inward current is thus calculated to be -41 ± 4 pA ($n = 17$) and -33 ± 2 pA ($n = 16$) ($p = 0.0164$) for Myo7a^{+/sh6j} and Myo7a^{sh6j/sh6j} OHCs respectively. At -154 mV the peak current is smaller in the neonatal Myo7a^{sh6j/sh6j} OHCs compared to the Myo7a^{+/sh6j} OHCs. Although this difference was not seen at -124 mV this may well be because the currents are larger at -154 mV and so the difference is exaggerated. The decaying inward current at -154 mV is calculated to -61 ± 6 pA ($n = 17$) and -49 ± 5 pA ($n = 16$) ($p = 0.0288$) for Myo7a^{+/sh6j} and Myo7a^{sh6j/sh6j} OHCs respectively. This shows that the size of the decaying inward current is reduced in the neonatal Myo7a^{sh6j/sh6j} OHCs. The size of the decaying inward current in both cell types is comparable to those previously recorded for neonatal OHCs (Marcotti and Kros, 1999). So although reduced in size the decaying inward current in the Myo7a^{sh6j/sh6j} is within the normal range for neonatal OHCs. This data suggests that Myo7a is required for the modulation of the development of the decaying inward current in the neonatal OHCs. . A summary of this data can be seen in Figure 4-4**Error! Reference source not found.** and **Error! Reference source not found.**

At -124 mV the $I_{K,n}$ current for mature Myo7a^{+/sh6j} and Myo7a^{sh6j/sh6j} OHCs measures -371 ± 34 pA ($n = 23$) and -52 ± 6 pA ($n = 13$) ($p < 0.0001$) respectively. At -154 mV the $I_{K,n}$ current for mature Myo7a^{+/sh6j} and Myo7a^{sh6j/sh6j} OHCs measures -668 ± 65 pA ($n = 23$)

and -82 ± 16 pA ($n = 13$) ($p < 0.0001$) respectively. The larger currents seen in the mature $\text{Myo7a}^{+/sh6j}$ OHCs are comparable with those previously recorded for mature OHCs (Marcotti and Kros, 1999), with those seen for the mature $\text{Myo7a}^{sh6j/sh6j}$ OHCs comparing with those reported for typical neonatal OHCs. The currents recorded here for the $\text{Myo7a}^{sh6j/sh6j}$ OHCs are comparable with those reported here for the neonatal $\text{Myo7a}^{+/sh6j}$ and $\text{Myo7a}^{sh6j/sh6j}$ OHCs. This suggests that the $I_{K,n}$ current does not develop in the $\text{Myo7a}^{sh6j/sh6j}$ OHCs and that these cells maintain a neonatal compliment of basolateral currents.

4.2.3 Cellular properties of the OHCs

The whole cell capacitance of the neonatal $\text{Myo7a}^{+/sh6j}$ OHCs is 6.4 ± 0.1 pF ($n = 17$) compared to 6.5 ± 0.1 pF ($n = 16$) (NS) in the neonatal $\text{Myo7a}^{sh6j/sh6j}$ OHCs. Neonatal $\text{Myo7a}^{+/sh6j}$ OHCs have a linear leak conductance of 1.2 ± 0.1 nS ($n = 17$), whilst neonatal $\text{Myo7a}^{sh6j/sh6j}$ OHCs have a linear leak of 0.9 ± 0.2 nS ($n = 16$) (NS). Despite the differences seen in the basolateral currents of the neonatal OHCs there is no difference in the whole cell capacitance and leak measurements between the neonatal $\text{Myo7a}^{+/sh6j}$ and $\text{Myo7a}^{sh6j/sh6j}$ OHCs. The whole cell capacitance measurements recorded here are comparable to those previously recorded (Marcotti and Kros, 1999) suggesting that the whole cell capacitance is unaffected by loss of Myo7a function and so growth to this stage of development is not affected by loss of this protein. The resting potential was -54 ± 3 mV ($n = 16$) and -51 ± 2 mV ($n = 14$) (NS) in the neonatal $\text{Myo7a}^{+/sh6j}$ and $\text{Myo7a}^{sh6j/sh6j}$ OHCs respectively. Interestingly there is no difference in the resting membrane potential between the neonatal $\text{Myo7a}^{+/sh6j}$ and $\text{Myo7a}^{sh6j/sh6j}$ OHCs. A difference here would have been expected due to the lack of the MET current in the $\text{Myo7a}^{sh6j/sh6j}$ OHCs which contributes significantly to the resting potential (Johnson et al., 2012). The reduced decaying inward current in the neonatal $\text{Myo7a}^{sh6j/sh6j}$ OHCs may explain this. The decaying inward current would hyperpolarise the resting membrane potential and so reduction in this current would depolarize the resting membrane potential and so counteract the hyperpolarization caused by the lack of the MET current. The resting membrane potentials recorded here are comparable to those previously recorded (Marcotti and Kros, 1999).

Mature $\text{Myo7a}^{+/sh6j}$ and $\text{Myo7a}^{sh6j/sh6j}$ OHCs have a whole cell capacitance of 8.4 ± 0.2 pF ($n = 44$) and 7.1 ± 0.2 pF ($n = 46$) ($p < 0.001$). The whole cell capacitance of the $\text{Myo7a}^{+/sh6j}$ OHCs is comparable with those reported previously for mature OHCs (Marcotti and Kros, 1999). Mature $\text{Myo7a}^{sh6j/sh6j}$ OHCs have a whole cell capacitance that is similar but larger than that of

the neonatal OHCs previously reported (Marcotti and Kros, 1999). The leak conductance measured between -164 mV and -154 mV in mature Myo7a^{+/sh6j} and Myo7a^{sh6j/sh6j} OHCs was 14 ± 1 nS (n = 23) and 2 ± 0.4 nS (n = 13) ($p < 0.0001$) respectively. A summary of these data can be seen in Figure 4-3C, D and E and **Error! Reference source not found.** The increased leak in the mature Myo7a^{+/sh6j} OHCs is likely to be due to the presence of the $I_{K,n}$ current in these cells, which is absent in the mature Myo7a^{sh6j/sh6j} OHCs. The $I_{K,n}$ current has a hyperpolarised activation range and is half activated at resting membrane potentials around -60 mV, this means that at rest a significant proportion of the current is activated. During the voltage step when the leak is measured this value is contaminated by the presence of the $I_{K,n}$ current, as the linear leak measurement is increased. The resting potential of the mature Myo7a^{+/sh6j} OHCs is -69 ± 2.1 mV (n = 12) and -62 ± 3 mV (n = 5) (NS) in the mature Myo7a^{sh6j/sh6j} OHCs suggesting that there is no difference in the resting membrane potential between the two cell types. The values for the resting membrane potential recorded here are comparable to those previously seen (Marcotti and Kros, 1999). A difference in the resting membrane potentials may have been expected due to the loss of the MET current which would cause the Myo7a^{sh6j/sh6j} OHCs to sit at a more hyperpolarised resting potential. However, this is not the case and may be explained by the concomitant loss of the $I_{K,n}$ current. As the $I_{K,n}$ current is activated at hyperpolarised potentials it is partially open at rest (Marcotti and Kros, 1999) and this current will then contribute to the resting membrane potential of the OHC making it more hyperpolarised. The lack of the $I_{K,n}$ current in the mature Myo7a^{sh6j/sh6j} OHCs means that the resting membrane potential will sit more depolarised than in the Myo7a^{+/sh6j} OHCs. As a consequence of losing both the MET current and the $I_{K,n}$ current the resting membrane potential may remain unaffected if the loss of both more or less cancels each other out.

4.2.4 Presence of prestin in the mature OHCs

Electromotility was seen in mature Myo7a^{+/sh6j} OHCs (16 out of 16 cells) (**Error! Reference source not found.**) and Myo7a^{sh6j/sh6j} OHCs (13 out of 13 cells) (**Error! Reference source not found.**). The white arrows in figures 4-5 and 4-6 outline the basal membrane of the OHC which is being recorded from at rest, the membrane potential is then stepped to +76 mV and the prestin in the cell membrane begins to contract causing a shortening of the cell body length, this is at its shortest length at time 750 ms (**Error! Reference source not found.**, 4-6 C) the membrane potential is then stepped back to -84 mV and the prestin in the cell membrane

beings to relax and the cell body elongates back to its resting position (**Error! Reference source not found.**, 4-6 E). Non-linear capacitance transients can be seen when there are changes to either the series resistance or whole cell capacitance of a cell whilst they are being recorded from. Non-linear capacitance transients can be seen in the traces in Figure 4-1C and D and are associated with the changes in whole cell capacitance with the electromotility of the mature OHC. The observed electromotility and presence of the non-linear capacitance transients suggests that the OHC adult marker protein prestin has been expressed in the mature Myo7a^{sh6j/sh6j} OHCs and that this developmental pathway is unaffected by the loss of function of the hair bundle.

4.2.5 Effect of linopirdine on the basolateral currents

Linopirdine is a known blocker of the KCNQ4 channel which carries the $I_{K,n}$ current (Marcotti and Kros, 1999). In the presence of linopirdine the size of the peak current is reduced and so the size of the $I_{K,n}$ current is also smaller. At -124 mV the steady state current in mature Myo7a^{+sh6j} OHCs -115 ± 107 pA ($n = 4$), the peak current is -175 ± 110 pA ($n = 4$) ($p = 0.0104$) and $I_{K,n}$ is -60 ± 7 pA ($n = 4$) ($p = 0.001$). At the same membrane potential in the presence of linopirdine mature Myo7a^{sh6j/sh6j} OHCs have a steady state current of -16 ± 33 pA ($n = 4$), a peak current of -60 ± 33 pA ($n = 4$) (NS) and $I_{K,n}$ is -44 ± 4 pA ($n = 4$) (NS). At -154 mV the steady state current in the presence of 100 μ M linopirdine in mature Myo7a^{+sh6j} OHCs is -140 ± 165 pA ($n = 4$) (NS) and -262 ± 184 pA ($n = 4$) ($p = 0.0173$) for the peak current, $I_{K,n}$ is calculated to be -121 ± 30 pA ($n = 4$) ($p = 0.0019$). The steady state current is -2 ± 44 pA ($n = 4$) (NS) and the peak current is -75 ± 44 pA ($n = 4$) (NS) in mature Myo7a^{sh6j/sh6j} OHCs in the presence of linopirdine and at -154 mV, $I_{K,n}$ is calculated to be -73 ± 7 pA ($n = 4$) (NS) (Figure 4-1F). A summary of this data can be seen in Figure 4-4 and **Error! Reference source not found.**. The IV plots in Figure 4-2 show that linopirdine reduces the peak and steady state currents in the mature Myo7a^{+sh6j} OHCs at membrane potentials negative to -80 mV, but has very little effect on these currents in the mature Myo7a^{sh6j/sh6j} OHCs. As linopirdine exerts a significant reduction on the $I_{K,n}$ current in the mature Myo7a^{+sh6j} OHCs and not the Myo7a^{sh6j/sh6j} OHCs the inward current present in the Myo7a^{sh6j/sh6j} is unlikely to be $I_{K,n}$, this confirms the results seen previously in that there is no $I_{K,n}$ current present in the mature Myo7a^{sh6j/sh6j} OHCs.

Application of 100 μ M linopirdine had no effect on the leak measured in the mature Myo7a^{sh6j/sh6j} OHCs 1.3 ± 0.1 nS ($n = 4$) (NS). However in the mature Myo7a^{+sh6j} OHCs the leak

was reduced significantly 3 ± 0.9 nS ($n = 4$) ($p = 0.0024$) in the presence of linopirdine, confirming that the increased leak measured in these mature cells is likely to be due to the $I_{K,n}$ current being active at these hyperpolarised (-154 mV) potentials.

4.3 Discussion

In similarity to the results found in the previous chapter with the IHCs the basolateral currents remain immature in the mature $Myo7a^{sh6j/sh6j}$ OHCs. This suggests that defects in the hair bundle are required for the development of the $I_{K,n}$ current in mature OHCs. As with the IHCs it is hypothesized that this developmental stunting may be due to the lack of the MET current causing hyperpolarisation of the resting membrane potential and a potential decrease in the intracellular concentration of calcium within the OHC cell body. In IHCs it has recently been discovered that under lower extracellular calcium concentrations, which are much closer to the physiological endolymph conditions, spontaneous spiking activity continues through into the second postnatal week of development (Johnson et al., 2012), it is feasible that this same thing happens in OHCs and that these cells are able to produce action potentials in the first postnatal weeks of development and that this activity is important in the electrical development of the OHCs.

I have shown that mature $Myo7a^{+/sh6j}$ OHCs are larger than $Myo7a^{sh6j/sh6j}$ OHCs, but that these cells are larger than those seen at a neonatal age, this may be due to the presence of prestin within the cellular membrane of the mature OHCs. Prestin is associated with an increase in the cell capacitance and so increase in cell size of the mature OHC. Given that the mature $Myo7a^{sh6j/sh6j}$ OHCs do possess electromotile behaviour, but have a cell capacitance smaller than typical mature OHCs and larger than typical neonatal OHCs it may be that the electromotile behaviour is smaller than that seen in wild type mature OHCs. However investigation of prestin levels in the mature $Myo7a^{+/sh6j}$ and $Myo7a^{sh6j/sh6j}$ is beyond the scope of this body of work.

It is intriguing that $Myo7a^{sh6j/sh6j}$ OHCs develop electromotility despite the basolateral currents remaining immature. This suggests that the programming for prestin development lies on a different pathway than that of the basolateral currents. Prestin is present in the cell membrane at low levels of expression in the neonatal OHCs (Belyantseva et al., 2000), therefore it may be that hair bundle function is required for the presence of new proteins and

or ion channels in the membrane but not for the up-regulation of proteins already present within the neonatal OHC cell membrane.

4.4 Conclusions

The adult marker current $I_{K,n}$ does not appear in the mature $\text{Myo7a}^{\text{sh6j/sh6j}}$ OHCs suggesting that Myo7a is required for the development of this current in the OHCs. The development of electromotility is not dependent on the presence of Myo7a as this does develop in the $\text{Myo7a}^{\text{sh6j/sh6j}}$ mature OHCs.

4.5 Future experiments

The voltage responses of the OHCs are known to change with development, resulting in smaller deviations from the resting membrane potential as the OHCs increase in age with the same size current injections (Marcotti and Kros, 1999). It would be interesting to find out if the voltage responses in the $\text{Myo7a}^{\text{sh6j/sh6j}}$ OHCs develop normally or remain immature.

The difference in the steady state currents seen in the neonatal OHCs here may be due in part to differences in the calcium currents. It would be interesting to further investigate this to find out if there is a difference in these currents. However, the calcium currents in neonatal OHCs are small and so it may be difficult to detect a difference in the current size.

It would also be interesting to look at slightly older OHCs (P20-30) to see whether the lack of development of the basolateral current described is due to a stunting of development or a delay in the development. Investigation of OHCs that are fully adult would be interesting, but it is likely that the cells would be far too fragile to be able to record from 6 months of age onwards.

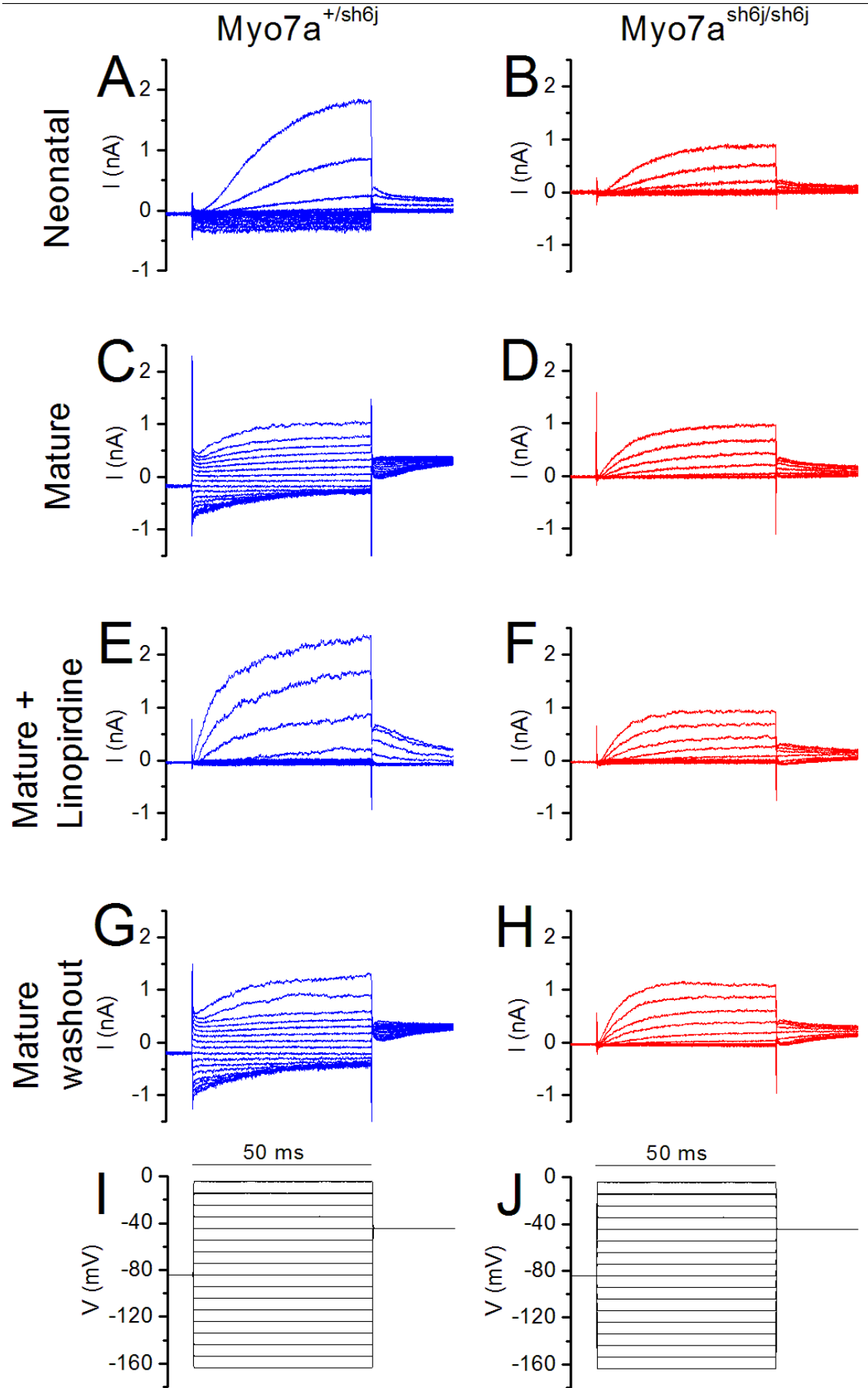


Figure 4-1 Steady state currents in neonatal and mature *Myo7a*^{+/sh6j} and *Myo7a*^{sh6j/sh6j} OHCs.

Figure 4-1 Steady state currents in neonatal and mature Myo7a^{+/sh6J} and Myo7a^{sh6J/sh6J} OHCs.

Typical whole cell current recordings seen in response to voltage steps in:

- A. Myo7a^{+/sh6J} neonatal OHC (C_m 6.9 pF, R_s 3.0 M Ω , Leak 9.3 nS, P2)
- B. Myo7a^{sh6J/sh6J} neonatal OHC (C_m 6.8 pF, R_s 3.4 M Ω , Leak 4.6 nS, P3)
- C. Myo7a^{+/sh6J} mature OHC (C_m 9.6 pF, R_s 3.4 M Ω , Leak 9.7 nS, P15)
- D. Myo7a^{sh6J/sh6J} mature OHC (C_m 6.6 pF, R_s 2.7 M Ω , Leak 0.5 nS, P11)
- E. Myo7a^{+/sh6J} mature OHC + linopirdine (C_m 7.8 pF, R_s 2.1 M Ω , Leak 2.3 nS, P15)
- F. Myo7a^{sh6J/sh6J} mature OHC + Linopirdine (C_m 6.1 pF, R_s 3.2 M Ω , Leak 1.5 nS, P11)
- G. Myo7a^{+/sh6J} mature OHC linopirdine washout (C_m 5.9 pF, R_s 4.5 M Ω , Leak 4.1 nS, P15)
- H. Myo7a^{sh6J/sh6J} mature OHC linopirdine washout (C_m 5.6 pF, R_s 3.1 M Ω , Leak 1.5 nS, P11)
- I. Voltage command
- J. Voltage command

Traces have been corrected for linear leak conductance assuming Ohms law, baselines haven't been adjusted to 0 pA.

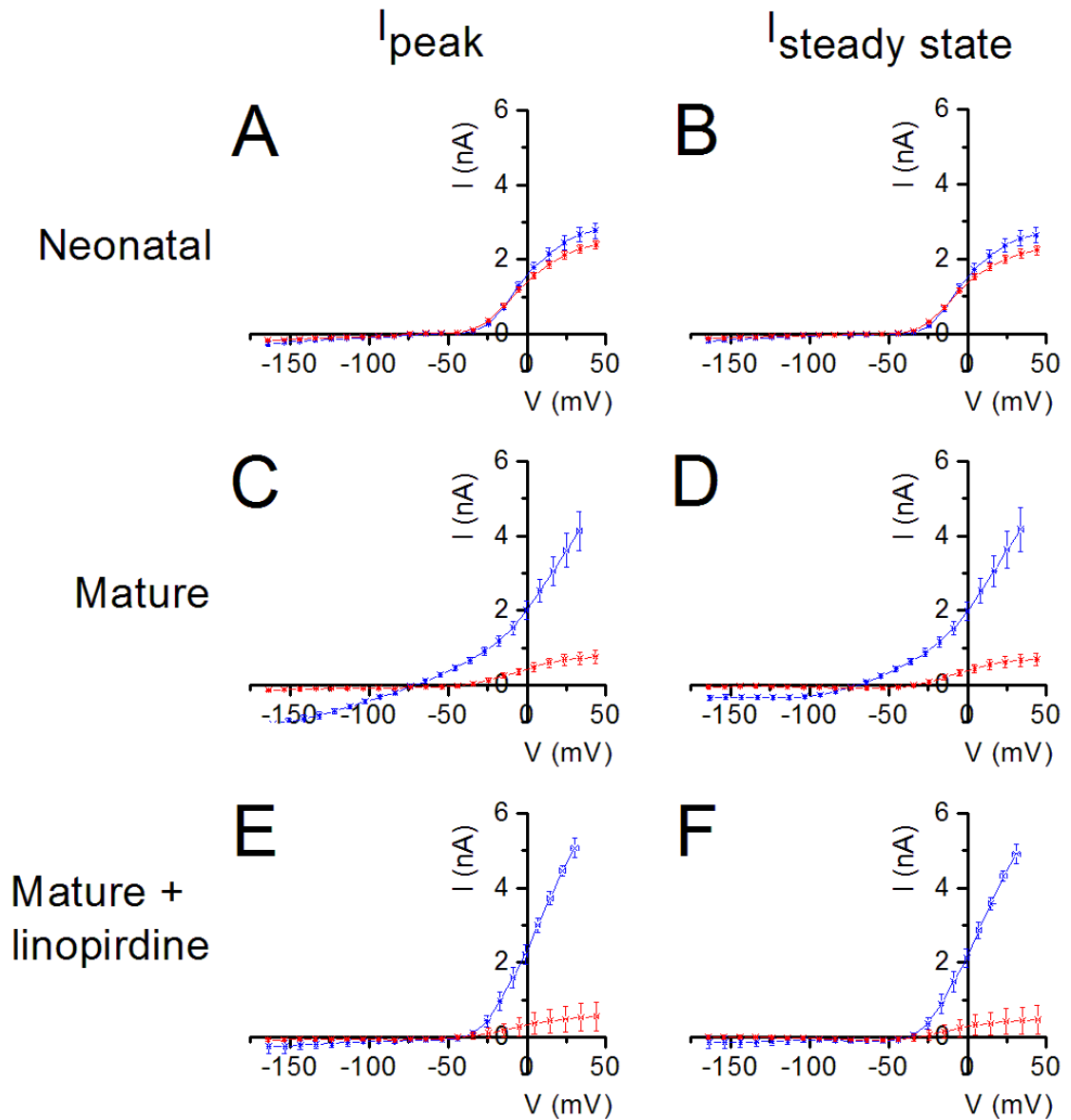


Figure 4-2 IV plots for the peak and steady state currents in neonatal and mature $Myo7a^{+/sh6j}$ and $Myo7a^{sh6j/sh6j}$ OHCs.

IV plots of the leak subtracted steady state and $I_{K,f}$ currents measured during the voltage step in:

- Peak currents in neonatal $Myo7a^{+/sh6j}$ (blue) ($n = 23$) and $Myo7a^{sh6j/sh6j}$ (red) ($n = 13$) OHCS
- Steady state currents in neonatal $Myo7a^{+/sh6j}$ (blue) ($n = 23$) and $Myo7a^{sh6j/sh6j}$ (red) ($n = 13$) OHCS
- Peak state currents in mature $Myo7a^{+/sh6j}$ (blue) ($n = 17$) and $Myo7a^{sh6j/sh6j}$ (red) ($n = 16$) OHCS
- Steady state currents in adult mature $Myo7a^{+/sh6j}$ (blue) ($n = 17$) and $Myo7a^{sh6j/sh6j}$ (red) ($n = 16$) OHCS
- Peak currents in mature $Myo7a^{+/sh6j}$ (blue) ($n = 4$) and $Myo7a^{sh6j/sh6j}$ (red) ($n = 4$) OHCS + linopirdine
- Steady state currents in mature $Myo7a^{+/sh6j}$ (blue) ($n = 4$) and $Myo7a^{sh6j/sh6j}$ (red) ($n = 4$) OHCS + linopirdine

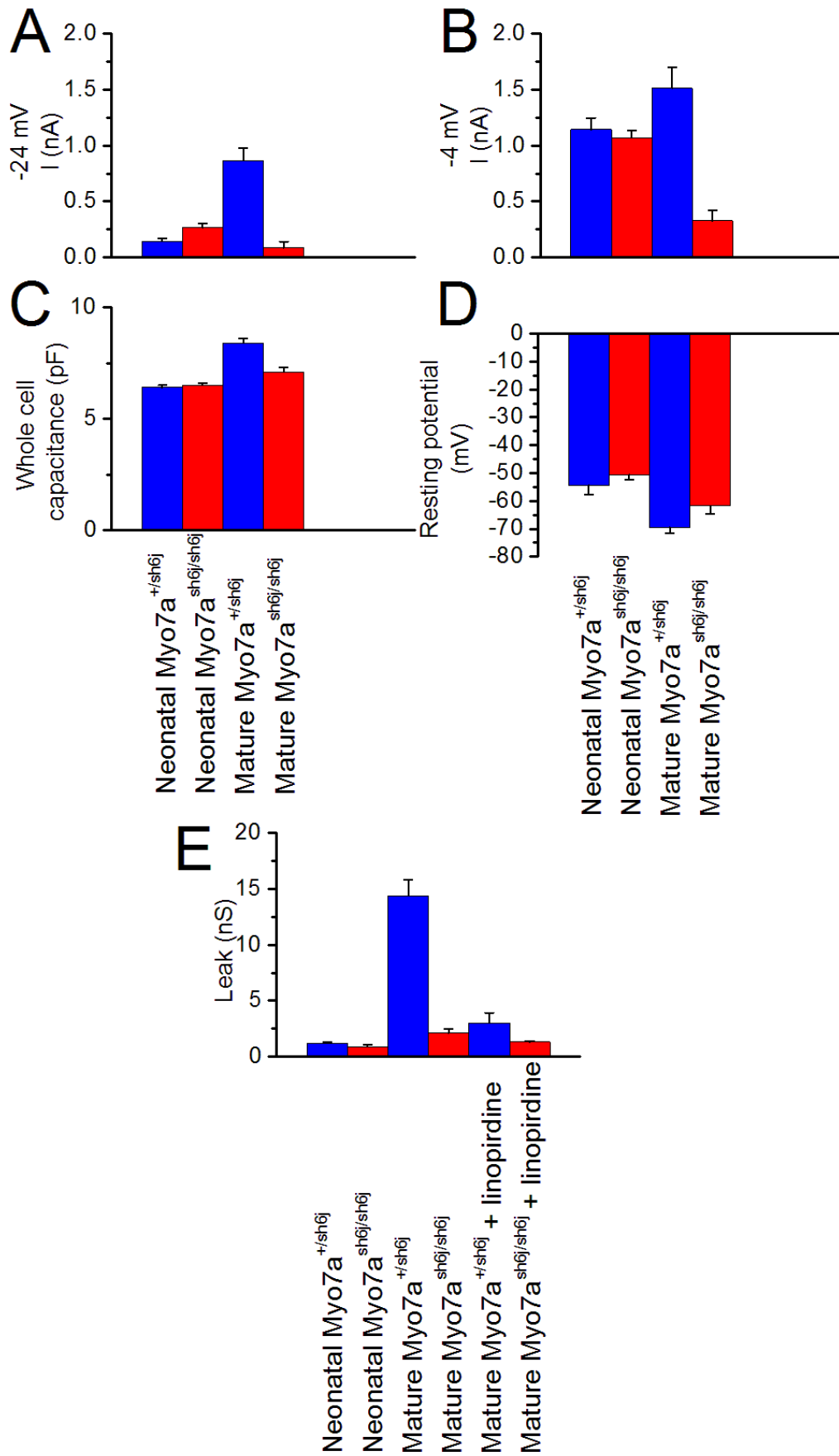


Figure 4-3 Bar graphs to represent the steady state currents at -24 mV, -4 mV, the whole cell capacitance, the resting membrane potential and the leak measurements.

Figure 4-3 Bar graphs to represent the steady state currents at -24 mV, -4 mV, the whole cell capacitance, the resting membrane potential and the leak measurements.

Leak subtracted current measurements for:

- A. Steady state currents at -24 mV (n = 17,16,23,13)
- B. Steady state currents at -4 mV (n = 17,16,23,13)
- C. Whole cell capacitance (n = 17,16,44,46)
- D. Resting membrane potential (n = 16,14,12,5)
- E. Leak measurements (n = 17,16,23,13)

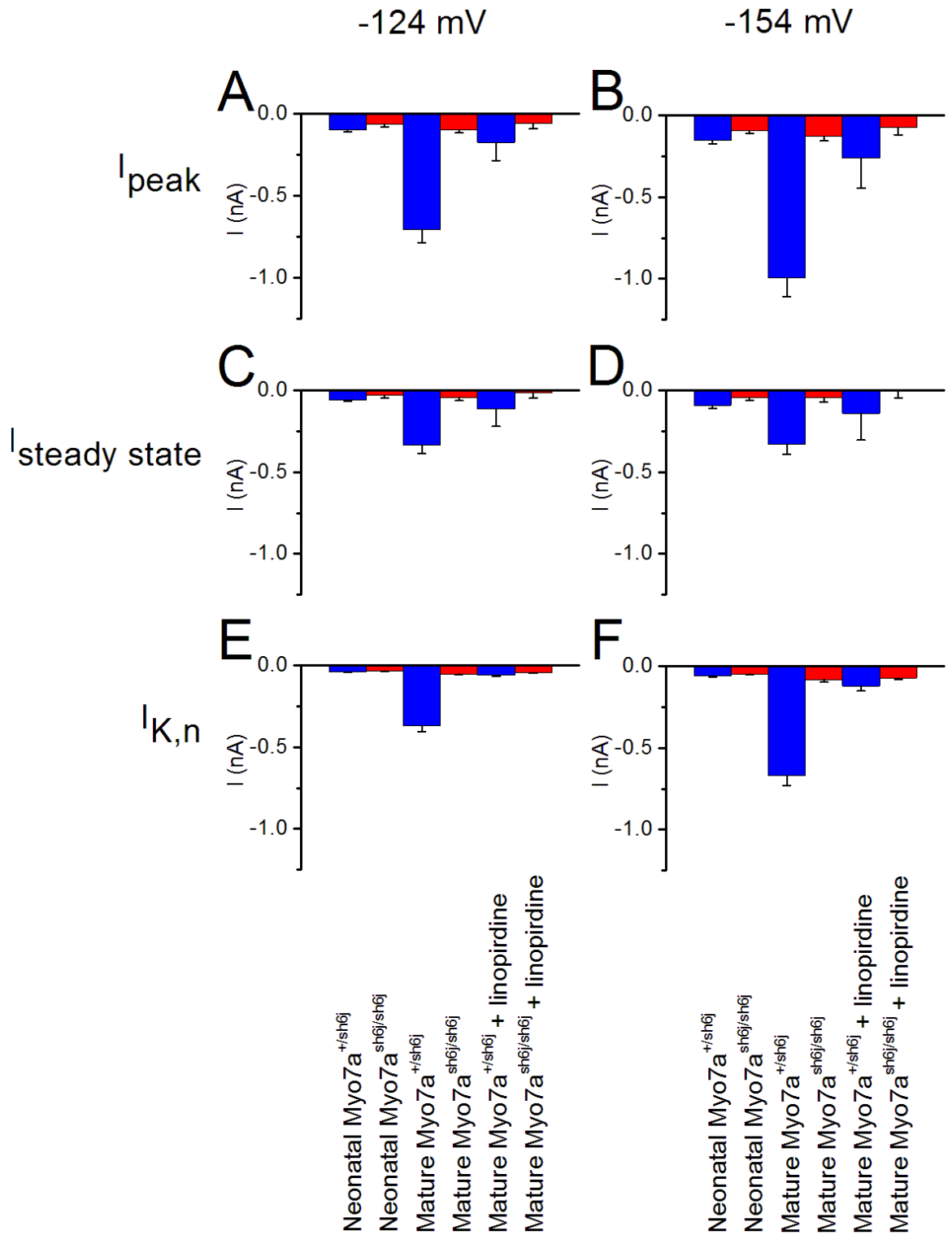


Figure 4-4 Bar graphs to show the peak, steady state and $I_{\text{K,n}}$ currents at -124 mV and -154 mV

Figure 4-4 Bar graphs to show the peak, steady state and $I_{K,n}$ currents at -124 mV and -154 mV.

- A. Peak currents at -124 mV (n = 17,16,23,13,4,4)
- B. Peak currents at -154 mV (n = 17,16,23,13,4,4)
- C. Steady state currents at -124 mV (n = 17,16,23,13,4,4)
- D. Steady state currents at -154 mV (n = 17,16,23,13,4,4)
- E. $I_{K,n}$ currents at -124 mV (n = 17,16,23,13,4,4)
- F. $I_{K,n}$ currents at -154 mV (n = 17,16,23,13,4,4)

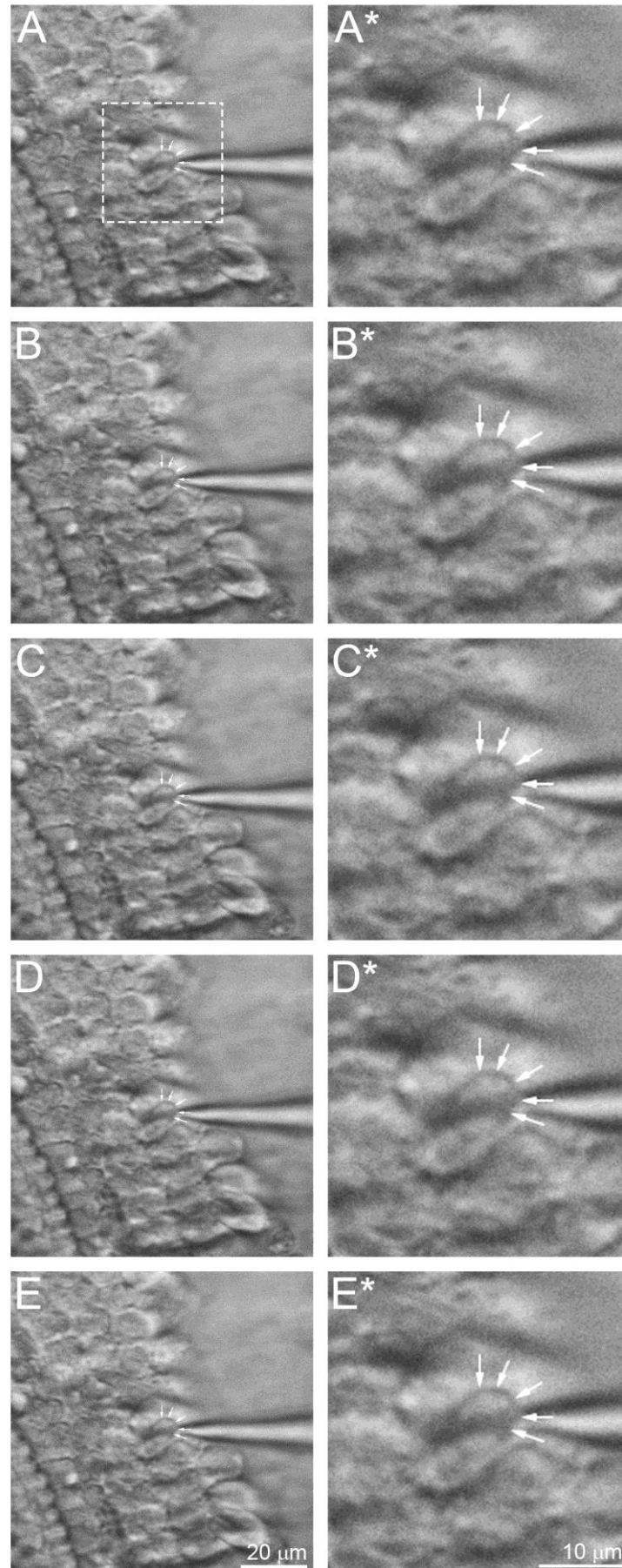


Figure 4-5 presence of electromotility – $Myo7a^{+/sh6j}$ electromotility movie.

Figure 4-5 presence of electromotility – Myo7a^{+sh6j} electromotility movie.

Electromotile response seen in P12 mature OHCs when the membrane potential is stepped from -84 mV to +76 mV. The white arrows mark the outline of the cell, the membrane of the cell pulls away from these markers during the depolarising step.

The OHC is held at -84 mV and is in a resting position, time 0 ms.

The OHC membrane potential has been stepped to +76 mV and the cell body is beginning to contract, time 500 ms.

The OHC membrane potential is still held at +76 mV and the cell body is fully contracted, time 750 ms.

The OHC membrane potential has been stepped back to -86 mV and the cell body is beginning to elongate, time 1000 ms.

The OHC membrane potential is still held at -84 mV and the cell body has elongated back to its resting position, times 1250 ms.

A*,B*,C*D* and E* are zoomed in images of the square outlined in A in A,B,C,D and E respectively and allow the small movements of the OHC cell body to be seen clearly.

The movie itself is attached to the accompanying C.D.

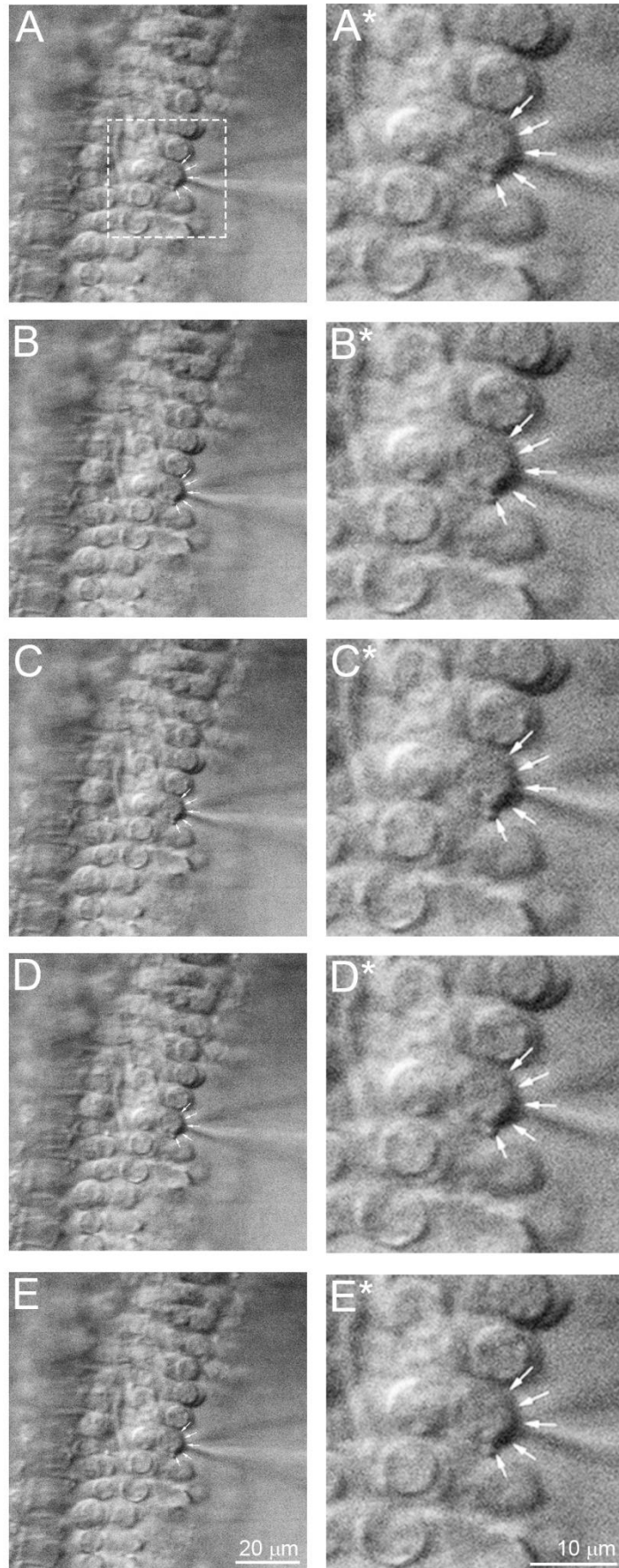


Figure 4-6 presence of electromotility – $Myo7a^{sh6j/sh6j}$ electromotility movie.

Figure 4-6 presence of electromotility – Myo7a^{sh6j/sh6j} electromotility movie.

Electromotile response seen in P12 mature OHCs when the membrane potential is stepped from -84 mV to +76 mV. The white arrows mark the outline of the cell, the membrane of the cell pulls away from these markers during the depolarising step.

The OHC is held at -84 mV and is in a resting position, time 0 ms.

The OHC membrane potential has been stepped to +76 mV and the cell body is beginning to contract, time 500 ms.

The OHC membrane potential is still held at +76 mV and the cell body is fully contracted, time 750 ms.

The OHC membrane potential has been stepped back to -86 mV and the cell body is beginning to elongate, time 1000 ms.

The OHC membrane potential is still held at -84 mV and the cell body has elongated back to its resting position, times 1250 ms.

A*,B*,C*D* and E* are zoomed in images of the square outlined in A in A,B,C,D and E respectively and allow the small movements of the OHC cell body to be seen clearly.

The movie itself is attached to the accompanying C.D.

	Neonatal				Mature				Mature + linopirdine			
	Myo7a ^{+/sh6j}		Myo7a ^{sh6j/sh6j}		Myo7a ^{+/sh6j}		Myo7a ^{sh6j/sh6j}		Myo7a ^{+/sh6j}		Myo7a ^{sh6j/sh6j}	
	mean ± SEM	n	mean ± SEM	n	mean ± SEM	n	mean ± SEM	n	mean ± SEM	n	mean ± SEM	n
C _{whole cell} (pF)	6.4 ±0.1	17	6.5 ±0.1	16	8.4 ±0.2	44	7.1 ±0.2	46				
V _m (mV)	-54.4 ±3.3	16	-50.6 ±1.8	14	-69.4 ±2.1	12	-61.8 ±2.9	5				
g _{leak} (nS)	1.2 ±0.1	17	0.9 ±0.2	16	14.4 ±1.4	23	2.1 ±0.4	13	3 ±0.9	4	1.3 ±0.1	4
I _{steady state} @-24mV (pA)	143.7 ±25.5	17	265.5 ±38.7	16	866.3 ±108.5	23	86.3 ±55.3	13				
I _{steady state} @-4mV (pA)	1143.6 ±101.3	17	1068.7 ±65.5	16	1512.4 ±187.7	23	326.3 ±91	13				
I _{steady state} @-124mV (pA)	-57.4 ±10.2	17	-30.2 ±15.6	16	-336.5 ±51	23	-46.3 ±17.5	13	-114.6 ±106.8	4	-15.7 ±33.1	4
I _{inward peak} @-124mV (pA)	-97.9 ±11.7	17	-62.9 ±15.6	16	-707.7 ±77.1	23	-98.4 ±18.5	13	-174.9 ±109.8	4	-60.1 ±32.6	4
I _{K,n} @-124mV (pA)	-40.5 ±3.5	17	-32.7 ±2.2	16	-371.2 ±34.2	23	-52.2 ±5.9	13	-60.2 ±6.8	4	-44.4 ±4.2	4
I _{steady state} @-154mV (pA)	-91.8 ±18.5	17	-45.9 ±17.1	16	-328 ±65.5	23	-46.9 ±25.6	13	-140.4 ±164.6	4	-2.3 ±44.3	4
I _{inward peak} @-154mV (pA)	-153 ±21.4	17	-94.9 ±17.5	16	-995.6 ±114.7	23	-128.9 ±27.5	13	-261.7 ±183.7	4	-75.2 ±43.5	4
I _{K,n} @-154mV (pA)	-61.2 ±5.8	17	-48.9 ±4.8	16	-667.5 ±64.6	23	-667.5 ±15.6	13	-121.2 ±30	4	-72.9 ±7.4	4

Table 4-1 Summary of the basolateral currents and cellular properties in the neonatal and mature OHCs

Steady state, Inward peak and I_{K,n} current measurements. All current measurements are mean ± SEM. All recordings were measured from a holding potential of -84 mV. Steady state currents were measured over 10 ms towards the end of the 50 ms voltage step. Peak currents were measured as the largest current seen during the 50 ms step. I_{K,n} is the subtraction between the two, I_{K,f} currents are averaged over 0.2 ms 0.7 ms after the step onset, I_{K,s} is the subtraction between the steady state and I_{K,f} current measurements

5 PRESENCE OF AN ACID SENSITIVE CURRENT IN THE HAIR CELLS

5.1 Introduction

Previous work (Ugawa et al., 2006) has shown that in the stereocilia of both the IHCs and OHCs an acid sensing ion channel (ASIC) is present. This work also shows that in the hair cells themselves the ASIC present is ASIC1b, ASIC1a expression is also found in organ of Corti but is not thought to be present in the hair cells (Ugawa et al., 2006). In this chapter I investigate the presence of an acid sensitive current in the hair cells by reducing the extracellular pH from 7.5 to 5.0 for a 10 second period and recording the resulting current. I also investigate the idea of this current being carried by the ASIC1b channel subtype by investigating the presence of an acid sensitive current in an ASIC1b knock out mouse model. It has been shown that ASIC currents are blocked by amiloride, (Waldmann et al., 1997) and nafamostat (Ugawa et al., 2007) with a IC_{50} of 20 μ M and 2.5 μ M, respectively. Both of these drugs have been shown to reduce the size of the inward peak current response to a reduction in the extracellular pH reversibly. The effects of these drugs on the acid sensitive current and the resting currents in the hair cells have also been investigated to help identify the channel carrying the acid sensitive current.

5.2 Results

All electrophysiology recordings were performed using standard ECS and K^+ ICS (see Table 2-1 and Table 2-2 for composition), the temperature was held at either 21°C (room temperature – RT) or 35°C (body temperature - BT) depending on the experimental condition.

5.2.1 Acid sensitive currents in the inner and outer hair cells

A reduction in the extracellular pH from 7.5 to 5.0 (Δ pH response) typically elicited an inward peak current followed by a smaller steady state current in ASIC1b^{+/+} neonatal IHCs and OHCs at both RT and BT. A large drop in extracellular pH from 7.5 to 5.0 was chosen to try and reduce the large variation in cell to cell responses to extracellular protons seen with these experiments. This large change in extracellular pH ensured that all ASICs were fully activated

during the ΔpH response, although not investigated it was assumed that smaller pH changes would activate the ASIC channels to a lesser extent and the proton depend current would be more variable. Typical responses can be seen in the left hand panel of Figure 5-1. Statistical comparisons were carried out using a two way ANOVA, significant differences were achieved with a p value of <0.05 (NS for non-significant differences $p >0.05$).

The inward peak current response (measured as the largest inward current during the step to pH 5.0 minus the baseline current before the step to pH 5.0 at pH 7.5) at a holding potential of -84 mV was for ASIC1b^{+/+} neonatal IHCs (P6) at RT -244 ± 55 pA (mean \pm SEM, $n = 25$) with a steady state current response (measured as the steady state current during ΔpH minus the baseline current at pH 7.5) of -16 ± 11 pA ($n = 25$) (Figure 5-1A). ASIC1b^{+/+} neonatal OHCs (P6) at RT the inward peak current response was -404 ± 133 pA ($n = 19$) and the steady state current response was 14 ± 11 pA ($n = 19$) (Figure 5-1C).

At BT ASIC1b^{+/+} neonatal IHCs have an inward peak current response of -122 ± 31 pA ($n = 11$) and a steady state current response of 0.4 ± 8 pA ($n = 10$) (Figure 5-1B). Neonatal OHCs have an inward peak current response of -372 ± 68 pA ($n = 24$) and a steady state current response of 16 ± 10 pA ($n = 23$) (Figure 5-1D).

When comparing the inward peak current responses between neonatal ASIC1b^{+/+} IHCs and OHCs, it is interesting to note that the current is almost double in size in OHCs compared to IHCs at both RT and BT, although this difference was not statistically significant. This is likely to be due to the high variation in the size of the inward peak current responses between individual cells. Although again there is no statistical difference between the steady state current responses of the IHCs and OHCs it is intriguing that this current in the IHCs is on average inward at RT and very small at BT whereas in the OHCs the steady state current is outward. The result being not significant is likely to be due to the high variation in the steady state current response between individual cells.

At BT the inward peak current response is ~ 100 pA smaller than at RT in both the ASIC1b^{+/+} neonatal IHCs and OHCs. This is known to be typical of ASIC ΔpH responses (Askwith et al., 2001). Although different ASIC subtypes respond differently to changes in temperature, larger inward peak current response are seen at lower temperatures ($6-22^\circ\text{C}$) when compared to 35°C . This difference may be a consequence of slower desensitization kinetics at room temperature, meaning that the conformational change the channel is required to undergo in

order to desensitize occurs over a longer time period at RT allowing a larger current to flow before the channels close.

Mature ASIC1b^{+/+} IHCs (P20 - 30) at BT have an inward peak current response of -44 ± 10 pA ($n = 13$) and a steady state current response of 18 ± 13 pA ($n = 11$) (Figure 5-1E). The mature ASIC1b^{+/+} IHCs have an inward peak current response much less than half the size of the neonatal IHCs at BT suggesting a developmental reduction in the size of the Δ pH response, although this did not reach statistical significance. This is likely to be due to the high variation in the size of the inward peak current responses between individual cells. The steady state current responses show no statistical difference in their size, but it is interesting to note that in neonatal IHCs this current varies little from the baseline current whereas in mature IHCs the average steady state response is outward. In mature IHCs the steady state current response recorded was typically an outward current; however in neonatal IHCs the steady state current response was variable between individual cells and was recorded as both an inward and an outward current when compared to the baseline current. Mature ASIC1b^{+/+} OHCs (P11 – 18) at RT have an inward peak current response of -56 ± 17 pA ($n = 10$) and a steady state current response of 58 ± 6 pA ($n = 10$) (Figure 5-1F). The inward peak current response in ASIC1b^{+/+} OHCs at RT do change significantly with age reducing from -404 ± 133 pA ($n = 19$) at P6 to -56 ± 17 pA ($n = 10$) at P11-18 ($p < 0.05$). The steady state current response, although not significantly different, does appear to change with development. Both steady state current responses are outward relative to the baseline current and 40 pA larger in the mature OHCs. The steady state current responses recorded in mature OHCs was always outwards, whereas in neonatal OHCs this current was quite variable and could be both inward and outward between individual cells compared to the baseline current. A summary of these data can be seen in Figure 5-7A and B and Table 5-1.

The acid sensitive currents recorded in an ASIC1b knock out mouse model will now be described as in ASIC1b^{-/-} IHCs and OHCs. The response seen is similar to that seen in the ASIC1b^{+/+} hair cells in that in neonatal IHCs and OHCs there is an inward peak current followed by a steady state current in response to a fall in the extracellular pH. Examples of typical responses can be seen in the right-hand panels of Figure 5-1.

At a holding potential of -84 mV ASIC1b^{-/-} neonatal IHCs at RT show an inward peak current response of -185 ± 35 pA ($n = 19$) and a steady state current response of 2 ± 5 pA ($n = 19$) (Figure 5-1G). ASIC1b^{-/-} neonatal OHCs at RT have an inward peak current response of -201 ± 39 pA ($n = 21$) and a steady state current response of 5 ± 5 pA ($n = 21$) (Figure 5-1I).

At BT ASIC1b^{-/-} neonatal IHCs have an inward peak current response of -48 ± 10 pA ($n = 14$) with a steady state current response of -14 ± 8 pA ($n = 13$) (Figure 5-1H). Neonatal ASIC1b^{-/-} OHCs at BT have a Δ pH response with an inward peak current response of -185 ± 27 pA ($n = 10$) and a steady state current response of 22 ± 6 pA ($n = 10$) (Figure 5-1J).

Although at RT there appears to be little difference in the size of the inward peak current response between the neonatal IHCs and OHCs, at BT the size of the inward peak current response appears to be much larger in OHCs than IHCs. The difference of over 100 pA is comparable to the difference in size seen between ASIC1b^{+/+} neonatal IHCs and OHCs at BT. This suggests that there might be a larger inward peak current response in the OHCs than in the IHCs (NS). The steady state current response in the ASIC1b^{-/-} neonatal IHCs and OHCs does not differ at RT. At BT however, the current does appear to be different (NS). The steady state current response is inward in the ASIC1b^{-/-} OHCs and outward in the IHCs. As previously mentioned the steady state current responses were quite variable and could be both inward and outward between individual cells. This is similar to the difference seen in the steady state currents between ASIC1b^{+/+} IHCs and OHCs.

Much like the ASIC1b^{+/+} IHCs, at BT the inward peak current response in the neonatal ASIC^{-/-} IHCs is much less than half the size of that seen at RT (NS). In ASIC1b^{-/-} neonatal OHCs there appears to be no temperature dependency on the size of the inward peak current response.

ASIC1b^{-/-} mature IHCs at BT show an inward peak current response to Δ pH of -28 ± 7 pA ($n = 16$) and a steady state current response of 17 ± 5 pA ($n = 16$) (Figure 5-1K). ASIC1b^{-/-} mature OHCs at RT have a Δ pH response of -22 ± 3 pA ($n = 5$) for the inward peak current response and 43 ± 8 pA ($n = 5$) for the steady state current response (Figure 5-1L). A summary of these data can be seen in Figure 5-7A and B and Table 5-1

Like the ASIC1b^{+/+} IHCs the ASIC1b^{-/-} IHCs show a developmental reduction (not statistically significant) in the peak inward current response at BT, with the peak current in response to Δ pH being about half the size in the mature IHCs when compared to the neonatal IHCs. There seems to be no difference in the steady state current response upon maturation in the ASIC1b^{-/-} IHCs. The peak inward current responses are reduced about 10-fold in the mature ASIC1b^{-/-} OHCs compared to their neonatal counterparts, a relative difference comparable to that seen in the ASIC1b^{+/+} OHCs (although not reaching statistical significance). This suggests a reduction in the size of the current as the OHCs develop. Although there is again no statistically significant difference in the steady state current responses between neonatal and mature ASIC1b^{-/-} OHCs at RT the currents reduce in size again by 40 pA from neonatal to mature when

compared to the baseline. Again this is likely to be due to the variation in the steady state current responses seen in the neonatal hair cells.

It is interesting to note that the current sizes in the ASIC1b^{-/-} hair cells are smaller than those in the ASIC1b^{+/+} hair cells when comparing both IHCs and OHCs in matching temperature conditions. Although these differences are not statistically significant it may suggest that the ASIC1b^{-/-} hair cells are not as sensitive to changes in the pH of their extracellular environment.

5.2.2 Effect of nafamostat on the pH sensitive current in the hair cells.

Reducing the extracellular pH from 7.5 to 5.0 in the presence of 100 μ M nafamostat evoked a current response which was much smaller than that seen without the presence of nafamostat. There was a small inward peak current response followed by a steady state response. Statistical comparisons were carried out using a two-tailed *t*-test, significant differences were achieved with a *p* value of <0.05 (NS for non-significant differences *p* >0.05).

Nafamostat reduced the size of the inward peak current recorded in all neonatal cell types and conditions suggesting that this component of the pH sensitive current is carried through ASIC channels. Nafamostat does not significantly change the steady state current response in any cell type or condition that was investigated, suggesting that the steady state current may be carried by a combination of non-ASIC pH sensitive ion channels.

At a holding potential of -84 mV ASIC1b^{+/+} IHCs at RT the Δ pH plus nafamostat inward peak current response is -7 ± 2 pA (*n* = 4) (*p* = 0.0002) and has a steady state current of 0 ± 4 pA (*n* = 4) (NS) (Figure 5-2A). ASIC1b^{+/+} OHCs at RT have an inward peak current response of -25 ± 12 pA (*n* = 3) (*p* = 0.0107) and a steady state current response of 71 ± 33 pA (*n* = 3) (NS) in response to Δ pH plus nafamostat (Figure 5-2C).

ASIC1b^{+/+} neonatal IHCs at BT show a Δ pH plus nafamostat inward peak current response of -41 ± 22 pA (*n* = 5) (*p* = 0.048) and a steady state current response of 7 ± 7 pA (*n* = 5) (NS) (Figure 5-2B). At BT ASIC1b^{+/+} neonatal OHCs show a Δ pH plus nafamostat response with an inward peak current response of -60 ± 26 pA (*n* = 6) (*p* = 0.0002) and a steady state current response of -21 ± 34 pA (*n* = 6) (NS) (Figure 5-2D).

Mature ASIC1b^{+/+} IHCs at BT in response to Δ pH plus nafamostat show an inward peak current response of -32 ± 8 pA (*n* = 4) (NS) and a steady state current response of 24 ± 16 pA (*n* = 4)

(NS) (Figure 5-2E). ASIC1b^{+/+} mature OHCs at RT have an inward peak current response of -33 ± 15 pA (n = 3) (NS) and a steady state current response of 79 ± 25 pA (n = 3) (NS) in response to Δ pH plus nafamostat (Figure 5-2F). A summary of these data can be seen in Table 5-1 and Figure 5-7C and D.

Neonatal ASIC1b^{-/-} IHCs at RT show a Δ pH plus nafamostat response with an inward peak current response of -23 ± 8 pA (n = 5) (p = 0.0002) and a steady state current response of 9 ± 5 pA (n = 5) (NS) (Figure 5-2G). Neonatal ASIC1b^{-/-} OHCs at RT show an inward peak current response of -8 ± 3 pA (n = 3) (p = <0.0001) and a steady state current response of 5 ± 1 pA (NS) (n = 3) in response to Δ pH 5.0 plus nafamostat (Figure 5-2I).

ASIC1b^{-/-} neonatal IHCs at BT show a Δ pH plus nafamostat inward peak current response of -8 ± 2 pA (n = 4) (p = 0.0016) and a steady state current response of 4 ± 3 pA (n = 4) (NS) (Figure 5-2H). Neonatal ASIC1b^{-/-} OHCs at BT have an inward peak current response of -18 ± 10 pA (n = 4) (p = 0.0002) and a steady state current response of 46 ± 2 pA (n = 4) (NS) in response to Δ pH plus nafamostat (Figure 5-2J).

Mature ASIC1b^{-/-} IHCs at BT respond to Δ pH plus nafamostat with an inward peak current response of -19 ± 17 pA (n = 3) (NS) and a steady state current response of 23 ± 9 pA (n = 3) (NS) (Figure 5-2K). ASIC1b^{-/-} mature OHCs at RT have an inward peak current response of -15 ± 2 pA (n = 3) (NS) and a steady state current response of 36 ± 10 pA (n = 3) (NS) in response to Δ pH plus nafamostat (Figure 5-2L). A summary of these data can be seen in Figure 5-7C and D and Table 5-1.

Nafamostat does not appear to affect the inward peak current response in mature ASIC1b^{+/+} and ASIC1b^{-/-} IHCs and OHCs with the peak currents being comparable in size both with and without the presence of nafamostat and Δ pH. This suggests the pH sensitive current in mature hair cells is carried through a non- pH sensitive ion channel.

5.2.3 Effect of amiloride on the pH sensitive current in the hair cells.

Reducing the extracellular pH in the presence of 100 μ M amiloride causes a current similar to that seen with Δ pH with nafamostat. The inward peak current is much reduced when compared to that seen with Δ pH only. Statistical comparisons were carried out using a two-

tailed *t*-test, significant differences were achieved with a *p* value of <0.05 (NS for non-significant differences *p* >0.05).

Amiloride reduced the size of the inward peak current in all cell types and conditions recorded from except neonatal ASIC^{+/+} and ASIC^{-/-} IHCs at BT and mature ASIC^{+/+} and ASIC^{-/-} IHCs and OHCs. Amiloride had no effect on the steady state currents in all cell types and conditions recorded from except neonatal ASIC^{+/+} IHCs at RT.

At a holding potential of -84 mV ASIC1b^{+/+} neonatal IHCs at RT have an inward peak current response of -21 ± 16 pA (*n* = 3) (*p* = 0.0029) and a steady state current response of 31 ± 11 pA (*n* = 3) (*p* = 0.0218) in response to Δ pH plus amiloride (Figure 5-3A). ASIC1b^{+/+} neonatal OHCs at RT have a Δ pH plus amiloride response of -65 ± 9 pA (*n* = 12) (*p* = 0.0014) for the inward peak current response and 9 ± 6 pA (*n* = 12) (NS) for the steady state current response (Figure 5-3C).

ASIC1b^{+/+} neonatal IHCs at BT show a Δ pH plus amiloride response with an inward peak current response of -9 ± 4 pA (*n* = 3) (NS) and a steady state current response of 8 ± 5 pA (*n* = 3) (Figure 5-3B). At BT neonatal ASIC1b^{+/+} OHCs have an inward peak current response of -72 ± 11 pA (*n* = 15) (*p* = 0.0005) and a steady state current response of 25 ± 7 pA (*n* = 15) (NS) in response to Δ pH plus nifedipine (Figure 5-3D).

Mature ASIC1b^{+/+} IHCs at BT show an inward peak current response of -12 ± 4 pA (*n* = 4) (NS) and a steady state current response of 4 ± 2 pA (*n* = 4) (NS) to Δ pH plus amiloride (Figure 5-3E). ASIC1b^{+/+} OHCs at RT in response to Δ pH plus amiloride show an inward peak current response of -28 ± 8 pA (*n* = 5) (NS) and a steady state current response of 69 ± 20 pA (*n* = 5) (NS) (Figure 5-3F). A summary of these data can be seen in Figure 5-7E and F and Table 5-1.

ASIC1b^{-/-} neonatal IHCs at RT have a Δ pH plus amiloride response of -53 ± 20 pA (*n* = 7) (*p* = 0.0006) for the inward peak current response and -4 ± 4 pA (*n* = 7) (NS) for the steady state current response (Figure 5-3G). Neonatal ASIC1b^{-/-} OHCs at RT have an inward peak current response of -51 ± 13 pA (*n* = 9) (*p* = 0.0201) and a steady state current response of 16 ± 8 pA (*n* = 9) (NS) in response to Δ pH plus amiloride (Figure 5-3I).

ASIC1b^{-/-} neonatal IHCs at BT respond to Δ pH plus amiloride with an inward peak current response of -41 ± 13 pA (*n* = 3) (NS) and a steady state current response of -17 ± 4 pA (*n* = 3) (NS) (Figure 5-3H). ASIC1b^{-/-} neonatal OHCs at BT have an inward peak current response of -42 ± 5 pA (*n* = 3) (*p* = 0.0002) and a steady state current response of 13 ± 3 pA (*n* = 3) (NS) to Δ pH plus amiloride (Figure 5-3J).

Mature ASIC1b^{-/-} IHCs at BT have a Δ pH plus amiloride response with -17 ± 5 pA (n = 4) (NS) for the inward peak current response and 2 ± 8 pA (n = 4) (NS) for the steady state current response (Figure 5-3K). ASIC1b^{-/-} mature OHCs at RT respond to Δ pH plus amiloride with an inward peak current response of -13 ± 3 pA (n = 3) (NS) and a steady state current response of 59 ± 16 pA (n = 3) (NS) (Figure 5-3L).

5.2.4 Effect of nafamostat on the resting current in the hair cells.

There is no significant difference between the inward peak current response seen during the application of nafamostat and that seen during Δ pH plus nafamostat in any of the recording conditions.

Maintaining the extracellular pH at 7.5 but applying 100 μ M nafamostat causes the inward baseline current recorded in hair cells at a holding potential of -84 mV to be reduced. ASIC1b^{+/+} neonatal IHCs at RT had an inward peak current response of -10 ± 7 pA (n = 3) (NS) and a steady state current response of 35 ± 8 pA (n = 3) in response to the application of nafamostat (Figure 5-4A). ASIC1b^{+/+} neonatal OHCs at RT responded to nafamostat with an inward peak current response of -11 ± 4 pA (n = 6) (NS) and a steady state current response of -1 ± 3 pA (n = 6) (Figure 5-4C).

At BT ASIC1b^{+/+} IHCs respond to application of nafamostat with an inward peak current response of -16 ± 7 pA (n = 3) (NS) and a steady state current response of 30 ± 13 pA (n = 3) (Figure 5-4B). ASIC1b^{+/+} OHCs respond with an inward peak current response of -7 ± 7 pA (n = 11) (NS) and a steady state current response of 45 ± 12 pA (n = 11) (Figure 5-4D).

Mature ASIC1b^{+/+} IHCs at BT have an inward peak current response of -11 ± 4 pA (n = 4) (NS) and a steady state current response of 14 ± 8 pA (n = 8) during application of nafamostat (Figure 5-4E). ASIC1b^{+/+} mature OHCs at RT respond to nafamostat with an inward peak response of -29 ± 15 pA (n = 4) (NS) and a steady state current response of 107 ± 20 pA (n = 4) (Figure 5-4F). A summary of these data can be seen in Figure 5-8 and Table 5-1.

ASIC1b^{-/-} neonatal IHCs at RT have an inward peak current response of -16 ± 8 pA (n = 4) (NS) and a steady state current response of 12 ± 2 pA (n = 4) in response to nafamostat (Figure 5-4G). Neonatal ASIC1b^{-/-} OHCs at RT respond to nafamostat with an inward peak current response of -12 ± 4 pA (n = 3) (NS) and a steady state current response of 30 ± 10 pA (n = 3) (Figure 5-4).

At BT ASIC1b^{-/-} neonatal IHCs respond to nafamostat with an inward peak current response of -9 ± 2 pA ($n = 3$) (NS) and a steady state current response of 14 ± 5 pA ($n = 3$) (Figure 5-4H). ASIC1b^{-/-} neonatal OHCs respond with an inward peak current response of -10 ± 7 pA ($n = 3$) (NS) and a steady state current response of 23 ± 4 pA ($n = 3$) (Figure 5-4J).

Application of nafamostat causes an inward peak current response of -9 ± 3 pA ($n = 3$) (NS) and a steady state current response of 24 ± 2 pA ($n = 3$) in mature ASIC1b^{-/-} IHCs at BT (Figure 5-4K). ASIC1b^{-/-} mature OHCs at RT respond to nafamostat with an inward peak current response of -10 ± 4 pA ($n = 3$) (NS) and a steady state current response of 90 ± 35 pA ($n = 3$) (Figure 5-4L). A summary of these data can be seen in Table 5-1 and Figure 5-8

5.2.5 Effect of amiloride on the baseline currents in the hair cells.

Applying 100 μ M amiloride to the hair cells whilst maintaining the extracellular pH at pH 7.5 evokes a current response similar to what is seen with the application of nafamostat at pH 7.5. There is very little inward peak current response and a sustained steady state current response is seen with a similar magnitude as was seen in previous conditions. There is no significant difference between the inward peak current response seen during the application of amiloride and that seen during Δ pH plus amiloride in any of the recording conditions.

ASIC1b^{+/+} neonatal IHCs at RT had an inward peak current response of -4 ± 3 pA ($n = 3$) (NS) and a steady state current response of 4 ± 3 pA ($n = 3$) (Figure 5-5A). Neonatal ASIC1b^{+/+} OHCs at RT showed an inward peak response of -33 ± 4 pA ($n = 3$) (NS) and a steady state current response of 3 ± 5 pA ($n = 3$) during the application of amiloride (Figure 5-5C).

At BT ASIC1b^{+/+} neonatal IHCs responded to amiloride with an inward peak current response of -13 ± 3 pA ($n = 3$) (NS) and steady state current response of 0 ± 2 pA ($n = 3$) (Figure 5-5B) shows a typical example of this response. ASIC1b^{+/+} neonatal OHCs responded with an inward peak current response of -9 ± 2 pA ($n = 3$) (NS) and a steady state current response of 9 ± 3 pA ($n = 3$) (Figure 5-5D).

Mature ASIC1b^{+/+} IHCs at BT responded to the application of amiloride with an inward peak current response of -49 ± 23 pA ($n = 3$) (NS) and a steady state current response of 10 ± 9 pA ($n = 3$) (Figure 5-5E). ASIC1b^{+/+} mature OHCs had an inward peak current response of -36 ± 29 pA ($n = 3$) (NS) and a steady state current response of 110 ± 35 pA ($n = 3$) in

response to amiloride (Figure 5-5F). A summary of these data can be seen in Figure 5-8 and Table 5-1.

ASIC1b^{-/-} neonatal IHCs at RT responded to amiloride with an inward peak current response of -21 ± 9 pA (n = 3) (NS) and a steady state current response of 16 ± 3 pA (n = 3) (Figure 5-5G). Neonatal ASIC1b^{-/-} OHCs at RT had an inward peak current response of -8 ± 1 pA (n = 3) (NS) and a steady state current response of 1 ± 1 pA (n = 3) in response to amiloride (Figure 5-5I).

Neonatal ASIC1b^{-/-} IHCs at BT had an inward peak current response of -6 ± 4 pA (n = 4) (NS) and a steady state current response of 6 ± 3 pA (n = 4) in response to amiloride (Figure 5-5H). At BT ASIC1b^{-/-} neonatal OHCs responded to amiloride with an inward peak current response of -22 ± 4 pA (n = 3) (NS) and a steady state current response of 5 ± 2 pA (n = 3) (Figure 5-5J).

ASIC1b^{-/-} mature IHCs at BT responded to amiloride with an inward peak current response of -18 ± 5 pA (n = 4) (NS) and a steady state current response of 27 ± 15 pA (n = 4) (Figure 5-5K). Mature ASIC1b^{-/-} OHCs at RT had an inward peak current response of -10 ± 10 pA (n = 3) (NS) and a steady state current response of 28 ± 13 pA (n = 3) in response to amiloride (Figure 5-5L). A summary of these data can be seen in Figure 5-8 and Table 5-1.

5.3 Discussion

Despite previous publications finding that although other classes of ASIC channels are present in the organ of Corti, only ASIC1b is found in the hair cells (Ugawa et al., 2006), an acid sensitive current is clearly still present in the ASIC1b^{-/-} hair cells, although confirmation of lack of ASIC1b expression in these mouse models is required by genotyping. This suggests that the currents elicited in response to lowering the extracellular pH may be carried by a different channel as yet unidentified or that the cells are able to substitute another channel if the ASIC1b channel is not available. This current may well be carried by another acid sensitive channel of which two have been reported in the hair cells. The first is a type of TRP channel (Suzuki et al., 2003). Although activated by an increase in H⁺ ions which would show as an inward current, the current produced by these channels is sustained and does not desensitize as seen in my recordings, and so it is unlikely that the currents recorded here are carried by TRP channels. The second channel type which is pH sensitive are the P2X receptors, which can be both potentiated and inhibited by changes in the extracellular pH (Burgard et al., 1999).

However, the currents recorded here are unlikely to be carried by this channel as H^+ itself merely modulates the P2X current and increases in the extracellular ATP concentration would also be required in order to activate the channel. ATP concentration should not be changing between experimental conditions as all extracellular solutions have no ATP in them and so release from surrounding cells should have minimal effect and it would be very unlikely for such effects to be timed with application of ΔpH . As neither of these channels are likely to carry the pH sensitive current seen it is most likely that the currents are indeed being carried by an ASIC channel. Work by Donier et al. (2008) has shown that in CHO-K1 cells up-regulation of ASIC4 protein expression results in a decrease in the expression of both ASIC1b and ASIC3. It is not unreasonable to speculate that lack of expression of ASIC1b in the ASIC1b^{-/-} mouse models may result in the up-regulation in expression of one or more of the other ASIC subtypes and that it is this which is carrying the acid sensitive current in the ASIC1b^{-/-} hair cells. Changes in the ASIC channel subtype that are carrying the channel may change features of the current itself, and may explain why the current is smaller (albeit not significantly so) in the ASIC1b^{-/-} hair cells.

Nafamostat does not appear to affect the inward peak current response in mature ASIC1b^{+/+} and ASIC1b^{-/-} IHCs and OHCs with the peak currents being comparable in size both with and without the presence of nafamostat and ΔpH . This is likely to be due to the inward peak current response measured in both the mature hair cells and in the presence of both amiloride and nafamostat being a consequence of the data analysis technique. The inward peak current response is defined as the largest inward current during the 10 second drug application minus the steady state current prior to drug application. This procedure will measure a peak current response even without the presence of a true peak current; when the inward peak current response is small it is likely to be measuring noise within the steady state current. In these conditions very small inward peak current responses are seen and so the measurements made here are likely to be noise within the experimental and analytical techniques.

Nafamostat does not significantly change the steady state current response in any cell type or condition that was investigated, suggesting that the steady state current may be carried by a combination of non-ASIC pH sensitive ion channels. The steady state current response to lowering the pH in ASIC1b^{-/-} neonatal IHCs and OHCs at RT is not significantly affected by the presence of nafamostat, thus supporting this hypothesis, however neonatal IHCs and OHCs at BT do have a smaller outward steady state current response in the presence of nafamostat. This suggests that loss of the ASIC1b channel causes temperature sensitivity due to the effect of nafamostat on the steady state current. Nafamostat does not significantly change the

steady state current response in ASIC1b^{+/+} and ASIC1b^{-/-} mature IHCs and OHCs, again supporting the idea that this current may be carried by multiple channel types.

Amiloride blocks the inward peak current response in all ASIC1b^{+/+} neonatal IHCs at RT, OHCs at RT and OHCs at BT and ASIC1b^{-/-} neonatal IHCs at RT, OHCs at RT and OHCs at BT, reducing the size of the peak current response. Amiloride does not appear to affect the inward peak current response in neonatal ASIC1b^{+/+} and ASIC1b^{-/-} IHCs at BT, mature ASIC1b^{+/+} and ASIC1b^{-/-} IHCs and OHCs with the peak current responses being comparable in size both with and without the presence of nafamostat and Δ pH. This is probably again because there is little inward peak current with Δ pH to block with amiloride, and the inward peak current response measured in both the mature IHCs and in the presence of amiloride being associated with noise rather than a definite inward peak current response.

The steady state current response seen with Δ pH plus amiloride does not seem to differ when compared to the response seen with Δ pH in ASIC1b^{+/+} neonatal IHCs at BT, OHCs at RT and BT, mature IHCs at BT and OHCs at RT and ASIC1b^{-/-} neonatal IHCs and OHCs at RT and BT and mature IHCs and OHCs. Interestingly ASIC1b^{+/+} neonatal IHCs at RT do show a significant difference in the steady state current response with Δ pH with and without amiloride.

There is no significant difference between the inward peak current response seen during the application of nafamostat and that seen during Δ pH plus nafamostat in any of the recording conditions. This is likely to be due to the inward peak current responses measured here being noise rather than a true inward peak current. This is also true for the inward peak current response measured during Δ pH plus amiloride and during the application of amiloride alone. The size of the inward peak current response also remains unchanged between nafamostat and amiloride conditions. During application of either nafamostat or amiloride alone the ASIC should not be activated and so no inward peak current response should be measurable suggesting that these measurements are an artefact of the analytical technique. If this is indeed true then there is also no inward peak current response found in Δ pH with either nafamostat or amiloride. In mature hair cells of both phenotypes there is no significant difference between the size of the inward peak current response during Δ pH and Δ pH plus either nafamostat and amiloride. This suggests that there is no true ASIC inward peak current response present in the mature hair cells, this maybe because the ASIC channel disappears during development. Work by Ugawa et al. (2006) shows that at P7 there is expression of ASIC1b channels, however expression has not been investigated at older ages and so there

may well be down regulation of the ASIC1b protein upon maturation. It is also possible that the acid sensitive current is being carried through a different channel type in the mature hair.

It is unlikely that blockage of the MET current by either nafamostat or amiloride (see section 6.2.7) is responsible for the outward steady state current response. The steady state current responses are not different between ΔpH and ΔpH plus either nafamostat or amiloride in both ASIC1b^{+/+} and ASIC1b^{-/-} hair cells, therefore it is unlikely that the reduction in the baseline current is a result of a reduction of the MET current. As the MET channel has a finite probability of being open at rest blockers of the channel would decrease this probability and so there will be a slight reduction in the resting baseline current. As I have shown that (section 6.2.7), as well as amiloride, nafamostat is also a blocker of the MET channel this is one explanation for the smaller steady state current response seen during ΔpH plus either amiloride or nafamostat. However as I have also shown that ΔpH has no effect on the transduction currents, the smaller steady state current response compared to the baseline current seen during ΔpH cannot be attributed to closure of the MET channel. It is typical of ASIC currents to desensitize (Askwith et al., 2001), but it is unusual for the steady state current responses to be outward relative to the baseline current. Typically the steady state current responses are inward relative to the baseline currents. One possible reason for this is other channels that are regulated by H⁺ in the hair cells. It is well documented that TRPV1 and TRPV4 channels can be activated by a decrease in the extracellular pH (Suzuki et al., 2003). As these channels carry a non-specific cation current, activation would cause an inward current at a holding potential of -84 mV and so the steady state current response would be a larger inward current than the baseline current. It is also known that P2X receptors, present in the hair cells, can be modulated by changes in the extracellular pH (Burgard et al., 1999). The presence of H⁺ can potentiate the P2X current in the additional presence of ATP. H⁺ alone can activate the P2X receptor but this current is small (Burgard et al., 1999). Given that it is unlikely that intrinsic extracellular ATP concentrations are high enough to activate these channels in a sustained manner at rest (Johnson et al., 2011), it is doubtful that inhibition of the P2X receptors would have a noticeable effect of the currents during ΔpH . As to the best of my knowledge there are no further pH sensitive ion channels present in the hair cells, the reduction in the steady state currents when compared to the baseline during ΔpH can best be explained by complete desensitization of ASIC channels that are somewhat open at a resting pH of 7.5. This desensitization would cause closure of channels that are opened in response to ΔpH as well as those that are open at rest, causing a reduction in the inward current that is recorded.

5.4 Conclusions

In this chapter I have shown that there is an acid sensitive current present in mouse hair cells in the organ of Corti. In neonatal IHCs and OHCs there is a large inward peak current which desensitizes to a steady state level typical of a current carried through ASIC. I have shown the presence of a proton-dependent current in mature IHCs and OHCs but can be less certain of the channel carrying this current. I have, using ASIC1b^{-/-} mice, shown that the current is not carried by purely ASIC1b channels despite previous evidence suggesting this to be the only subtype found in the hair cells. I have also shown block of this channel by nafamostat and amiloride, typical ASIC blockers.

5.5 Future experiments

As this work on ASIC1b^{-/-} hair cells has proved inconclusive as to the channel carrying the acid sensitive current future work should focus on identifying the ASIC channel subtype. The effect of specific subtype blockers such as psalmotoxin 1 (PcTx1) could be used to implicate or eliminate ASIC1a (Chen et al., 2005). The formation of heteromers (Askwith et al., 2004) between ASIC variants has been shown in other cell types with heteromers between ASIC1a and ASIC2a being most common in the CNS (Chen et al., 2005) and may complicate the responses that are seen. It has also been shown that PcTx1 may promote the acid sensitive current carried by ASIC1b channels, which could make data interpretation difficult (Chen et al., 2006). Another method that could be used to identify channel subtypes is to use varying sizes of ΔpH : ASIC1 and ASIC3 are much more sensitive to changes in the extracellular pH, as inward currents can be seen with a reduction in the pH of -0.4 and -0.2 respectively from a holding pH of 7.4 whereas ASIC2 has an activation pH of 6. Again, these experiments may be complicated if heteromers are present and would be less definitive than specific drug blockade.

The production of action potentials is well documented in the neonatal IHCs (Kros et al., 1998; Marcotti et al., 2003a, 2003b). Activation of ASIC would at first depolarise the hair cell potentially triggering this activity and then with an outward steady state current cause a hyperpolarisation which may reduce the likelihood of action potential generation. An inward steady state current would cause sustained depolarisation and increase the likelihood of action potential generation. Given that I have shown in previous chapters the importance of action

potential activity on the development of the hair cells it would be interesting to investigate the effects of ΔpH on this activity in the neonatal IHCs.

As I previously described, TRP channels are present in the hair cells and are known to have some H^+ dependence (Suzuki et al., 2003). To exclude TRP channel activity from the acid sensitive current identified here it would be interesting to examine the effects of capsazepine, a blocker of TRP channels (Peier et al., 2002), on the pH sensitive current in the hair cells.

Another way of determining if there is a second channel carrying an acid sensitive current is to change the pH of the extracellular environment with either nafamostat or amiloride already present and blocking ASICs. If a current can be recorded then it is likely that the H^+ sensitive current is not solely carried by ASIC.

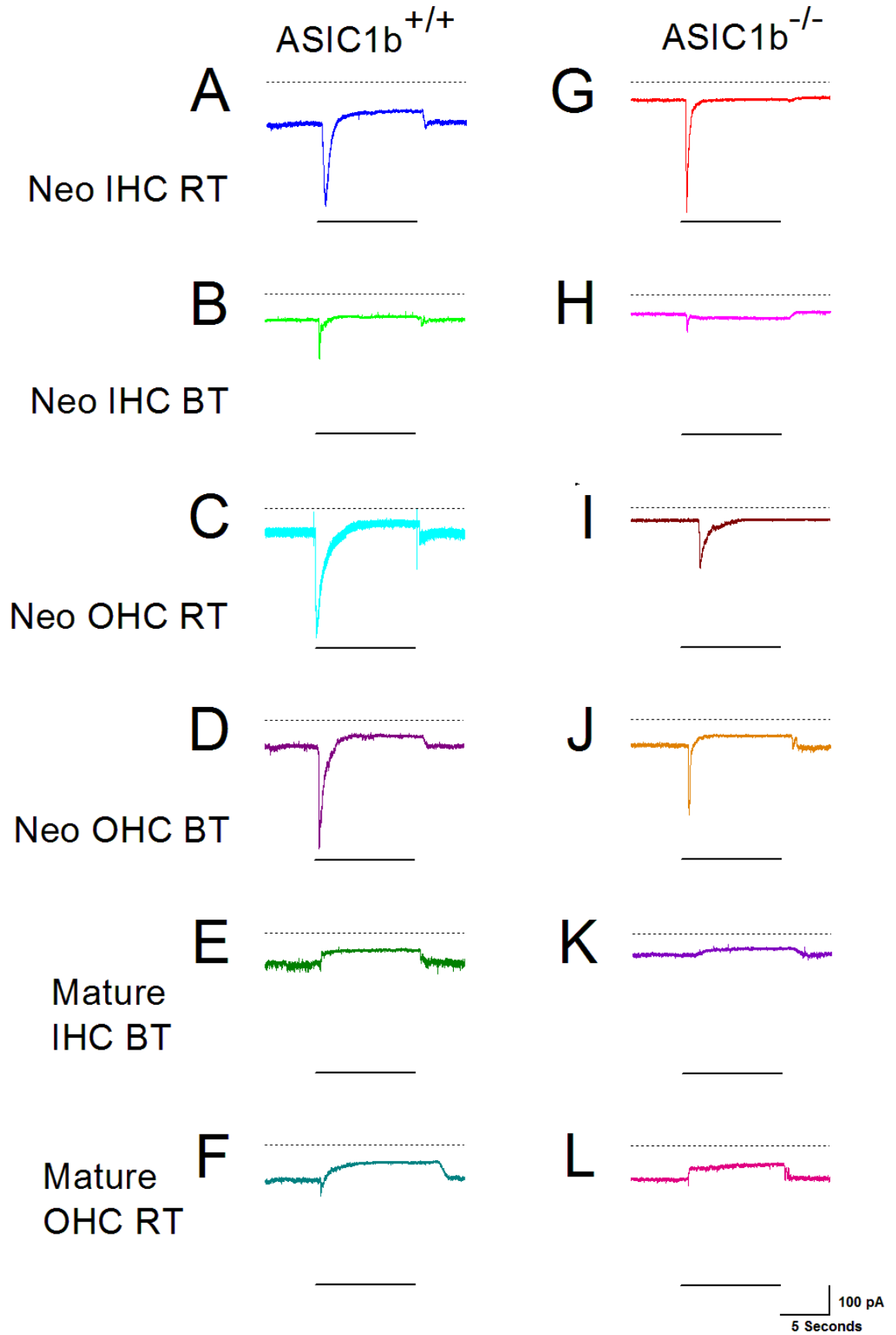


Figure 5-1 Representative examples of the current response seen when the pH of the extracellular solution is dropped from pH 7.5 to pH 5.0.

Figure 5-1 Representative examples of the current response seen when the pH of the extracellular solution is dropped from pH 7.5 to pH 5.0.

Typical whole-cell current recordings seen when the extracellular pH was changed from pH 7.5 to pH 5.0 for ~10 seconds as shown by a solid black line in:

- A. *Asic1b*^{+/+} Neonatal IHC at 21°C (C_m 9.6 pF, R_s 0.72 M Ω)
- B. *Asic1b*^{+/+} Neonatal IHC at 35°C (C_m 8.3 pF, R_s 2.22 M Ω)
- C. *Asic1b*^{+/+} Neonatal OHC at 21°C (C_m 5.4 pF, R_s 0.84 M Ω)
- D. *Asic1b*^{+/+} Neonatal OHC at 35°C (C_m 5.2 pF, R_s 0.62 M Ω)
- E. *Asic1b*^{+/+} Adult IHC at 35°C (C_m 13.8 pF, R_s 2.8 M Ω)
- F. *Asic1b*^{+/+} Adult OHC at 21°C (C_m 6.0 pF, R_s 0.96 M Ω)
- G. *Asic1b*^{-/-} Neonatal IHC at 21°C (C_m 8.7 pF, R_s 0.9 M Ω)
- H. *Asic1b*^{-/-} Neonatal IHC at 35°C (C_m 7.9 pF, R_s 0.84 M Ω)
- I. *Asic1b*^{-/-} Neonatal OHC at 21°C (C_m 5.9 pF, R_s 0.86 M Ω)
- J. *Asic1b*^{-/-} Neonatal OHC at 35°C (C_m 5.1 pF, R_s 1.12 M Ω)
- K. *Asic1b*^{-/-} Adult IHC at 35°C (C_m 11.8 pF, R_s 0.96 M Ω)
- L. *Asic1b*^{-/-} Adult OHC at 21°C (C_m 6.2 pF, R_s 1.82 M Ω)

Traces have not been corrected for linear leak conductance and baselines have not been adjusted to zero. 0 pA is shown by the dotted line.

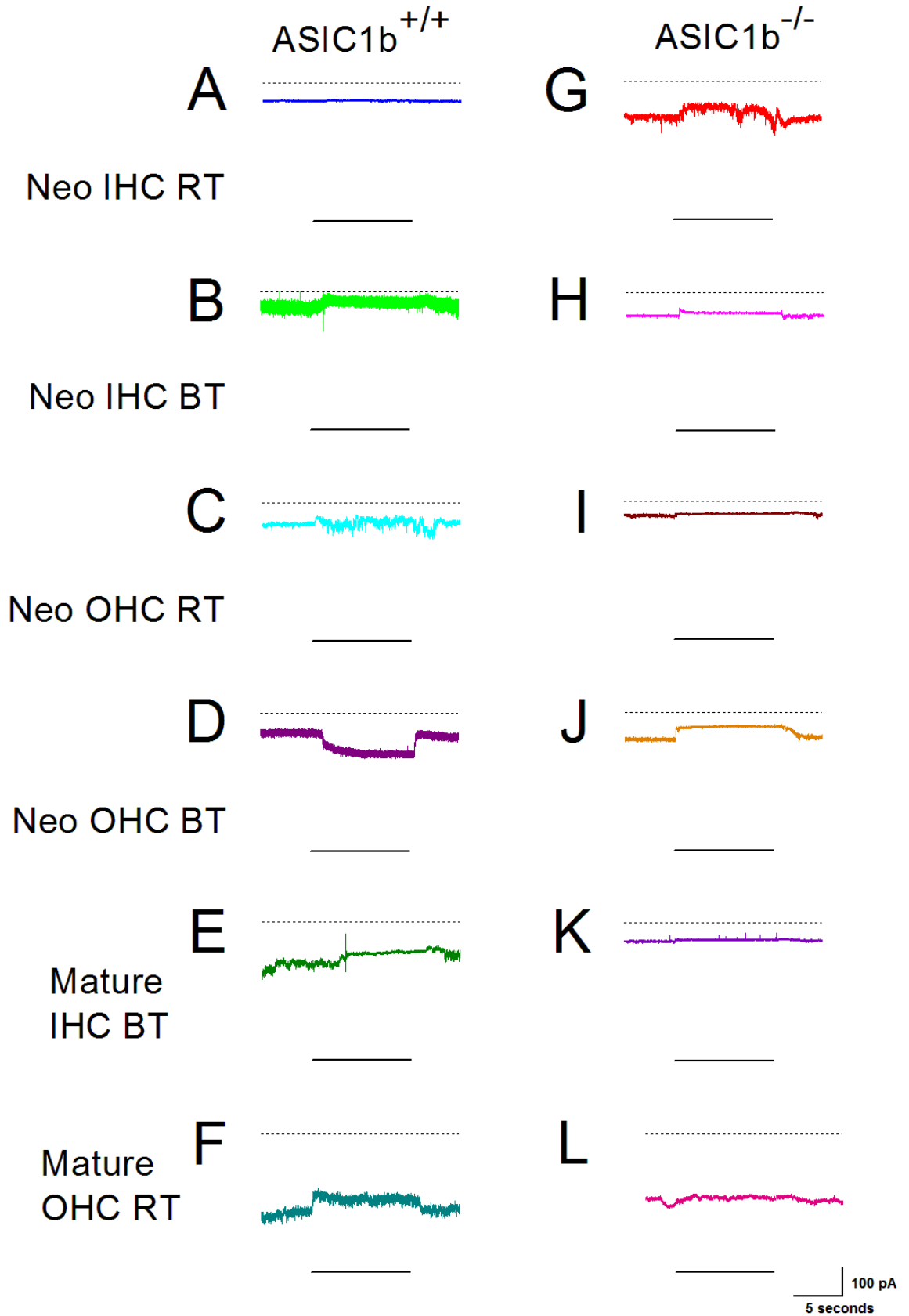


Figure 5-2 Representative examples of the current response seen when the pH of the extracellular solution is dropped from pH 7.5 to pH 5.0 with 100 μ M nafamostat.

Figure 5-2 Representative examples of the current response seen when the pH of the extracellular solution is dropped from pH 7.5 to pH 5.0 with 100 μ M nafamostat.

Typical whole-cell current recordings seen when the extracellular pH was changed from pH 7.5 to pH 5.0 100 μ M nafamostat for ~10 seconds as shown by a solid black line in:

- A. *Asic1b*^{+/+} Neonatal IHC at 21°C (C_m 7.5 pF, R_s 1.82 M Ω)
- B. *Asic1b*^{+/+} Neonatal IHC at 35°C (C_m 6.7 pF, R_s 1.42 M Ω)
- C. *Asic1b*^{+/+} Neonatal OHC at 21°C (C_m 5.3 pF, R_s 0.92 M Ω)
- D. *Asic1b*^{+/+} Neonatal OHC at 35°C (C_m 5.7 pF, R_s 0.72 M Ω)
- E. *Asic1b*^{+/+} Adult IHC at 35°C (C_m 13.8 pF, R_s 0.74 M Ω)
- F. *Asic1b*^{+/+} Adult OHC at 21°C (C_m 7.0 pF, R_s 2.80 M Ω)
- G. *Asic1b*^{-/-} Neonatal IHC at 21°C (C_m 8.7 pF, R_s 2.15 M Ω)
- H. *Asic1b*^{-/-} Neonatal IHC at 35°C (C_m 8.3 pF, R_s 0.86 M Ω)
- I. *Asic1b*^{-/-} Neonatal OHC at 21°C (C_m 6.3 pF, R_s 1.00 M Ω)
- J. *Asic1b*^{-/-} Neonatal OHC at 35°C (C_m 5.1 pF, R_s 1.12 M Ω)
- K. *Asic1b*^{-/-} Adult IHC at 35°C (C_m 10.3 pF, R_s 2.10 M Ω)
- L. *Asic1b*^{-/-} Adult OHC at 21°C (C_m 6.1 pF, R_s 2.15 M Ω)

Traces have not been corrected for linear leak conductance and baselines have not been adjusted to zero. 0 pA is shown by the dotted line.

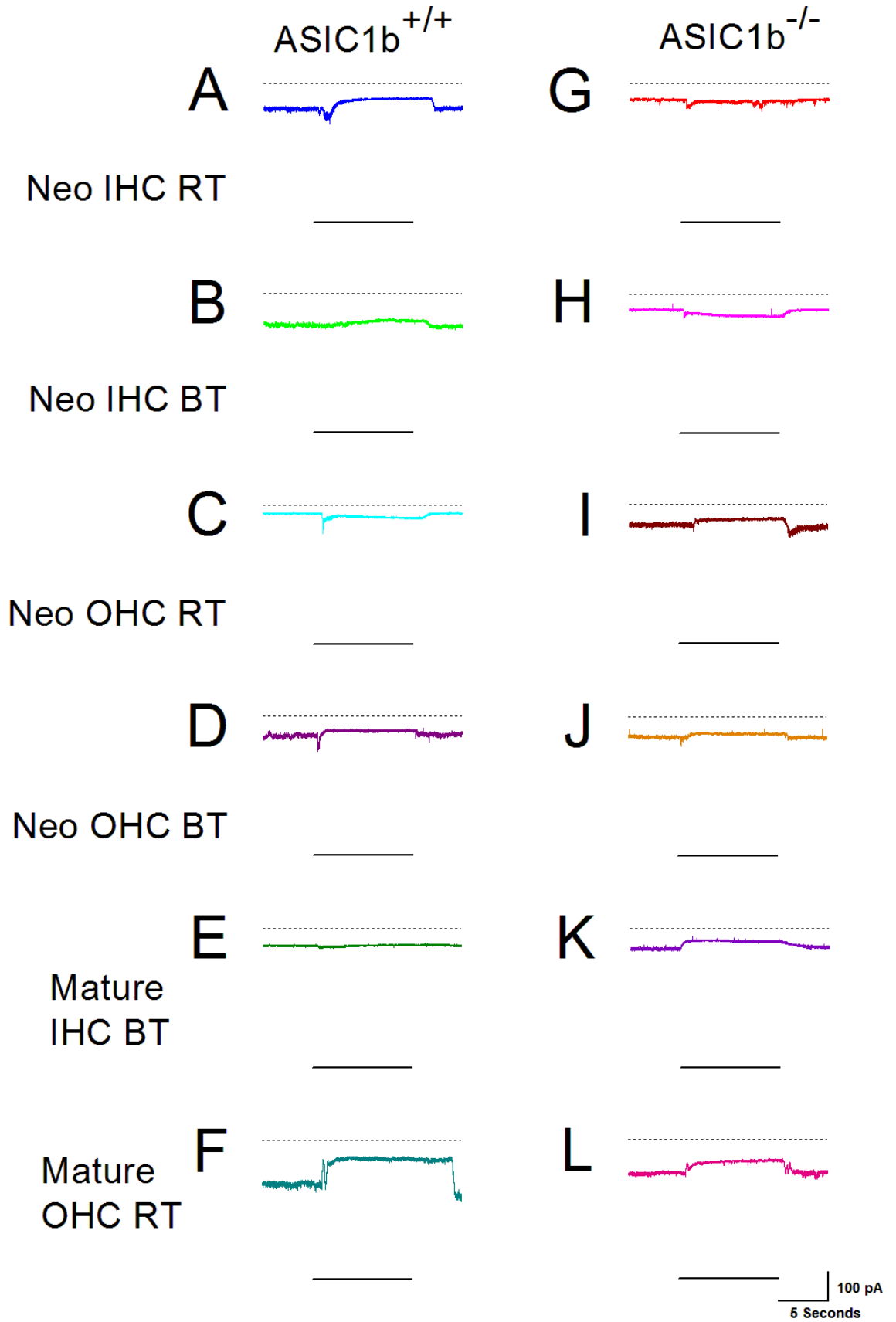


Figure 5-3 Representative examples of the current response seen when the pH of the extracellular solution is dropped from pH 7.5 to pH 5.0 with 100 μ M amiloride.

Figure 5-3 Representative examples of the current response seen when the pH of the extracellular solution is dropped from pH 7.5 to pH 5.0 with 100 μ M amiloride.

Typical whole-cell current recordings seen when the extracellular pH was changed from pH 7.5 to pH 5.0 100 μ M amiloride for ~10 seconds as shown by a solid black line in:

- A. *Asic1b*^{+/+} Neonatal IHC at 21°C (C_m 5.6 pF, R_s 0.96 M Ω)
- B. *Asic1b*^{+/+} Neonatal IHC at 35°C (C_m 7.3 pF, R_s 0.84 M Ω)
- C. *Asic1b*^{+/+} Neonatal OHC at 21°C (C_m 6.9 pF, R_s 0.96 M Ω)
- D. *Asic1b*^{+/+} Neonatal OHC at 35°C (C_m 6.1 pF, R_s 1.34 M Ω)
- E. *Asic1b*^{+/+} Adult IHC at 35°C (C_m 9.2 pF, R_s 0.54 M Ω)
- F. *Asic1b*^{+/+} Adult OHC at 21°C (C_m 6.3 pF, R_s 1.26 M Ω)
- G. *Asic1b*^{-/-} Neonatal IHC at 21°C (C_m 8.7 pF, R_s 0.90 M Ω)
- H. *Asic1b*^{-/-} Neonatal IHC at 35°C (C_m 7.3 pF, R_s 1.18 M Ω)
- I. *Asic1b*^{-/-} Neonatal OHC at 21°C (C_m 5.7 pF, R_s 1.12 M Ω)
- J. *Asic1b*^{-/-} Neonatal OHC at 35°C (C_m 5.6 pF, R_s 0.70 M Ω)
- K. *Asic1b*^{-/-} Adult IHC at 35°C (C_m 10.4 pF, R_s 0.80 M Ω)
- L. *Asic1b*^{-/-} Adult OHC at 21°C (C_m 6.2 pF, R_s 1.82 M Ω)

Traces have not been corrected for linear leak conductance and baselines have not been adjusted to zero. 0 pA is shown by the dotted line.

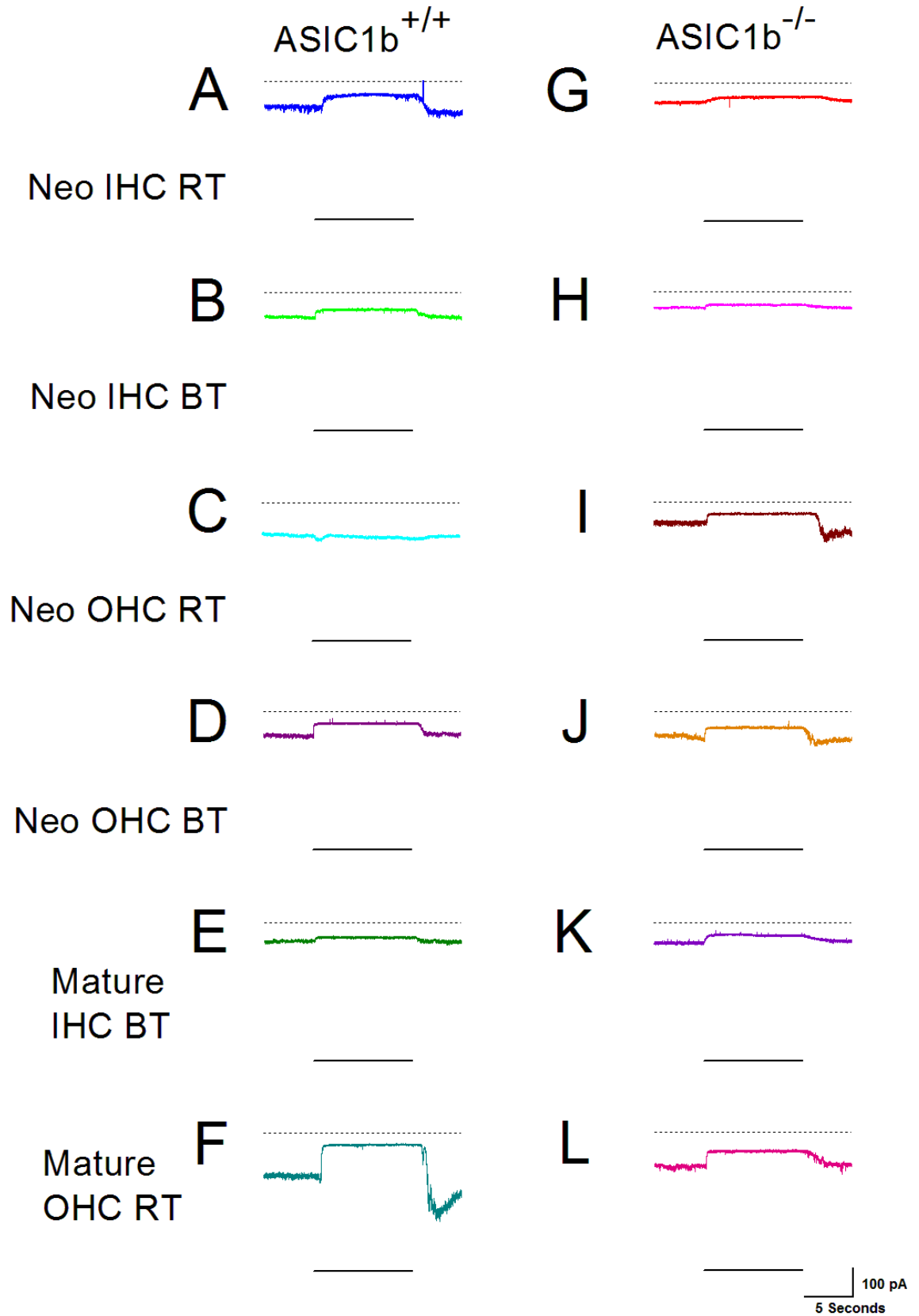


Figure 5-4 Representative examples of the current seen with the presence of 100 μ M nafamostat in the extracellular solution.

Figure 5-4 Representative examples of the current seen with the presence of 100 μ M nafamostat in the extracellular solution.

- A. Typical whole-cell current recordings seen with the presence of 100 μ M nafamostat in the extracellular solution for ~10 seconds as shown by a solid black line in:
- B. *Asic1b* *+/+* Neonatal IHC at 21oC (Cm 5.6 pF, Rs 2.40 M Ω)
- C. *Asic1b* *+/+* Neonatal IHC at 35oC (Cm 8.1 pF, Rs 0.86 M Ω)
- D. *Asic1b* *+/+* Neonatal OHC at 21oC (Cm 6.5 pF, Rs 0.74 M Ω)
- E. *Asic1b* *+/+* Neonatal OHC at 35oC (Cm 5.5 pF, Rs 0.96 M Ω)
- F. *Asic1b* *+/+* Adult IHC at 35oC (Cm 9.8 pF, Rs 1.42 M Ω)
- G. *Asic1b* *+/+* Adult OHC at 21oC (Cm 6.3 pF, Rs 1.26 M Ω)
- H. *Asic1b* *-/-* Neonatal IHC at 21oC (Cm 8.5 pF, Rs 0.74 M Ω)
- I. *Asic1b* *-/-* Neonatal IHC at 35oC (Cm 7.3 pF, Rs 1.18 M Ω)
- J. *Asic1b* *-/-* Neonatal OHC at 21oC (Cm 5.7 pF, Rs 1.12 M Ω)
- K. *Asic1b* *-/-* Neonatal OHC at 35oC (Cm 5.6 pF, Rs 0.64 M Ω)
- L. *Asic1b* *-/-* Adult IHC at 35oC (Cm 10.4 pF, Rs 0.80 M Ω)
- M. *Asic1b* *-/-* Adult OHC at 21oC (Cm 6.2 pF, Rs 1.82 M Ω)

Traces have not been corrected for linear leak conductance and baselines have not been adjusted to zero. 0 pA is shown by the dotted line.

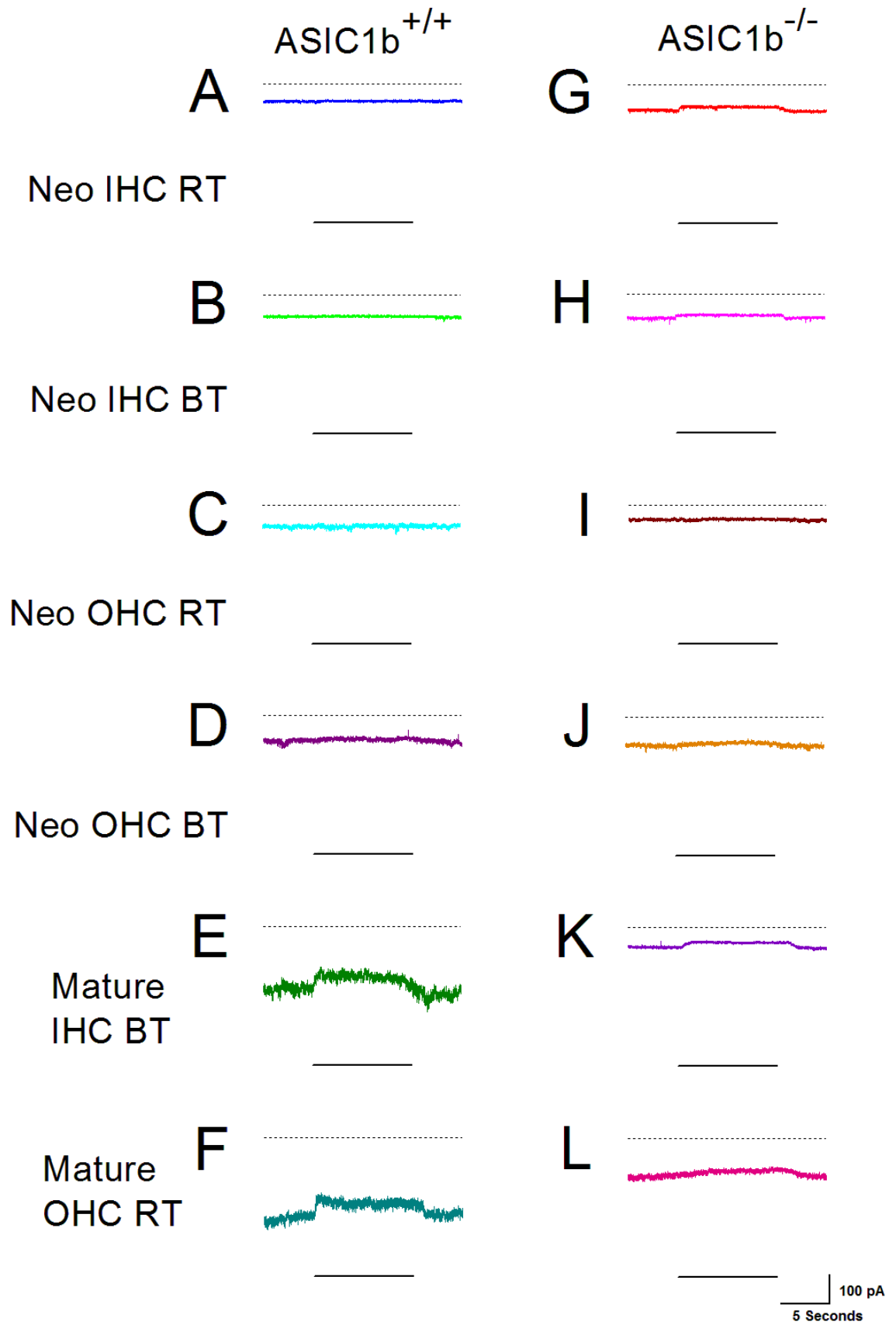


Figure 5-5 Representative examples of the current seen with the presence of 100 μ M amiloride in the extracellular solution.

Figure 5-5 Representative examples of the current seen with the presence of 100 μ M amiloride in the extracellular solution.

Typical whole-cell current recordings seen with the presence of 100 μ M nafamostat in the extracellular solution for ~10 seconds as shown by a solid black line in:

- A. *Asic1b*^{+/+} Neonatal IHC at 21°C (C_m 8.8 pF, R_s 0.90 M Ω)
- B. *Asic1b*^{+/+} Neonatal IHC at 35°C (C_m 8.5 pF, R_s 1.42 M Ω)
- C. *Asic1b*^{+/+} Neonatal OHC at 21°C (C_m 5.3 pF, R_s 1.42 M Ω)
- D. *Asic1b*^{+/+} Neonatal OHC at 35°C (C_m 5.7 pF, R_s 0.90 M Ω)
- E. *Asic1b*^{+/+} Adult IHC at 35°C (C_m 15.3 pF, R_s 3.00 M Ω)
- F. *Asic1b*^{+/+} Adult OHC at 21°C (C_m 7.0 pF, R_s 2.80 M Ω)
- G. *Asic1b*^{-/-} Neonatal IHC at 21°C (C_m 9.1 pF, R_s 0.86 M Ω)
- H. *Asic1b*^{-/-} Neonatal IHC at 35°C (C_m 8.3 pF, R_s 0.86 M Ω)
- I. *Asic1b*^{-/-} Neonatal OHC at 21°C (C_m 6.3 pF, R_s 1.00 M Ω)
- J. *Asic1b*^{-/-} Neonatal OHC at 35°C (C_m 5.1 pF, R_s 1.12 M Ω)
- K. *Asic1b*^{-/-} Adult IHC at 35°C (C_m 10.3 pF, R_s 2.10 M Ω)
- L. *Asic1b*^{-/-} Adult OHC at 21°C (C_m 8.2 pF, R_s 4.55 M Ω)

Traces have not been corrected for linear leak conductance and baselines have not been adjusted to zero. 0 pA is shown by the dotted line.

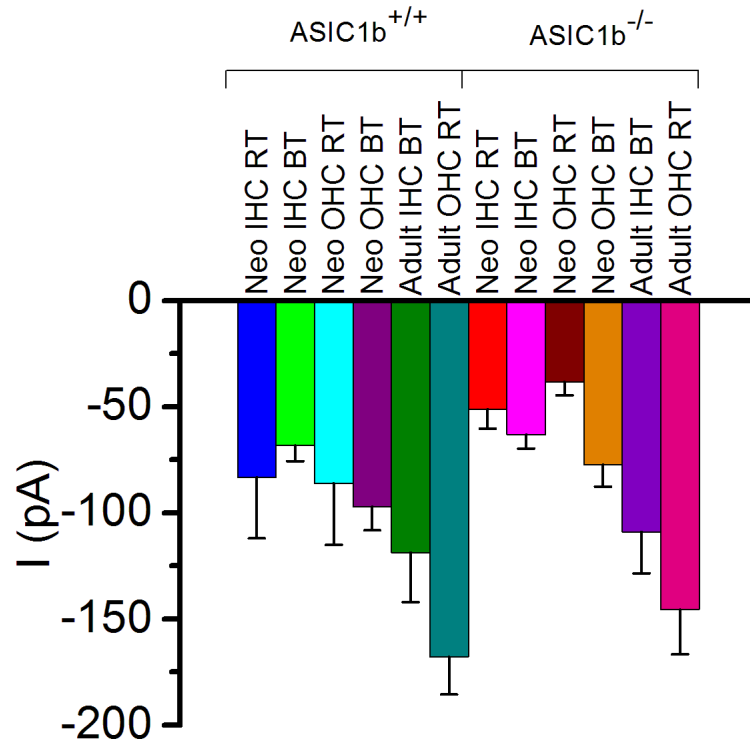


Figure 5-6 baseline current measurements

Resting current levels measured over a 2 second period 2 seconds at pH 7.5 before a change in the extracellular environment at a holding potential of -84mV. Mean currents \pm SEM are shown (N=25,11,19,24,13,10,19,14,21,10,16,5).

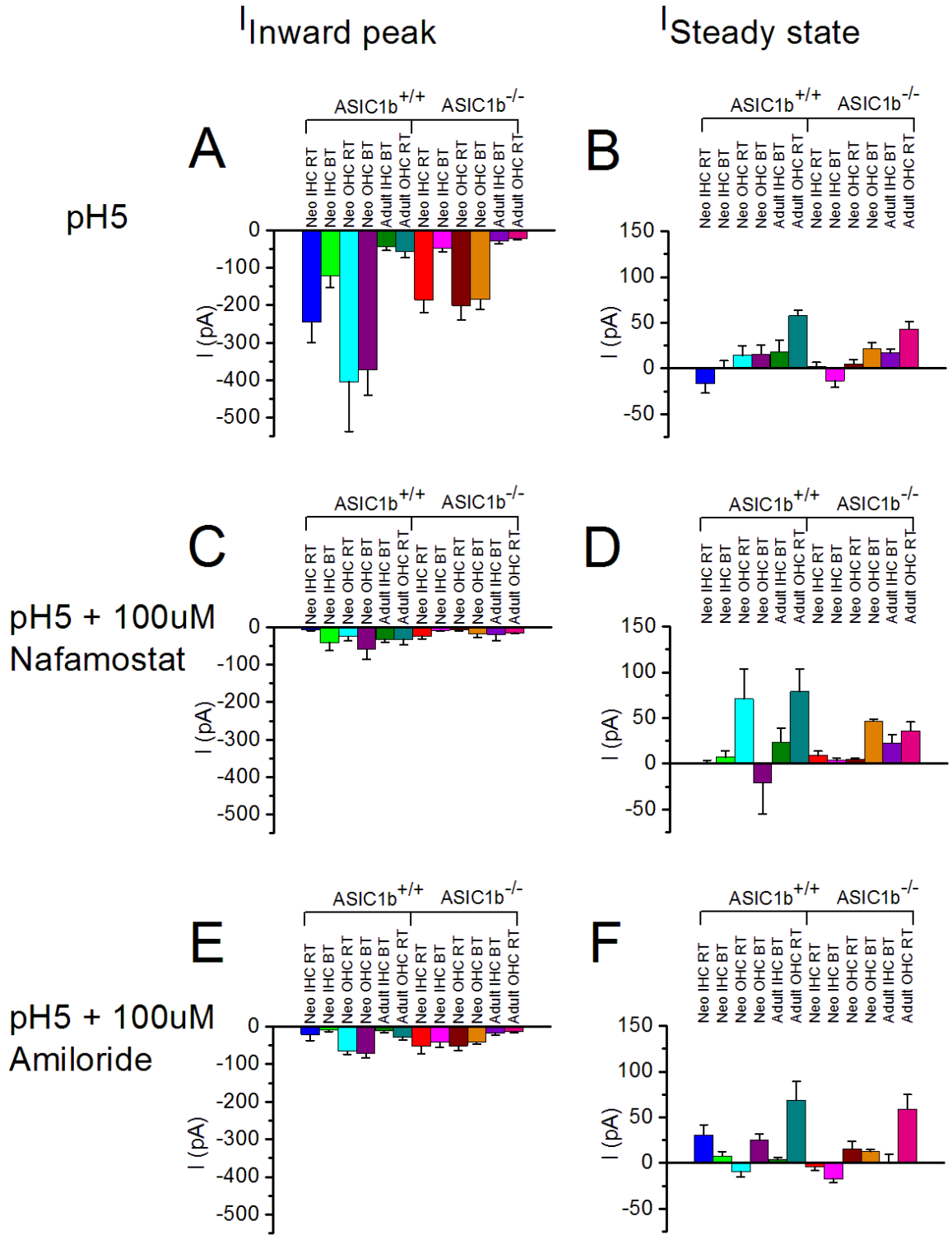


Figure 5-7 Inward peak and steady state current responses measured during Δ pH

Figure 5-7 Inward peak and steady state current responses measured during Δ pH

Inward peak and steady state currents seen in:

- A. pH drop from pH 7.5 to pH 5.0 (N=25,11,19,24,13,10,19,14,21,10,16,5)
- B. pH drop from pH 7.5 to pH 5.0 (N=25,10,19,23,11,10,19,13,21,10,16,5)
- C. pH drop from pH 7.5 to pH 5.0 with 100 μ M nafamostat (N=4,5,3,6,4,3,5,4,3,3,3,3)
- D. pH drop from pH 7.5 to pH 5.0 with 100 μ M nafamostat (N=4,5,3,6,4,3,5,4,3,3,3,3)
- E. pH drop from pH 7.5 to pH 5.0 with 100 μ M amiloride (N=3,3,12,15,4,5,7,3,9,3,4,3)
- F. pH drop from pH 7.5 to pH 5.0 with 100 μ M amiloride (N=3,3,12,15,4,5,7,3,9,3,4,3)

Graphs A,C and E show mean $I_{inward\ peak} \pm SEM$. Graphs B,D and F show $I_{steady\ state} \pm SEM$. All recordings were measured from a holding potential of -84 mV. Inward peak currents were measured as the largest inward current seen during the 10 second period in which the extracellular environment was altered. Steady state currents were measured over 1 second where the current had stabilised after the peak current, towards the end of the 10 second period in which the extracellular environment was changed.

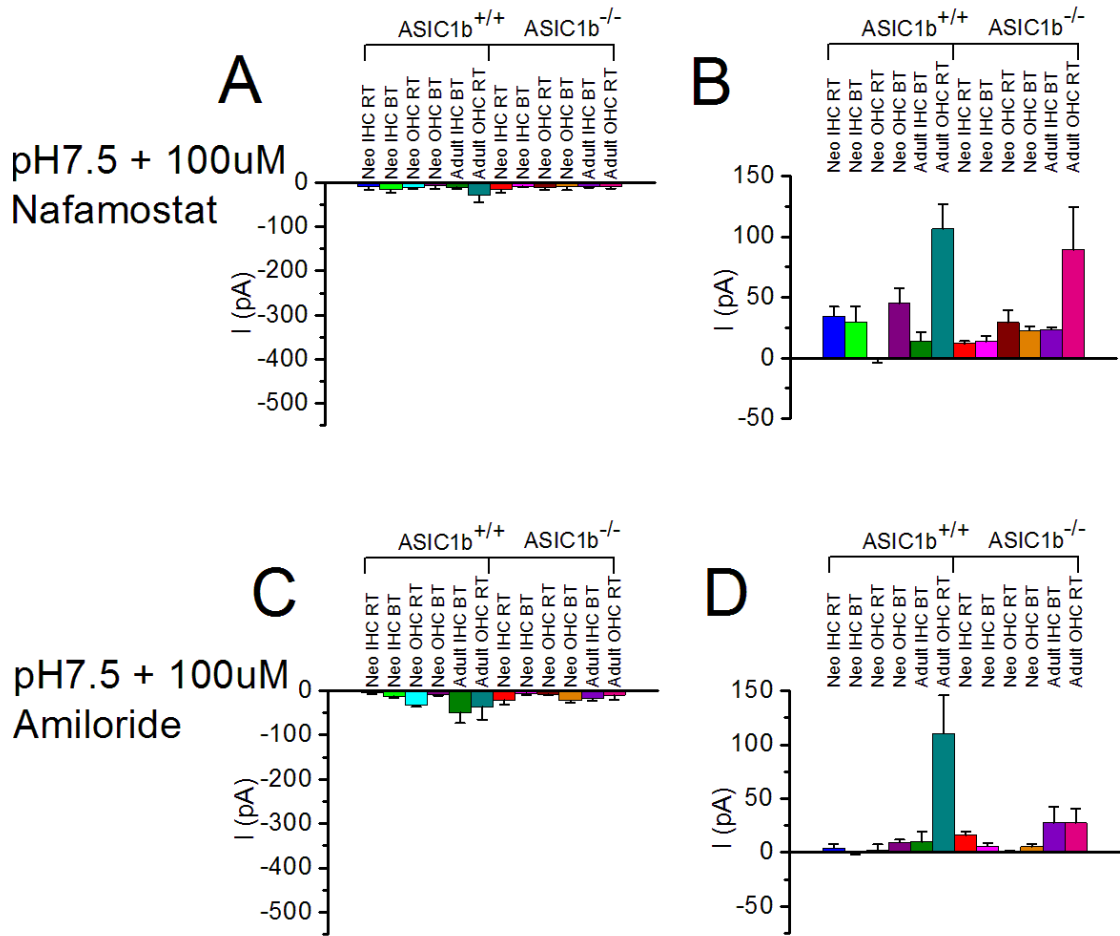


Figure 5-8 Inward peak and steady state current responses measured without ΔpH

Inward peak and steady state currents seen in:

- application of 100 μM nafamostat (N=3,3,6,11,4,4,4,3,3,3,3,3)
- application of 100 μM nafamostat (N=3,3,6,11,4,4,4,3,3,3,3,3)
- application of 100 μM amiloride (N=3,3,3,3,3,3,3,4,3,3,4,3)
- application of 100 μM amiloride (N=3,3,3,3,3,3,3,4,3,3,4,3)

Graphs A and C show mean $I_{inward\ peak} \pm SEM$. Graphs B and D show $I_{steady\ state} \pm SEM$. All recordings were measured from a holding potential of $-84\ mV$. Inward peak currents were measured as the largest inward current seen during the 10 second period in which the extracellular environment was altered. Steady state currents were measured over 1 second where the current had stabilised after the peak current, towards the end of the 10 second period in which the extracellular environment was changed.

		pH7.5		pH5				pH5 = 100uM nafamostat				pH5 + 100uM amiloride				pH7.5 + 100uM nafamostat				pH7.5 + 100uM amiloride			
		Leak measurements		Inward current		Steady state		Inward current		Steady state		Inward current		Steady state		Inward current		Steady state		Inward current		Steady state	
		I (pA)	n	I (pA)	n	I (pA)	n	I (pA)	n	I (pA)	n	I (pA)	n	I (pA)	n	I (pA)	n	I (pA)	n	I (pA)	n	I (pA)	n
+/-	neonatal IHC RT	-83.2 ±28.8	25	-244.4 ±55.2	25	-16.4 ±10.5	25	-7.0 ±2.3	4	0.1 ±3.5	4	-20.8 ±15.8	3	30.6 ±11.1	3	-9.5 ±6.7	3	34.5 ±7.9	3	-4.4 ±2.6	3	4.3 ±3.4	3
	neonatal IHC BT	-68.3 ±7.3	11	-122.0 ±30.6	11	0.4 ±7.9	10	-40.7 ±21.5	5	7.2 ±6.9	5	-8.8 ±4.3	3	7.6 ±4.9	3	-16.1 ±6.7	3	29.7 ±13	3	-12.6 ±2.7	3	-0.1 ±1.5	3
	neonatal OHC RT	-86.0 ±29.1	19	-404.2 ±132.8	19	14.2 ±10.7	19	-24.6 ±12.2	3	70.9 ±33	3	-64.9 ±8.5	12	-9.2 ±6.2	12	-11.1 ±3.5	6	-0.6 ±3	6	-32.5 ±3.8	3	2.6 ±5.1	3
	neonatal OHC BT	-97.1 ±11.2	24	-372.4 ±68	24	15.6 ±10	23	-59.5 ±26.2	6	-20.8 ±33.8	6	-72.1 ±11.1	15	24.8 ±7	15	-7.1 ±7	11	45.3 ±11.9	11	-9.1 ±1.8	3	9.2 ±3	3
	adult IHC BT	-118.7 ±23.4	13	-44.4 ±9.5	13	18.2 ±13.1	11	-31.7 ±7.5	4	23.5 ±15.6	4	-11.6 ±3.5	4	3.8 ±2.1	4	-10.6 ±4.3	4	14.2 ±7.5	4	-49.2 ±23.3	3	10.0 ±9.4	3
	adult OHC RT	-167.9 ±17.7	10	-56.4 ±16.9	10	57.6 ±6.3	10	-32.5 ±14.5	3	79.0 ±24.5	3	-27.9 ±7.5	5	68.9 ±20.2	5	-28.6 ±15.3	4	106.6 ±20.2	4	-36.2 ±28.6	3	110.3 ±35.3	3
-/-	neonatal IHC RT	-51.1 ±9.2	19	-185.2 ±34.7	19	2.3 ±4.6	19	-23.3 ±7.9	5	9.0 ±5	5	-52.7 ±19.5	7	-4.3 ±3.7	7	-15.6 ±7.8	4	12.1 ±2.1	4	-21.1 ±9.4	3	16.1 ±2.9	3
	neonatal IHC BT	-63.2 ±6.6	14	-48.0 ±9.9	14	-13.5 ±7.1	13	-8.0 ±1.6	4	3.5 ±2.8	4	-41.4 ±13.3	3	-17.2 ±4.2	3	-8.5 ±2	3	13.7 ±4.7	3	-5.8 ±4	4	5.9 ±3	4
	neonatal OHC RT	-38.3 ±6.3	21	-200.7 ±39	21	4.8 ±4.8	21	-7.5 ±3.3	3	4.6 ±1.3	3	-51.3 ±13.3	9	15.7 ±7.8	9	-11.9 ±4.3	3	29.4 ±10.1	3	-8.1 ±1.3	3	0.8 ±0.6	3
	neonatal OHC BT	-77.2 ±10.4	10	-184.5 ±26.8	10	21.7 ±6.4	10	-18.2 ±9.6	3	46.4 ±2.1	3	-41.7 ±4.8	3	12.5 ±2.9	3	-9.7 ±7.3	3	22.5 ±3.9	3	-22.4 ±3.5	3	5.3 ±2.3	3
	adult IHC BT	-109.0 ±19.5	16	-28.3 ±6.9	16	16.9 ±4.7	16	-19.3 ±17	3	22.7 ±8.8	3	-16.5 ±5.3	4	1.5 ±8.2	4	-8.9 ±2.7	3	23.6 ±1.7	3	-17.9 ±5.2	4	27.4 ±15.4	4
	adult OHC RT	-145.7 ±21.0	5	-21.8 ±3.3	5	43.1 ±8.1	5	-14.6 ±2.4	3	36.2 ±9.5	3	-13.3 ±2.6	3	58.9 ±16	3	-9.7 ±3.5	3	89.3 ±35.2	3	-10.1 ±9.5	3	27.7 ±12.9	3

Table 5-1 Inward peak and steady state current responses. Both $I_{\text{inward peak}}$ and $I_{\text{steady state}}$ measurements are mean \pm SEM. All recordings were measured from a holding potential of -84 mV. Inward peak currents were measured as the largest inward current seen during the 10 second period in which the extracellular environment was altered. Steady state currents were measured over 1 second where the current had stabilised after the peak current, towards the end of the 10 second period in which the extracellular environment was changed.

6 BASOLATERAL CURRENTS IN THE HAIR CELLS OF ASIC1B MOUSE MODELS

6.1 Introduction

The development of the hair cells in the organ of Corti can easily be described by the appearance of certain currents ($I_{K,f}$ for mature IHCs and $I_{K,n}$ for mature OHCs) and by other cellular properties (electromotility in the mature OHCs). In this chapter I investigate the development of the hair cells from neonatal to mature and examine the effect of the ASIC1b knockout mutation on this process.

It is known that ASIC channels can be involved in mechanosensation (Page et al., 2005; Price et al., 2001) and so I investigate the effect on the ASIC1b knock out mutation on the MET current in the neonatal OHCs. It is known that amiloride is a blocker of the MET current (Rüsch et al., 1994) and so I also investigate the effect of nafamostat, a second blocker of the ASIC current, on the MET current.

6.2 Results

All electrophysiology recordings were performed using standard ECS and K^+ ICS (see Table 2-1 and Table 2-2 for composition), the temperature was held at either 21°C (room temperature – RT) or 35°C (body temperature - BT) depending on the experimental condition. Mechano-electrical transduction experiments were performed using Cs^+ ICS with standard ECS.

6.2.1 Steady state currents in the hair cells.

At both room and body temperature neonatal ASIC1b^{+/+} and ASIC1b^{-/-} IHCs and OHCs (P4-P6) all show outward K^+ currents with slow activation reaching a steady state within 25 ms of a depolarising step in membrane potential to -4 mV, typical of IHCs and OHCs at this point in development. At body temperature mature ASIC1b^{+/+} and ASIC1b^{-/-} IHCs display large outward K^+ currents with fast activation in response to depolarizing voltage steps to -4 mV which reach a steady state within 0.5 ms of a change in membrane potential. Mature ASIC1b^{+/+} and ASIC1b^{-/-} OHCs have inward K^+ currents which instantly reaches a peak which then deactivates

to a steady state level, the outward currents are slowly activating reaching a steady state level within 25 ms (Figure 6-1).

At -24 mV neonatal IHCs at RT the steady state current for ASIC1b^{+/+} and ASIC1b^{-/-} is 491 ± 50 pA (mean \pm SEM) (n = 32) and 399 ± 65 pA (n = 18) (NS). Neonatal IHCs ASIC1b^{+/+} and ASIC1b^{-/-} at BT have a steady state current of 581 ± 49 pA (n = 16) and 673 ± 96 pA (n = 15) (NS) respectively. Neonatal OHCs IHCs ASIC1b^{+/+} and ASIC1b^{-/-} at RT have a steady state current of 610 ± 159 pA (n = 10) and 385 ± 108 pA (n = 14) (NS) at BT the steady state currents measure 507 ± 106 pA (n = 21) and 635 ± 26 pA (n = 6) (NS). ASIC1b^{+/+} and ASIC1b^{-/-} mature IHCs at BT have a steady state current of 4398 ± 360 pA (n = 15) and 2988 ± 465 pA (n = 11) (p < 0.001). Mature ASIC1b^{+/+} and ASIC1b^{-/-} OHCs at RT have a steady state current of 743 ± 195 pA (n = 12) and 64 ± 121 pA (n = 7) (NS). Example traces can be seen in Figure 6-1

At -4 mV ASIC1b^{+/+} and ASIC1b^{-/-} neonatal IHCs at RT have a steady state current of 2091 ± 143 pA (n = 32) and 2104 ± 147 pA (n = 18) (NS). Neonatal ASIC1b^{+/+} and ASIC1b^{-/-} IHCs at BT have a steady state current of 2403 ± 274 pA (n = 16) and 3296 ± 193 pA (n = 15) (NS). Neonatal ASIC1b^{+/+} and ASIC1b^{-/-} OHCs at RT have a steady state current of 1919 ± 275 pA (n = 10) and 1779 ± 302 pA (n = 14) (NS). At BT these currents measure 2355 ± 221 pA (n = 21) and 3397 ± 447 pA (n = 6) (NS). Mature ASIC1b^{+/+} and ASIC1b^{-/-} IHCs at BT have a steady state current of 12706 ± 1375 pA (n = 15) and 8335 ± 1238 pA (n = 11) (p < 0.001) respectively. Mature ASIC1b^{+/+} and ASIC1b^{-/-} OHCs have a steady state current of 1546 ± 211 pA (n = 12) and 730 ± 253 pA (n = 7) (NS). A summary of these data can be seen in Figure 6-5A and B and Table 6-1.

Figure 6-2 shows IV plots comparing the steady state currents in the ASIC1b^{+/+} and ASIC1b^{-/-} hair cells. The current sizes recorded in the neonatal IHCs and OHCs are comparable to those recorded in (Marcotti et al., 2003a) and (Marcotti and Kros, 1999) respectively. This shows that the neonatal hair cells have developed their normal complement of K⁺ currents in both ASIC1b^{+/+} and ASIC1b^{-/-} genotypes. ASIC1b^{+/+} and ASIC1b^{-/-} mature IHCs have steady state currents which resemble those seen in (Marcotti et al., 2003a). Steady state currents in the mature ASIC1b^{+/+} and ASIC1b^{-/-} OHCs are similar to those recorded in (Marcotti and Kros, 1999), suggesting that these currents develop to maturity in ASIC1b^{+/+} and ASIC1b^{-/-} hair cells.

There is a significant difference in the steady state currents between ASIC1b^{+/+} neonatal IHCs at BT and mature IHCs at BT (p < 0.001) and ASIC1b^{-/-} neonatal IHCs at BT and mature IHCs at BT (p < 0.001), this is at a holding potential of both -24 mV and 4 mV. This difference is due to

the presence of the $I_{K,f}$ current in the mature IHCs increasing the size of the steady state current.

There is also a significant difference in the steady state current at both -24 mV and -4 mV between ASIC1b^{+/+} and ASIC1b^{-/-} mature IHCs at BT ($p < 0.001$) (Figure 6-2E, Figure 6-5A and B). This difference is likely to be due to the difference in the $I_{K,f}$ current which is discussed below.

6.2.2 Presence of adult current $I_{K,f}$

In ASIC1b^{+/+} and ASIC1b^{-/-} mature IHCs at BT the early current (measured 0.7 ms after the step onset) is 1658 ± 246 pA (mean \pm SEM) ($n = 12$) and 721 ± 335 pA ($n = 8$) ($p = 0.0225$) at a membrane potential of -24 mV. At -4 mV the same current measures 7265 ± 1019 pA ($n = 12$) and 3696 ± 950 pA ($n = 8$) ($p = 0.0325$) for ASIC1b^{+/+} and ASIC1b^{-/-} mature IHCs respectively. (Figure 6-3). Neonatal ASIC1b^{+/+} and ASIC1b^{-/-} IHCs at BT have an early current of -499 ± 141 pA ($n = 6$) and -323 ± 46 pA ($n = 9$) (NS) for a membrane potential of -24 mV. At -4 mV these currents measure at -413 ± 82 pA ($n = 6$) and -353 ± 48 pA ($n = 9$) (NS) respectively. A summary of these data can be seen in Figure 6-5C and D and Table 6-1.

The IV plot shown in Figure 6-4B shows the early current measured in neonatal ASIC1b^{+/+} and ASIC1b^{-/-} IHCs at BT. There is no statistical difference in the size of this current between ASIC1b^{+/+} and ASIC1b^{-/-} neonatal IHCs. The early current measured in neonatal IHCs is likely to be dominated by calcium currents. The size of the early current measured here is comparable to that seen in (Kros et al., 1998) at -4 mV, showing that the ASIC1b knockout mutation has no effect on the development of the early current.

There is a significant difference in the size of the early current between both ASIC1b^{+/+} and ASIC1b^{-/-} neonatal and mature IHCs with p values of < 0.001 . This difference is because the $I_{K,f}$ current is not present in the neonatal IHCs and is present in the mature IHCs.

Figure 6-4A shows an IV plot for the early current measured in the mature IHCs. There is a significant difference in the size of the $I_{K,f}$ current between ASIC1b^{+/+} and ASIC1b^{-/-} mature IHCs at body temperature at both -24 mV or -4 mV. This suggests that ASIC1b is required for the development of the $I_{K,f}$ current to its normal size. Although the $I_{K,f}$ current is present in the ASIC1b^{-/-} mature IHCs it is smaller in size suggesting that ASIC1b offers some small modulatory effects on this current.

6.2.3 Presence of $I_{K,s}$

ASIC1b^{+/+} and ASIC1b^{-/-} mature IHCs at BT have an $I_{K,s}$ current of 2945 ± 356 pA ($n = 12$) and 641 ± 1021 pA ($n = 9$) (NS) at -24 mV. The same current measures 6384 ± 1070 pA ($n = 12$) and 578 ± 2505 pA ($n = 9$) (NS) at -4 mV. A summary of these data can be seen in Figure 6-5E and F and Table 6-1.

ASIC1b^{+/+} and ASIC1b^{-/-} neonatal IHCs at BT have an $I_{K,neo}$ current of 1095 ± 151 pA ($n = 6$) and 938 ± 137 pA ($n = 9$) (NS) at -24 mV. At -4 mV the same current measures 3566 ± 417 pA ($n = 6$) and 3552 ± 307 pA ($n = 9$) (NS) respectively. Figure 6-5E and F and Table 6-1 give a summary of these data.

There is no significant difference in the size of the $I_{K,neo}$ and $I_{K,s}$ currents respectively between ASIC1b^{-/-} neonatal and mature IHCs at BT at either -24 mV or -4 mV. Between ASIC1b^{+/+} neonatal and mature IHCs at BT there is a significant difference in the size of the slow outward potassium currents ($I_{K,neo}$ and $I_{K,s}$, respectively) at -24 mV with a p value of <0.05, this difference does not however extend to the current size at -4 mV.

6.2.4 Presence of adult current $I_{K,n}$

Figure 6-4D shows an IV plot of the peak current measured from the ASIC1b^{+/+} and ASIC1b^{-/-} mature OHCs at RT. It can be seen that this current is larger at both negative and positive potentials in the ASIC1b^{+/+} mature OHCs compared to ASIC1b^{-/-} mature OHCs.

The $I_{K,n}$ current is defined at the peak current minus the steady state current (Marcotti and Kros, 1999) as described in chapter 2 and Figure 2-3, a full description of the peak and steady state currents can be seen in Figure 6-4, 6 and Table 6-2. The size of the $I_{K,n}$ current in ASIC1b^{+/+} and ASIC1b^{-/-} mature OHC is -413 ± 66 pA ($n = 8$) and -140 ± 21 pA ($n = 7$) ($p = 0.0042$) respectively. In ASIC1b^{+/+} and ASIC1b^{-/-} mature OHCs $I_{K,n}$ was calculated to be -767 ± 139 pA ($n = 8$) and -223 ± 51 pA ($n = 7$) ($P = 0.0061$) respectively (Figure 6-3).

The inward peak and $I_{K,n}$ currents recorded here in the ASIC1b^{+/+} mature OHCs are of a similar size to those seen in (Marcotti and Kros, 1999). Mature ASIC1b^{-/-} OHC the inward peak current and the decaying inward current sizes are of a similar size to the neonatal OHCs seen in the

same paper. This suggests that the ASIC1b^{-/-} OHCs do not develop the I_{k,n} current and maintain an immature complement of inward rectifying currents.

The size of I_{k,n} at -124 mV in ASIC1b^{+/+} and ASIC1b^{-/-} mature IHCs is calculated to be -450 ± 274 pA (n = 5) and $1-271 \pm 67$ pA (n = 6) (NS) respectively. At -154 mV ASIC1b^{+/+} and ASIC1b^{-/-} mature IHCs at BT the I_{k,n} current is calculated to be -737 ± 466 pA (n = 5) and -436 ± 149 pA (n = 6) in ASIC1b^{+/+} and ASIC1b^{-/-} mature IHCs respectively (Figure 6-3). A summary of these data can be seen in Figure 6-4C and D, Figure 6-5 and Table 6-2.

Figure 6-4C show the IV plot for the peak currents measured in the ASIC1b^{+/+} and ASIC1b^{-/-} mature IHCs. The sizes of the peak and I_{k,n} currents measured here are comparable to those seen in (Marcotti et al., 2003a). There is no significant difference in the peak current, steady state current or the size of I_{k,n} between ASIC1b^{+/+} and ASIC1b^{-/-} mature IHCs at BT at either -124 or -154 mV. This suggests that ASIC1b does not affect the development of the I_{k,n} current in mature IHCs, unlike that seen in mature OHCs.

6.2.5 Presence of prestin

The presence of electromotility in mature ASIC1b^{+/+} OHCs can be determined both by observing the electromotile behaviour and by looking at the un-compensatable capacitance transients at the beginning of the steps in changes of the membrane potential in the voltage clamp recordings (Figure 6-1F). This transient can clearly be seen at the start of the membrane potential steps and is absent in the neonatal OHC recordings. The transients arise from the contraction of the cell body resulting in a reduced whole capacitance which is then not compensated for using the series resistance compensation circuitry of the amplifier. This capacitance transient is reduced in the ASIC1b^{-/-} mature OHCs (Figure 6-1M), suggesting that prestin expression is reduced and electromotility does not occur.

In ASIC1b^{+/+} mature OHCs electromotility was seen in 5 out of 5 cells in response to a change in the membrane potential from -84 mV to +76 mV. The white arrows in figures 6-9 outline the basal membrane of the OHC which is being recorded from at rest, the membrane potential is then stepped to +76 mV and the prestin in the cell membrane begins to contract causing a shortening of the cell body length, this is at its shortest length at time 750 ms (Figure 4-5, 6-11 C) the membrane potential is then stepped back to -84 mV and the prestin in the cell

membrane begins to relax and the cell body elongates back to its resting position (Figure 4-5, 6-11 E). An example of this can be seen in Figure 6-10 and Figure 8-5.

In ASIC1b^{-/-} mature OHCs electromotility was seen in 0 out of 4 cells in response to depolarising membrane potentials from -84 mV to +76 mV. The white arrows in figure 6-10 which outline the basolateral membrane of the mature OHC continue to outline the membrane throughout the depolarising membrane step (Figure 6-10C) suggesting that the cell body does not contract and electromotility is not present.

Taken together with the reduced capacitive transients this suggests that ASIC1b is required for either the expression of prestin or for the function of prestin in the OHC basolateral membrane.

6.2.6 Cellular properties

The whole cell capacitance of the ASIC1b^{+/+} and ASIC1b^{-/-} neonatal IHCs at RT is 7.4 ± 0.2 pF ($n = 34$) and 8.0 ± 0.2 pF ($n = 31$) (NS). At BT the same cells have a whole cell capacitance of 7.8 ± 0.2 pF ($n = 20$) and 7.9 ± 0.3 pF ($n = 22$) (NS) respectively. ASIC1b^{+/+} and ASIC1b^{-/-} neonatal OHCs at RT have a whole cell capacitance of 6.0 ± 0.2 pF ($n = 24$) and 6.3 ± 0.2 pF ($n = 24$) (NS) respectively. ASIC1b^{+/+} and ASIC1b^{-/-} neonatal OHCs at BT have a whole cell capacitance of 5.8 ± 0.1 pF ($n = 32$) and 5.5 ± 0.2 pF ($n = 10$) (NS) respectively. Mature ASIC1b^{+/+} and ASIC1b^{-/-} IHCs at BT have a whole cell capacitance of 11.0 ± 0.4 pF ($n = 26$) and 10.5 ± 0.3 pF ($n = 22$) (NS). ASIC1b^{+/+} and ASIC1b^{-/-} mature OHCs at RT have a whole cell capacitance of 8.0 ± 0.2 pF ($n = 11$) and 7.1 ± 0.3 pF ($n = 8$). A summary of these data can be seen in Table 6-3 and Figure 6-7B.

This data shows that the whole cell capacitance of both the ASIC1b^{+/+} and ASIC1b^{-/-} neonatal hair cells is unaffected by ASIC1b^{-/-} and that ASIC1b is not required for the cell size of the maintaining the correct cell size of neonatal hair cells.

There is a significant difference between the whole cell capacitance of the ASIC1b^{+/+} IHCs and OHCs, this is true at both RT and BT and for neonatal and mature hair cells. All differences have a p value of <0.001 . There is a significant difference between the whole cell capacitance of the ASIC1b^{-/-} IHCs and OHCs, this is true at both RT and BT and for neonatal and mature hair cells.

All differences have a p value of <0.001. The differences seen here are normal and compare with previous data showing that IHCs are larger in size than OHCs (Marcotti et al., 2003a).

There is a significant difference in the capacitance, and hence cell size, between both ASIC1b^{+/+} and ASIC1b^{-/-} neonatal and mature IHCs at BT, both with a p value of <0.001. This is consistent with previous work (Marcotti et al., 2003a) that shows IHCs increase in size during development.

There is a significant difference in the whole cell capacitance between ASIC1b^{+/+} neonatal and mature OHCs, this has a p value of <0.001. This is consistent with previous work that shows there is an increase in the whole cell capacitance during the development of the OHCs (Marcotti and Kros, 1999). Interestingly there is no significant difference between neonatal and mature ASIC1b^{-/-} OHCs, suggesting that the mature OHCs remain neonatal in size. This fits with the other results seen here showing that the ASIC1b^{-/-} OHCs do not develop to maturity.

ASIC1b^{+/+} and ASIC1b^{-/-} neonatal IHCs at RT have a resting membrane potential of -59 ± 5 mV (n = 6) and -63 ± 3 mV (n = 7) (NS). At BT these values are -56 ± 5 mV (n = 4) and -62 ± 4 mV (n = 4) (NS). ASIC1b^{+/+} and ASIC1b^{-/-} neonatal OHCs at RT have resting membrane potentials of -59 ± 8 mV (n = 4) and -65 ± 6 mV (n = 6) (NS), at BT the resting membrane potentials are -53 ± 4 mV (n = 10) and -45 ± 1 mV (n = 2) (NS). Mature ASIC1b^{+/+} and ASIC1b^{-/-} IHCs at BT have a resting membrane potential of -67 ± 2 mV (n = 7) and -58 ± 3 mV (n = 6) (NS). The data for mature OHCs has not been collected directly but has been interpolated from the voltage clamp recordings and ASIC1b^{+/+} and ASIC1b^{-/-} mature OHCs have a resting membrane potential of -64 ± 5 mV (n = 12) and -52 ± 7 mV (n = 7). A summary of this data can be seen in Figure 6-7A and Table 6-3.

The lack of significant differences seen in the resting membrane potentials between all cell types and conditions is likely to be due to low n numbers. However it is interesting to note that there is a large difference in the resting membrane potentials between ASIC1b^{+/+} and ASIC1b^{-/-} mature OHCs with the ASIC1b^{+/+} sitting more than 10 mV more hyperpolarised than the ASIC1b^{-/-} mature OHCs. This difference is likely to be due to the $I_{K,n}$ current not being present in the mature ASIC1b^{-/-} OHCs. The $I_{K,n}$ current is some 50% (Housley and Ashmore, 1992) open at the resting membrane potential and so this K^+ current will cause the resting membrane potential to hyperpolarise. As the current is missing in the ASIC1b^{-/-} mature OHCs sit more depolarised than the ASIC1b^{+/+} mature OHCs.

6.2.7 Mechanoelectrical transduction current

The MET current is activated by deflection of the hair bundles in both the IHCs and OHCs. The MET current is examined only in the neonatal OHCs as the hair bundle is clearly visible and much more readily available for manipulation by the fluid jet used for deflecting the hair bundle compared to neonatal IHCs. All transduction experiments were performed at room temperature and with a Cs⁺ based intracellular solution (for composition see Table 2-2).

For comparisons MET currents have been measured at -104 mV and +96 mV. In pH 7.5 extracellular solution ASIC1b^{+/+} neonatal OHCs at RT had a MET current of -303 ± 169 pA (mean \pm SEM) (n = 7) and 660 ± 267 pA (n = 7) at -104 mV and +96 mV respectively. Figure 6-8A shows a typical example. ASIC1b^{-/-} neonatal OHCs had a MET current at -104 mV of -302 ± 92 pA (n = 7) and at +96 mV 404 ± 108 pA (n = 7), an example can be seen in Figure 6-8G.

In pH 5.0 extracellular solution the ASIC1b^{+/+} OHCs had a MET current of -92 ± 36 pA (n = 3) at -104 mV and 407 ± 296 pA (n = 3) at +96 mV, an example can be seen in Figure 6-8B. ASIC1b^{-/-} OHCs had a MET current of -250 ± 129 pA (n = 3) and 381 ± 201 pA (n = 3) at -104 mV and +96 mV respectively. A typical example can be seen in Figure 6-8G.

In the presence of 100 μ M nifedipine the ASIC1b^{+/+} OHCs at RT had a much reduced MET current of -3 ± 4 pA (n = 3) at -104 mV and 29 ± 29 pA (n = 3) at +96 mV, a typical example can be seen in Figure 6-8C. ASIC1b^{-/-} OHCs at RT had a MET current of -2 ± 1 pA (n = 2) at -104mV in the presence of nifedipine and at +96 mV the MET current is 42 ± 34 pA (n = 2), Figure 6-8H shows a typical example.

In the presence of reduced extracellular pH and 100 μ M nifedipine ASIC1b^{+/+} OHCs had a MET current of -15 ± 4 pA (n = 3) at -104 mV and 165 ± 165 pA (n = 3) at -96 mV, Figure 6-8D shows a typical example. ASIC1b^{-/-} OHCs had a MET current -5 pA (n = 2) at -104 mV and -6 ± 34 pA (n = 2) at +96 mV in the presence of nifedipine at pH 5.0.

There is no statistical difference in the size of the MET current between ASIC1b^{+/+} and ASIC1b^{-/-} OHCs, suggesting that loss of ASIC1b has no effect on the mechanical electrical transduction in the neonatal OHCs.

There is no statistical difference in the size of the MET current in pH 7.5 and 5.0 suggesting that pH changes do not affect the transduction current. However results show that the

currents may be smaller in pH 5.0 extracellular solution, which suggests there may be a small modulatory effect of H^+ on the MET channel. Although there is no significant difference in the size of the MET current when comparing with and without the presence of nafamostat, this is likely because of low repetitions as it can be clearly seen that nafamostat does block this current both at pH 7.5 and at pH 5.0.

6.3 Discussion

The data presented in the chapter suggests that the development of the basolateral currents in the IHCs is unaffected by the loss of function of the ASIC1b channel. I have shown that the $I_{K,f}$ and $I_{K,s}$ currents develop to maturity along with the ASIC1b^{-/-} mature IHCs having typical resting membrane potentials and whole cell capacitances. There does however seem to be some modulatory effect of the ASIC1b channel on the effect of the $I_{K,f}$ current with this current being larger in the ASIC1b^{+/+} mature IHCs. Previous work by (Petroff et al., 2008) has shown that in HEK cells co-expression of ASIC1a and BK channels results in a reduction of the BK current. Although opposite to the result seen here it is possible that removal of the ASIC1b channel causes an up-regulation of the ASIC1a channel and a reduction in the $I_{K,f}$ current. The idea of ASIC channel substitution, up-regulation and down-regulation is discussed in Chapter 5.

In this chapter I have shown that the development of the OHCs to a neonatal stage is unaffected by the loss of the ASIC1b channel. However unlike IHCs this does not extend to maturity with the mature ASIC1b^{-/-} OHCs remaining functionally immature with a lack of expression of the $I_{K,n}$ current and a reduced whole cell capacitance, along with a lack of electromotile function.

It is interesting that prestin is not functional in the cell membrane of the ASIC1b^{-/-} mature OHCs, suggesting that ASIC1b is important for the development of electromotility. This loss of prestin is supported by unpublished data by Ugawa which shows ASIC1b^{-/-} mice have a slight increase in their hearing threshold by around 20 dB, indicative of mild hearing loss. Previous work by (Wu et al., 2004) has shown that loss of prestin causes an elevation in the hearing threshold by 40 – 60 dB. The hearing threshold shift seen in the ASIC1b^{-/-} mice matches with that seen in the prestin knockout mice and could explain the shift that has been seen.

Paired together the lack of development of the $I_{K,n}$ current and the non-appearance of electromotility in the mature ASIC1b^{-/-} OHCs suggests that the ASIC1b channel is necessary for the OHCs to develop into fully functioning mature cells.

Previous work has shown that ASIC channels can be involved in mechanosensation (Page et al., 2005; Price et al., 2001). Whilst investigating the MET current in neonatal OHCs I have found that this current is unaffected by the loss of function of the ASIC1b channel. This suggests that in neonatal OHCs at least the ASIC1b channel is not required for the normal function of the hair bundle and thus detection of sound within the mouse.

It was previously known that amiloride was a blocker of the MET current (Rüsch et al., 1994), given the similar blocking effect nafamostat and amiloride had on the ASIC currents recorded in chapter 5 I investigated the effect of nafamostat on the MET current. Much like amiloride nafamostat was able to completely block the MET currents recorded (Figure 6-8). The blocking effect of nafamostat is reversible and the MET currents after washout can be seen in Figure 6-8E and K. Nafamostat appears to block the MET current more strongly at the more hyperpolarised potentials with the block being removed at positive potentials. This is consistent with the blocking activity of many MET current blockers such as aminoglycosides and amiloride. This typical blocking activity is due to the positive potential repelling the positive charge of the blocker, removing it from the pore of the channel (Kroese et al., 1989; Marcotti et al., 2005).

6.4 Conclusions

The development of $I_{K,f}$ and so the development of the IHC's electrical properties is unaffected by the loss of function of the ASIC1b channel. ASIC1b does offer modulatory effects on the size of the $I_{K,f}$ current, as shown by a reduction in the early current in the ASIC1b^{-/-} mature IHCs.

ASIC1b appears to be required for the development of the OHCs into fully functioning mature cells, shown by the lack of the $I_{K,n}$ current and the non-appearance of electromotility and the reduction in cell size in the ASIC1b^{-/-} mature OHCs.

Mechanoelectrical transduction appears to remain normal in the ASIC1b^{-/-} neonatal OHCs. A new blocker of the MET current has been identified in nafamostat.

6.5 Future experiments

It would be useful to continue to investigate the effects of nafamostat at various concentrations on the MET current in order to get a dose response curve. It would also be interesting to see if there are smaller modulatory effects of pH change on the size of the MET currents.

The number of cells used for recordings of basolateral currents for mature OHCs needs to be increased to examine whether differences seen are real or a consequence of low numbers and to see if there is an effect of ASIC1b^{-/-}. This will also allow exploration of the resting membrane potential of the mature OHCs, to see if there is a difference here. As $I_{K,n}$ is about 50% active at rest this inward potassium current drives the membrane potential more negative and so differs from the potential recorded in the neonatal OHCs. Although it has been interpolated from the voltage clamp recordings it would be interesting to directly measure any potential differences in the resting membrane potential between ASIC1b^{+/+} and ASIC1b^{-/-} mature OHCs.

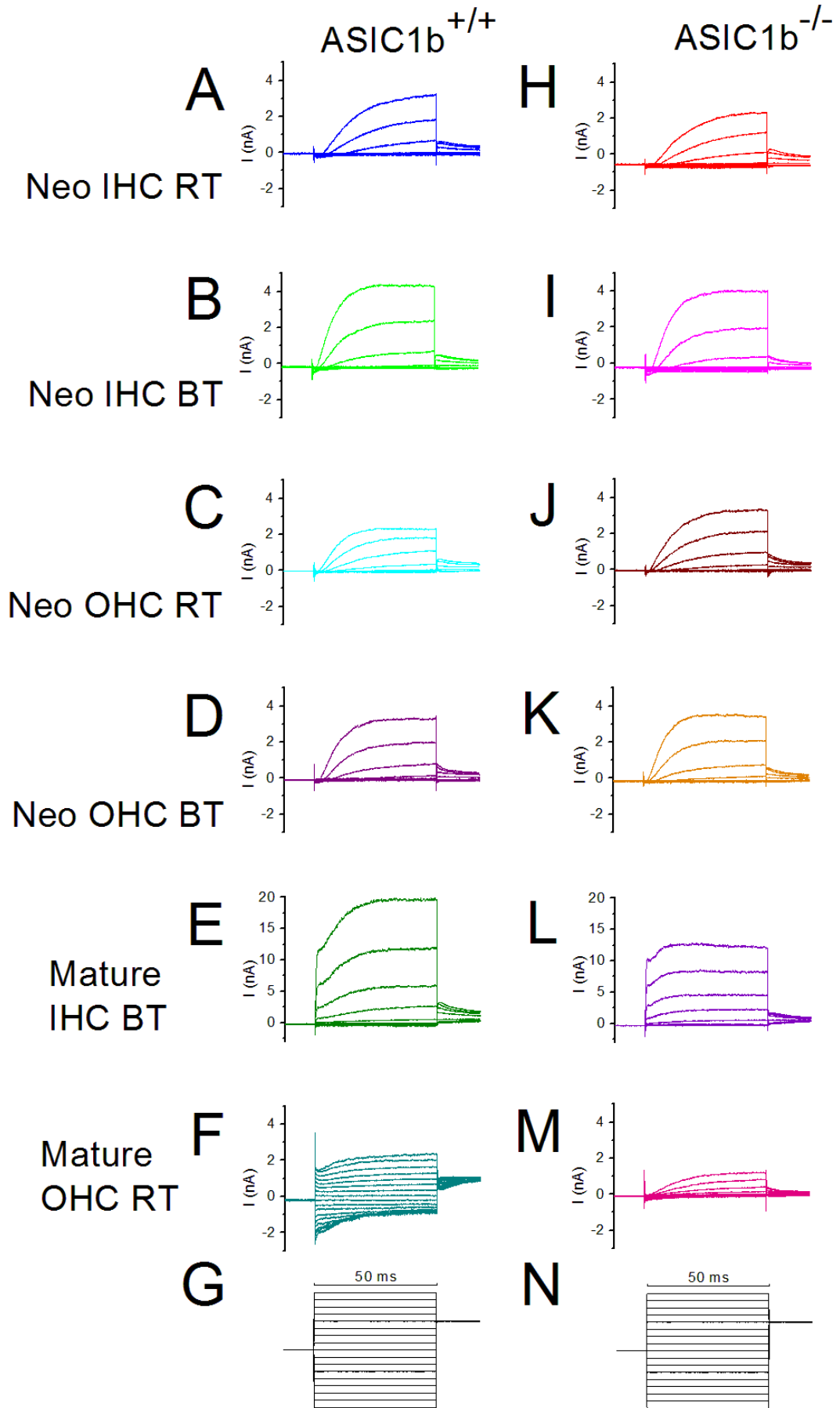


Figure 6-1 Representative current traces seen with various voltage steps

Figure 6-1 Representative current traces seen with various voltage steps

Typical whole-cell current recordings seen in response to changes in the command voltages. Steps are 50 ms long and range from -164 mV to 0 mV.

- A. Asic1b ^{+/+} Neonatal IHC at 21°C (C_m 9.0 pF, R_s 1.26 MΩ, Leak 1.6 nS, P6)
- B. Asic1b ^{+/+} Neonatal IHC at 35°C (C_m 7.8 pF, R_s 0.74 MΩ, Leak 3.3 nS, P6)
- C. Asic1b ^{+/+} Neonatal OHC at 21°C (C_m 8.4 pF, R_s 0.6 MΩ, Leak 1.3 nS, P6)
- D. Asic1b ^{+/+} Neonatal OHC at 35°C (C_m 5.6 pF, R_s 1.0 MΩ, Leak 3.1 nS, P6)
- E. Asic1b ^{+/+} Adult IHC at 35°C (C_m 9.5 pF, R_s 0.58 MΩ, Leak 4.3 nS, P24)
- F. Asic1b ^{+/+} Adult OHC at 21°C (C_m 9.7 pF, R_s 2.95 MΩ, Leak 1.0 nS, P13)
- G. Voltage command
- H. Asic1b ^{-/-} Neonatal IHC at 21°C (C_m 7.6 pF, R_s 0.84 MΩ, Leak 9.1 nS, P6)
- I. Asic1b ^{-/-} Neonatal IHC at 35°C (C_m 6.9 pF, R_s 1.38 MΩ, Leak 1.2 nS, P6)
- J. Asic1b ^{-/-} Neonatal OHC at 21°C (C_m 6.8 pF, R_s 1.54 MΩ, Leak 1.3 nS, P6)
- K. Asic1b ^{-/-} Neonatal OHC at 35°C (C_m 5.3 pF, R_s 0.8 MΩ, Leak 3.7 nS, P6)
- L. Asic1b ^{-/-} Adult IHC at 35°C (C_m 12.2 pF, R_s 0.84 MΩ, Leak 13.5 nS, P25)
- M. Asic1b ^{-/-} Adult OHC at 21°C (C_m 7.7 pF, R_s 3.55 MΩ, Leak 2.7 nS, P11)
- N. Voltage command

Traces have been corrected for linear leak conductance assuming Ohms law and baselines have not been adjusted to zero.

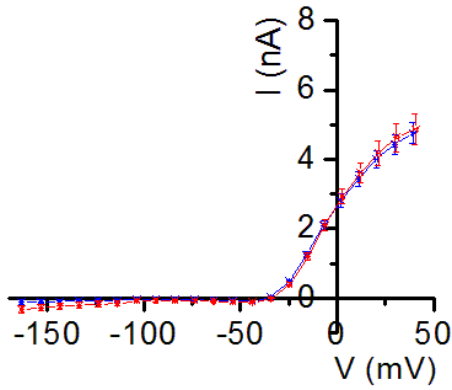
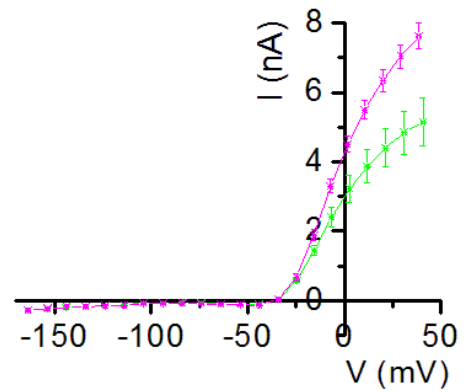
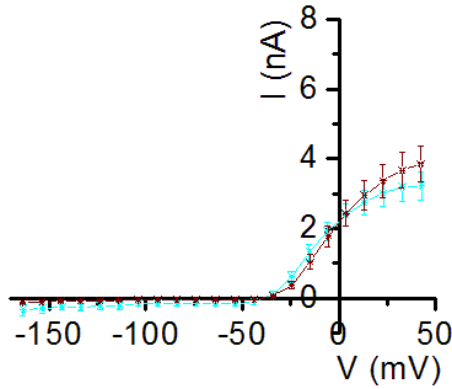
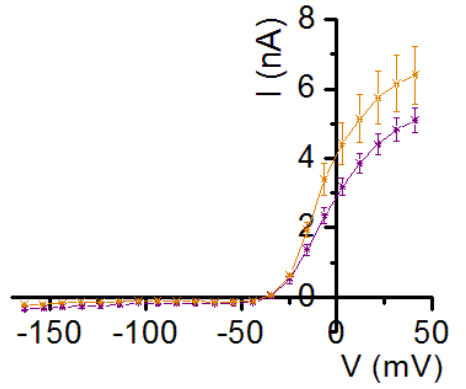
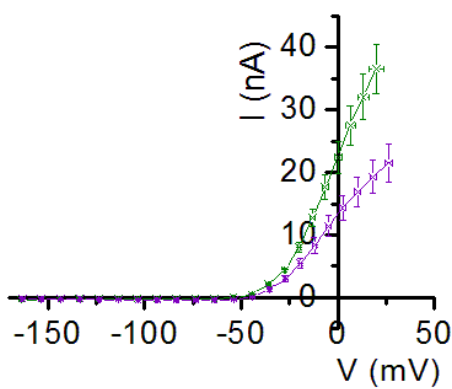
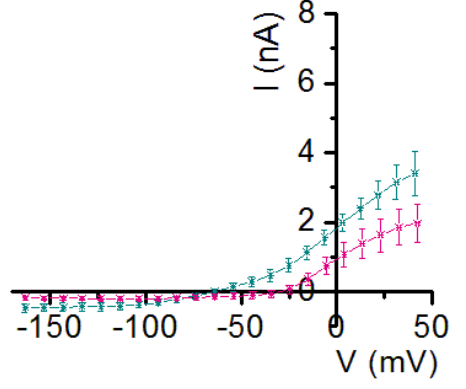
A Neo IHC RT**B** Neo IHC BT**C** Neo OHC RT**D** Neo OHC BT**E** Mature IHC BT**F** Mature OHC RT

Figure 6-2 IV plots of the steady state currents.

Figure 6-2 IV plots of the steady state currents.

An IV plot of the leak subtracted steady state currents measured during the voltage step in:

A. Neonatal IHCs at RT

ASIC1b^{+/+} (blue) (n = 7,7,7,7,32,32,32,32,32,32,32,32,32,32,32,32) and
ASIC1b^{-/-} (pink) (n = 7,7,7,7,18,18,18,18,18,18,18,18,18,18,18,18)

B. Neonatal IHCs at BT

ASIC1b^{+/+} (green) (n = 3,3,3,3,16,16,16,16,16,16,16,16,16,16,16,16) and
ASIC1b^{-/-} (pink) (n = 5,5,5,5,16,16,16,16,16,16,16,16,16,16,16,16)

C. Neonatal OHCs at RT

ASIC1b^{+/+} (blue) (n = 8,8,8,8,10,10,10,10,10,10,10,10,10,10,10,10) and
ASIC1b^{-/-} (plum) (n = 8,8,8,8,14,14,14,14,14,14,14,14,14,14,14,14)

D. Neonatal OHCs at BT

ASIC1b^{+/+} (purple) (n = 15,15,15,15,15,21,21,21,21,21,21,21,21,21,21,21) and
ASIC1b^{-/-} (orange) (n = 5,5,5,5,5,6,6,6,6,6,6,6,6,6,6,6)

E. Mature IHCs at BT

ASIC1b^{+/+} (green) (n = 9,9,9,9,15,15,15,15,15,15,15,15,15,15,15,15) and
ASIC1b^{-/-} (purple) (n = 6,6,6,6,11,11,11,11,11,11,11,11,11,11,11,11)

F. Mature OHCs at RT

ASIC1b^{+/+} (blue) (n = 12)
ASIC1b^{-/-} (pink) (n = 7)

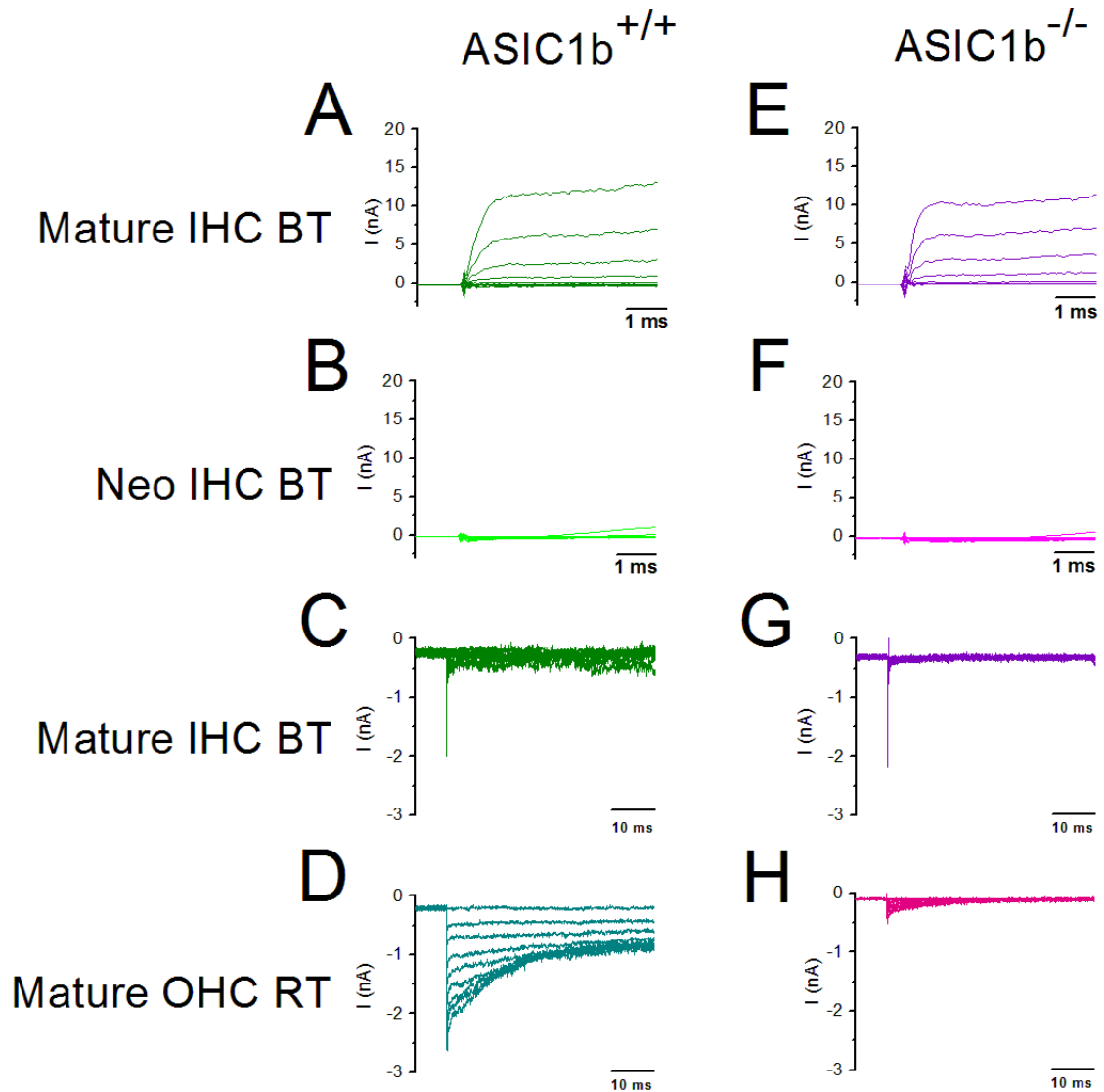


Figure 6-3 Representative current traces seen with various voltage steps highlighting $I_{K,f}$ and $I_{K,n}$.

Typical whole-cell current recordings seen in response to changes in the command voltages. Figures A,B,E and F has had the time axis expanded to show the first 5 ms after the voltage change to highlight $I_{K,f}$, and show all current recordings between -164 mV and 0 mV (10 mV steps) Figures C,D,G and H have had the current axis expanded to highlight $I_{K,n}$ and show traces only between -164 mV and -84 mV (10 mV steps).

- A. *Asic1b*^{+/+} Mature IHC at BT (C_m 9.5 pF, R_s 0.58 M Ω , Leak 4.3 nS, P24)
- B. *Asic1b*^{+/+} Neonatal IHC at BT (C_m 7.8 pF, R_s 0.74 M Ω , Leak 3.3 nS, P6)
- C. *Asic1b*^{+/+} Mature IHC at BT C_m 9.5 pF, R_s 0.58 M Ω , Leak 4.3 nS, P24)
- D. *Asic1b*^{+/+} Mature OHC at RT (C_m 9.7 pF, R_s 2.95 M Ω , Leak 1.0 nS, P13)
- E. *Asic1b*^{-/-} Mature IHC at BT (C_m 11.2 pF, R_s 0.846 M Ω , Leak 13.5 nS, P25)
- F. *Asic1b*^{-/-} Neonatal IHC at BT (C_m 6.9 pF, R_s 1.38 M Ω , Leak 1.2 nS, P6)
- G. *Asic1b*^{-/-} Mature IHC at BT (C_m 11.2 pF, R_s 0.846 M Ω , Leak 13.5 nS, P25)
- H. *Asic1b*^{-/-} Mature OHC at RT (C_m 7.7 pF, R_s 3.55 M Ω , Leak 2.7 nS, P11)

Traces have been corrected for linear leak conductance assuming Ohms law and baselines have not been adjusted to zero.

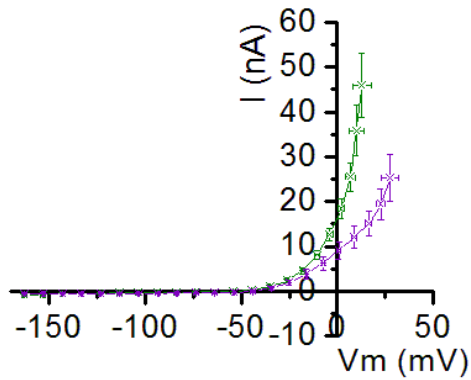
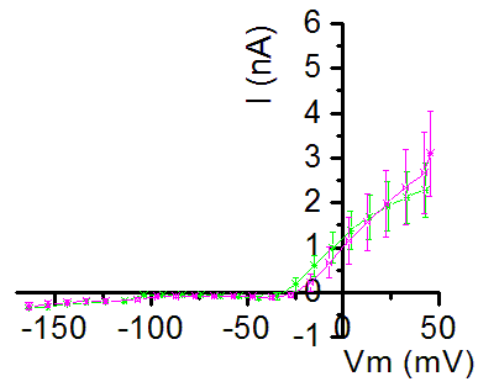
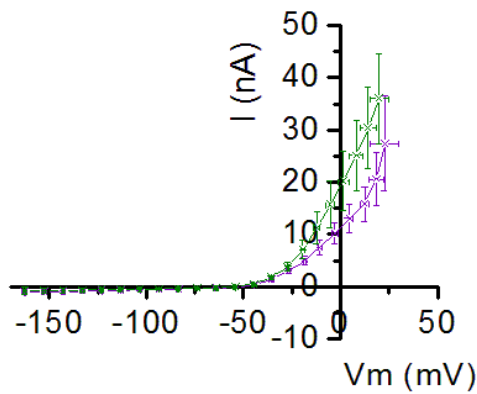
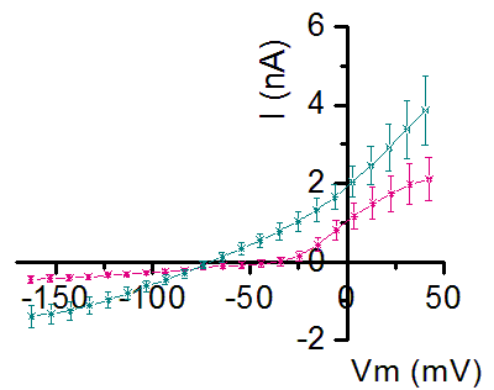
A Mature IHC BT**B** Neo IHC BT**C** Mature IHC BT**D** Mature OHC RT

Figure 6-4. IV plots of the leak subtracted $I_{K,f}$ and inward peak currents.

IV plots of the leak subtracted $I_{K,f}$ and inward peak currents measured during the voltage step in:

- A. Early currents in mature IHCs at BT
 - ASIC1b^{+/+} (green) (n = 9,9,9,9,12,12,12,12,12,12,12,12,12,12,12,12,12)
 - ASIC1b^{-/-} (purple) (n = 6,6,6,6,6,8,8,8,8,8,8,8,8,8,8,8,8)
- B. Early currents in neonatal IHCs at BT
 - ASIC1b^{+/+} (green) (n = 3,3,3,3,3,6,6,6,6,6,6,6,6,6,6,6,6)
 - ASIC1b^{-/-} (pink) (n = 5,5,5,5,5, 9,9,9,9,9,9,9,9,9,9,9,9,9,9,9)
- C. Peak currents in mature IHCs at BT
 - ASIC1b^{+/+} (green) (n = 5) and
 - ASIC1b^{-/-} (purple) (n = 6)
- D. Peak currents in mature OHCs at RT
 - ASIC1b^{+/+} (blue) (n = 8) and
 - ASIC1b^{-/-} (pink) (n = 7)

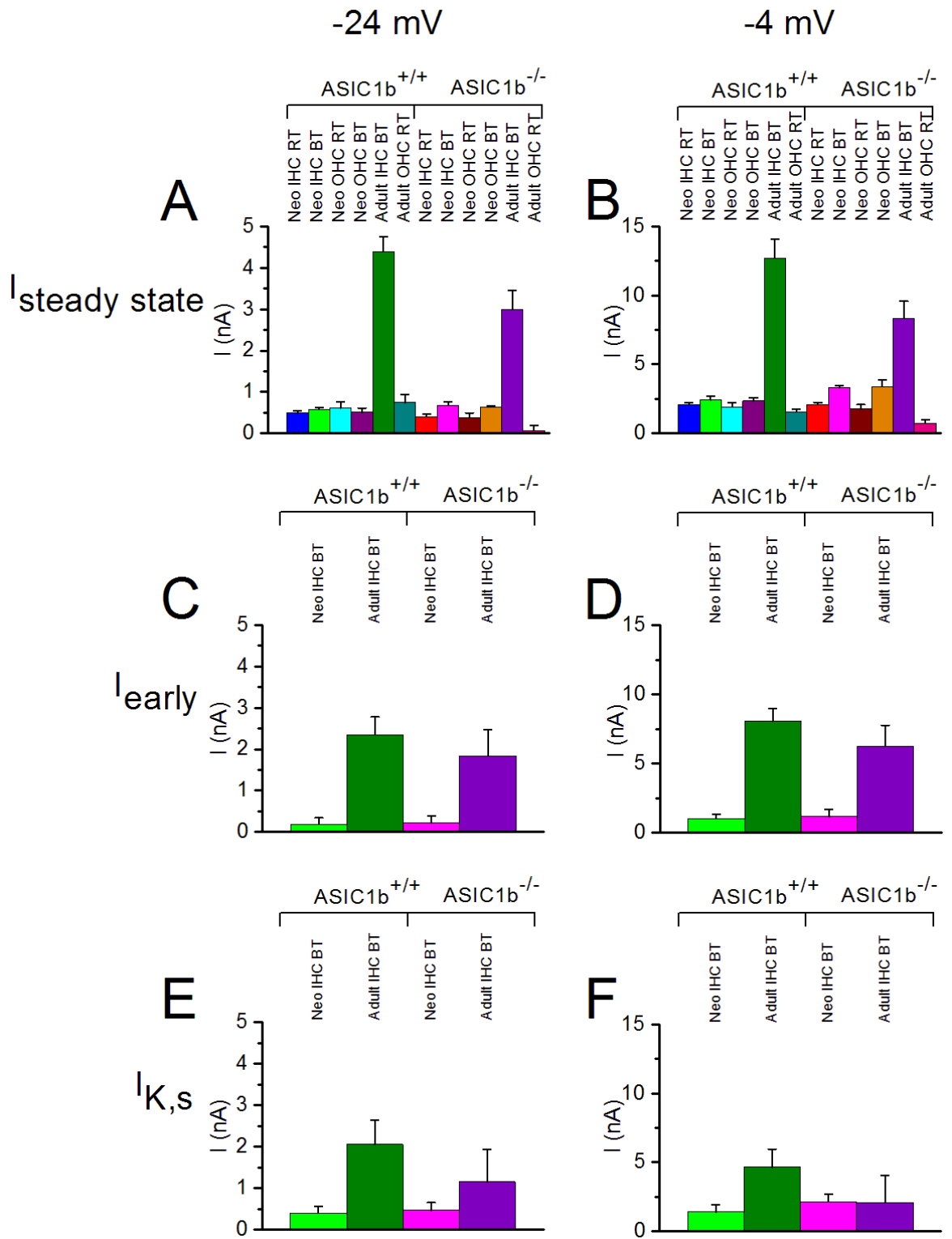


Figure 6-5 Current measurements for steady state currents, $I_{K,f}$ and $I_{K,s}$.

Figure 6-5 Current measurements for steady state currents, $I_{K,f}$ and $I_{K,s}$.

Leak subtracted current measurements for:

- A. Steady state currents at -20 mV (n = 32,16,10,21,15,12,18,15,14,6,11,7)
- B. Steady state currents at 0 mV (n = 32,16,10,21,15,12,18,15,14,6,11,7)
- C. Early currents at -20 mV (n = 6,12,9,8)
- D. Early currents at 0 mV (n = 6,12,9,8)
- E. $I_{K,s}$ at -20 mV (n = 6,12,9,8)
- F. $I_{K,s}$ at 0 mV (n = 6,12,9,8)

All graphs show mean Current measurements \pm SEM. All recordings were measured from a holding potential of -84 mV. Steady state currents were measured over 10 ms towards the end of the 50 ms voltage step $I_{K,f}$ currents were measured 0.02 ms after the voltage step onset. Peak currents were measured as the largest current seen during the 50 ms step.

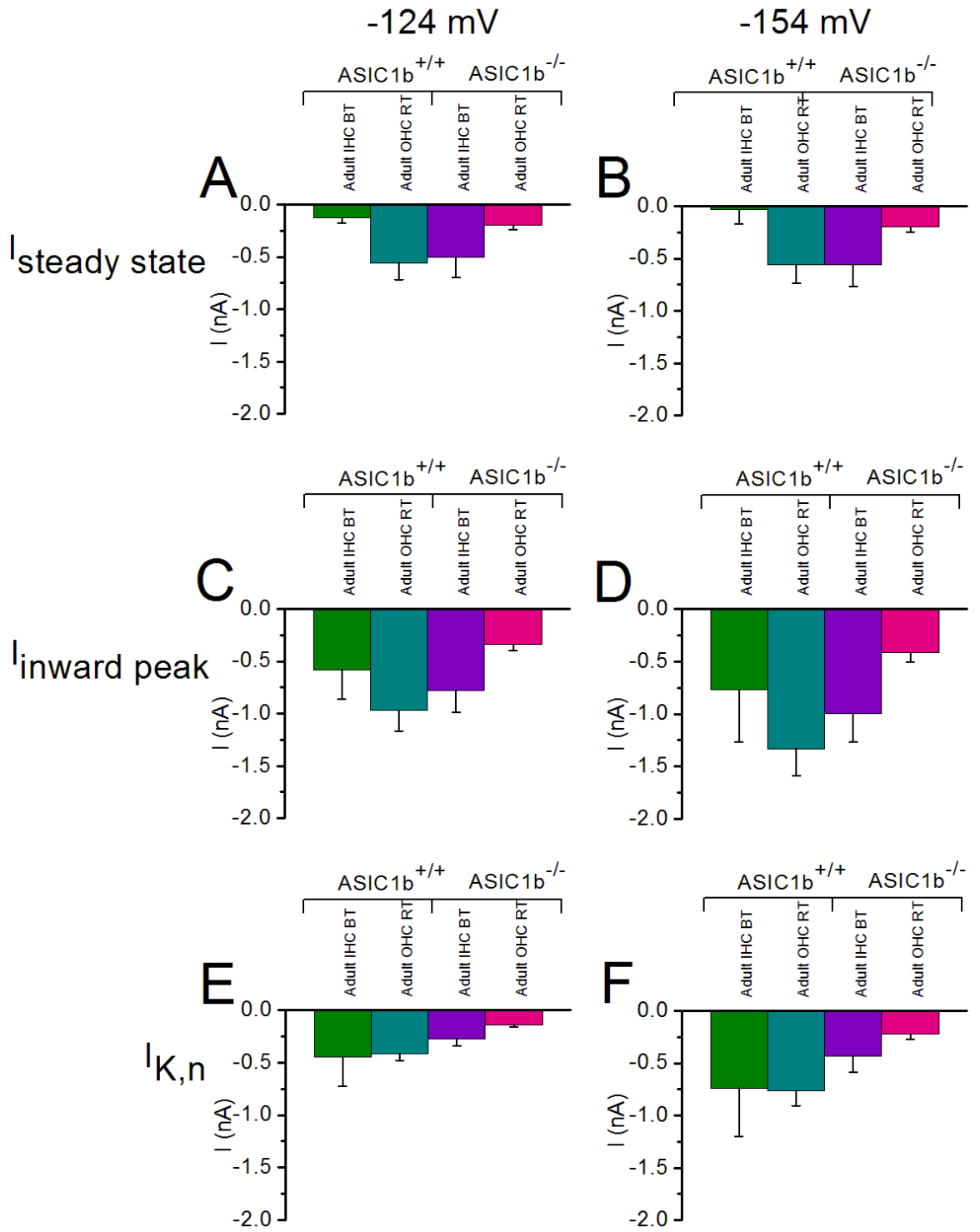


Figure 6-6 Current measurements for steady state currents, inward peak currents and $I_{K,n}$

Figure 6-6 Current measurements for steady state currents, inward peak currents and $I_{K,n}$

Leak subtracted current measurements for:

- A. Steady state currents at -124 mV (n = 5,8,6,7)
- B. Steady state currents at -154 mV (n = 5,8,6,7)
- C. Peak currents at -124 mV (n = 5,8,6,7)
- D. Peak currents at -154 mV (n = 5,8,6,7)
- E. $I_{K,n}$ at -124 mV (n = 5,8,6,7)
- F. $I_{K,n}$ at -154 mV (n = 5,8,6,7)

All graphs show mean Current measurements \pm SEM. All recordings were measured from a holding potential of -84 mV. Steady state currents were measured over 10 ms towards the end of the 50 ms voltage step. Peak currents were measured as the largest current seen during the 50 ms step.

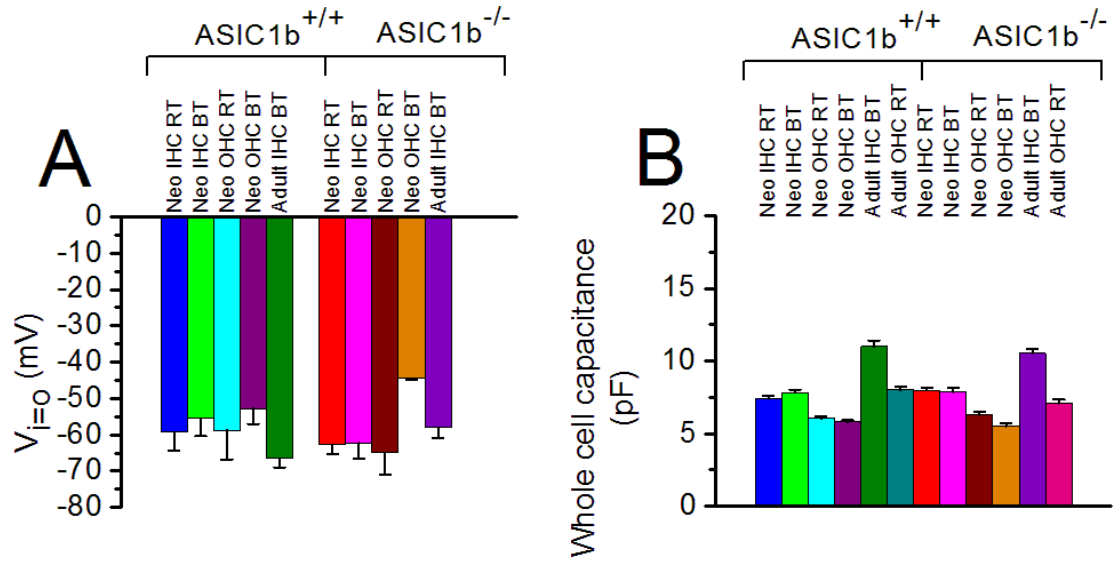


Figure 6-7 Whole cell capacitance and resting membrane potential measurements.

- A. Shows the mean \pm SEM resting membrane potential values for the hair cells (n = 6,4,4,10,7,0,7,4,6,2,6,0)
- B. Shows the mean \pm SEM whole cell capacitance measurements for the hair cells (n = 34,20,24,32,26,11,31,22,24,10,22,8)

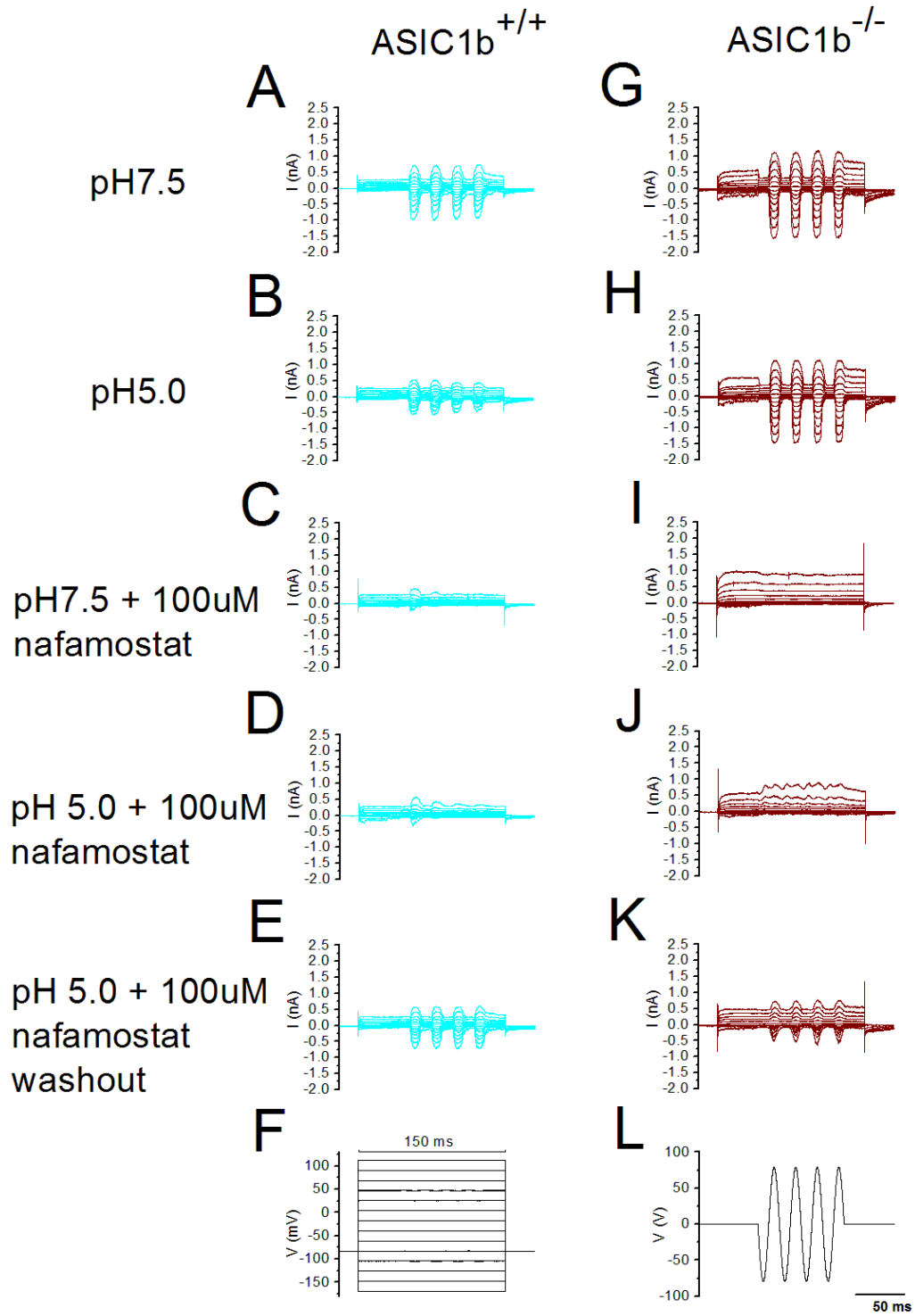


Figure 6-8 Typical whole-cell current recordings seen in OHCs in response to deflection of the hair bundles in various extracellular conditions:

Figure 6-8 Typical whole-cell current recordings seen in OHCs in response to deflection of the hair bundles in various extracellular conditions:

- A. Asic1b^{+/+} pH 7.5 (C_m 7.6 pF, R_s 5.8 MΩ P2)
- B. Asic1b^{+/+} pH 5.0 (C_m 7.6 pF, R_s 5.8 MΩ P2)
- C. Asic1b^{+/+} pH 7.5 plus 100 μM nafamostat (C_m 7.6 pF, R_s 5.8 MΩ P2)
- D. Asic1b^{+/+} pH 5.0 plus 100 μM nafamostat (C_m 7.6 pF, R_s 5.8 MΩ P2)
- E. ASIC1b^{+/-} pH 5.0 plus 100 μM nafamostat washout (C_m 7.6 pF, R_s 5.8 MΩ P2)
- F. Voltage command protocol
- G. Asic1b^{-/-} pH 7.5 (C_m 7.4 pF, R_s 4.3 MΩ P4)
- H. Asic1b^{-/-} pH 5.0 (C_m 7.4 pF, R_s 4.3 MΩ P4)
- I. Asic1b^{-/-} pH 7.5 plus 100 μM nafamostat (C_m 8.2 pF, R_s 5.1 MΩ P3)
- J. Asic1b^{-/-} pH 5.0 plus 100 μM nafamostat (C_m 7.3 pF, R_s 5.2 MΩ P4)
- K. ASIC1b^{+/-} pH 5.0 plus 100 μM nafamostat washout (C_m 7.3 pF, R_s 5.2 MΩ P4)
- L. Fluid jet stimulus for deflection of the hair bundle.

All recordings were performed at RT and from a holding potential of -84 mV. Voltage command potentials haven't been corrected for series resistance errors as this difference is less than 5 mV. Recordings haven't been corrected for linear leak conductance and baselines have not been adjusted to zero.

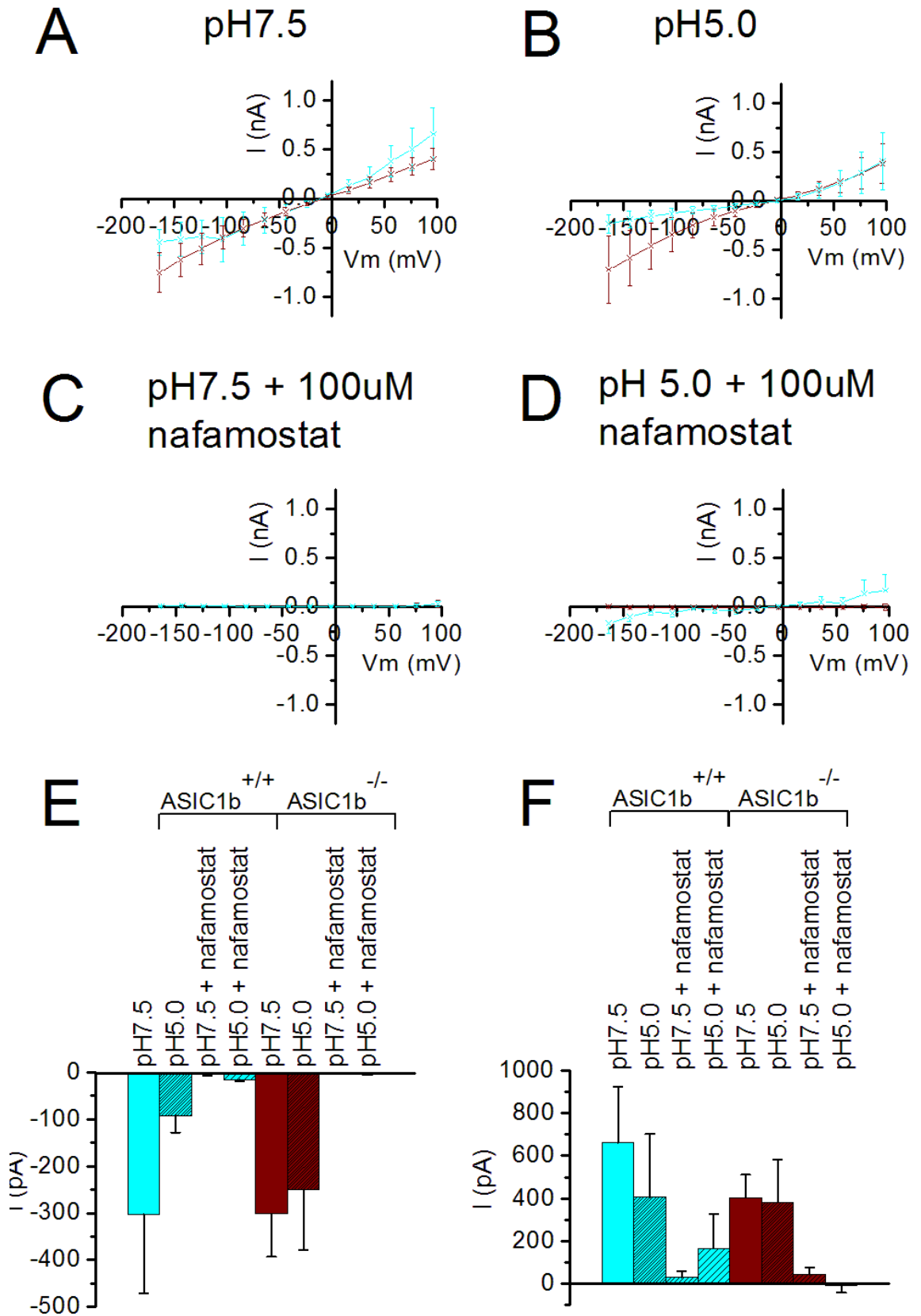


Figure 6-9 IV plots and bar graphs to describe the MET current in the neonatal OHCs.

Figure 6-9 IV plots and bar graphs to describe the MET current in the neonatal OHCs.

Figures A,B,C and D show IV plots for the MET current (ASIC1b^{+/+} in blue, and ASIC1b^{-/-} in plum) in:

- A. pH 7.5 extracellular solution (n = 7,7)
- B. pH 5.0 extracellular solution (n = 3,3)
- C. pH 7.5 plus 100 μ M nafamostat (n = 3,2)
- D. pH 5.0 plus 100 μ M nafamostat (n = 3,2)

Figures E and F show bar graphs of the MET currents measured at:

- E. -96 mV (n = 7,3,3,3,7,3,2,2)
- F. 86 mV (n = 7,3,3,3,7,3,2,2)

MET currents were measured as the average of the centre peak currents with the inhibitory phase currents subtracted

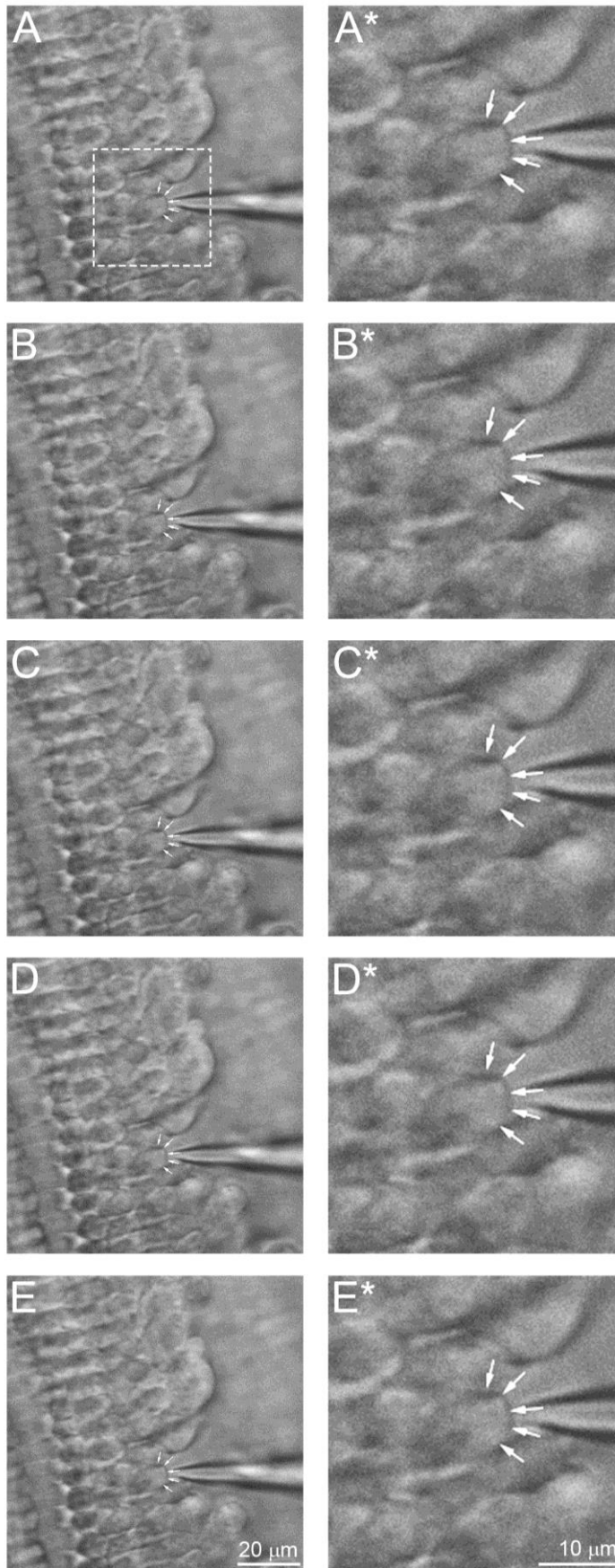


Figure 6-10 presence of electromotility $ASIC1b^{+/+}$ electromotility movie.

Figure 6-10 presence of electromotility ASIC1b^{+/+} electromotility movie.

Electromotile response seen in P12 mature OHCs when the membrane potential is stepped from -84 mV to +76 mV. The white arrows mark the outline of the cell, the membrane of the cell pulls away from these markers during the depolarising step.

The OHC is held at -84 mV and is in a resting position, time 0 ms.

The OHC membrane potential has been stepped to +76 mV and the cell body is beginning to contract, time 500 ms.

The OHC membrane potential is still held at +76 mV and the cell body is fully contracted, time 750 ms.

The OHC membrane potential has been stepped back to -86 mV and the cell body is beginning to elongate, time 1000 ms.

The OHC membrane potential is still held at -84 mV and the cell body has elongated back to its resting position, times 1250 ms.

A*,B*,C*D* and E* are zoomed in images of the square outlined in A in A,B,C,D and E respectively and allow the small movements of the OHC cell body to be seen clearly.

The movie itself is attached to the accompanying C.D.

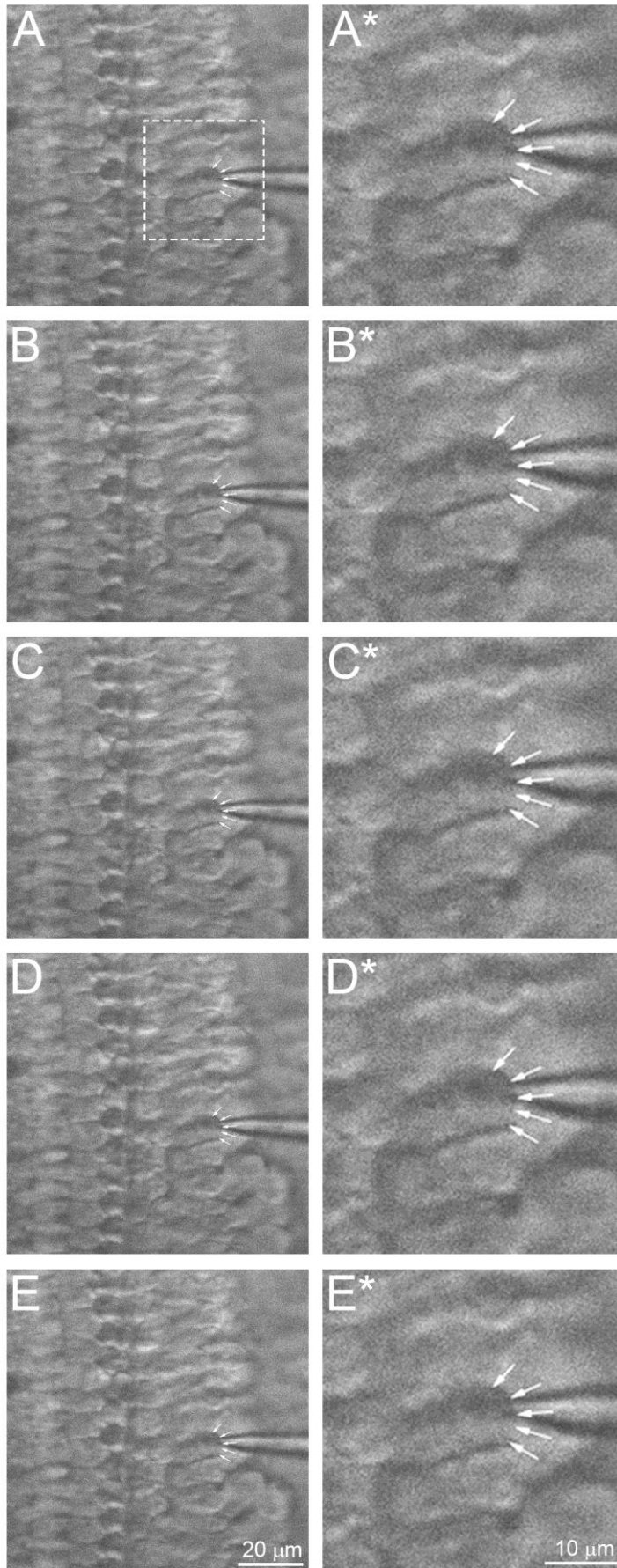


Figure 6-11 absence of electromotility ASIC1b^{-/-} electromotility movie.

Figure 6-11 absence of electromotility ASIC1b^{-/-} electromotility movie.

Electromotile response seen in P12 mature OHCs when the membrane potential is stepped from -84 mV to +76 mV. The white arrows mark the outline of the cell, the membrane of the cell pulls away from these markers during the depolarising step.

- A. The OHC is held at -84 mV and is in a resting position, time 0 ms.
- B. The OHC membrane potential has been stepped to +76 mV and the cell body does not contract, time 500 ms.
- C. The OHC membrane potential is still held at +76 mV and the cell body is still in the resting position, time 750 ms.
- D. The OHC membrane potential has been stepped back to -86 mV and the cell body length has remained unchanged, time 1000 ms.
- E. The OHC membrane potential is still held at -84 mV and the cell body has remained in its resting position, times 1250 ms.

A*,B*,C*D* and E* are zoomed in images of the square outlined in A in A,B,C,D and E respectively and allow the small movements of the OHC cell body to be seen clearly.

The movie itself is attached to the accompanying C.D.

		$I_{\text{steady state}}$		$I_{\text{steady state}}$		$I_{\text{instantaneous}}$		$I_{\text{instantaneous}}$		I_{K_s}		I_{K_s}	
		-24 mV		-4 mV		-24 mV		-4 mV		-24 mV		-4 mV	
		I (pA)	n	I (pA)	n	I (pA)	n	I (pA)	n	I (pA)	n	I (pA)	n
+/-	neonatal IHC RT	491.4 ±50.4	32	2090.8 ±142.6	32								
	neonatal IHC BT	581.6 ±48.6	16	2402.9 ±273.9	16	-499.3 ±141	6	-413.4 ±82.1	6	1095.101 ±150.8	6	3566.158 ±417.3	6
	neonatal OHC RT	610.9 ±158.7	10	1919.2 ±275.2	10								
	neonatal OHC BT	507.8 ±105.6	21	2355.4 ±220.5	21								
	adult IHC BT	4398.0 ±359.7	15	12706.0 ±1374.9	15	1658.4 ±246.3	12	7235.1 ±1019.3	12	2945.146 ±358.8	12	6384.45 ±1069.8	12
	adult OHC RT	743.2 ±194.9	12	1545.7 ±210.8	12								
-/-	neonatal IHC RT	398.5 ±64.7	18	2104.1 ±146.9	18								
	neonatal IHC BT	672.7 ±95.8	15	3295.6 ±193.4	15	-323.8 ±45.6	9	-353.4 ±47.9	9	937.9793 ±136.7411	9	3552.735 ±307.3	9
	neonatal OHC RT	385.4 ±108	14	1778.9 ±302.2	14								
	neonatal OHC BT	634.6 ±26	6	3397.8 ±447.4	6								
	adult IHC BT	2987.8 ±465.3	11	8335.4 ±1237.6	11	721.4 ±335.3	8	3696.2 ±949.5	8	641.7256 ±1021	8	578.5755 ±2504.8	8
	adult OHC RT	64.3 ±121.1	7	730.1 ±253.2	7								

Table 6-1 Steady state, I_{K_f} and I_{K_s} current measurements.. All current measurements are mean ± SEM. All recordings were measured from a holding potential of -84 mV. Steady state currents were measured over 10 ms towards the end of the 50 ms voltage step. I_{K_f} currents were measured 0.02 ms after the voltage step onset. I_{K_s} is the subtraction between these two currents.

		$I_{inward\ peak}$		$I_{inward\ peak}$		$I_{steady\ state}$		$I_{steady\ state}$		$I_{k,n}$		$I_{k,n}$	
		-124 mV		-154 mV		-124 mV		-154 mV		-124 mV		-154 mV	
		I (pA)	n	I (pA)	n	I (pA)	n	I (pA)	n	I (pA)	n	I (pA)	n
+/-	neonatal IHC RT												
	neonatal IHC BT												
	neonatal OHC RT												
	neonatal OHC BT												
	adult IHC BT	-578.7 ±281.1	5	-768.7 ±500.2	5	-128.5 ±51	5	-31.9 ±136.4	5	-450.2 ±274.3	5	-736.8 ±465.8	5
	adult OHC RT	-971.8 ±193.3	8	-1329.4 ±259.7	8	-558.4 ±159.7	8	-562.6 ±171.6	8	-413.4 ±65.8	8	-766.9 ±138.6	8
-/-	neonatal IHC RT												
	neonatal IHC BT												
	neonatal OHC RT												
	neonatal OHC BT												
	adult IHC BT	-778.4 ±213.3	6	-993.3 ±275	6	-507.1 ±186.2	6	-557.6 ±212.3	6	-271.3 ±66.7	6	-435.8 ±149.2	6
	adult OHC RT	-339.0 ±54.6	7	-419.0 ±86.8	7	-198.6 ±44	7	-196.3 ±55.4	7	-140.4 ±20.7	7	-222.6 ±50.6	7

Table 6-2 Inward peak, Steady state and $I_{k,n}$ current measurements.. All current measurements are mean \pm SEM. All recordings were measured from a holding potential of -84 mV. Steady state currents were measured over 10 ms towards the end of the 50 ms voltage step. Peak currents were measured as the largest current seen during the 50 ms step. $I_{k,n}$ is the subtraction between the two.

		Whole cell capacitance		$V_{i=0}$	
		F (pF)	n	V (mV)	n
+/-	neonatal IHC RT	7.4 ±0.2	34	-59.3 ±5	6
	neonatal IHC BT	7.8 ±0.2	20	-55.5 ±4.9	4
	neonatal OHC RT	6.0 ±0.2	24	-58.8 ±8.1	4
	neonatal OHC BT	5.8 ±0.1	32	-52.8 ±4.2	10
	adult IHC BT	11.0 ±0.4	26	-66.6 ±2.4	7
	adult OHC RT	8.0 ±0.2	11		
-/-	neonatal IHC RT	8.0 ±0.2	31	-62.7 ±2.5	7
	neonatal IHC BT	7.9 ±0.3	22	-62.3 ±4.3	4
	neonatal OHC RT	6.3 ±0.2	24	-65.0 ±6	6
	neonatal OHC BT	5.5 ±0.2	10	-44.5 ±0.5	2
	adult IHC BT	10.5 ±0.3	22	-58.0 ±2.9	6
	adult OHC RT	7.1 ±0.3	8		

Table 6-3 Whole cell capacitance and resting membrane potential values. Values shown are mean ± SEM.

		pH7.5		pH5.0		pH7.5 + nafamostat		pH5.0 + nafamostat	
		I (pA)	n	I (pA)	n	I (pA)	n	I (pA)	n
-104 mV	+/+	-303.31 ±168.64	7	-92.30 ±36.1	3	-2.93 ±4.44	3	-14.85 ±4.02	3
	-/-	-302.31 ±91.82	7	-250.05 ±128.72	3	-1.98 ±0.77	2	-5.29 ±0.26	2
+96 mV	+/+	659.79 ±266.78	7	406.83 ±296.19	3	29.00 ±28.69	3	165.23 ±164.47	3
	-/-	404.43 ±107.7	7	381.05 ±201.16	3	42.42 ±33.98	2	-6.63 ±33.74	2

Table 6-4 MET current measurements. All current measurements are mean ± SEM. All recordings were measured from a holding potential of -84 mV. MET currents were measured as the average of the centre peak currents with the inhibitory phase currents subtracted

6.6 Amendment

Since the completion of both the first draft of this thesis and *viva voce* I have collected more data on the presence of electromotility within the ASIC1b^{-/-} mature OHCs. I have seen the presence of electromotility in 9 out of 9 cells that have since been recorded from. Although movies and the subsequent images have not yet been recorded and so cannot be shown here, this new result does suggest that OHCs are able to develop to maturity in terms of their electromotile behaviour in the ASIC1b^{-/-} mouse model.

I have not been able to collect any further data on the lack of expression of the $I_{K,n}$ current in these hair cells and so more work is required to be sure that this loss of current expression is still present despite the change in the presence of electromotility.

In order to confirm that this change of functionality is not due to any genetic alterations in the mouse models used the genotyping of these mice is currently being undertaken.

The increase of hearing threshold seen in the ASIC1b^{-/-} mouse models (Ugawa. S., personal communication) that had previously been attributed to a lack of electromotile function in the mature OHCs may further be explained by loss of function of the ASIC1b channel within the hair cells with the loss of function of the $I_{K,n}$ current within the mature OHCs and the reduced $I_{K,f}$ current within the mature IHCs. The lack of expression of the $I_{K,n}$ current in the mature OHCs will increase the time constant of the membrane of the hair cell meaning that the cells will be less sensitive to incoming sound signals and increasing the hearing threshold of these mice. The smaller $I_{K,f}$ current in the mature ASIC1b^{-/-} IHCs will mean that the IHCs will require a larger input stimulus for a similar activation of the $I_{K,f}$ current in the ASIC1b^{+/+} mature IHCs. This increase in stimulus size will increase the hearing threshold in these mice and may account for the changes that have been detected.

In conclusion I can now say that ASIC1b is required for the development of the basolateral current $I_{K,n}$ in mature OHCs whilst it is not required for the development of the electromotile behaviour in these cells.

7 FINAL CONCLUSIONS

In the previous four results chapters I have shown that maturation of the hair cells of the auditory organ is a complex process and can be inhibited through the loss of function of the proteins Myo7a, Hrm, PCDH15 and ASIC1b. Although the effects of mutations in ASIC1b and the Usher proteins are somewhat dissimilar in that ASIC1b^{-/-} mature IHCs do have the I_{K,f} current which is absent in Myo7a^{sh6j/sh6j}, Ush1c^{-/-}, PCDH15^{AV3J/AV3J} and PCDH15^{AV6J/AV6J} mature IHCs, there are also some similarities with the I_{K,f} current in the ASIC1b^{-/-} mature IHCs being smaller compared to that seen in ASIC1b^{+/+} mature IHCs. This suggests that although ASIC1b is not required for the appearance or targeting to the cell membrane of the BK channels, it may be important in the regulation of the I_{K,f} current.

I have also shown that mature homozygous mutant OHCs which lack the function of all of the Usher proteins mentioned above, fail to develop the I_{K,n} current. Interestingly in ASIC1b^{-/-} mature OHCs there is also a lack of electromotility, this dysfunction however does not extend to the mature Myo7a^{sh6j/sh6j} OHCs and electromotility is likely to also be present in Ush1c^{-/-}, PCDH15^{AV3J/AV3J} and PCDH15^{AV6J/AV6J} mature OHCs given the similarity of affect of these mutations in the IHCs. It might be possible that ASIC1b is required for the modulation of prestin activity rather than its expression alone, meaning that prestin may be expressed but is non-functional without the presence of ASIC1b, and it is this that causes the difference between the two mature OHCs I have investigated. However, this statement is purely speculative and would require further investigation to be certain. It may also be that ASIC1b is required for the expression of prestin and that it is this which causes the lack of electromotility seen in the ASIC1b^{-/-} mature OHCs. It appears that the ASIC1b protein is required for the development of prestin function in the OHCs, but the Usher proteins are not.

In all of the mouse models investigated here it is interesting to note that the developmental failure of the electrical properties of the hair cells is a secondary effect to the loss of the function of a specific protein, rather than as a direct result of the lack of protein function. Although uncertain, I have speculated that action potential generation in neonatal hair cells is an important signalling factor for the correct development of both the IHCs and OHCs. In hair cells that lack the function of one of the Usher proteins this activity is likely to be reduced due to the decreased open probability of the MET channel. Although not investigated, loss of function of the ASIC1b channel may cause smaller modulatory effects on the spiking activity in the neonatal hair cells which may account for the reduced I_{K,f} current in the mature ASIC1b^{-/-} IHCs and lack of I_{K,n} current and prestin expression in the mature ASIC1b^{-/-} OHCs. It is also possible that the reduced I_{K,f} current in the ASIC1b^{-/-} mature IHCs is unrelated to the action potential activity in the neonatal IHCs and is as a consequence of up-regulation of another ASIC

channel subtype such as ASIC1a, that may modulate the activity of the BK channels and cause a reduction in the size of the $I_{K,f}$ current (Donier et al., 2008; Petroff et al., 2008).

This work agrees with results previously published which found that lack of Myo6 function caused a failure of the IHCs to develop to maturity with a lack of $I_{K,f}$ and $I_{K,n}$ expression along with the presence of immature ribbon synapses in the mature IHC (Roux et al., 2009). This work, along with the work I have described here, suggests that a functional hair bundle is required for the correct development of the hair cells. Lack of function of the $Ca_v1.3$ calcium channel in the mature IHCs also results in a similar phenotype to that seen here with the loss of function of the Usher proteins. Neonatal $Ca_v1.3^{-/-}$ IHCs are unable to produce action potentials due to the loss of the voltage gated calcium channels and when these cells have reached maturity they continue to express an immature complement of currents, with the $I_{K,f}$ current not being expressed (Brandt et al., 2003b). This result agrees with the data I present here if we believe that mis-functioning hair bundles decreases the likelihood of spontaneous action potential generation in the Usher protein mutant neonatal IHCs, and that this is important in the developmental failure of the mature IHCs in these mouse models. The exact mechanism behind the failure of the hair cells to develop their full complement of mature currents is unknown. From this work I am speculating that initiation of this process is multi-layered with the correct function of at least the hair bundle and a pH sensitive current being required for the hair cells to develop electrically to maturity.

8 SUPPLEMENTARY INFORMATION

Figure 8-1 - Immature organ of Corti dissection video.

Video of the removal of the apical section of the organ of Corti from a P4 CD-1 mouse. For ease of viewing certain events have been time-stamped:

0:00 the nose of the mouse is to the left of the screen with the cochlea on the right

0:15 gently pulling on the temporal bone removes the cochlea

0:30 the cochlea has been removed from the skull

1:54 the outer casing of the cochlea has been removed

2:06 the soft tissue including the organ of Corti and the stria Vascularis has been unwound from the central modiolus

2:45 the stria Vascularis has been removed leaving the organ of Corti

3:11 the organ of Corti has been cut into apical and basal sections with the apical region sitting above the basal.

Figure 8-2 - Mature organ of Corti dissection video.

Video of the removal of the apical section of the organ of Corti from a P20 CD-1 mouse. For ease of viewing certain events have been time-stamped:

0:00 the cochlea is sitting at the top of the screen with the vestibular system sitting at the bottom

1:00 the outer casing of the cochlea has been removed

2:00 the organ of Corti has been separated from the central modiolus

2:21 the apical section of the organ of Corti has been removed from the cochlea

3:00 increased magnification of the mature organ of Corti preparation

Figure 8-3 Electromotility in mature Myo7a^{+/sh6j} OHCs video

Figure 8-4 Electromotility in mature Myo7a^{sh6j/sh6j} OHCs video

Figure 8-5 Electromotility in mature ASIC1b^{+/+} OHCs video

Figure 8-6 Electromotility in mature ASIC1b^{-/-} OHCs video

9 REFERENCES

- Adato, A., Michel, V., Kikkawa, Y., Reiners, J., Alagramam, K.N., Weil, D., Yonekawa, H., Wolfrum, U., El-Amraoui, A., and Petit, C. (2005). Interactions in the network of Usher syndrome type 1 proteins. *Hum. Mol. Genet.* *14*, 347–356.
- Ahmed, Z.M., Riazuddin, S., Bernstein, S.L., Ahmed, Z., Khan, S., Griffith, A.J., Morell, R.J., Friedman, T.B., Riazuddin, S., and Wilcox, E.R. (2001). Mutations of the protocadherin gene PCDH15 cause Usher syndrome type 1F. *Am. J. Hum. Genet.* *69*, 25–34.
- Ahmed, Z.M., Goodyear, R., Riazuddin, S., Lagziel, A., Legan, P.K., Behra, M., Burgess, S.M., Lilley, K.S., Wilcox, E.R., Riazuddin, S., et al. (2006). The Tip-Link Antigen, a Protein Associated with the Transduction Complex of Sensory Hair Cells, Is Protocadherin-15. *J. Neurosci.* *26*, 7022–7034.
- Akopian, A.N., Chen, C.C., Ding, Y., Cesare, P., and Wood, J.N. (2000). A new member of the acid-sensing ion channel family. *Neuroreport* *11*, 2217–2222.
- Alagramam, K.N., Murcia, C.L., Kwon, H.Y., Pawlowski, K.S., Wright, C.G., and Woychik, R.P. (2001). The mouse Ames waltzer hearing-loss mutant is caused by mutation of *Pcdh15*, a novel protocadherin gene. *Nat. Genet.* *27*, 99–102.
- el-Amraoui, A., Sahly, I., Picaud, S., Sahel, J., Abitbol, M., and Petit, C. (1996). Human Usher 1B/mouse shaker-1: the retinal phenotype discrepancy explained by the presence/absence of myosin VIIA in the photoreceptor cells. *Hum. Mol. Genet.* *5*, 1171–1178.
- Anniko, M. (1983). Cytodifferentiation of cochlear hair cells. *Am J Otolaryngol* *4*, 375–388.
- Askwith, C.C., Benson, C.J., Welsh, M.J., and Snyder, P.M. (2001). DEG/ENaC ion channels involved in sensory transduction are modulated by cold temperature. *PNAS* *98*, 6459–6463.
- Askwith, C.C., Wemmie, J.A., Price, M.P., Rokhlina, T., and Welsh, M.J. (2004). Acid-sensing ion channel 2 (ASIC2) modulates ASIC1 H⁺-activated currents in hippocampal neurons. *J. Biol. Chem.* *279*, 18296–18305.
- Assad, J.A., Shepherd, G.M.G., and Corey, D.P. (1991). Tip-link integrity and mechanical transduction in vertebrate hair cells. *Neuron* *7*, 985–994.
- Babini, E., Paukert, M., Geisler, H.-S., and Grunder, S. (2002). Alternative splicing and interaction with di- and polyvalent cations control the dynamic range of acid-sensing ion channel 1 (ASIC1). *J. Biol. Chem.* *277*, 41597–41603.
- Babinski, K., Catarsi, S., Biagini, G., and Séguéla, P. (2000). Mammalian ASIC2a and ASIC3 subunits co-assemble into heteromeric proton-gated channels sensitive to Gd³⁺. *J. Biol. Chem.* *275*, 28519–28525.
- Bahloul, A., Michel, V., Hardelin, J.-P., Nouaille, S., Hoos, S., Houdusse, A., England, P., and Petit, C. (2010). Cadherin-23, myosin VIIa and harmonin, encoded by Usher syndrome type I genes, form a ternary complex and interact with membrane phospholipids. *Hum. Mol. Genet.* *19*, 3557–3565.

- Baron, A., Waldmann, R., and Lazdunski, M. (2002). ASIC-like, proton-activated currents in rat hippocampal neurons. *J Physiol* 539, 485–494.
- Bassilana, F., Champigny, G., Waldmann, R., de Weille, J.R., Heurteaux, C., and Lazdunski, M. (1997). The acid-sensitive ionic channel subunit ASIC and the mammalian degenerin MDEG form a heteromultimeric H⁺-gated Na⁺ channel with novel properties. *J. Biol. Chem.* 272, 28819–28822.
- Bässler, E.L., Ngo-Anh, T.J., Geisler, H.S., Ruppertsberg, J.P., and Gründer, S. (2001). Molecular and functional characterization of acid-sensing ion channel (ASIC) 1b. *J. Biol. Chem.* 276, 33782–33787.
- Belyantseva, I.A., Adler, H.J., Curi, R., Frolenkov, G.I., and Kachar, B. (2000). Expression and Localization of Prestin and the Sugar Transporter GLUT-5 during Development of Electromotility in Cochlear Outer Hair Cells. *J. Neurosci.* 20, RC116–RC116.
- Berg, J.S., Powell, B.C., and Cheney, R.E. (2001). A millennial myosin census. *Mol. Biol. Cell* 12, 780–794.
- Beurg, M., Nam, J.-H., Crawford, A., and Fettiplace, R. (2008). The actions of calcium on hair bundle mechanics in mammalian cochlear hair cells. *Biophys. J.* 94, 2639–2653.
- Beurg, M., Fettiplace, R., Nam, J.-H., and Ricci, A.J. (2009). Localization of inner hair cell mechanotransducer channels using high-speed calcium imaging. *Nat. Neurosci.* 12, 553–558.
- Beutner, D., and Moser, T. (2001a). The Presynaptic Function of Mouse Cochlear Inner Hair Cells during Development of Hearing. *J. Neurosci.* 21, 4593–4599.
- Beutner, D., and Moser, T. (2001b). The Presynaptic Function of Mouse Cochlear Inner Hair Cells during Development of Hearing. *J. Neurosci.* 21, 4593–4599.
- Blanchet, C., Eróstegui, C., Sugasawa, M., and Dulon, D. (1996). Acetylcholine-induced potassium current of guinea pig outer hair cells: its dependence on a calcium influx through nicotinic-like receptors. *J. Neurosci.* 16, 2574–2584.
- Boëda, B., El-Amraoui, A., Bahloul, A., Goodyear, R., Daviet, L., Blanchard, S., Perfettini, I., Fath, K.R., Shorte, S., Reiners, J., et al. (2002). Myosin VIIa, harmonin and cadherin 23, three Usher I gene products that cooperate to shape the sensory hair cell bundle. *EMBO J.* 21, 6689–6699.
- Bolz, H., von Brederlow, B., Ramírez, A., Bryda, E.C., Kutsche, K., Nothwang, H.G., Seeliger, M., del C-Salcedó Cabrera, M., Vila, M.C., Molina, O.P., et al. (2001). Mutation of CDH23, encoding a new member of the cadherin gene family, causes Usher syndrome type 1D. *Nat. Genet.* 27, 108–112.
- Bork, J.M., Peters, L.M., Riazuddin, S., Bernstein, S.L., Ahmed, Z.M., Ness, S.L., Polomeno, R., Ramesh, A., Schloss, M., Srisailpathy, C.R., et al. (2001). Usher syndrome 1D and nonsyndromic autosomal recessive deafness DFNB12 are caused by allelic mutations of the novel cadherin-like gene CDH23. *Am. J. Hum. Genet.* 68, 26–37.
- Brandt, A., Striessnig, J., and Moser, T. (2003a). CaV1.3 channels are essential for development and presynaptic activity of cochlear inner hair cells. *J. Neurosci.* 23, 10832–10840.

- Brandt, A., Striessnig, J., and Moser, T. (2003b). CaV1.3 Channels Are Essential for Development and Presynaptic Activity of Cochlear Inner Hair Cells. *J. Neurosci.* *23*, 10832–10840.
- Brown, D.A., and Adams, P.R. (1980). Muscarinic suppression of a novel voltage-sensitive K⁺ current in a vertebrate neurone. *Nature* *283*, 673–676.
- Brownell, W.E., Bader, C.R., Bertrand, D., and de Ribaupierre, Y. (1985). Evoked mechanical responses of isolated cochlear outer hair cells. *Science* *227*, 194–196.
- Burgard, E.C., Niforatos, W., Biesen, T. van, Lynch, K.J., Touma, E., Metzger, R.E., Kowaluk, E.A., and Jarvis, M.F. (1999). P2X Receptor–Mediated Ionic Currents in Dorsal Root Ganglion Neurons. *J Neurophysiol* *82*, 1590–1598.
- Chambard, J.-M., and Ashmore, J.F. (2005). Regulation of the voltage-gated potassium channel KCNQ4 in the auditory pathway. *Pflügers Archiv European Journal of Physiology* *450*, 34–44.
- Champigny, G., Voilley, N., Waldmann, R., and Lazdunski, M. (1998). Mutations causing neurodegeneration in *Caenorhabditis elegans* drastically alter the pH sensitivity and inactivation of the mammalian H⁺-gated Na⁺ channel MDEG1. *J. Biol. Chem.* *273*, 15418–15422.
- Chen, X., and Gründer, S. (2007). Permeating protons contribute to tachyphylaxis of the acid-sensing ion channel (ASIC) 1a. *J. Physiol. (Lond.)* *579*, 657–670.
- Chen, C.C., England, S., Akopian, A.N., and Wood, J.N. (1998). A sensory neuron-specific, proton-gated ion channel. *Proc. Natl. Acad. Sci. U.S.A.* *95*, 10240–10245.
- Chen, X., Kalbacher, H., and Gründer, S. (2005). The tarantula toxin psalmotoxin 1 inhibits acid-sensing ion channel (ASIC) 1a by increasing its apparent H⁺ affinity. *J. Gen. Physiol.* *126*, 71–79.
- Chen, X., Kalbacher, H., and Gründer, S. (2006). Interaction of Acid-sensing Ion Channel (ASIC) 1 with the Tarantula Toxin Psalmotoxin 1 is State Dependent. *J Gen Physiol* *127*, 267–276.
- Chu, X.-P., Wemmie, J.A., Wang, W.-Z., Zhu, X.-M., Saugstad, J.A., Price, M.P., Simon, R.P., and Xiong, Z.-G. (2004). Subunit-dependent high-affinity zinc inhibition of acid-sensing ion channels. *J. Neurosci.* *24*, 8678–8689.
- Chu, X.-P., Papasian, C.J., Wang, J.Q., and Xiong, Z.-G. (2011). Modulation of acid-sensing ion channels: molecular mechanisms and therapeutic potential. *Int J Physiol Pathophysiol Pharmacol* *3*, 288–309.
- Corey, D.P., and Hudspeth, A.J. (1979). Response latency of vertebrate hair cells. *Biophysical Journal* *26*, 499–506.
- Dallos, P. (2008). Cochlear amplification, outer hair cells and prestin. *Curr Opin Neurobiol* *18*, 370–376.
- Dallos, P., and Harris, D. (1978). Properties of auditory nerve responses in absence of outer hair cells. *Journal of Neurophysiology* *41*, 365–383.

- Donier, E., Rugiero, F., Jacob, C., and Wood, J.N. (2008). Regulation of ASIC activity by ASIC4 – new insights into ASIC channel function revealed by a yeast two-hybrid assay. *European Journal of Neuroscience* 28, 74–86.
- Dulon, D., and Lenoir, M. (1996). Cholinergic Responses in Developing Outer Hair Cells of the Rat Cochlea. *European Journal of Neuroscience* 8, 1945–1952.
- Dulon, D., Luo, L., Zhang, C., and Ryan, A.F. (1998). Expression of small-conductance calcium-activated potassium channels (SK) in outer hair cells of the rat cochlea. *Eur. J. Neurosci.* 10, 907–915.
- El-Amraoui, A., and Petit, C. (2005). Usher I syndrome: unravelling the mechanisms that underlie the cohesion of the growing hair bundle in inner ear sensory cells. *J Cell Sci* 118, 4593–4603.
- Elgoyhen, A.B., Vetter, D.E., Katz, E., Rothlin, C.V., Heinemann, S.F., and Boulter, J. (2001). $\alpha 10$: A determinant of nicotinic cholinergic receptor function in mammalian vestibular and cochlear mechanosensory hair cells. *Proc Natl Acad Sci U S A* 98, 3501–3506.
- Evans, M.G. (1996). Acetylcholine activates two currents in guinea-pig outer hair cells. *J. Physiol. (Lond.)* 491 (Pt 2), 563–578.
- Firsov, D., Gautschi, I., Merillat, A.M., Rossier, B.C., and Schild, L. (1998). The heterotetrameric architecture of the epithelial sodium channel (ENaC). *EMBO J.* 17, 344–352.
- Frank, G., Hemmert, W., and Gummer, A.W. (1999). Limiting dynamics of high-frequency electromechanical transduction of outer hair cells. *Proc. Natl. Acad. Sci. U.S.A.* 96, 4420–4425.
- Gamper, N., and Shapiro, M.S. (2003). Calmodulin Mediates Ca^{2+} -dependent Modulation of M-type K^+ Channels. *J Gen Physiol* 122, 17–31.
- Garner, C.C., Nash, J., and Haganir, R.L. (2000). PDZ domains in synapse assembly and signalling. *Trends Cell Biol.* 10, 274–280.
- Garza, A., López-Ramírez, O., Vega, R., and Soto, E. (2010). The aminoglycosides modulate the acid-sensing ionic channel currents in dorsal root ganglion neurons from the rat. *J. Pharmacol. Exp. Ther.* 332, 489–499.
- Geisler, C.D. (1998). *From Sound to Synapse: Physiology of the Mammalian Ear* (OUP USA).
- Gillespie, P.G., and Cyr, J.L. (2004). Myosin-1c, the hair cell's adaptation motor. *Annu. Rev. Physiol.* 66, 521–545.
- Gillespie, P.G., and Müller, U. (2009). Mechanotransduction by Hair Cells: Models, Molecules, and Mechanisms. *Cell* 139, 33–44.
- Glowatzki, E., and Fuchs, P.A. (2000). Cholinergic Synaptic Inhibition of Inner Hair Cells in the Neonatal Mammalian Cochlea. *Science* 288, 2366–2368.
- Goodyear, R., and Richardson, G. (1999). The Ankle-Link Antigen: an Epitope Sensitive to Calcium Chelation Associated with the Hair-Cell Surface and the Calycal Processes of Photoreceptors. *J. Neurosci.* 19, 3761–3772.

Goodyear, R.J., and Richardson, G.P. (2003). A Novel Antigen Sensitive to Calcium Chelation That is Associated with the Tip Links and Kinocilial Links of Sensory Hair Bundles. *J. Neurosci.* *23*, 4878–4887.

Goodyear, R.J., Kros, C.J., and Richardson, G.P. (2006). The development of hair cells in the inner ear.

Grati, M., and Kachar, B. (2011). Myosin VIIa and sans localization at stereocilia upper tip-link density implicates these Usher syndrome proteins in mechanotransduction. *Proc Natl Acad Sci U S A* *108*, 11476–11481.

Gregory, F.D., Bryan, K.E., Pangršič, T., Calin-Jageman, I.E., Moser, T., and Lee, A. (2011). Harmonin inhibits presynaptic Cav1.3 Ca²⁺ channels in mouse inner hair cells. *Nat Neurosci* *14*, 1109–1111.

Grillet, N., Xiong, W., Reynolds, A., Kazmierczak, P., Sato, T., Lillo, C., Dumont, R.A., Hintermann, E., Sczaniecka, A., Schwander, M., et al. (2009). Harmonin mutations cause mechanotransduction defects in cochlear hair cells. *Neuron* *62*, 375–387.

Gründer, S., and Chen, X. (2010). Structure, function, and pharmacology of acid-sensing ion channels (ASICs): focus on ASIC1a. *Int J Physiol Pathophysiol Pharmacol* *2*, 73–94.

Gründer, S., Geissler, H.S., Bässler, E.L., and Ruppertsberg, J.P. (2000). A new member of acid-sensing ion channels from pituitary gland. *Neuroreport* *11*, 1607–1611.

Hamill, O.P., Marty, A., Neher, E., Sakmann, B., and Sigworth, F.J. (1981). Improved patch-clamp techniques for high-resolution current recording from cells and cell-free membrane patches. *Pflugers Arch.* *391*, 85–100.

Hasson, T., Heintzelman, M.B., Santos-Sacchi, J., Corey, D.P., and Mooseker, M.S. (1995). Expression in cochlea and retina of myosin VIIa, the gene product defective in Usher syndrome type 1B. *Proc. Natl. Acad. Sci. U.S.A.* *92*, 9815–9819.

Hasson, T., Gillespie, P.G., Garcia, J.A., MacDonald, R.B., Zhao, Y., Yee, A.G., Mooseker, M.S., and Corey, D.P. (1997). Unconventional Myosins in Inner-Ear Sensory Epithelia. *J Cell Biol* *137*, 1287–1307.

Helyer, R.J., Kennedy, H.J., Davies, D., Holley, M.C., and Kros, C.J. (2005). Development of Outward Potassium Currents in Inner and Outer Hair Cells from the Embryonic Mouse Cochlea. *Audiology and Neuro-Otology* *10*, 22–34.

Hildebrand, M.S., de Silva, M.G., Klockars, T., Rose, E., Price, M., Smith, R.J.H., McGuirt, W.T., Christopoulos, H., Petit, C., and Dahl, H.-H.M. (2004). Characterisation of DRASIC in the mouse inner ear. *Hear. Res.* *190*, 149–160.

Housley, G.D., and Ashmore, J.F. (1992). Ionic currents of outer hair cells isolated from the guinea-pig cochlea. *Journal of Physiology* *448*, 73–98.

Howard, J., and Hudspeth, A.J. (1987). Mechanical relaxation of the hair bundle mediates adaptation in mechano-electrical transduction by the bullfrog's saccular hair cell. *Proc. Natl. Acad. Sci. U.S.A.* *84*, 3064–3068.

- Immke, D.C., and McCleskey, E.W. (2003). Protons Open Acid-Sensing Ion Channels by Catalyzing Relief of Ca²⁺ Blockade. *Neuron* 37, 75–84.
- Inoue, A., and Ikebe, M. (2003). Characterization of the motor activity of mammalian myosin VIIA. *J. Biol. Chem.* 278, 5478–5487.
- Jagger, D.J., and Ashmore, J.F. (1999). Regulation of ionic currents by protein kinase A and intracellular calcium in outer hair cells isolated from the guinea-pig cochlea. *Pflügers Archiv European Journal of Physiology* 437, 409–416.
- Jasti, J., Furukawa, H., Gonzales, E.B., and Gouaux, E. (2007). Structure of acid-sensing ion channel 1 at 1.9 Å resolution and low pH. *Nature* 449, 316–323.
- Johnson, K.R., Gagnon, L.H., Webb, L.S., Peters, L.L., Hawes, N.L., Chang, B., and Zheng, Q.Y. (2003). Mouse models of USH1C and DFNB18: phenotypic and molecular analyses of two new spontaneous mutations of the Ush1c gene. *Hum. Mol. Genet.* 12, 3075–3086.
- Johnson, S.L., Marcotti, W., and Kros, C.J. (2005). Increase in efficiency and reduction in Ca²⁺ dependence of exocytosis during development of mouse inner hair cells. *J. Physiol. (Lond.)* 563, 177–191.
- Johnson, S.L., Adelman, J.P., and Marcotti, W. (2007). Genetic deletion of SK2 channels in mouse inner hair cells prevents the developmental linearization in the Ca²⁺ dependence of exocytosis. *J Physiol* 583, 631–646.
- Johnson, S.L., Eckrich, T., Kuhn, S., Zampini, V., Franz, C., Ranatunga, K.M., Roberts, T.P., Masetto, S., Knipper, M., Kros, C.J., et al. (2011). Position-dependent patterning of spontaneous action potentials in immature cochlear inner hair cells. *Nat Neurosci* 14, 711–717.
- Johnson, S.L., Kennedy, H.J., Holley, M.C., Fettiplace, R., and Marcotti, W. (2012). The resting transducer current drives spontaneous activity in prehearing Mammalian cochlear inner hair cells. *J. Neurosci.* 32, 10479–10483.
- Jørgensen, F., and Ohmori, H. (1988). Amiloride blocks the mechano-electrical transduction channel of hair cells of the chick. *J Physiol* 403, 577–588.
- Kachar, B., Parakkal, M., Kurc, M., Zhao, Y., and Gillespie, P.G. (2000). High-resolution structure of hair-cell tip links. *PNAS* 97, 13336–13341.
- Takehata, S., and Santos-Sacchi, J. (1996). Effects of Salicylate and Lanthanides on Outer Hair Cell Motility and Associated Gating Charge. *J. Neurosci.* 16, 4881–4889.
- Kawashima, Y., Géléoc, G.S.G., Kurima, K., Labay, V., Lelli, A., Asai, Y., Makishima, T., Wu, D.K., Della Santina, C.C., Holt, J.R., et al. (2011). Mechanotransduction in mouse inner ear hair cells requires transmembrane channel-like genes. *Journal of Clinical Investigation* 121, 4796–4809.
- Kazmierczak, P., Sakaguchi, H., Tokita, J., Wilson-Kubalek, E.M., Milligan, R.A., Müller, U., and Kachar, B. (2007). Cadherin 23 and protocadherin 15 interact to form tip-link filaments in sensory hair cells. *Nature* 449, 87–91.
- Kennedy, H.J., Evans, M.G., Crawford, A.C., and Fettiplace, R. (2003). Fast adaptation of mechano-electrical transducer channels in mammalian cochlear hair cells. *Nat. Neurosci.* 6, 832–836.

- Kharkovets, T., Dedek, K., Maier, H., Schweizer, M., Khimich, D., Nouvian, R., Vardanyan, V., Leuwer, R., Moser, T., and Jentsch, T.J. (2006). Mice with altered KCNQ4 K⁺ channels implicate sensory outer hair cells in human progressive deafness. *The EMBO Journal* 25, 642–652.
- Kikkawa, Y.S., Pawlowski, K.S., Wright, C.G., and Alagramam, K.N. (2008). Development of Outer Hair Cells in Ames Waltzer Mice: Mutation in Protocadherin 15 Affects Development of Cuticular Plate and Associated Structures. *The Anatomical Record: Advances in Integrative Anatomy and Evolutionary Biology* 291, 224–232.
- Kremer, H., van Wijk, E., Märker, T., Wolfrum, U., and Roepman, R. (2006). Usher syndrome: molecular links of pathogenesis, proteins and pathways. *Hum. Mol. Genet.* 15 *Spec No 2*, R262–270.
- Krishtal, O. (2003). The ASICs: signaling molecules? Modulators? *Trends Neurosci.* 26, 477–483.
- Krishtal, O.A., and Pidoplichko, V.I. (1981). A receptor for protons in the membrane of sensory neurons may participate in nociception. *Neuroscience* 6, 2599–2601.
- Kroese, A.B., Das, A., and Hudspeth, A.J. (1989). Blockage of the transduction channels of hair cells in the bullfrog's sacculus by aminoglycoside antibiotics. *Hear. Res.* 37, 203–217.
- Kros, C.J. (2007). How to build an inner hair cell: Challenges for regeneration. *Hearing Research* 227, 3–10.
- Kros, C.J., and Crawford, A.C. (1990). Potassium currents in inner hair cells isolated from the guinea-pig cochlea. *J Physiol* 421, 263–291.
- Kros, C.J., Ruppertsberg, J.P., and Rüsch, A. (1998). Expression of a potassium current in inner hair cells during development of hearing in mice. *Nature* 394, 281–284.
- Kros, C.J., Marcotti, W., Netten, S.M. van, Self, T.J., Libby, R.T., Brown, S.D.M., Richardson, G.P., and Steel, K.P. (2001). Reduced climbing and increased slipping adaptation in cochlear hair cells of mice with Myo7a mutations. *Nature Neuroscience* 5, 41–47.
- Kubisch, C., Schroeder, B.C., Friedrich, T., Lütjohann, B., El-Amraoui, A., Marlin, S., Petit, C., and Jentsch, T.J. (1999). KCNQ4, a novel potassium channel expressed in sensory outer hair cells, is mutated in dominant deafness. *Cell* 96, 437–446.
- Küssel-Andermann, P., El-Amraoui, A., Safieddine, S., Nouaille, S., Perfettini, I., Lecuit, M., Cossart, P., Wolfrum, U., and Petit, C. (2000). Vezatin, a novel transmembrane protein, bridges myosin VIIA to the cadherin-catenins complex. *EMBO J.* 19, 6020–6029.
- Lagziel, A., Ahmed, Z.M., Schultz, J.M., Morell, R.J., Belyantseva, I.A., and Friedman, T.B. (2005). Spatiotemporal pattern and isoforms of cadherin 23 in wild type and waltzer mice during inner ear hair cell development. *Dev. Biol.* 280, 295–306.
- Lefèvre, G., Michel, V., Weil, D., Lepelletier, L., Bizard, E., Wolfrum, U., Hardelin, J.-P., and Petit, C. (2008). A core cochlear phenotype in USH1 mouse mutants implicates fibrous links of the hair bundle in its cohesion, orientation and differential growth. *Development* 135, 1427–1437.
- Lelli, A., Asai, Y., Forge, A., Holt, J.R., and Geleoc, G.S.G. (2009). Tonotopic Gradient in the Developmental Acquisition of Sensory Transduction in Outer Hair Cells of the Mouse Cochlea. *Journal of Neurophysiology* 101, 2961–2973.

- Lelli, A., Kazmierczak, P., Kawashima, Y., Müller, U., and Holt, J.R. (2010). Development and regeneration of sensory transduction in auditory hair cells requires functional interaction between cadherin-23 and protocadherin-15. *J. Neurosci.* *30*, 11259–11269.
- Lenoir, M., Shneron, A., and Pujol, R. (1980). Cochlear receptor development in the rat with emphasis on synaptogenesis. *Anat. Embryol.* *160*, 253–262.
- Liberman, M.C., Gao, J., He, D.Z.Z., Wu, X., Jia, S., and Zuo, J. (2002). Prestin is required for electromotility of the outer hair cell and for the cochlear amplifier. *Nature* *419*, 300–304.
- Lingueglia, E., de Weille, J.R., Bassilana, F., Heurteaux, C., Sakai, H., Waldmann, R., and Lazdunski, M. (1997). A modulatory subunit of acid sensing ion channels in brain and dorsal root ganglion cells. *J. Biol. Chem.* *272*, 29778–29783.
- Lustig, L.R., Peng, H., Hiel, H., Yamamoto, T., and Fuchs, P.A. (2001). Molecular cloning and mapping of the human nicotinic acetylcholine receptor alpha10 (CHRNA10). *Genomics* *73*, 272–283.
- Mammano, F., and Ashmore, J.F. (1996). Differential expression of outer hair cell potassium currents in the isolated cochlea of the guinea-pig. *J Physiol* *496*, 639–646.
- Mammano, F., Kros, C.J., and Ashmore, J.F. (1995). Patch clamped responses from outer hair cells in the intact adult organ of Corti. *Pflugers Arch.* *430*, 745–750.
- Marcotti, W., and Kros, C.J. (1999). Developmental expression of the potassium current $I_{K,n}$ contributes to maturation of mouse outer hair cells. *The Journal of Physiology* *520*, 653–660.
- Marcotti, W., Johnson, S.L., Holley, M.C., and Kros, C.J. (2003a). Developmental changes in the expression of potassium currents of embryonic, neonatal and mature mouse inner hair cells. *J Physiol* *548*, 383–400.
- Marcotti, W., Johnson, S.L., Rusch, A., and Kros, C.J. (2003b). Sodium and calcium currents shape action potentials in immature mouse inner hair cells. *J. Physiol. (Lond.)* *552*, 743–761.
- Marcotti, W., Johnson, S.L., and Kros, C.J. (2004a). A transiently expressed SK current sustains and modulates action potential activity in immature mouse inner hair cells. *J Physiol* *560*, 691–708.
- Marcotti, W., Johnson, S.L., and Kros, C.J. (2004b). Effects of intracellular stores and extracellular Ca^{2+} on Ca^{2+} -activated K^{+} currents in mature mouse inner hair cells. *The Journal of Physiology* *557*, 613–633.
- Marcotti, W., Netten, S.M. van, and Kros, C.J. (2005). The aminoglycoside antibiotic dihydrostreptomycin rapidly enters mouse outer hair cells through the mechano-electrical transducer channels. *J Physiol* *567*, 505–521.
- Mazurek, B., Winter, E., Fuchs, J., Haupt, H., and Gross, J. (2003). Susceptibility of the hair cells of the newborn rat cochlea to hypoxia and ischemia. *Hear. Res.* *182*, 2–8.
- Meyer, A.C., Frank, T., Khimich, D., Hoch, G., Riedel, D., Chapochnikov, N.M., Yarin, Y.M., Harke, B., Hell, S.W., Egner, A., et al. (2009). Tuning of synapse number, structure and function in the cochlea. *Nature Neuroscience* *12*, 444–453.

Michalski, N., Michel, V., Caberlotto, E., Lefèvre, G., van Aken, A., Tinevez, J.-Y., Bizard, E., Houbron, C., Weil, D., Hardelin, J.-P., et al. (2009). Harmonin-b, an actin-binding scaffold protein, is involved in the adaptation of mechano-electrical transduction by sensory hair cells. *Pflügers Archiv European Journal of Physiology* 459, 115–130.

Michel, V., Goodyear, R.J., Weil, D., Marcotti, W., Perfettini, I., Wolfrum, U., Kros, C.J., Richardson, G.P., and Petit, C. (2005). Cadherin 23 is a component of the transient lateral links in the developing hair bundles of cochlear sensory cells. *Dev. Biol.* 280, 281–294.

Michna, M., Knirsch, M., Hoda, J.-C., Muenkner, S., Langer, P., Platzer, J., Striessnig, J., and Engel, J. (2003). Cav1.3 (alpha1D) Ca²⁺ currents in neonatal outer hair cells of mice. *J. Physiol. (Lond.)* 553, 747–758.

Muallem, D., and Ashmore, J. (2006). An anion antiporter model of prestin, the outer hair cell motor protein. *Biophysical Journal* 90, 4035–4045.

Müller, U. (2008). Cadherins and mechanotransduction by hair cells. *Curr. Opin. Cell Biol.* 20, 557–566.

Müller, U., and Gillespie, P. (2008). Silencing the Cochlear Amplifier by Immobilizing Prestin. *Neuron* 58, 299–301.

Neher, E. (1992). [6] Correction for liquid junction potentials in patch clamp experiments. In *Ion Channels*, (Academic Press), pp. 123–131.

Nenov, A.P., Norris, C., and Bobbin, R.P. (1997). Outwardly rectifying currents in guinea pig outer hair cells. *Hearing Research* 105, 146–158.

Ogden, D. (1994). *Microelectrode Techniques: The Plymouth Workshop Handbook* (Company of Biologists).

Oliver, D., Plinkert, P., Zenner, H.P., and Ruppertsberg, J.P. (1997). Sodium current expression during postnatal development of rat outer hair cells. *Pflügers Archiv European Journal of Physiology* 434, 772–778.

Oliver, D., Knipper, M., Derst, C., and Fakler, B. (2003). Resting potential and submembrane calcium concentration of inner hair cells in the isolated mouse cochlea are set by KCNQ-type potassium channels. *J. Neurosci.* 23, 2141–2149.

Page, A.J., Brierley, S.M., Martin, C.M., Price, M.P., Symonds, E., Butler, R., Wemmie, J.A., and Blackshaw, L.A. (2005). Different contributions of ASIC channels 1a, 2, and 3 in gastrointestinal mechanosensory function. *Gut* 54, 1408–1415.

Di Palma, F., Holme, R.H., Bryda, E.C., Belyantseva, I.A., Pellegrino, R., Kachar, B., Steel, K.P., and Noben-Trauth, K. (2001). Mutations in *Cdh23*, encoding a new type of cadherin, cause stereocilia disorganization in waltzer, the mouse model for Usher syndrome type 1D. *Nat. Genet.* 27, 103–107.

Paukert, M., Babini, E., Pusch, M., and Gründer, S. (2004). Identification of the Ca²⁺ blocking site of acid-sensing ion channel (ASIC) 1: implications for channel gating. *J. Gen. Physiol.* 124, 383–394.

- Peier, A.M., Reeve, A.J., Andersson, D.A., Moqrich, A., Earley, T.J., Hergarden, A.C., Story, G.M., Colley, S., Hogenesch, J.B., McIntyre, P., et al. (2002). A Heat-Sensitive TRP Channel Expressed in Keratinocytes. *Science* *296*, 2046–2049.
- Peng, B.-G., Ahmad, S., Chen, S., Chen, P., Price, M.P., and Lin, X. (2004). Acid-sensing ion channel 2 contributes a major component to acid-evoked excitatory responses in spiral ganglion neurons and plays a role in noise susceptibility of mice. *J. Neurosci.* *24*, 10167–10175.
- Petit, C. (2001). USHER SYNDROME: From Genetics to Pathogenesis. *Annual Review of Genomics and Human Genetics* *2*, 271–297.
- Petroff, E.Y., Price, M.P., Snitsarev, V., Gong, H., Korovkina, V., Abboud, F.M., and Welsh, M.J. (2008). Acid-sensing ion channels interact with and inhibit BK K⁺ channels. *Proc. Natl. Acad. Sci. U.S.A.* *105*, 3140–3144.
- Phillips, K.R., Tong, S., Goodyear, R., Richardson, G.P., and Cyr, J.L. (2006). Stereociliary myosin-1c receptors are sensitive to calcium chelation and absent from cadherin 23 mutant mice. *J. Neurosci.* *26*, 10777–10788.
- Pickles, J.O. (2008). *An Introduction to the Physiology of Hearing* (Academic Press).
- Pickles, J.O., Comis, S.D., and Osborne, M.P. (1984). Cross-links between stereocilia in the guinea pig organ of Corti, and their possible relation to sensory transduction. *Hearing Research* *15*, 103–112.
- Platzer, J., Engel, J., Schrott-Fischer, A., Stephan, K., Bova, S., Chen, H., Zheng, H., and Striessnig, J. (2000). Congenital Deafness and Sinoatrial Node Dysfunction in Mice Lacking Class D L-Type Ca²⁺ Channels. *Cell* *102*, 89–97.
- Price, M.P., McIlwrath, S.L., Xie, J., Cheng, C., Qiao, J., Tarr, D.E., Sluka, K.A., Brennan, T.J., Lewin, G.R., and Welsh, M.J. (2001). The DRASIC cation channel contributes to the detection of cutaneous touch and acid stimuli in mice. *Neuron* *32*, 1071–1083.
- Pujol, R., Lavigne-Rebillard, M, and Lenoir, M. (1998). *Development of the Auditory System*. (Springer-Verlag, New York).
- Purves, D., Augustine, G.J., Fitzpatrick, D., Hall, W.C., LaMantia, A.-S., McNamara, J.O., and White, L.E. (2007). *Neuroscience* (Sinauer Associates).
- Reiners, J., Märker, T., Jürgens, K., Reidel, B., and Wolfrum, U. (2005). Photoreceptor expression of the Usher syndrome type 1 protein protocadherin 15 (USH1F) and its interaction with the scaffold protein harmonin (USH1C). *Mol. Vis.* *11*, 347–355.
- Revenu, C., Athman, R., Robine, S., and Louvard, D. (2004). The co-workers of actin filaments: from cell structures to signals. *Nat. Rev. Mol. Cell Biol.* *5*, 635–646.
- Ricci, A.J., and Fettiplace, R. (1998). Calcium permeation of the turtle hair cell mechanotransducer channel and its relation to the composition of endolymph. *J Physiol* *506*, 159–173.
- Roux, I., Hosie, S., Johnson, S.L., Bahloul, A., Cayet, N., Nouaille, S., Kros, C.J., Petit, C., and Safieddine, S. (2009). Myosin VI is required for the proper maturation and function of inner hair cell ribbon synapses. *Hum. Mol. Genet.* *18*, 4615–4628.

- Ruben, R.J. (1967). Development of the inner ear of the mouse: a radioautographic study of terminal mitoses. *Acta Otolaryngol. Suppl* 220:1–44.
- Rüsch, A., Kros, C.J., and Richardson, G.P. (1994). Block by amiloride and its derivatives of mechano-electrical transduction in outer hair cells of mouse cochlear cultures. *J Physiol* 474, 75–86.
- Ryan, A., and Dallos, P. (1975). Effect of absence of cochlear outer hair cells on behavioural auditory threshold. , Published Online: 03 January 1975; | Doi:10.1038/253044a0 253, 44–46.
- Rzadzinska, A.K., Schneider, M.E., Davies, C., Riordan, G.P., and Kachar, B. (2004). An actin molecular treadmill and myosins maintain stereocilia functional architecture and self-renewal. *J. Cell Biol.* 164, 887–897.
- Santos-Sacchi, J. (1991). Reversible inhibition of voltage-dependent outer hair cell motility and capacitance. *J. Neurosci.* 11, 3096–3110.
- Schaechinger, T.J., and Oliver, D. (2007). Nonmammalian orthologs of prestin (SLC26A5) are electrogenic divalent/chloride anion exchangers. *PNAS* 104, 7693–7698.
- Schneider, M.E., Belyantseva, I.A., Azevedo, R.B., and Kachar, B. (2002). Rapid renewal of auditory hair bundles. *Nature* 418, 837–838.
- Self, T., Mahony, M., Fleming, J., Walsh, J., Brown, S.D., and Steel, K.P. (1998). Shaker-1 mutations reveal roles for myosin VIIA in both development and function of cochlear hair cells. *Development* 125, 557–566.
- Sellick, P.M., Kirk, D.L., Patuzzi, R., and Robertson, D. (2007). Does BAPTA leave outer hair cell transduction channels closed? *Hearing Research* 224, 84–92.
- Selyanko, A.A., Hadley, J.K., Wood, I.C., Abogadie, F.C., Jentsch, T.J., and Brown, D.A. (2000). Inhibition of KCNQ1-4 potassium channels expressed in mammalian cells via M1 muscarinic acetylcholine receptors. *J. Physiol. (Lond.)* 522 Pt 3, 349–355.
- Senften, M., Schwander, M., Kazmierczak, P., Lillo, C., Shin, J.-B., Hasson, T., Géléoc, G.S.G., Gillespie, P.G., Williams, D., Holt, J.R., et al. (2006). Physical and functional interaction between protocadherin 15 and myosin VIIa in mechanosensory hair cells. *J. Neurosci.* 26, 2060–2071.
- Sgard, F., Charpantier, E., Bertrand, S., Walker, N., Caput, D., Graham, D., Bertrand, D., and Besnard, F. (2002). A novel human nicotinic receptor subunit, alpha10, that confers functionality to the alpha9-subunit. *Mol. Pharmacol.* 61, 150–159.
- Siemens, J., Kazmierczak, P., Reynolds, A., Sticker, M., Littlewood-Evans, A., and Müller, U. (2002). The Usher syndrome proteins cadherin 23 and harmonin form a complex by means of PDZ-domain interactions. *Proc. Natl. Acad. Sci. U.S.A.* 99, 14946–14951.
- Siemens, J., Lillo, C., Dumont, R.A., Reynolds, A., Williams, D.S., Gillespie, P.G., and Müller, U. (2004). Cadherin 23 is a component of the tip link in hair-cell stereocilia. *Nature* 428, 950–955.
- Sotomayor, M., and Schulten, K. (2008). The allosteric role of the Ca²⁺ switch in adhesion and elasticity of C-cadherin. *Biophys. J.* 94, 4621–4633.

- Staruschenko, A., Dorofeeva, N.A., Bolshakov, K.V., and Stockand, J.D. (2007). Subunit-dependent cadmium and nickel inhibition of acid-sensing ion channels. *Dev Neurobiol* 67, 97–107.
- Stepanyan, R., and Frolenkov, G.I. (2009). Fast adaptation and Ca²⁺ sensitivity of the mechanotransducer require myosin-XVa in inner but not outer cochlear hair cells. *J. Neurosci.* 29, 4023–4034.
- Sutherland, S.P., Benson, C.J., Adelman, J.P., and McCleskey, E.W. (2001). Acid-sensing ion channel 3 matches the acid-gated current in cardiac ischemia-sensing neurons. *Proc. Natl. Acad. Sci. U.S.A.* 98, 711–716.
- Suzuki, M., Mizuno, A., Kodaira, K., and Imai, M. (2003). Impaired Pressure Sensation in Mice Lacking TRPV4. *J. Biol. Chem.* 278, 22664–22668.
- Tilney, L.G., Tilney, M.S., and DeRosier, D.J. (1992). Actin filaments, stereocilia, and hair cells: how cells count and measure. *Annu. Rev. Cell Biol.* 8, 257–274.
- Tritsch, N.X., Yi, E., Gale, J.E., Glowatzki, E., and Bergles, D.E. (2007). The origin of spontaneous activity in the developing auditory system. *Nature* 450, 50–55.
- Ugawa, S., Ueda, T., Ishida, Y., Nishigaki, M., Shibata, Y., and Shimada, S. (2002). Amiloride-blockable acid-sensing ion channels are leading acid sensors expressed in human nociceptors. *Journal of Clinical Investigation* 110, 1185–1190.
- Ugawa, S., Inagaki, A., Yamamura, H., Ueda, T., Ishida, Y., Kajita, K., Shimizu, H., and Shimada, S. (2006). Acid-sensing ion channel-1b in the stereocilia of mammalian cochlear hair cells. *NeuroReport* 17, 1235–1239.
- Ugawa, S., Ishida, Y., Ueda, T., Inoue, K., Nagao, M., and Shimada, S. (2007). Nafamostat mesilate reversibly blocks acid-sensing ion channel currents. *Biochemical and Biophysical Research Communications* 363, 203–208.
- Verpy, E., Leibovici, M., Zwaenepoel, I., Liu, X.Z., Gal, A., Salem, N., Mansour, A., Blanchard, S., Kobayashi, I., Keats, B.J., et al. (2000). A defect in harmonin, a PDZ domain-containing protein expressed in the inner ear sensory hair cells, underlies Usher syndrome type 1C. *Nat. Genet.* 26, 51–55.
- Waguespack, J., Salles, F.T., Kachar, B., and Ricci, A.J. (2007). Stepwise morphological and functional maturation of mechanotransduction in rat outer hair cells. *J. Neurosci.* 27, 13890–13902.
- Waldmann, R., and Lazdunski, M. (1998). H(+)-gated cation channels: neuronal acid sensors in the NaC/DEG family of ion channels. *Curr. Opin. Neurobiol.* 8, 418–424.
- Waldmann, R., Champigny, G., Bassilana, F., Heurteaux, C., and Lazdunski, M. (1997). A proton-gated cation channel involved in acid-sensing. *Nature* 386, 173–177.
- Wang, W., Duan, B., Xu, H., Xu, L., and Xu, T.-L. (2006). Calcium-permeable acid-sensing ion channel is a molecular target of the neurotoxic metal ion lead. *J. Biol. Chem.* 281, 2497–2505.
- Wang, W., Yu, Y., and Xu, T.-L. (2007). Modulation of acid-sensing ion channels by Cu²⁺ in cultured hypothalamic neurons of the rat. *Neuroscience* 145, 631–641.

- Weil, D., Blanchard, S., Kaplan, J., Guilford, P., Gibson, F., Walsh, J., Mburu, P., Varela, A., Leveilliers, J., and Weston, M.D. (1995). Defective myosin VIIA gene responsible for Usher syndrome type 1B. *Nature* 374, 60–61.
- Weil, D., Levy, G., Sahly, I., Levi-Acobas, F., Blanchard, S., El-Amraoui, A., Crozet, F., Philippe, H., Abitbol, M., and Petit, C. (1996). Human myosin VIIA responsible for the Usher 1B syndrome: a predicted membrane-associated motor protein expressed in developing sensory epithelia. *Proc. Natl. Acad. Sci. U.S.A.* 93, 3232–3237.
- Weil, D., El-Amraoui, A., Masmoudi, S., Mustapha, M., Kikkawa, Y., Lainé, S., Delmaghani, S., Adato, A., Nadifi, S., Zina, Z.B., et al. (2003). Usher syndrome type I G (USH1G) is caused by mutations in the gene encoding SANS, a protein that associates with the USH1C protein, harmonin. *Hum. Mol. Genet.* 12, 463–471.
- De Weille, J., and Bassilana, F. (2001). Dependence of the acid-sensitive ion channel, ASIC1a, on extracellular Ca(2+) ions. *Brain Res.* 900, 277–281.
- Wells, A.L., Lin, A.W., Chen, L.-Q., Safer, D., Cain, S.M., Hasson, T., Carragher, B.O., Milligan, R.A., and Sweeney, H.L. (1999). Myosin VI is an actin-based motor that moves backwards. *Nature* 401, 505–508.
- Wu, T., Lv, P., Kim, H.J., Yamoah, E.N., and Nuttall, A.L. (2010). Effect of salicylate on KCNQ4 of the guinea pig outer hair cell. *J. Neurophysiol.* 103, 1969–1977.
- Wu, X., Gao, J., Guo, Y., and Zuo, J. (2004). Hearing threshold elevation precedes hair-cell loss in prestin knockout mice. *Molecular Brain Research* 126, 30–37.
- Wu, Y.C., Ricci, A.J., and Fettiplace, R. (1999). Two components of transducer adaptation in auditory hair cells. *J. Neurophysiol.* 82, 2171–2181.
- Xia, X.-M., Fakler, B., Rivard, A., Wayman, G., Johnson-Pais, T., Keen, J.E., Ishii, T., Hirschberg, B., Bond, C.T., Lutsenko, S., et al. (1998). Mechanism of calcium gating in small-conductance calcium-activated potassium channels. *Nature* 395, 503–507.
- Xiong, Z.-G., Pignataro, G., Li, M., Chang, S., and Simon, R.P. (2008). Acid-sensing ion channels (ASICs) as pharmacological targets for neurodegenerative diseases. *Curr Opin Pharmacol* 8, 25–32.
- Xu, T., Nie, L., Zhang, Y., Mo, J., Feng, W., Wei, D., Petrov, E., Calisto, L.E., Kachar, B., Beisel, K.W., et al. (2007). Roles of Alternative Splicing in the Functional Properties of Inner Ear-specific KCNQ4 Channels. *J. Biol. Chem.* 282, 23899–23909.
- Yermolaieva, O., Leonard, A.S., Schnizler, M.K., Abboud, F.M., and Welsh, M.J. (2004). Extracellular acidosis increases neuronal cell calcium by activating acid-sensing ion channel 1a. *Proc. Natl. Acad. Sci. U.S.A.* 101, 6752–6757.
- Zheng, J., Shen, W., He, D.Z., Long, K.B., Madison, L.D., and Dallos, P. (2000). Prestin is the motor protein of cochlear outer hair cells. *Nature* 405, 149–155.
- Ziemann, A.E., Schnizler, M.K., Albert, G.W., Severson, M.A., Howard, M.A., 3rd, Welsh, M.J., and Wemmie, J.A. (2008). Seizure termination by acidosis depends on ASIC1a. *Nat. Neurosci.* 11, 816–822.

